

Some pages of this thesis may have been removed for copyright restrictions.

If you have discovered material in AURA which is unlawful e.g. breaches copyright, (either yours or that of a third party) or any other law, including but not limited to those relating to patent, trademark, confidentiality, data protection, obscenity, defamation, libel, then please read our [Takedown Policy](#) and [contact the service](#) immediately

**KINETO-ELASTODYNAMIC ANALYSIS OF HIGH-SPEED
FOUR-BAR MECHANISM**

ABDESLAM AANNAQUE

Doctor of Philosophy

THE UNIVERSITY OF ASTON IN BIRMINGHAM

January 1996

This copy of the thesis has been supplied on condition that anyone who consults it is understood to recognise that its copyright rests with its author and that no quotation from the thesis and no information derived from it may be published without the author's prior, written consent.

THE UNIVERSITY OF ASTON IN BIRMINGHAM

**KINETO-ELASTODYNAMIC ANALYSIS OF HIGH-SPEED FOUR-BAR
MECHANISM**

ABDESLAM AANNAQUE, Doctor of Philosophy
January 1996

SYNOPSIS

This thesis addresses the kineto-elastodynamic analysis of a four-bar mechanism running at high-speed where all links are assumed to be flexible. First, the mechanism, at static configurations, is considered as structure. Two methods are used to model the system, namely the finite element method (FEM) and the dynamic stiffness method. The natural frequencies and mode shapes at different positions from both methods are calculated and compared.

The FEM is used to model the mechanism running at high-speed. The governing equations of motion are derived using Hamilton's principle. The equations obtained are a set of stiff ordinary differential equations with periodic coefficients. A model is developed whereby the FEM and the dynamic stiffness method are used conjointly to provide high-precision results with only one element per link.

The principal concern of the mechanism designer is the behaviour of the mechanism at steady-state. Few algorithms have been developed to deliver the steady-state solution without resorting to costly time marching simulation. In this study two algorithms are developed to overcome the limitations of the existing algorithms. The superiority of the new algorithms is demonstrated.

The notion of critical speeds is clarified and a distinction is drawn between "critical speeds", where stresses are at a local maximum, and "unstable bands" where the mechanism deflections will grow boundlessly. Floquet theory is used to assess the stability of the system. A simple method to locate the critical speeds is derived. It is shown that the critical speeds of the mechanism coincide with the local maxima of the eigenvalues of the transition matrix with respect to the rotational speed of the mechanism.

Every mechanism has some limiting critical speeds at which the stresses will become unacceptable. A method is proposed whereby the mechanism can be run above one or more limiting critical speeds by changing a geometrical parameter of the mechanism.

The experimental work is carried out in two parts. In the first part the mechanism at different static configurations is considered. Modal testing method is used to extract the natural frequencies, mode shapes of the mechanism and the damping ratios. In the second part, the mechanism is run at different speeds. The strains and stresses at different locations of the mechanism are measured. The effect of the distance between the ground pivots is demonstrated.

Key words: Elastodynamic, critical speeds, Transition matrix, FEM.

ACKNOWLEDGEMENTS

The author wishes to express his sincere appreciation to Dr J. E. T Penny and Dr S. D. Garvey at Aston University (UK) and Prof. M. Bennouna at Ecole Mohammedia d'Ingénieurs (Morocco) for their supervision, guidance, support and many fruitful discussions throughout the course of this research. The author is very grateful to the British Council for their financial support.

Thanks should go to the technicians in the Department of Mechanical and Electrical Engineering, particularly Mr. Brian Muddyman, Mr. Jim Jeffs and Mr. Paul Pizer.

Thanks are also due to my friends Bing, Fathi, Kamel and Patrick for their kindness, help and encouragement.

Finally, I would like to express my appreciation and sincere thanks to all members of my family for their moral support and encouragement, particularly my parents, my wife Khadija and my two daughters Imane and Kawthar.

LIST OF CONTENTS

SYNOPSIS.....	2
ACKNOWLEDGEMENTS	3
LIST OF CONTENTS	4
LIST OF FIGURES	7
LIST OF TABLES	13
 Chapter 1: INTRODUCTION.....	 14
1.1 INTRODUCTION	14
1.2 AIM OF THIS RESEARCH.....	15
1.3 OUTLINE OF THE THESIS.....	17
 Chapter 2: LITERATURE REVIEW	 20
2.1 INTRODUCTION	20
2.2 FINITE ELEMENT METHOD	22
2.2.1 Equations of motion	24
2.2.2 Solution of the equations of motion	26
2.3 STABILITY.....	30
2.4 EXPERIMENTAL STUDIES	36
2.5 OTHER METHODS.....	39
2.6 CONCLUSION.....	40
 Chapter 3: KINETO-DYNAMIC ANALYSIS	 41
3.1 INTRODUCTION	41
3.2 MOBILITY	43
3.3 TRANSMISSION ANGLE	43
3.4 CLASSIFICATION OF FOUR-BAR MECHANISMS	46
3.5 KINEMATIC ANALYSIS	49
3.6 COUPLER CURVES	54
3.7 DYNAMIC ANALYSIS.....	55
3.8 GENERALISED RIGID-BODY ACCELERATIONS	57
3.9 CONCLUSION.....	58
 Chapter 4: FINITE ELEMENT METHOD IN THE ANALYSIS OF A FOUR-BAR MECHANISM	 59
4.1 INTRODUCTION	59
4.2 APPLICATION OF THE FEM TO THE ANALYSIS OF FOUR-BAR MECHANISMS.....	63
4.2.1 Shape functions for a Beam Element.	63
4.2.2 The equations of motion of the mechanism	66
4.2.3 Transformation to global coordinates.....	71
4.2.4 Assembly of the overall matrices.	73
4.2.5 Damping effect	76
4.2.6 Stiffening effect	77

4.3 NATURAL FREQUENCIES AND MODE SHAPES IN A STATIONARY MECHANISM	78
4.4 CONCLUSION.....	84
Chapter 5: DYNAMIC STIFFNESS METHOD	86
5.1 INTRODUCTION	86
5.2 APPLICATION OF THE DYNAMIC STIFFNESS METHOD TO THE ANALYSIS OF FOUR-BAR MECHANISMS.....	88
5.2.1 Exact displacement functions.....	88
5.2.2 Stiffness and mass matrices.....	91
5.3 WITTRICK-WILLIAMS ALGORITHM.....	95
5.4 APPLICATIONS	97
5.4.1 Portal frame	98
5.4.2 Four-bar mechanism.....	107
5.5 CONCLUSION.....	109
Chapter 6: SOLUTION OF THE EQUATIONS OF MOTION FOR STEADY STATE	111
6.1 INTRODUCTION	111
6.2 DIRECT INTEGRATION METHOD.....	112
6.2.1 Newmark method	113
6.2.2 Consistency of a scheme	115
6.2.3 Stability	116
6.3 MODAL ANALYSIS.....	118
6.4 FOURIER SERIES METHOD.....	124
6.5 NEW ALGORITHM 1: USING THE TRANSITION MATRIX TO CALCULATE THE STEADY-STATE SOLUTION	126
6.6 NEW ALGORITHM 2: VARIATION ON THE ESTABLISHED "CLOSED-FORM" ALGORITHMS.....	128
6.7 EQUIVALENCE BETWEEN THE TWO ALGORITHMS	131
6.8 COMPARISON OF EFFICIENCY OF DIFFERENT ALGORITHMS	131
6.9 CONCLUSION.....	135
Chapter 7: A METHOD OF RUNNING THE MECHANISM ABOVE SEVERAL CRITICAL SPEEDS.....	136
7.1 INTRODUCTION	136
7.2 TRANSITION MATRIX AND STABILITY ANALYSIS.....	137
7.2.1 Floquet Theorem for Analysing Periodic Systems.....	139
7.2.2 Definition of the Transition Matrix and its use for Assessing Stability.	140
7.2.3 Use of the Transition Matrix to Compute Critical Speeds.....	142
7.3 CRITICAL SPEEDS.....	149
7.4 MAXIMUM STRESS AS A FUNCTION OF RUNNING SPEED	152
7.4.1 Influence of the number of elements	153
7.4.2 The role of damping	155

7.5 PROPOSED DESIGN METHOD FOR HIGH-SPEED OPERATION.....	157
7.6 CONCLUSION.....	161
Chapter 8: EXPERIMENTAL INVESTIGATION	162
8.1 INTRODUCTION	162
8.2 DESIGN OF THE TEST RIG	162
8.3 PATH GENERATED BY THE COUPLER MID-POINT.....	165
8.4 NATURAL FREQUENCIES AND MODE SHAPES AT STATIC CONFIGURATIONS	169
8.5 MECHANISM RUNNING AT HIGH SPEED	184
8.5.1. Effect of L_4	185
8.5.2. Effect of L_2	189
8.6 CONCLUSION.....	190
Chapter 9: CONCLUSIONS AND SUGGESTIONS FOR FURTHER WORK	192
9.1 CONCLUSIONS	192
9.2 FURTHER WORK.....	195
REFERENCES.....	199
Appendix A: MATRIX ELEMENTS FOR THE p-VERSION	209
A.1. BEAM ELEMENT WITH 1 INTERNAL NODE.....	209
A.2. BEAM ELEMENT WITH CURVATURES	211
Appendix B: FREQUENCY FUNCTIONS F_1 and G_1	213
Appendix C: EXPERIMENTAL RESULTS FOR $L_2=0.328$ m	215
Appendix D: EXPERIMENTAL RESULTS FOR $L_2=0.636$ m.....	239
Appendix E: STABILITY REGIONS OF MATHIEU'S EQUATION	265

LIST OF FIGURES

Fig. 3.1: Schematic of the four-bar mechanism	42
Fig. 3.2: Two extreme cases of the transmission angle.....	44
Fig. 3.3: Locking toggle plier.....	45
Fig. 3.4: Zero mobility plane and base plane.....	47
Fig. 3.5: Base plane for typical values of λ	49
Fig. 3.6: The two mechanisms solution for a given input angle.	51
Fig. 3.7: Relative angular velocity of the coupler and the follower.....	53
Fig. 3.8: Relative angular accelerations of the coupler and the follower.....	53
Fig. 3.9: Transmission angle versus input angle.....	54
Fig. 3.10: Path generated by some points on the coupler.....	55
Fig. 3.11.a: Free-body diagramme of the input link	56
Fig. 3.11.b: Free-body diagramme of the coupler.....	56
Fig. 3.11.c: Free-body diagramme of the follower	56
Fig. 4.1: Mechanism at a given position	63
Fig. 4.2: Beam element with its nodal coordinates	64
Fig. 4.3: elemental mass displacement in local and global coordinate system	69
Fig. 4.4: transformation between local and reference coordinate system	72
Fig. 4.5: Four bar mechanism modelled with 1 element per link	75
Fig. 4.6.a: First natural frequency	82
Fig. 4.6.b: Second natural frequency	82
Fig. 4.6.c: Third natural frequency.....	83
Fig. 4.6.d: Fourth natural frequency.....	83
Fig. 4.7: Nodal coordinates in the p-version of the FEM.....	84
Fig. 5.1: eigenvalues of D for one and two element/bar models.....	99
Fig. 5.2: Schematic of square portal frame and its data	100
Fig. 5.3.a: First natural frequency	108
Fig. 5.3.b: Second natural frequency	108
Fig. 5.3.c: Third natural frequency.....	109
Fig. 5.3.d: Fourth natural frequency.....	109
Fig. 6.1: Limits of stability of Newmark method	118
Fig. 6.2: Form of the equation system obtained by Xiaochun <i>et al.</i> (1988).....	120
Fig. 6.3.a: Displacement of the coupler midpoint for $\omega = 35$ rad/s and $\zeta = 0.02$. 122	
Fig. 6.3.b: Displacement of the follower midpoint for $\omega = 35$ rad/s and $\zeta = 0.02$. 123	
Fig. 6.4.a: Contributions of different modes to the global deflection at the coupler mid-point for $\omega = 35$ rad/s and $\zeta = 0.02$	123
Fig. 6.4.b: Contributions of different modes to the global deflection at the follower mid-point for $\omega = 35$ rad/s and $\zeta = 0.02$	124
Fig. 6.5: Convergence of the deflection at the midpoint of the follower at $\omega = 62$ rad/s	134
Fig. 6.6: Comparison of the number of flops between different algorithms.....	135
Fig 7.1: Local maxima of stress and the real part of the maximum eigenvalue of the transition matrix.....	144
Fig. 7.2: Instability regions corresponding to $J_2 = \pm 1$	147
Fig. 7.3: Comparison between the functions J and the real part of one of the eigenvalues of the monodromy matrix.....	148

Fig. 7.4: Predicted response of follower midpoint.....	151
Fig. 7.5: Predicted maximum stress on the input link.....	151
Fig. 7.6: Predicted strain energy of the system	151
Fig. 7.7: Maximum stress for a damping ratio of 0.01	153
Fig. 7.8: Influence of the number of elements	154
Fig. 7.9: Stress at the follower midpoint for different models at $\omega = 30$ rad/s	155
Fig. 7.10: Maximum stress versus speed for a damping ratio of 0.03	156
Fig. 7.11: Maximum stress versus speed for a damping ratio of 0.06	156
Fig. 7.12: Acceleration of the follower for various transmission angles	159
Fig. 7.13: Response of the follower for various transmission angles	160
Fig. 8.1: Photograph of the test-rig	164
Fig. 8.2.a: Path generated at a low speed	167
Fig. 8.2.b: Path generated at higher speed	168
Fig. 8.3: Comparison between the paths generated experimentally and theoretically.....	168
Fig. 8.4: Comparison between the path generated experimentally at a low speed and at a higher speed.....	169
Fig. 8.5: Experimental modal analysis using a hammer and an accelerometer	170
Fig. 8.6: Modules of SMS-STAR package	172
Fig. 8.7: Wire frame representation of the mechanism at $t_1 = 0^\circ$	172
Fig. 8.8: FRF corresponding to the accelerometer at the midpoint of the follower.	173
Fig. 8.9: Mode shapes and frequencies for $t_1 = 0^\circ$	174
Fig. 8.10: Mode shapes and frequencies for $t_1 = 36^\circ$	175
Fig. 8.11: Mode shapes and frequencies for $t_1 = 72^\circ$	176
Fig. 8.12: Mode shapes and frequencies for $t_1 = 108^\circ$	177
Fig. 8.13: Mode shapes and frequencies for $t_1 = 144^\circ$	178
Fig. 8.14: Mode shapes and frequencies for $t_1 = 180^\circ$	179
Fig. 8.15: Mode shapes and frequencies for $t_1 = 216^\circ$	180
Fig. 8.16: Mode shapes and frequencies for $t_1 = 252^\circ$	181
Fig. 8.17: Mode shapes and frequencies for $t_1 = 288^\circ$	182
Fig. 8.18: Mode shapes and frequencies for $t_1 = 316^\circ$	183
Fig. 8.19: Maximum stress at follower midpoint for $L_4 = 0.547$ m.	184
Fig. 8.20: Maximum stress at follower midpoint for $L_4 = 0.632$ m.	186
Fig. 8.21: Maximum stress at follower midpoint for $L_4 = 0.642$ m.	187
Fig. 8.22: Maximum stress at follower midpoint for $L_4 = 0.652$ m.	187
Fig. 8.23: Maximum stress at follower midpoint for $L_4 = 0.662$ m.	188
Fig. 8.24: Stress at the midpoint of the follower for $\omega = 17$ rad/s and $L_4 = 0.662$ m	189
Fig. 8.25: Maximum stress at coupler midpoint for $L_2 = 0.636$ m.....	190
Fig. 8.26: Maximum stress at follower midpoint for $L_2 = 0.636$ m.	190
Fig. 9.1: Variation of natural frequencies with L_2	197
Fig. C.1.a: Stress at the input link midpoint for $\omega = 7.11$ rad/s	215
Fig. C.1.b: Stress at the coupler midpoint for $\omega = 7.11$ rad/s	215
Fig. C.1.c: Stress at the follower midpoint for $\omega = 7.11$ rad/s	215
Fig. C.2.a: Stress at the input link midpoint for $\omega = 9.71$ rad/s	216
Fig. C.2.b: Stress at the coupler midpoint for $\omega = 9.71$ rad/s	216
Fig. C.2.c: Stress at the follower midpoint for $\omega = 9.71$ rad/s	216

Fig. C.3.a: Stress at the input link midpoint for $\omega = 11.1$ rad/s	217
Fig. C.3.b: Stress at the coupler midpoint for $\omega = 11.1$ rad/s	217
Fig. C.3.c: Stress at the follower midpoint for $\omega = 11.1$ rad/s	217
Fig. C.4.a: Stress at the input link midpoint for $\omega = 13.43$ rad/s	218
Fig. C.4.b: Stress at the coupler midpoint for $\omega = 13.43$ rad/s	218
Fig. C.4.c: Stress at the follower midpoint for $\omega = 13.43$ rad/s	218
Fig. C.5.a: Stress at the input link midpoint for $\omega = 15.44$ rad/s	219
Fig. C.5.b: Stress at the coupler midpoint for $\omega = 15.44$ rad/s	219
Fig. C.5.c: Stress at the follower midpoint for $\omega = 15.44$ rad/s	219
Fig. C.6.a: Stress at the input link midpoint for $\omega = 16.28$ rad/s	220
Fig. C.6.b: Stress at the coupler midpoint for $\omega = 16.28$ rad/s	220
Fig. C.6.c: Stress at the follower midpoint for $\omega = 16.28$ rad/s	220
Fig. C.7.a: Stress at the input link midpoint for $\omega = 16.71$ rad/s	221
Fig. C.7.b: Stress at the coupler midpoint for $\omega = 16.71$ rad/s	221
Fig. C.7.c: Stress at the follower midpoint for $\omega = 16.71$ rad/s	221
Fig. C.8.a: Stress at the input link midpoint for $\omega = 17.7$ rad/s	222
Fig. C.8.b: Stress at the coupler midpoint for $\omega = 17.7$ rad/s	222
Fig. C.8.c: Stress at the follower midpoint for $\omega = 17.7$ rad/s	222
Fig. C.9.a: Stress at the input link midpoint for $\omega = 18.27$ rad/s	223
Fig. C.9.b: Stress at the coupler midpoint for $\omega = 18.27$ rad/s	223
Fig. C.9.c: Stress at the follower midpoint for $\omega = 18.27$ rad/s	223
Fig. C.10.a: Stress at the input link midpoint for $\omega = 20.07$ rad/s	224
Fig. C.10.b: Stress at the coupler midpoint for $\omega = 20.07$ rad/s	224
Fig. C.10.c: Stress at the follower midpoint for $\omega = 20.07$ rad/s	224
Fig. C.11.a: Stress at the input link midpoint for $\omega = 20.40$ rad/s	225
Fig. C.11.b: Stress at the coupler midpoint for $\omega = 20.40$ rad/s	225
Fig. C.11.c: Stress at the follower midpoint for $\omega = 20.40$ rad/s	225
Fig. C.12.a: Stress at the input link midpoint for $\omega = 21.01$ rad/s	226
Fig. C.12.b: Stress at the coupler midpoint for $\omega = 21.01$ rad/s	226
Fig. C.12.c: Stress at the follower midpoint for $\omega = 21.01$ rad/s	226
Fig. C.13.a: Stress at the input link midpoint for $\omega = 21.08$ rad/s	227
Fig. C.13.b: Stress at the coupler midpoint for $\omega = 21.08$ rad/s	227
Fig. C.13.c: Stress at the follower midpoint for $\omega = 21.08$ rad/s	227
Fig. C.14.a: Stress at the input link midpoint for $\omega = 21.89$ rad/s	228
Fig. C.14.b: Stress at the coupler midpoint for $\omega = 21.89$ rad/s	228
Fig. C.14.c: Stress at the follower midpoint for $\omega = 21.89$ rad/s	228
Fig. C.15.a: Stress at the input link midpoint for $\omega = 22.52$ rad/s	229
Fig. C.15.b: Stress at the coupler midpoint for $\omega = 22.52$ rad/s	229
Fig. C.15.c: Stress at the follower midpoint for $\omega = 22.52$ rad/s	229
Fig. C.16.a: Stress at the input link midpoint for $\omega = 22.60$ rad/s	230
Fig. C.16.b: Stress at the coupler midpoint for $\omega = 22.60$ rad/s	230
Fig. C.16.c: Stress at the follower midpoint for $\omega = 22.60$ rad/s	230
Fig. C.17.a: Stress at the input link midpoint for $\omega = 23.44$ rad/s	231
Fig. C.17.b: Stress at the coupler midpoint for $\omega = 23.44$ rad/s	231
Fig. C.17.c: Stress at the follower midpoint for $\omega = 23.44$ rad/s	231
Fig. C.18.a: Stress at the input link midpoint for $\omega = 24.35$ rad/s	232
Fig. C.18.b: Stress at the coupler midpoint for $\omega = 24.35$ rad/s	232
Fig. C.18.c: Stress at the follower midpoint for $\omega = 24.35$ rad/s	232

Fig. C.19.a: Stress at the input link midpoint for $\omega = 25.96$ rad/s	233
Fig. C.19.b: Stress at the coupler midpoint for $\omega = 25.96$ rad/s	233
Fig. C.19.c: Stress at the follower midpoint for $\omega = 25.96$ rad/s	233
Fig. C.20.a: Stress at the input link midpoint for $\omega = 27.32$ rad/s	234
Fig. C.20.b: Stress at the coupler midpoint for $\omega = 27.32$ rad/s	234
Fig. C.20.c: Stress at the follower midpoint for $\omega = 27.32$ rad/s	234
Fig. C.21.a: Stress at the input link midpoint for $\omega = 29.09$ rad/s	235
Fig. C.21.b: Stress at the coupler midpoint for $\omega = 29.09$ rad/s	235
Fig. C.21.c: Stress at the follower midpoint for $\omega = 29.09$ rad/s	235
Fig. C.22.a: Stress at the input link midpoint for $\omega = 30.21$ rad/s	236
Fig. C.22.b: Stress at the coupler midpoint for $\omega = 30.21$ rad/s	236
Fig. C.22.c: Stress at the follower midpoint for $\omega = 30.21$ rad/s	236
Fig. C.23.a: Stress at the input link midpoint for $\omega = 31.42$ rad/s	237
Fig. C.23.b: Stress at the coupler midpoint for $\omega = 31.42$ rad/s	237
Fig. C.23.c: Stress at the follower midpoint for $\omega = 31.42$ rad/s	237
Fig. C.24.a: Stress at the input link midpoint for $\omega = 35.30$ rad/s	238
Fig. C.24.b: Stress at the coupler midpoint for $\omega = 35.30$ rad/s	238
Fig. C.24.c: Stress at the follower midpoint for $\omega = 35.30$ rad/s	238
Fig. D.1.a: Stress at the input link midpoint for $\omega = 6.84$ rad/s	239
Fig. D.1.b: Stress at the coupler midpoint for $\omega = 6.84$ rad/s	239
Fig. D.1.c: Stress at the follower midpoint for $\omega = 6.84$ rad/s	239
Fig. D.2.a: Stress at the input link midpoint for $\omega = 7.86$ rad/s	240
Fig. D.2.b: Stress at the coupler midpoint for $\omega = 7.86$ rad/s	240
Fig. D.2.c: Stress at the follower midpoint for $\omega = 7.86$ rad/s	240
Fig. D.3.a: Stress at the input link midpoint for $\omega = 9.11$ rad/s	241
Fig. D.3.b: Stress at the coupler midpoint for $\omega = 9.11$ rad/s	241
Fig. D.3.c: Stress at the follower midpoint for $\omega = 9.11$ rad/s	241
Fig. D.4.a: Stress at the input link midpoint for $\omega = 9.68$ rad/s	242
Fig. D.4.b: Stress at the coupler midpoint for $\omega = 9.68$ rad/s	242
Fig. D.4.c: Stress at the follower midpoint for $\omega = 9.68$ rad/s	242
Fig. D.5.a: Stress at the input link midpoint for $\omega = 10.23$ rad/s	243
Fig. D.5.b: Stress at the coupler midpoint for $\omega = 10.23$ rad/s	243
Fig. D.5.c: Stress at the follower midpoint for $\omega = 10.23$ rad/s	243
Fig. D.6.a: Stress at the input link midpoint for $\omega = 11.38$ rad/s	244
Fig. D.6.b: Stress at the coupler midpoint for $\omega = 11.38$ rad/s	244
Fig. D.6.c: Stress at the follower midpoint for $\omega = 11.38$ rad/s	244
Fig. D.7.a: Stress at the input link midpoint for $\omega = 11.90$ rad/s	245
Fig. D.7.b: Stress at the coupler midpoint for $\omega = 11.90$ rad/s	245
Fig. D.7.c: Stress at the follower midpoint for $\omega = 11.90$ rad/s	245
Fig. D.8.a: Stress at the input link midpoint for $\omega = 12.44$ rad/s	246
Fig. D.8.b: Stress at the coupler midpoint for $\omega = 12.44$ rad/s	246
Fig. D.8.c: Stress at the follower midpoint for $\omega = 12.44$ rad/s	246
Fig. D.9.a: Stress at the input link midpoint for $\omega = 13.40$ rad/s	247
Fig. D.9.b: Stress at the coupler midpoint for $\omega = 13.40$ rad/s	247
Fig. D.9.c: Stress at the follower midpoint for $\omega = 13.40$ rad/s	247
Fig. D.10.a: Stress at the input link midpoint for $\omega = 14.28$ rad/s	248
Fig. D.10.b: Stress at the coupler midpoint for $\omega = 14.28$ rad/s	248
Fig. D.10.c: Stress at the follower midpoint for $\omega = 14.28$ rad/s	248

Fig. E.1: Variation of the first eigenvalue of the monodromy matrix versus d and ϵ	265
Fig. E.2: Variation of the second eigenvalue of the monodromy matrix versus d and ϵ	266
Fig. E.3: Stability chart in (d, ϵ) space.	267

LIST OF TABLES

Table 3.1: Classification of four-bar mechanisms by Barker (1985).....	48
Table 3.2: Characteristics of the mechanism.	53
Table 4.1: Mechanism data	81
Table 5.1.a: Natural frequencies of portal frame	101
Table 5.1.b: Relative error in %	101
Table 6.1 Number of Flops for different algorithms.....	132
Table 6.2 Comparison of number of flops between different algorithms	133
Table 6.3 Comparison between algorithm 1 and the Fourier Series analysis	133
Table 8.1 Dimensions of the mechanism	163

Chapter 1

INTRODUCTION

1.1. INTRODUCTION

Reuleaux (1875), a German kinematician, defined a machine as "a combination of resistant bodies so arranged that by their means the mechanical forces of nature can be compelled to do work accompanied by certain determinate motions". Further, he defined a mechanism as "an assemblage of resistant bodies, connected by movable joints, to form a closed kinematic chain with one link fixed and having the purpose of transforming motion". For the 90 years which followed, this definition has been the core of almost all investigations of the dynamics of mechanisms. Stresses in the members were assumed to be only due to inertia and external forces. Based on these stress calculations, the mechanism was designed, built and tested. As mechanisms were made of relatively stiff components and the running speed was relatively low and quite below their fundamental frequency, the assumptions that mechanisms parts behave as rigid bodies have not been challenged.

The competition in the international marketplace prompted the development of machines and mechanisms which run at even higher speeds. However, the higher operating speeds generated larger inertial forces and the mechanism members suffered considerable deformation. Under these circumstances the rigid body assumption was no longer valid. A new approach was needed where the members were allowed to deflect when loaded. A new discipline was born: the elastodynamic analysis of mechanisms.

When the operational speed increases, inertia forces, being proportional to the square of the speed, could rise drastically. Hence the need for light-mass links in applications involving high speeds. This brought about a new challenge for the designer. The flexibility of such links increased and high precision motion could no longer be guaranteed. In applications where high-precision is required, mechanisms such as robot manipulators are made very stiff which means with high inertia if the components are made of commercial materials such as steel. This limits their use to relatively low operating speeds due to the torques and forces required for their operation. The other alternative is to use high stiffness-to-density ratio materials such as fibre-reinforced composite materials.

1.2. AIM OF THIS RESEARCH

The purpose of this research is to model a flexible four-bar mechanism running at high-speed. The model used was derived from the finite element method (FEM). The main objectives of the study are outlined in the following:

- 1- In the FEM the accuracy of the solution increases with the number of elements used to model the system. However, this leads to a bigger equation system and the central processing unit (CPU) time required for the solution to converge becomes a limiting factor. Hence, the first objective of this study is to develop an efficient model with the minimum number of elements per link.
- 2- The literature review shows that there is a lack of algorithms to yield the steady-state solution of the mechanism quickly and efficiently. The few algorithms which exist all suffer from some defects. The situation should be addressed by developing new algorithms to calculate the steady-state solution of the mechanism running at high-speed.

3- When the mechanism is running at high-speed, the stresses in the links exhibit a series of local maxima with respect to speed. The speeds at which the stresses are bigger than at neighbouring speeds are called critical speeds and, in the past, they have been found theoretically and verified experimentally. Some of these critical speeds, called here *limiting* critical speeds, cannot be exceeded because the stress in one or more of the linkages will exceed the safe working stress. However, above some limiting critical speeds there may be a safe speed band, or quiet speed band, where the mechanism could be run without the mechanism being over stressed. The problem of running the mechanism over some limiting critical speeds is addressed in this study.

4- The localisation of the critical speeds of a mechanism is an important issue for the designer. If such information is not available, the designer would have to run a costly simulation at different speeds with small step size in the range of speeds for which the mechanism was designed. The result of this simulation would be a graph of the maximum stresses endured by the linkages against speed. Once this achieved, the designer would locate the critical speeds, determine which link suffers most and finally locate the first limiting critical speed. One of the purposes of this study is to develop a simple method to locate the critical speeds of the mechanism. Once this information is made available, the designer would run the simulation at only a limited number of speeds thus saving valuable CPU time.

5- The experimental work aims mainly at verifying the theoretical findings. Broadly it can be divided into two parts. The first part deals with the mechanism as a structure at static configurations and in the second part, the mechanism is run at different speeds.

1.3. OUTLINE OF THE THESIS

This thesis is organised into nine chapters. The present chapter serves as an introduction to the subject and outlines the overall research programme. The rest of the chapters are as follows:

Chapter 2 critically reviews the literature relevant to the subject being investigated. Since there are different aspects to the subject, the review is not limited to papers on the elastodynamics of four-bar mechanisms.

Chapter 3 deals with the kineto-dynamic analysis of the four-bar mechanism. In this part the links are assumed to be rigid. First, kinematic characteristics, such as velocities and accelerations, are derived. The effect of the transmission angle on these characteristics is discussed. The inertia forces and the torque required to drive the mechanism are presented. Speed is assumed constant and the only forces being applied to the mechanism are inertia forces. Finally, a classification of four-bar mechanisms is given with the help of the solution space concept.

Chapter 4 gives a detailed presentation of the application of the FEM to the analysis of the four-bar mechanism. The links of the mechanism are modelled as beam elements in axial and bending vibration modes. The equations of motion are obtained by means of Hamilton's principle. In the derivation of these equations, the effects of the rigid-body motion on the elastic deflections are included. Also the stiffening effect is discussed. The two versions of the FEM are considered, namely the h-version and the p-version.

The dynamic stiffness method is described and developed in Chapter 5. The expressions of the system matrices are derived in terms of transcendental functions which are frequency-dependent. The advantage of this method over the conventional

FEM is that the interpolation functions are based on the exact solution of the differential equation governing the vibration of a beam in the mode considered (bending or axial). Therefore very accurate natural frequencies and mode shapes are determined and the accuracy does not depend on the number of "elements" used. However, this method leads to a non-linear eigenvalue problem and the classical algorithms are not suitable to solve the problem. A special algorithm is discussed. The dynamic stiffness method is compared to the conventional FEM for two cases: a portal frame and the four-bar mechanism.

The solution of the equations of motion is developed in Chapter 6. An overview of the existing methods to calculate the steady-state solution is discussed. Two new algorithms are derived to overcome the shortcomings of the existing algorithms.

Chapter 7 deals with the critical speeds of a four-bar mechanism and it proposes a method to run the mechanism above several of these. The stability of the system is investigated using Floquet theory from which the monodromy matrix (called also the transition matrix) is defined. The critical speeds are related to the maximum of the real part of the eigenvalue of the monodromy matrix. The effect of the distance between the ground pivots of the mechanism on the maximum stresses is also investigated. The notion that increasing the damping to reduce stresses so that the mechanism could be run at a maximum higher speed is discussed. Finally a proposed design method is derived.

The experimental work is presented in Chapter 8. First a practical method is given for measuring the generated path by any point of the coupler. Modal characteristics of the mechanism at static configurations are presented. Then, the mechanism is run at different constant speeds and different distances between the ground pivots. The experimentally obtained stresses are compared to the model. The effect of the transmission angle on the maximum stresses is also shown. The transmission angle

is defined as the angle between the follower and the coupler, the performance of the mechanism depends very much on it.

Chapter 9 draws the conclusions and provides some recommendations for further research in this area.

Chapter 2

LITERATURE REVIEW

2.1. INTRODUCTION

Since the dawn of civilisation, man invented many mechanisms and basic machines to carry out simple operations in his struggle for survival. The machines were operated by either human or animal power. After the industrial revolution and the invention of the steam engine, a new source of energy became available. This prompted the invention of many new mechanisms and machines to respond to the increasing demand of the expanding industry for increase of production. Initially, mechanisms and machine theory was random in growth characterised by inventions and the establishment of a basic form of machines rather than by design and development. Steadily a theory emerged where the analysis and synthesis of mechanisms were based on principles of physics, kinematics and dynamics assuming that mechanism elements were rigid.

However, as a consequence of the need for increased productivity, mechanisms were run at ever higher speeds. The design engineers were faced with a dilemma, on one hand to increase productivity, the machines had to be operated at higher speeds which generated new problems not encountered when mechanisms run at lower speeds, such as noise radiation, early failure due to fatigue and vibration excess. On the other hand the precision requirements meant that the body parts of the machine have to be stiff, which meant more power was needed to operate these machines. Therefore the problem they were facing was how to run machines at higher speeds with a lower power consumption. New methods to understand the elastic behaviour

of mechanisms were needed. The assumptions that machine parts are rigid can no longer be made since they do deflect when the speed is high enough.

This chapter deals with the literature review relevant to high-speed flexible mechanisms and the four-bar mechanism in particular. There have been many survey papers published in the past. Erdman and Sandor (1972), and Lowen and Jandarists (1972) published one of the pioneer research surveys in this field. As computers became more and more powerful and accessible, less assumptions were made. Erdman and Sandor (1972) rightly reported that many simplifying assumptions made in order to yield solvable equations tend unfortunately to make the model and solution unrealistic. For example, at the beginning only one of the linkages of the four-bar mechanism was assumed flexible. An analytical solution was derived after many simplifications and assumptions. As the system became more difficult to solve, the use of numerical techniques was inevitable. Two widely used approaches exist. These are the lumped parameter approach and the Finite Element Method. The FE theory of structural analysis has been applied to the modelling of an elastic linkage using both the force (flexibility) method (Erdman *et al.*, 1972) as well as displacement (stiffness) method (Winfrey 1971, 1972). However, in general the stiffness matrix approach is more popular among researchers, as it is in many fields of structural design, than the flexibility method in the analysis of high-speed mechanisms.

Two of the most recent reviews in the area of dynamics of flexible mechanisms have been presented by Lowen and Chassapis (1986) and Thompson and Sung (1986c). In the first one, the reviewed publications have been grouped according to their basic premises: analytical methods, FE methods, optimisation schemes and general experimentation. Where appropriate, each of these categories was subjected to a further division of topics in order to be able to differentiate between publications which deal with vibration responses, quasi-static deflections or stability.

Throughout, special attention was paid to the derivation of the governing equations of motion, the methods of their solutions and, when possible, to the correlation of numerical results with experimental ones. In the second review paper, limited exclusively to the FE method, the authors presented a complete list of references on FEM for the design of planar mechanisms. In the latter paper, the literature was reviewed, by highlighting the phenomena being studied, the design function being undertaken and the different aspects of FE analyses such as element selection, formulation strategy and procedure employed to solve the equations of motion. Peng and Liou (1992), later presented a comprehensive study of the experimental studies achieved on flexible mechanisms. The authors carried out the investigation from a designer point of view. They started by exposing the parameters which affect the dynamic response of a flexible mechanism. They then discussed the common assumptions made in the analysis of such systems together with the experimental works whenever available to prove or disprove the assumptions. The subjects treated included the variation of stress along the cycle, the effect of non-linear terms, critical speeds, damping measurements, experimental set-up, etc. The authors concluded their review by suggesting more experimental work should be done in order to shed some light on the discrepancies between the model and the experimental results.

2.2. FINITE ELEMENT METHOD

One of the characteristics of the FEM is its ability to represent a continuous system which theoretically has an infinite number of degrees of freedom, by an approximate multi-degree of freedom system. Hence, it provides an easy and systematic technique for modelling complex structures and in particular it lays the groundwork for a general approach to the modelling of elastic mechanisms. As the size of the problem becomes bigger, the computational difficulty and the cost rise. This is where approximations in the methods of solution to reduce the computation time are

most needed. In the case of four-bar mechanisms the basic set of equations at any instant of time during the cycle is of low order; this is because the number of elements needed for the solution to converge is quite low. However, solving the system of equations corresponding to the steady-state solution can still be a time- or resource-consuming process. This problem is discussed later in more detail in chapter 6.

Winfrey (1971) was the first to apply FEM to analyse planar and spatial mechanisms with elastic links. It was shown that the FE solutions could systematically and easily be obtained as some or all of the links were considered to be elastic. Erdman *et al.* (1972) proposed a general method for kineto-elastodynamic analyses based on the flexibility approach of structural analysis. Bahgat and Willmert (1976) developed a computer program to analyse a variety of different planar elastic mechanisms with turning and sliding pairs. Their technique was based upon the FEM and utilised beam-type elements with four coordinates per node: 2 translations, 1 rotation and 1 curvature. In consequence, the shape functions chosen are high order polynomials of order 5; both transverse and longitudinal effects were taken into account.

There are two beam theories on which the FE models have been based, namely Euler-Bernoulli and Timoshenko theory. In the former, a plane section is assumed to remain plane and normal to the neutral axis after deformation. The Euler-Bernoulli theory is therefore limited to slender beams vibrating at lower modes. In order to model thick beams or a beams in higher modes, Timoshenko beam theory must be invoked since it accounts for the shear deformation and the rotatory inertia. Gamache and Thompson (1981) presented a comparative study of both theories applied to a four-bar mechanism. The first comparison concerned the effect of the number of elements used to model a beam on the accuracy of the maximum deflection. It was found that for slender links modelled with 1 element per link the error was 26.9% for the follower and 80.8% for the coupler when Euler-Bernoulli

beam theory was used. These errors dropped to 8.1% for the follower and 12.9% for the coupler when a model of 4 elements per link was used. When Timoshenko theory was used, the errors were 17.2% and 80.7% for 1 element per link and 0.95% and 10.9% for 4 elements per link. The errors were calculated with respect to a model of 10 elements per link. Gamache and Thompson also indicated that a two element model was adequate to represent the response of the follower but was inaccurate for the coupler. No explanation for this was given. The second comparison was made between the two theories for the same number of elements in the model. A small error was found between the two as was expected since the links were vibrating mainly in the first mode where the difference between the two theories is known to be negligible. Finally, link members with large thickness over length ratios were analysed. The authors demonstrated that Euler-Bernoulli theory predicts slightly larger deflections than Timoshenko theory for slender links, and for realistically proportioned linkages, Timoshenko model should be used.

2.2.1. Equations of motion

There are many ways of developing the equations of motion. The difference between the different methods used is purely procedural, they all lead to the same equations. Lagrange's equations are a popular choice among researchers (Bahgat and Willmert, 1976; Midha *et al.*, 1978; Nath and Ghosh, 1980; Cleghorn *et al.*, 1981; Turcic and Midha, 1984a; Chang and Chen, 1987; Nagarajan and Turcic, 1990a, 1990b). This is due to the ease and the systematic way with which the equations of motion can be established; the kinetic and potential energy are expressed in terms of a set of generalised coordinates (in this case the displacements and rotations at the nodes of the FE model). Then the equations of motion are derived from a set of equations relating the kinetic and potential energy to the generalised forces. Another approach favoured by others is a variational formulation (Thompson and Barr, 1975; Sung and Thompson, 1982; Thompson *et al.*, 1983; Thompson and Sung, 1984, 1986a). This

formulation consists of expressing the field equations and the boundary equations as a functional. The vanishing of the first variation of this provides the equations of motion. Any special relation between the coordinates is taken into account in the functional through Lagrange multipliers. Finally, some researchers established the equations of motion by means of the virtual work principle (Liou and Erdman, 1989). When a body is in equilibrium state and subjected to any compatible virtual displacement, the total external virtual work must be compensated by the total internal virtual work. As was mentioned earlier, the difference between the different methods is purely procedural; for example, and in general, Hamilton's principle is an integral form of the principle of virtual work. Also, Lagrange's equations can be derived from Hamilton's principle.

The equations of motion are developed for each link in the local coordinate system. The element matrices are then transformed into a global coordinate system common to all links. In order to obtain the global equations of motion, compatibility of displacements at nodes shared by two elements is considered. The global equations of motion take the form:

$$\mathbf{M}\ddot{\mathbf{q}} + (\mathbf{M}_c + \mathbf{C})\dot{\mathbf{q}} + (\mathbf{K} + \mathbf{M}_a)\mathbf{q} = \mathbf{p} - \mathbf{M}\ddot{\mathbf{q}}_r \quad (2.1)$$

where: \mathbf{M} , \mathbf{K} and \mathbf{C} are the mass, stiffness and the damping matrix,

\mathbf{M}_c the mass matrix associated with Coriolis effect,

\mathbf{M}_a the mass matrix due to normal and tangential accelerations,

\mathbf{p} is the external forces vector applied at the nodes

\mathbf{q} is the elastic deflections vector

\mathbf{q}_r : the displacements vector due to the rigid-body motion.

The dots denote differentiation with respect to time.

When the equations of motion are solved for the global displacements, the other characteristics such as stresses and strains could be obtained from the strain-displacement relationship and by Hooke's law. Many researchers neglected the effect of Coriolis, normal and tangential accelerations (Winfrey, 1971; Alexander and Lawrence, 1974; Midha *et al.*, 1978; Chang and Chen, 1987). This is referred to as the instantaneous structure formulation, the mechanism while rotating is considered as a series of structures upon which are applied the inertial forces and any other external forces. During the assemblage process of the matrices the rigid body degrees of freedom should be eliminated. This is because the stiffness matrix for a system which admits a rigid body motion is singular. The commonly made assumption is to consider the input link as a cantilever beam (Midha *et al.*, 1978; Cleghorn *et al.*, 1981). This suppresses any possible rigid body motion of the whole mechanism and therefore the stiffness matrix is no longer singular. The assumption is quite valid when the input link is attached to a large flywheel, which is the case in most papers investigating the elastodynamic of four-bar mechanisms. Others simply assumed that the input link was rigid (Sung and Thompson, 1982, 1984; Sung *et al.*, 1986). Winfrey (1971) took a different approach. He applied the principle of conservation of momentum to the whole mechanism.

2.2.2 Solution of the equations of motion

There are two aspects to the solution of the equations of motion. The first aspect deals with the solution of the basic differential equations during one step size. The second concerns the establishment of the steady-state solution. For the solution of the basic equation, the Newmark method is the most widely used because of its simplicity and, more importantly, for certain values of the method's parameters it provides an unconditionally stable solution. The Newmark method has gained widespread use in other areas of FE analysis and many commercial FE codes use it in their solution. ANSYS and PAFEC are just two examples. Another reason for the

popularity of this method is that the equations of motion in dealing with flexible mechanisms are stiff; methods such as Runge-Kutta would require a very small step size. The literature search reveals that much effort has been put in the establishment of the equations of motion in order to model the system accurately. Surprisingly, this effort has not been matched by a similar effort to solve these equations to yield the steady-state solution. There are many methods by which one can obtain the steady-state solution, the most straightforward one being time marching simulation. In this method the simulation is started from an arbitrary initial condition (usually from zero state vector). The transient associated with the initial conditions dies away naturally for stable systems, leaving the steady-state solution after a certain number of cycles. Yang and Sadler (1990) suggested to start the simulation from zero displacement and non-zero velocity conditions to accelerate the convergence. Alternatively, artificial damping could be added to damp out the transient response quickly. This damping decreases exponentially with time so that after a few cycles, its effect vanishes completely. Researchers who used time marching simulation in their analysis are, for example, Midha *et al.* (1979), Liou and Erdman (1989). Convergence to the steady-state solution can be very slow indeed for some input speeds, especially those near one of the critical speeds, or in general when there is relatively low damping in the system. In fact, if the effect of the damping is not taken into account in the model, the solution never converges. Sung and Thompson (1984) for example neglected the damping effect and were forced to assume that the steady-state solution was obtained just after the first cycle. This could be very misleading indeed as the solution could change drastically over the cycles.

Some methods inherently provide the steady-state solution. One of these methods uses the property that the steady-state vector, as well as the system matrices, are time periodic for a constant operational speed. The system matrices, the force vector and the state vector are developed into truncated Fourier series, then substituted into the equations of motion and the coefficients corresponding to the same harmonic terms

are equated. The system obtained is a large linear algebraic system which can be solved easily using the Gaussian elimination technique for example. The main advantage of this approach is that the time taken to obtain the steady-state solution is not affected by the rotational speed nor by the damping present in the system. Against this, however, is that (i) only the steady-state solution is obtained, the method does not allow the calculation of the transient response of the system; and (ii) the system can become extremely large depending on the number of terms in the truncated series and the number of degrees of freedom in the system. Cleghorn *et al.* (1984) suggested using 11 terms for the system matrices and 23 terms for the unknown displacements. Bahgat and Willmert (1976) used a similar approach. However, the solutions obtained corresponded only to the quasi-static response which could have been obtained by simpler means with less computation requirement. This came about because in their development the mass, stiffness and the damping matrices were not expressed as truncated Fourier series, only the forcing terms and the displacements were. A numerical problem arose using this method. The derived expressions contained the term $(\mathbf{K} - j^2\omega^2\mathbf{M})^{-1}$, where j is an integer used as an index of summation in the truncated Fourier series, ω is the rotational speed and \mathbf{M} and \mathbf{K} are the mass and stiffness matrices. The natural frequencies of the system depend on the input angle of the mechanism. It is possible that one or more of the eigenvalues of \mathbf{K} and \mathbf{M} will attain the value $j^2\omega^2$ somewhere in the cycle. When this is the case the expression above becomes indeterminate and there is no solution for the deflections. This problem can happen for any mechanism, even if the links are stiff. In the latter case this only happens for large values of j . Nath and Ghosh (1980a) employed different harmonic analysis. The truncated Fourier series were introduced at the element level before the assemblage process. The boundary conditions at the joints were introduced in the form of a set of compatibility equations. An elimination of these constraints in the end leads to a non-banded matrix in the final system. This disadvantage could have been avoided if

the system matrices and vectors were developed once the assemblage process had been achieved. In this case the system obtained is banded.

An approach to the solution of differential equations with time periodic coefficients, which resulted from analysis of elastic mechanisms, has been presented by Midha *et al.* (1979). The closed form numerical algorithm they developed is capable of calculating both the transient and steady-state response of any linear second order differential equations with time periodic coefficients. The numerical algorithm is based upon dividing the fundamental time period into discrete time sub-intervals; during each subinterval, the time-dependent coefficients are assumed to be constant. Modal analysis was carried out to uncouple the set of equations and each mode was then considered separately. The basic equations are then solved analytically during each sub-interval. Constraint equations, which require both displacement and velocity continuity, are applied at the boundaries of each time sub-interval. The algebraic set of constraint equations are then solved using Gaussian elimination technique. The equation system obtained is a large sparse system, except for two leading diagonals and the left bottom corner due to the periodicity of the state vector. The shortcoming of this method is that, unlike structures where modal analysis perfectly uncouples the equations, for mechanisms the modal matrix does change with time, and therefore its derivatives should be considered when the change of variable is conducted. Unfortunately this reduces the benefit of performing the modal analysis and leads to a set of coupled equations even in the natural coordinates. However, the method does give an accurate result for some generalised coordinates. When this is the case, the algorithm could still be improved. The unknowns of the problem chosen by Midha *et al.* (1979) were the constants obtained from the integration of the basic equations during the sub-interval. If the unknowns are chosen to be the actual displacements and velocities at the beginning of each sub-interval, then the equation system becomes simpler, the second diagonal is composed of blocks of the identity matrix (of order 2). Therefore only the leading

diagonal needs to be stored. A more general algorithm is proposed in this study, which takes full advantage of the latter property especially when memory storage is a problem, and also, unlike the previous study, the modal analysis is not required to solve the original system. Yang and Sadler (1993) used a different algorithm to calculate the steady-state solution. At each of the N sub-intervals, a new state vector was defined by adding two extra entries to the original one so that the matrix which links the N modal state vectors to the N modal forces has an almost block form. They argued that although the size of the system rose from $2N$ to $4(N+1)$, the solution of such a system is computationally less expensive than the Gaussian elimination method. The algorithm used to yield the steady-state solution was originally developed by Diaz *et al.* (1983).

2.3. STABILITY

The problem of stability became of concern at an early stage in the investigation of flexible high-speed mechanisms. Most early papers dealt with the dynamic stability of linkage mechanism systems where one link was flexible and the other links were assumed to be rigid. The flexible link was modelled as a pinned-pinned Euler-Bernoulli beam in flexure. The two typical mechanisms investigated were the slider crank mechanism and the four-bar mechanism (Jasinski *et al.*, 1971; Chu and Pan, 1975; Jandrasits and Lowen, 1979; Badlani and Klieinhenz, 1979; Badlani and Midha, 1982; Tadjbakhsh, 1982; Tadjbakhsh and Younes, 1986; Masurekar and Gupta, 1988a, 1988b). Jasinski *et al.* (1971) derived the equations of motion for the elastic response of the flexible connecting rod in a slider crank mechanism, and based the dynamic stability characteristics on the existence of algebraic steady-state solutions. Chu and Pan (1975) derived the equations of motion for the flexible connecting rod and the response was obtained by numerical methods. Stability criteria were derived based on Floquet theory. Jandrasits and Lowen (1979)

investigated the elastodynamics of a counter-weighted rocker link of a four-bar mechanism with an overhanging end-mass. After expressing the equations of motion in Hill's equation form, Floquet theory was used to investigate the stability of the system. A 2π periodic Fourier series solution form was assumed to calculate the steady-state solution. Computational results showed that when even the slightest viscous damping was included in the model, there were no instability regions in the operating speed range. However, when the mechanism was run at a speed which coincided with one of the resonance positions, the coefficient of the Fourier term, whose frequency was equal to the natural frequency of the link, was considerably amplified. The experiment generally verified the above. No instability was found in the test speed range of between 100 and 200 rpm and when the mechanism was run at speeds corresponding to a ratio between 1/10 and 1/6 of the natural frequency of the link, the predicted higher amplitude at the natural frequency could be clearly seen. At off-resonance speeds a very good agreement was found both in amplitude and phase between the experimental and analytical results for a wide range of damping ratios. In contrast, while there was a good phase agreement at the observed on-resonance speeds, the amplitude of the computational results was found to be very sensitive to the assumed damping ratio. Badlani and Klieinhenz (1979) modelled the connecting rod of a crank slider mechanism using the Euler-Bernoulli theory and the Timoshenko beam theory. Using the model based on the second theory which includes rotary inertia and shear deformation effects, additional regions of instability were found to exist. Badlani and Midha (1982) analysed an initially curved flexible rod and showed that a slider crank with curved connecting rod was less dynamically stable when compared to a slider crank with straight connecting rod. The equations of motion were expressed in the form of Hill's equation and solved by assuming trigonometric series solutions. Badlani and Midha (1982) have simplified the equation of motion into a Mathieu's type equation. The stability analysis was then investigated for a slider crank mechanism without taking the damping into account. Later, Badlani and Midha (1983) presented a study showing

the effect of internal material damping on the dynamic response of the mechanism. The connecting rod was assumed to be made of a linear viscoelastic material. They concluded that the inclusion of damping is not always beneficial in attenuating the vibration response of the connecting rod. Damping had a little effect and in some cases was even counterproductive when the speed was in a stable region, and had a big effect on the response when the speed was in an unstable region. Tadjbakhsh and Younes (1986) analysed the flexible connecting rod of a slider crank mechanism for dynamic stability and applied Floquet theory to the equations of motion represented in the form of Hill's equation.

Masurekar and Gupta (1988a, 1988b) investigated the stability of a four-bar mechanism with a flexible coupler. An Euler-Bernoulli beam element was used to model the coupler. After simplifications, a second order linear differential equation was obtained. In order to assess the stability, the homogenous part of the equation of motion was expressed in Hill's equation form. Floquet solution was considered. The stability boundaries were calculated by expressing the solution as 2π -periodic and 4π -periodic and therefore expressed as truncated Fourier series. Two infinite systems were obtained for each instability type by equating the expressions corresponding to the same cosine and sine terms. It was found that, as the speed increased, unstable regions became wider. Also the 2π -periodic unstable regions were larger than nearby 4π -periodic regions. An illustrative example revealed that when the mechanism was run at a speed in one of the 4π -periodic unstable zones the transient deflection increased every two cycles, and increased every cycle when the mechanism was operated at speeds in the 2π -periodic instability zone. Also the critical speeds corresponding to the 2π -periodic instability regions are centred around integer divisions of the natural frequency of the link.

When all links were considered to be flexible, in general the FEM was used to model the mechanism. The common assumption made is that the rotational speed was

constant, the equations of motion were linear differential equations with periodic coefficients. Many other engineering systems are governed by this type of equations. Some typical examples include rotating systems such as wind turbines and helicopter rotor blades (Peters and Hohenemser, 1971), parametrically excited elastic structures (Bolotin, 1964) and spin stabilised satellites (Tyc *et al.*, 1990). The stability of such systems has been the subject of investigation for many years. In general, the methods used could be cast into three categories:

(i) Perturbation methods: these are based on the assumption that the periodic coefficients could be expressed in terms of some small parameter. The stability boundaries are approximated by closed form expressions in the parameter space. The main limitation of the perturbation method is the small parameter assumption.

(ii) Infinite determinant method: The parameter space is divided into stable and unstable regions. At the boundaries between the two regions, one of the solutions of the homogenous part of the equations of motion is either 2π or 4π -periodic. In the infinite determinant method the boundaries of the stability regions are determined by expressing the solution and the coefficients of the equations of motion into Fourier series. In order that the system has no trivial solution, the determinant of the system obtained by replacing the Fourier series into the homogenous part of the equations of motion is set to zero. Initially the system obtained is infinite. An approximate solution is obtained by truncating the Fourier series and solving the resulting truncated determinant. Bolotin (1964) used Hill's method of infinite determinant extensively for scalar equations. He also provided an extension for multiple degree of freedom systems with certain restrictions placed on the damping matrix. He found that, for such systems, the equations became too cumbersome and impractical.

(iii) Floquet numerical integration method: This method, based on Floquet theory, is the most widely used as it does not suffer from the limitations of the above methods. The method is based on the evaluation of the called transition matrix over one period. The stability is assessed from the eigenvalues of the transition matrix. In the past, this method was avoided because of the high computational demands. Hsu and

Cheng (1973) and Friedmann *et al.* (1977) developed numerically efficient schemes that significantly reduce the number of required numerical integrations.

Kalaycioglu and Bagci (1979), investigated a four-bar mechanism with all links flexible. Critical speeds for a particular mode of vibration were defined as the lower bound values of the natural frequency for that mode. This was not a complete analysis because critical speeds have been shown to occur at speeds much lower than the lowest bounds of the natural frequencies both experimentally and theoretically. Cleghorn *et al.* (1984) used Fourier series analysis to investigate the stability of a flexible four-bar mechanism. The known periodic coefficients of the equations of motion and the unknown elastic steady-state response were expressed as truncated Fourier series and the steady-state response was determined. Also by using the criterion that at critical speeds the homogenous part of the equations of motion has non-trivial periodic solutions, critical speed ranges were determined by calculating speeds which provide non-trivial solutions. By comparing harmonic terms, the problem of determining critical speeds was reduced to that of solving an EVP. When damping was neglected it was shown that there was an infinite number of critical operating speeds.

The first attempt to develop a simple method to determine the critical speeds of mechanisms with all links considered flexible was made by Nagarajan and Turcic (1990c). They provided a simple approximate theoretical method to locate the critical speeds of a four-bar mechanism based on Floquet theory. First, the cycle was divided into a number of sub-intervals during which the coefficients of the equations of motion were assumed to be constant. The modal analysis technique was then used to uncouple the equations of motion and each mode was considered separately. An analytical solution was derived and the state vectors at the start and at the end of each sub-interval were linked. Using this elementary transformation, the state vector at the end of the cycle was expressed as a function of the state vector at the

beginning. By definition, these two state vectors are linked via the monodromy matrix. An alternative to computing the monodromy matrix is to integrate numerically the original equations of motion. Nagarajan and Turcic argued that their method was more efficient and was about 50 times faster than the method which involved integrating the equations of motion using Runge-Kutta for example. Once the monodromy matrix was obtained, stability of the system could be assessed. First the eigenvalues of the monodromy matrix, called characteristic multipliers, were calculated. It was shown that the system is stable if both characteristic multipliers were less than 1 in magnitude, marginally stable if one or both of them are equal to 1 in magnitude and finally unstable if the magnitude of at least one of them exceeds 1. In a second part, Nagarajan and Turcic (1990d) experimentally verified the critical speed ranges found by the method exposed in the first part. The critical speeds were located by examining three strain characteristics. The first characteristic was the maximum experimental strain amplitude. This characteristic shows the contribution of both the quasi-static and the dynamic responses. Since critical speeds are mainly due to the dynamic response being amplified, two extra characteristics were considered to show more of the dynamic contribution to the total response. A typical Fourier transform of the strain at any location on the link would exhibit two main peaks, the first corresponds to the rotational speed (quasi-static strain response) and the other occurring at higher frequency is related to the dynamic response. The second characteristic was therefore the amplitude at the second peak of the Fourier transform of strain. Finally the third characteristic was the vibration strain energy density which is proportional to the square value of vibration strain (difference of the total strain and the quasi-static strain). For the verification purpose only the first two modes of vibration were considered. It was shown that these two modes contributed most to the total response. It was also shown that the dynamic response peaked at the predicted critical speeds using the method of the monodromy matrix. The main disadvantage of this method, however, is that in one hand in some circumstances the modal analysis does not uncouple the equations of motion in case of mechanisms.

On the other hand when damping is included, the system ceases to be numerically unstable at some low speeds but these remain critical speeds in that the strains are bigger than at neighbouring speeds. To overcome the first difficulty, a method was developed in this study where uncoupling the equations of motion is not required. Further the critical speeds are not linked to the values of the characteristic multiplier modules but rather to their local maxima against speed.

2.4. EXPERIMENTAL STUDIES

Many experiments have been conducted to verify the theoretical results of displacements, strain and stresses. Lawrence and Alexander (1974, 1975) conducted one of the first experiments on a flexible four-bar mechanism and their experimental results latter became a reference among researchers. In their mechanism, the links were constructed of aluminium, and ball bearings were used to connect the coupler to the crank and the follower. The mechanism investigated was of quick-return type. The input link was driven by an electric motor through two belts placed on either side of the plane of motion so as to ensure symmetry of the input loading. Flywheels were used to minimise the crank speed fluctuation. Strain gauges were attached on both sides of the links and the strain were measured at 6 different locations on the coupler and the follower. Different crank length and different thicknesses of the links were tested. A good agreement in amplitude was found between the experiment and the model. Lawrence and Alexander linked the resonance frequencies (critical speeds) to the natural frequencies of the individual links, but Stamps and Bagci (1983) suggested that the critical speeds are linked to the average values of the natural frequencies of the whole mechanism. In fact, Fig. 7 of Lawrence and Alexander (1975) shows a contradiction . In that figure the results of the input link flexibility effect were presented. Two mechanisms were compared, and apart from the input links which were different, all other geometrical properties were identical.

Although the coupler and the follower in both mechanisms were identical the strain-speed curves showed different critical speeds for each mechanism. Stamp and Bagci investigated a spatial four-bar mechanism with out-of plane offset. They showed that the mechanism experienced critical speeds at integer divisions of the average value of its natural frequency. They recommended then that the mechanism should be run at speeds, which they called in-between efficiency speeds, between two integer divisions of the average natural frequency of the mechanism.

Liao *et al.* (1986) found that when the mechanism was run at various crank speeds, the links developed one of three modes: quasi-static, dynamic or resonance regimes. They also showed that while the main response is of the dynamic type over a wide range of speeds, the other responses may occur at any speed. Liao *et al.* (1986) reported from an experimental study that a quasi-static response could develop in one of the links while the other could be in a state of resonance. This phenomenon has never been predicted by existing models and no other experimental work conducted has shown this type of behaviour. Thompson and Ashworth (1976) investigated the response of a four-bar mechanism mounted on a vibrating foundation. They found that the resonance phenomenon occur whenever the sum or difference of the foundation's excitation frequency and the rotational speed of the mechanism, or their harmonics, were equal or near the natural frequency of transverse vibration of that member.

Unlike mass and stiffness distribution, it is difficult to model damping based on the geometry of the link, the properties of the material and the type of joints. In order to determine experimentally a damping factor, many researchers obtained an approximate damping ratio by fixing the mechanism at a series of static configurations and conducted the amplitude decay tests. An average value of the damping ratio over the cycle was calculated and used in the theoretical model (Alexander and Lawrence, 1973; Stamps and Bagci, 1983; Turcic *et al.*, 1983; Sung

et al., 1986). Karkoub and Erdman (1992) used a different technique, the mechanism was fixed at a given configuration and excited using a shock hammer; the response was recorded on a structural dynamic analyser. The displacements, at different locations of the links were measured using displacement transducers. The modal characteristics were then extracted by the windowing signal processing technique. The tests were carried out at increments of 20 degree intervals. Each link was modelled by six degrees of freedom elements and the damping matrix was assumed to be diagonal; each entry on the diagonal was measured by placing the transducer at the right location and direction. The experimental damping matrix was then added to the FE model. When compared to the model which used Rayleigh damping formulation, Karkoub and Erdman found that the coupler curves were improved compared to the coupler curves obtained experimentally by Liou and Erdman (1987, 1989) using the photogrammetry technique.

The photogrammetry technique analyses the motion of a four-bar mechanism without affecting any characteristic of the mechanism. Special reflectors were placed at different locations of the mechanism. The motion of the mechanism was captured by a high-speed movie camera capable of delivering high quality pictures at frame rates between 16 and 500 frames per second. The pictures were then digitised and processed on the computer to determine the path described by any point of the mechanism. Also the deflection of the entire mechanism could be reconstructed in slow motion and compared to the theoretical one. This method proved to be superior to the method where strain gauges were used to monitor the mechanisms deflections (Alexander and Lawrence, 1975). In the latter method, the wires used with the strain gauges do have an effect on the response. To account for this effect, Alexander and Lawrence recommended that the mass densities of the coupler and output links should be increased by 8% to account for the additional mass of the wires and strain gauges attached to these links in the experimental set-up.

From the equations of motion of a four-bar mechanism it can be seen that the elastodynamic response is substantially influenced by the stiffness-to-weight ratio of the links. In order to reduce the deflections and stresses in the links, two methods have been used in the past. First, for a given material, the stiffness was improved by optimising the cross sections of the links (Cleghorn et al., 1981; Imam and Sandor, 1975; Khan et al., 1978). Second, composite materials were used for their higher stiffness-to-weight ratio compared to carbon steel and aluminium alloy (Sung et al., 1986). It is believed that Thompson was the first to have considered the vibration problem of mechanism components made from fibre reinforced composite materials (Thompson and Barr, 1975; Sung and Thompson, 1982; Thompson *et al.*, 1983; Thompson and Sung, 1984, 1986). The advantage of using composite materials is not limited to their high stiffness-to-weight ratio; they also possess other interesting properties such as a good fatigue life and high material damping (Sung and Thompson, 1984).

2.5. OTHER METHODS

The lumped parameter approach has also been successfully implemented in the analysis of elastic mechanisms. The lumped parameter method consists of modelling the continuous mass distribution of a linkage by placing a number of lumped masses at discrete locations along the linkage. Sadler and Sandor (1973, 1975) developed a lumped parameter method for elastic mechanism analysis. The method applies Euler beam theory and finite difference approximations to yield a system of ordinary non-linear differential equations. These equations of motion were numerically integrated to yield the system response. The numerical results for an elastic four-bar mechanism are favourably compared with the experimental results of Alexander and Lawrence (1974). The only advantage of the lumped parameter method is that it leads to a diagonal mass matrix. Gao *et al.* (1989) combined the two methods (i.e.

the FEM and the lumped parameter approach) to make full use of the advantages of both methods. They developed a hybrid element whereby the mass was lumped and the distributed stiffness was considered. They argued that their model was more efficient than the conventional ones.

2.6. CONCLUSION

A literature survey has been carried out on the modelling of high-speed mechanisms. Although high-speed mechanisms have been the subject of investigation for more than twenty years, there are still areas where some improvements could be made. To date, the only way to improve the accuracy of the FE model has been achieved by increasing the number of elements in the model. Also only a few algorithms exist to yield the steady-state solution quickly and efficiently. Critical speeds have been known to exist for a long time, but no previous study has addressed the problem of running the mechanism over the highest of these where the stress in one of the links becomes unacceptable. These issues are developed in this study and an answer is provided for each one.

Chapter 3

KINETO-DYNAMIC ANALYSIS

3.1. INTRODUCTION

The study of mechanical systems has two distinct aspects: synthesis and analysis. The synthesis involves the prescription of sizes, shapes, materials, etc. so that the mechanism performs the functions for which it was designed. The analysis is the collection of scientific tools at the designer's disposal to analyse the suitability of the design. In this chapter, the analysis of a four-bar mechanism is undertaken. The geometrical data of the mechanism are assumed to be known *a priori*.

In the analysis and design of mechanisms, kinematic quantities such as velocities and accelerations are of great engineering importance. Velocities and displacements give an insight into the functional behaviour of the mechanism. The accelerations, on the other hand, are related to forces by Newton's principle which themselves are related to stresses and deformations in the mechanism's components. In the kinematic analysis, the mechanism is assumed to be made up of rigid bodies.

In order to determine velocities and accelerations in mechanisms, many methods of analysis have long been established. These include:

- Analysis using vector mathematics to express velocities and accelerations of bodies with respect to a set of coordinate systems.
- Analysis by use of complex numbers. The vector velocities and accelerations are represented by complex numbers.
- Analysis using graphical means. The equations of relative motion are solved graphically using polygons at every position of the mechanism. This method is

now rarely used today due to the wide-spread availability of computers and software tools which offer substantial improved flexibility, precision and speed in solving the problems of kinematics.

Fig. 3.1 shows a schematic of a four-bar mechanism. If the input link is free to rotate completely and the follower oscillates, this mechanism is called a Crank-Rocker. For a mechanism to be of this type a theorem by Grashof (1883) states that the sum of the longest link and the shortest should be less than the sum of the two other lengths. In the rest of this chapter, the four-bar mechanism analysed is assumed to be of this type. The four bar mechanism is widely used in machines to transmit motion or to provide mechanical advantage. It is also the most basic and fundamental linkage mechanism (three-bar linkage is a structure). Many more complex linkage mechanisms contain the four-bar linkage as elements. There are three main applications of the four-bar mechanism: path generation, function generation and motion generation. In the first application the path generated by a tracer point is the main concern. In the function generation application, the angle of the output link is a function of the input link position. Finally, in the motion generation application (or rigid body guidance) an entire body is guided through a prescribed motion sequences.

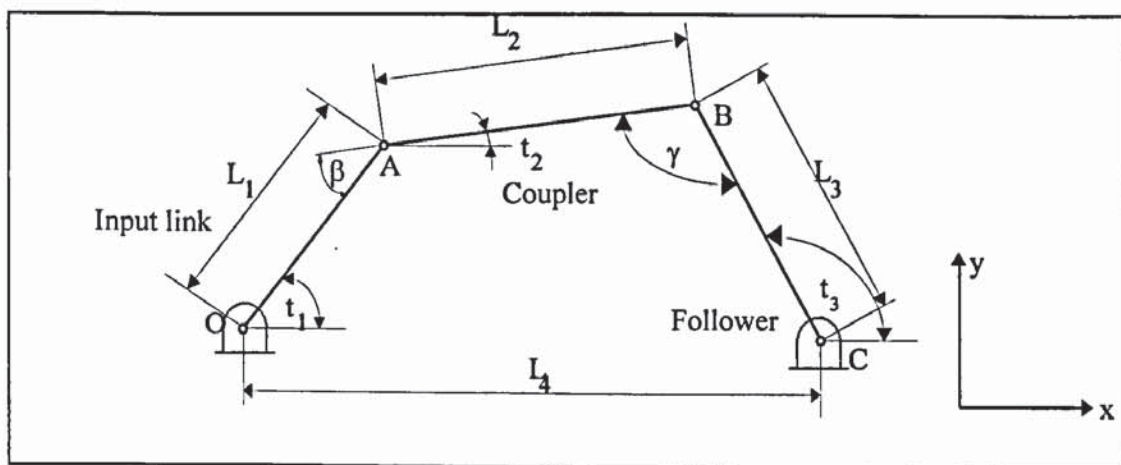


Fig. 3.1: Schematic of the four-bar mechanism.

Referring to Fig. 3.1, γ is the transmission angle, t_1 is the input angle and the distance between the two fix points, O and C, is always denoted by L_4 .

3.2. MOBILITY

Every mechanism has a number of degrees of freedom also called mobility. This defines the number of inputs that can be given to the mechanism so that it has a constrained motion. If a planar mechanism is made up of k rigid links, before assembly and counting the ground as a link, the system has $3(k - 1)$ degrees of freedom. Let j_1 be the number of single-degrees-of-freedom pairs (revolute joints for example) and j_2 be the number of two degrees of freedom pairs (cylinder pairs). Then the mobility m of the mechanism is given by Kutzbach's criterion (Shigley, 1969): $m = 3(k - 1) - 2j_1 - j_2$. In the particular case where $m = 0$ the system is not deformable and becomes a structure. If $m < 0$, the system is over-constrained and some constraints are redundant. In case of planar four-bar mechanism with revolute joints: $k = 4$, $j_1 = 4$ and $j_2 = 0$; therefore the mobility of such a mechanism is 1. The input angle is usually chosen as the reference parameter. Therefore all kinematic quantities are derived with respect to this reference.

A special case is considered for planar mechanisms with only revolute joints. The Grübler criterion (Shigley, 1969) gives the condition for this type of mechanisms to have 1 degree of freedom. For this to be satisfied, the following must hold: $m = 1 = 3(k - 1) - 2j_1$ and hence $3k - 2j_1 - 4 = 0$. From this, it is seen for example that a mechanism with odd number of links cannot have mobility equal to 1.

3.3. TRANSMISSION ANGLE

While the mechanism is rotating, some difficulties may arise if the angle between the coupler and the follower is too big or too small. This angle, γ , is called the

transmission angle. The quality of motion of the mechanism is dependent upon the minimum value of γ . The force transmission from the coupler to the output link is most effective when γ is 90° . As the input link rotates, the value of the transmission angle changes. It is desirable that the transmission angle does not deviate too much from the ideal value of 90° and it is recommended that γ should lie between 40° and 140° . If γ is too small high accelerations occur during the cycle and objectionable noise is generated at high speeds. Also, the accuracy of the output motion becomes very sensitive to the manufacturing tolerances of the link lengths and clearances between joints. On the other hand, if γ is too large uncertainty of movement arises and the two links, the coupler and the follower, may lock. However, the latter problem may be overcome by the presence of a large flywheel at the input link. The flywheel, by virtue of its high inertia, forces the mechanism to rotate in a prescribed way. Since the extreme values of γ are critical values in the design of a four-bar mechanism, it is essential for the designer to compute these values and the positions at which they occur. It is shown later in this chapter that the transmission angle is critical (i.e. maximum or minimum) at the two values of the input angle of 0° and 180° (Soni, 1974). Fig. 3.2 shows such extreme cases.

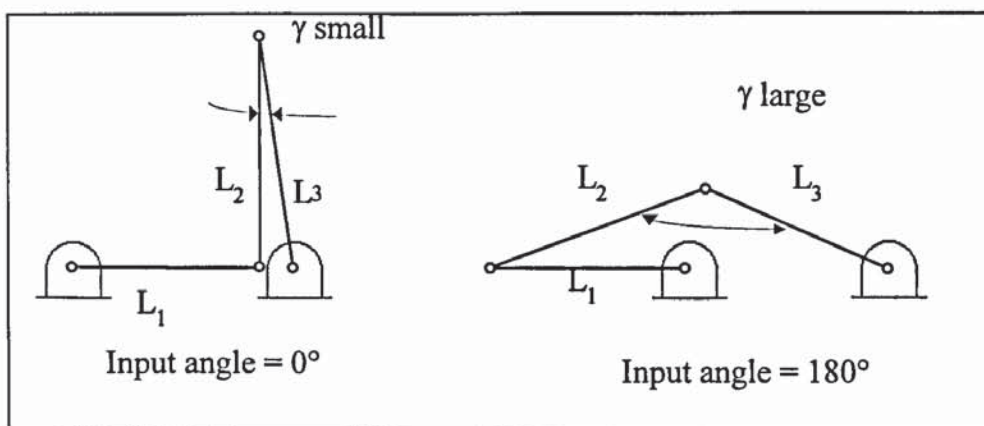


Fig. 3.2: Two extreme cases of the transmission angle.

There are many indexes which give an assessment of the performance of the mechanism. One of them is the ratio of input and output speeds, in this case the

index of merit is linked simply to the geometry of the mechanism. Another definition would be the mechanical advantage which is the ratio of input and output torques. In fact these two definitions are related if the joints are assumed frictionless and if the inertia forces are neglected. It can be shown that (Shigley, 1969):

$$\frac{T_3}{T_1} = \frac{\omega_1}{\omega_3} = \frac{L_3 \sin(\gamma)}{L_4 \sin(\beta)} \quad (3.1)$$

where T_1 and T_3 are the torques at the input and the follower, γ and β are shown in Fig. 3.1 and ω_1 and ω_3 are the corresponding speeds.

From (3.1) it is concluded that:

- The mechanical advantage is infinite when $\beta = 0^\circ$ or 180° . In this case, the mechanism is said to be in toggle. The output torque is infinite for a finite input torque, such a propriety is used in clamping mechanisms for example such as the pair of locking toggle pliers shown in Fig. 3.3.
- The transmission angle affects the mechanical advantage. If its is too small or too big, the mechanical advantage becomes very small, and the presence of even small friction torques in the joints may lock the links.



Fig. 3.3: Locking toggle plier (Sandor and Erdman, 1984).

3.4. CLASSIFICATION OF FOUR-BAR MECHANISMS

It is believed that the first attempt to classify the four-bar mechanisms was made by Grashof (1883). In his book, he classified the four-bar mechanisms into three types; namely double-cranks, rocker-cranks and double rockers. In one of his theorems, he stated that a four-bar mechanism has at least one revolving link (a crank) if $s + l \leq p + q$ and all links will be rockers if $s + l > p + q$; where s = length of the shortest link, l = length of the longest link and, p and q lengths of the intermediate links.

Barker (1985) was the first to introduce the solution space concept. He used a set of dimensionless parameters λ_2 , λ_3 and λ_4 defined by $\lambda_2 = L_2/L_1$, $\lambda_3 = L_3/L_1$ and $\lambda_4 = L_4/L_1$. The solution space is a volume in the $(\lambda_2, \lambda_3, \lambda_4)$ space where four-bar mechanisms can exist. Since all lengths must be positive, the solution space was included in the positive octant corresponding to the values of λ 's all positive. Also, the solution space was delimited by four planes which corresponded to mechanisms with zero mobility. These planes, called zero mobility planes, are defined by:

$$\begin{aligned}\lambda_2 &= 1 + \lambda_3 + \lambda_4 \\ 1 &= \lambda_2 + \lambda_3 + \lambda_4 \\ \lambda_3 &= \lambda_2 + 1 + \lambda_4 \\ \lambda_4 &= \lambda_2 + \lambda_3 + 1\end{aligned}\tag{3.2}$$

and represented graphically on Fig. 3.4 by:

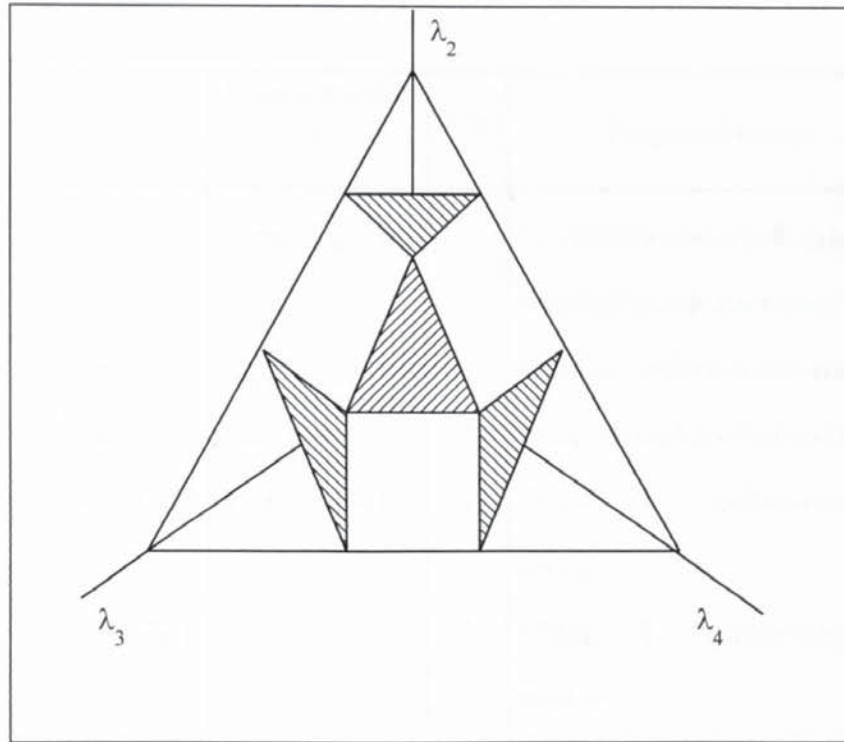


Fig. 3.4: Zero mobility plane and base plane.

Barker then considered a plane which he called base plane, at a distance λ from the origin and normal to the line $\lambda_2 = \lambda_3 = \lambda_4$ in order to focus on a two dimensional portion of the solution space. Different base planes can be investigated by varying λ given by $\frac{\lambda_2 + \lambda_3 + \lambda_4}{\sqrt{3}}$. Each base plane was then subdivided into regions, each of which corresponded to one type of the 14 mechanism classes he defined (see Table 3.1). In his classification system, a fully rotating link is called a crank whereas an oscillatory one is called a rocker. From Table 3.1 it can be seen that mechanisms of Grashof type are included in Barker's classification. In the latter case the symbol begins with the letter "G".

	$\begin{matrix} < \\ s+l=p+q \\ > \end{matrix}$	Category	Characteristic bar length	Class	Proposed name	Symbol
1	<	Grashof	frame, $L_4 = s$	1	Grashof crank-crank-crank	GCCC
2	<	Grashof	input, $L_1 = s$	2	Grashof crank-rocker-crank	GCRR
3	<	Grashof	coupler, $L_2 = s$	3	Grashof rocker-crank-rocker	GRCR
4	<	Grashof	output, $L_3 = s$	4	Grashof rocker-rocker-crank	GRRC
5	>	non-Grashof	frame, $L_4 = 1$	1	Class 1 rocker-rocker-rocker	RRR1
6	>	non-Grashof	input, $L_1 = 1$	2	Class 2 rocker-rocker-rocker	RRR2
7	>	non-Grashof	coupler, $L_2 = 1$	3	Class 3 rocker-rocker-rocker	RRR3
8	>	non-Grashof	output, $L_3 = 1$	4	Class 4 rocker-rocker-rocker	RRR4
9	=	change point	frame, $L_4 = s$	1	Change point crank-crank-crank	CPCCC
10	=	change point	input, $L_1 = s$	2	Change point crank-rocker-rocker	CPCRR
11	=	change point	coupler, $L_2 = s$	3	Change point rocker-crank-rocker	CPRCR
12	=	change point	output, $L_3 = s$	4	Change point rocker-rocker-crank	CPRRC
13	=	change point	two equal pairs	5	Double change point	CP2X
14	=	change point	$L_1=L_2=L_3=L_4$	6	Triple change point	CP3X

Table 3.1: Classification of four-bar mechanisms by Barker (1985).

Fig. 3.5 shows the base plane for three typical cases with the corresponding mechanism types in each region.

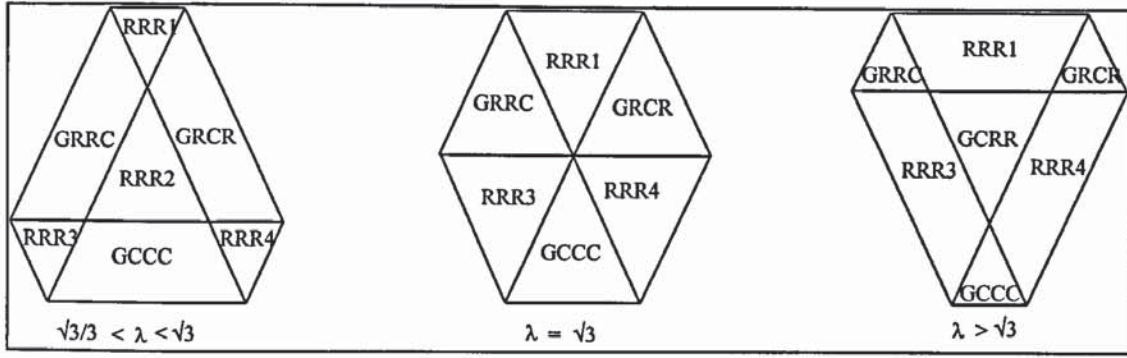


Fig. 3.5: Base plane for typical values of λ .

3.5. KINEMATIC ANALYSIS

Encyclopaedia Britannica (1980) defines kinematics as: "Branch of physics and subdivision of classical mechanics, concerns the description of the motion of objects without considering the forces that cause or result from the motion. It is an abstract study of motion that aims to provide a description of the spatial position of points in moving bodies, the rate at which the points are moving (velocity), and the rate at which their velocity is changing (acceleration). When the causative forces are disregarded, motion descriptions are possible only for points having constrained motion; i.e., moving on determinate paths. In unconstrained or free motion the forces determine the shape of the main path."

In the following, the complex number approach is used to carry out the kinematic analysis (Smith and Maunder, 1967; Erdman and Sandor, 1984). A linkage is represented by a complex number whereby the module is the link's length and the argument is the angle between the linkage and a certain reference, here the horizontal axis. From Fig. 3.1, the loop closure equation gives:

$$L_1 e^{it_1} + L_2 e^{it_2} = L_3 e^{it_3} + L_4 \quad (3.3)$$

separating the real parts and the imaginary parts in (3.3):

$$\begin{aligned} L_1 \cos(t_1) + L_2 \cos(t_2) - L_3 \cos(t_3) &= L_4 \\ L_1 \sin(t_1) + L_2 \sin(t_2) - L_3 \sin(t_3) &= 0 \end{aligned} \quad (3.4)$$

From (3.4) an expression for t_3 is derived with respect to t_1 by eliminating t_2 from the two equations in (3.4). The equation obtained is called Freudenstein's equation and can be used to synthesise a four-bar mechanism for three specified positions of the input link and three positions of the output link (Freudenstein, 1955).

$$\begin{aligned} K_1 \cos(t_3) - K_2 \cos(t_1) + K_3 &= \cos(t_1 - t_3) \\ \text{where } K_1 &= \lambda_4, K_2 = \frac{\lambda_4}{\lambda_3} \text{ and } K_3 = \frac{1 - \lambda_2^2 + \lambda_3^2 + \lambda_4^2}{2\lambda_3} \end{aligned} \quad (3.5)$$

Equation (3.5) can be simplified to yield an explicit expression of t_3 with respect to t_1 .

$$t_3 = 2 \tan^{-1} \left(\frac{2 \sin(t_1) \pm \sqrt{4 \sin^2(t_1) - 4[(1 - K_2) \cos(t_1) + K_3 - K_1][K_1 + K_3 - (1 + K_2) \cos(t_1)]}}{2[(1 - K_2) \cos(t_1) + K_3 - K_1]} \right) \quad (3.6)$$

Similarly an expression for the coupler angle t_2 is derived:

$$\begin{aligned} K_4 \cos(t_1) - K_1 \cos(t_2) + K_5 &= \cos(t_1 - t_2) \\ \text{where } K_4 &= \frac{\lambda_4}{\lambda_2} \text{ and } K_5 = \frac{\lambda_3^2 - \lambda_4^2 - 1 - \lambda_2^2}{2\lambda_2} \end{aligned} \quad (3.7)$$

$$t_2 = 2 \tan^{-1} \left(\frac{2 \sin(t_1) \pm \sqrt{4 \sin^2(t_1) - 4[(1 + K_4) \cos(t_1) + K_5 - K_1][K_1 + (K_4 - 1) \cos(t_1) + K_5]}}{2[K_5 - K_1 + (1 + K_4) \cos(t_1)]} \right) \quad (3.8)$$

In (3.6) and (3.8) two solutions are obtained for a given input angle which correspond to two different configurations of the mechanism. Fig. 3.6 shows the two solutions at a given configuration of the input link.

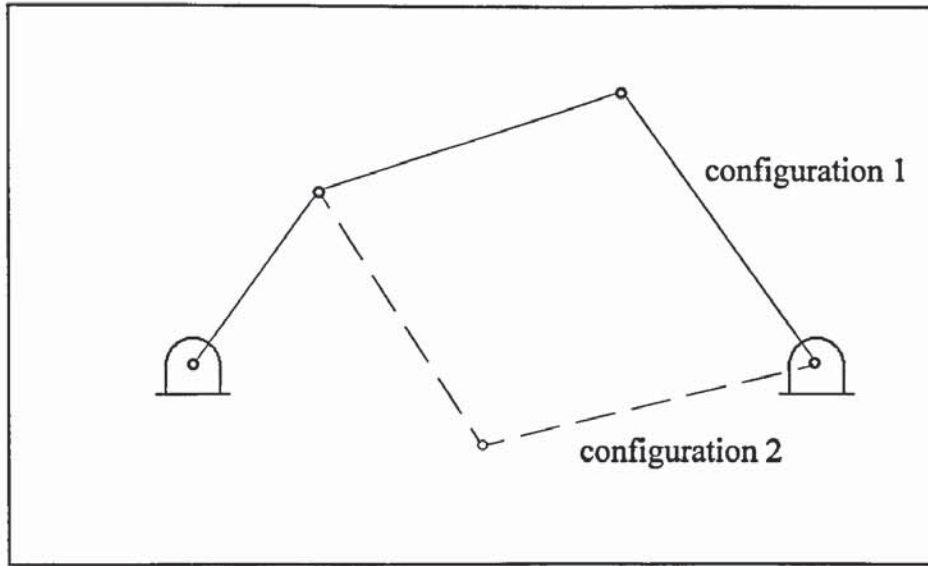


Fig. 3.6: The two mechanisms solution for a given input angle.

An expression for the transmission angle can also be derived from Fig. 3.1 by considering the two triangles OAC and ABC and expressing the distance AC in terms of the lengths of the links and the angles γ and t_1 .

$$\cos(\gamma) = \frac{L_2^2 + L_3^2 + 2L_1L_4\cos(t_1) - L_1^2 - L_4^2}{2L_2L_3} \quad (3.9)$$

Two values of γ are of particular interest. These are the maximum and minimum values of the transmission angle and correspond to $\cos(t_1) = -1$ and $\cos(t_1) = 1$ respectively. The designer should ensure that they are within an acceptable range. They are given by:

$$\cos(\gamma_{\min}) = \frac{L_2^2 + L_3^2 + 2L_1L_4 - L_1^2 - L_4^2}{2L_2L_3}$$

and

$$\cos(\gamma_{\max}) = \frac{L_2^2 + L_3^2 - 2L_1L_4 - L_1^2 - L_4^2}{2L_2L_3} \quad (3.10)$$

The angular velocities and accelerations of different links are obtained by differentiating (3.3) once to yield angular velocities, ω , and twice to give angular accelerations, α .

$$\begin{aligned}
\frac{\omega_2}{\omega_1} &= -\frac{L_1 \sin(t_3 - t_1)}{L_2 \sin(t_3 - t_2)} \\
\frac{\omega_3}{\omega_1} &= -\frac{L_1 \sin(t_2 - t_1)}{L_3 \sin(t_3 - t_2)} \\
\alpha_2 &= \frac{L_1 \omega_1^2 \cos(t_3 - t_1) + L_2 \omega_2^2 \cos(t_3 - t_2) - L_3 \omega_3^2}{L_2 \sin(t_3 - t_2)} \\
\alpha_3 &= \frac{L_1 \omega_1^2 \cos(t_2 - t_1) - L_3 \omega_3^2 \cos(t_2 - t_3) + L_2 \omega_2^2}{L_3 \sin(t_3 - t_2)}
\end{aligned} \tag{3.11}$$

These expressions will be used later in the derivation of inertia forces developed by the mechanism.

The characteristics of the mechanism investigated in this chapter are listed in Table 3.2. Relative angular velocities and accelerations over one cycle are given in figures 3.7 and 3.8 for the coupler and the follower respectively. The relative angular velocity is defined as the ratio of the angular speed of the link to the input speed, and the relative acceleration is defined by the ratio of the acceleration of the link considered to the square of the input speed. The variation of the acceleration over the cycle is important because the dynamic loads are proportional to these accelerations. Moreover, the deflections and stresses in the elements exhibit the same variation over the cycle as will be seen later. In Fig. 3.9 the variation of the transmission angle through one cycle is given. From this figure it is noticed that the maximum value of the transmission angle occurs at $t_1 = 180^\circ$ and the minimum at $t_1 = 0^\circ$. It is also seen that the mechanism being studied has a good transmission angle as it lies in the recommended band.

	Input Link	Coupler	Follower	Ground
Length [m]	$L_1 = 0.170$	$L_2 = 0.328$	$L_3 = 0.525$	$L_4 = 0.547$
Width [mm]	24.8	25	25	
Thickness [mm]	6.35	3.42	3.15	
Material : Steel, Density : $7.85 \cdot 10^3 \text{ kg/m}^3$.				

Table 3.2: Characteristics of the mechanism.

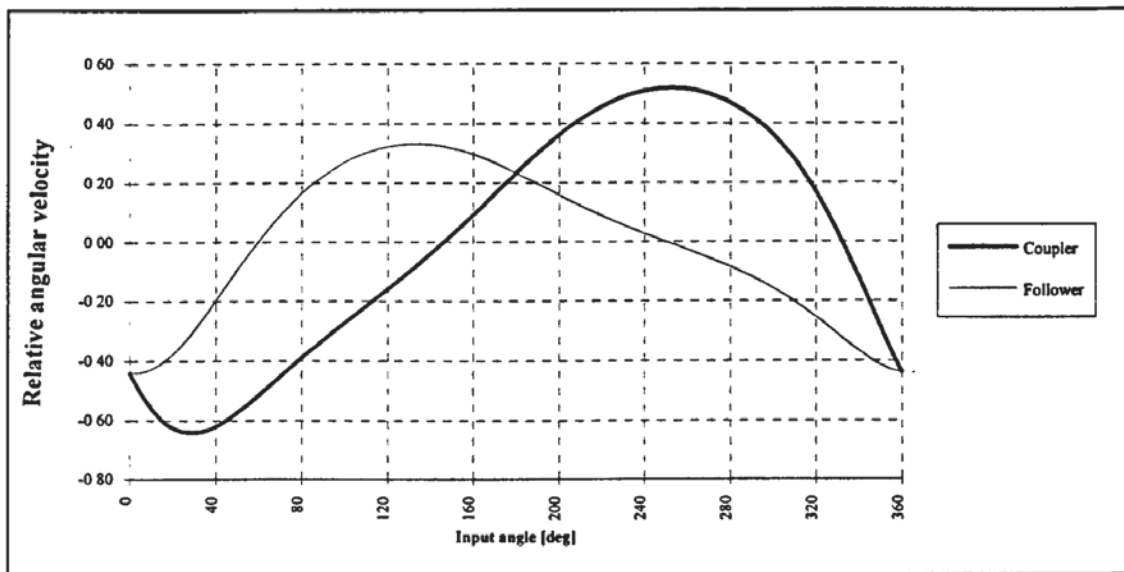


Fig. 3.7: Relative angular velocity of the coupler and the follower.

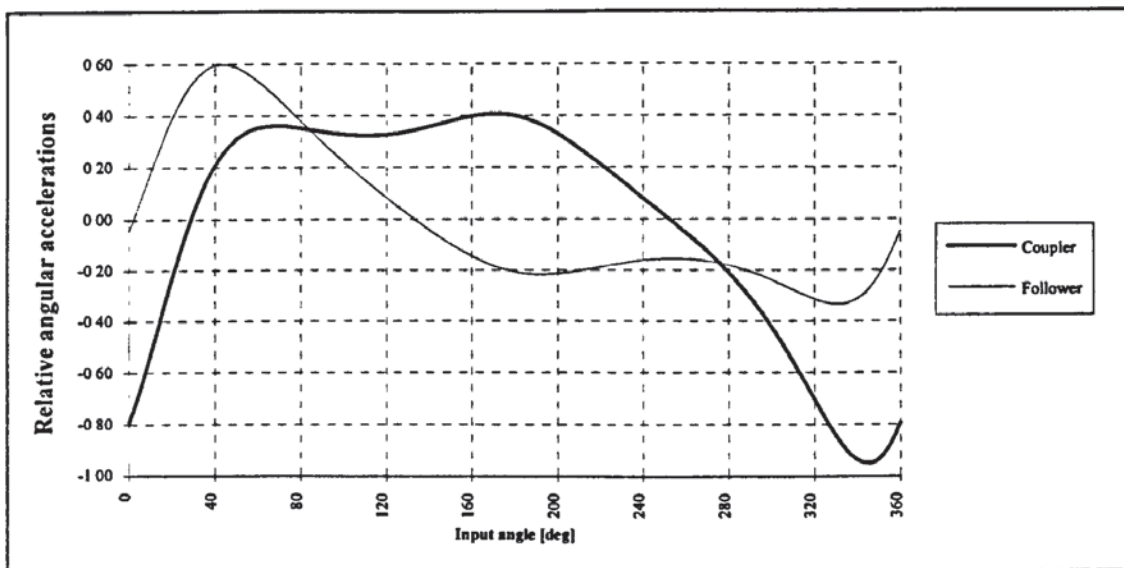


Fig. 3.8: Relative angular accelerations of the coupler and the follower.

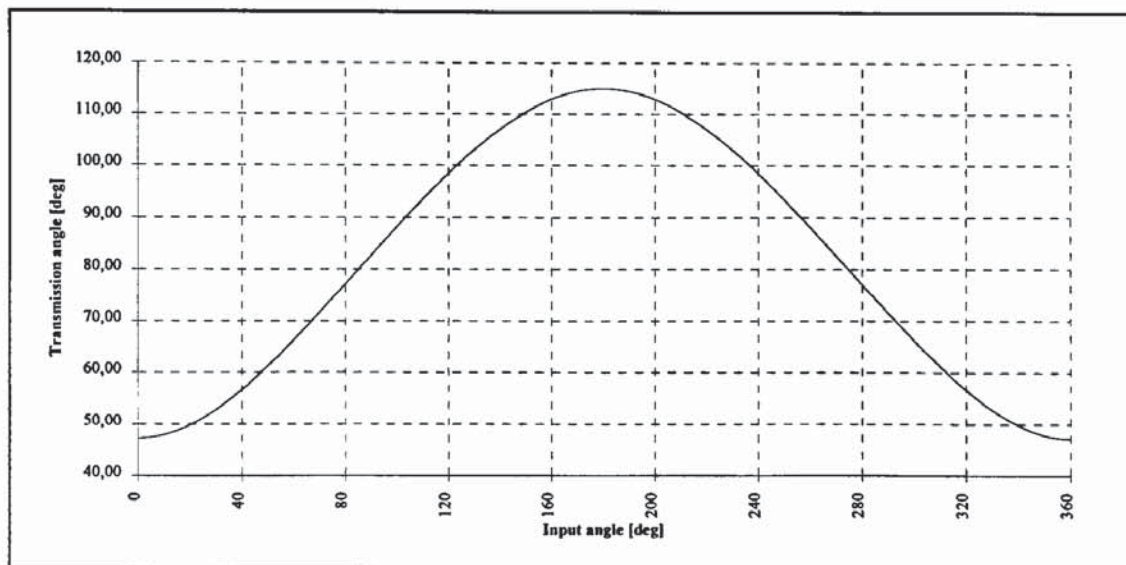


Fig. 3.9: Transmission angle versus input angle.

3.6. COUPLER CURVES

One application of the four-bar mechanism is to generate a prescribed path. The points on the coupler generate different paths with respect to the fixed link, these paths are called coupler curves. Two of these are obvious, the curves generated by the pins are either circles or arcs depending on the type of the mechanism. However, other points on the coupler generate much more complex curves. In this case it would be interesting to visualise the path generated by any point on the coupler. This can be used to validate the data of the mechanism synthesised by other means, or as part of a trial and error process. Fig. 3.10 shows a four-bar mechanism at different positions during one revolution and the path generated by some points on the coupler.

Hrones and Nelson (1951) produced an atlas of over 7000 coupler curves for different combinations of links in a four-bar mechanism. The book has been a valuable reference for decades to the designer who needs a specific mechanism for a specific path.

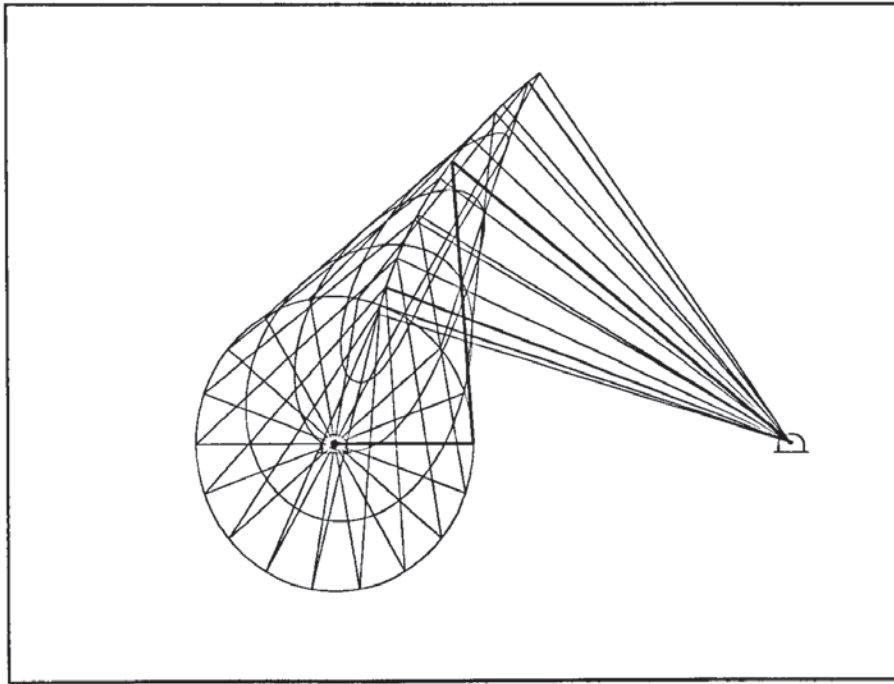
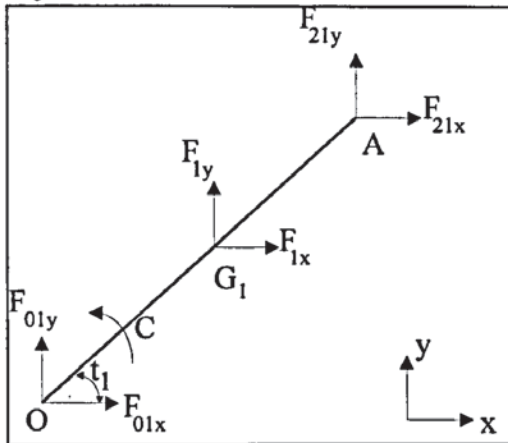


Fig. 3.10: Path generated by some points on the coupler.

3.7. DYNAMIC ANALYSIS

The forces in the linkages, by virtue of Newton's law, are proportional to the masses and accelerations of the linkages. The mechanism will now be analysed by considering the bars individually whereby the forces acting upon the linkages are the inertial forces due to the tangent and normal accelerations at the centre of gravity of each bar and the forces transmitted from the adjacent linkages by the joints. For each link three scalar equations are obtained: $\Sigma F_x = 0$, $\Sigma F_y = 0$ and $\Sigma M_G = J \alpha$. ΣF_x and ΣF_y are the sum of forces of a system of forces acting on the link in the plane of motion and along the x axis and y axis respectively. The forces comprise the external forces as well as the inertial forces F_{ix} and F_{iy} ($i = 1$ to 3). ΣM_G is the sum of moments of forces, and torque about an axis through the mass centre normal to the plane of motion; J is the moment of inertia of the bar about the same axis. Finally α is the angular acceleration of the link in the plane of motion. In the following F_{ij} is the force applied on link j by link i .

Input link:



$$F_{01x} + F_{21x} + F_{1x} = 0$$

$$F_{01y} + F_{21y} + F_{1y} = 0$$

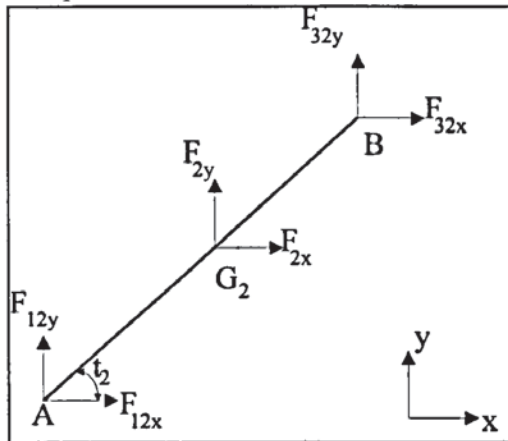
$$C + (F_{01x} - F_{21x}) \frac{L_1}{2} \sin(t_1) + (F_{21y} - F_{01y}) \frac{L_1}{2} \cos(t_1) = 0$$

C is the torque being applied to the crank.

N.B. The input angular speed is assumed to be constant in this analysis.

Fig. 3.11.a: Free-body diagramme of the input link

Coupler:



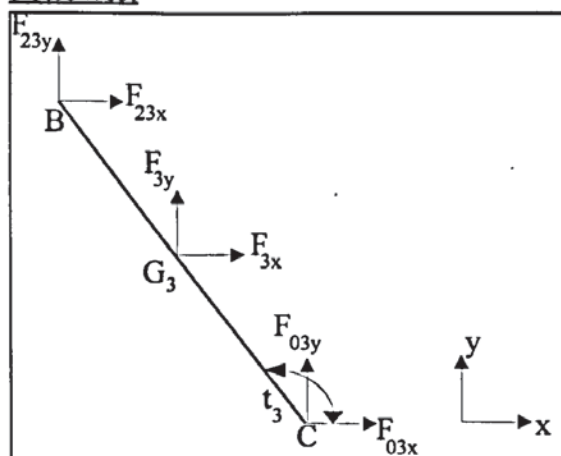
$$F_{12x} + F_{32x} + F_{2x} = 0$$

$$F_{12y} + F_{32y} + F_{2y} = 0$$

$$(F_{12x} - F_{32x}) \frac{L_2}{2} \sin(t_2) + (F_{32y} - F_{12y}) \frac{L_2}{2} \cos(t_2) = J_2 \alpha_2$$

Fig. 3.11.b: Free-body diagramme of the coupler

Follower:



$$F_{23x} + F_{03x} + F_{3x} = 0$$

$$F_{23y} + F_{03y} + F_{3y} = 0$$

$$(F_{03x} - F_{23x}) \frac{L_3}{2} \sin(t_3) + (F_{23y} - F_{03y}) \frac{L_3}{2} \cos(t_3) = J_3 \alpha_3$$

Fig. 3.11.c: Free-body diagramme of the follower

Grouping the previous equations and noting that $F_{ij} = -F_{ji}$ at all joints, a system of 9 equations with 9 unknowns is obtained. The unknowns of the problem are the forces in the joints (8 components) and the torque at the input link necessary to drive the mechanism. Thus

$$\begin{bmatrix} -1 & 0 & 1 & 0 & 0 & 0 & 0 & 0 & 0 \\ 0 & -1 & 0 & 1 & 0 & 0 & 0 & 0 & 0 \\ \frac{L_1}{2}\sin(t_1) & -\frac{L_1}{2}\cos(t_1) & \frac{L_1}{2}\sin(t_1) & -\frac{L_1}{2}\cos(t_1) & 0 & 0 & 0 & 0 & 1 \\ 0 & 0 & -1 & 0 & 1 & 0 & 0 & 0 & 0 \\ 0 & 0 & 0 & 1 & 0 & 1 & 0 & 0 & 0 \\ 0 & 0 & \frac{L_2}{2}\sin(t_2) & -\frac{L_2}{2}\cos(t_2) & \frac{L_2}{2}\sin(t_2) & -\frac{L_2}{2}\cos(t_2) & 0 & 0 & 0 \\ 0 & 0 & 0 & 0 & -1 & 0 & -1 & 0 & 0 \\ 0 & 0 & 0 & 0 & 0 & -1 & 0 & -1 & 0 \\ 0 & 0 & 0 & 0 & -\frac{L_3}{2}\sin(t_3) & \frac{L_3}{2}\cos(t_3) & \frac{L_3}{2}\sin(t_3) & -\frac{L_3}{2}\cos(t_3) & 0 \end{bmatrix} \begin{bmatrix} F_{01x} \\ F_{01y} \\ F_{12x} \\ F_{12y} \\ F_{23x} \\ F_{23y} \\ F_{30x} \\ F_{30y} \\ C \end{bmatrix} = \begin{bmatrix} F_{1x} \\ F_{1y} \\ 0 \\ F_{2x} \\ F_{2y} \\ J_2\alpha_2 \\ F_{3x} \\ F_{3y} \\ J_3\alpha_3 \end{bmatrix} \quad (3.12)$$

Once the solution of (3.12) is found, a preliminary check is carried out to ensure that the mechanism will withstand the forces due to the rigid body inertia forces. This is done by calculating the stresses sustained by each member as a result of the forces applied to the joints. If no flywheels are used, the torque of the motor is calculated as the maximum torque required during the cycle. If flywheels are used, however, the torque of the motor could be chosen to be lower. This is because the torque required to drive the mechanism fluctuates during the cycle and can even become negative. When this is the case the energy is stored by the flywheels and then restored when the torque becomes positive again. Therefore it is not required that the torque delivered by the motor be larger than the maximum torque needed during the cycle.

3.8. GENERALISED RIGID-BODY ACCELERATIONS

When the mechanism is rotating at a constant speed it deflects due to the inertia forces it is subjected to. In Chapter 4, the finite element method will be used to establish the equations of motion. It will be seen that the inertia forces acting upon the mechanism are expressed as $\mathbf{M}\ddot{\mathbf{q}}_r$, where \mathbf{M} is the mass matrix and $\ddot{\mathbf{q}}_r$ is the

generalised rigid-body acceleration. The latter is derived from purely kinematic quantities.

In this section, the rigid-body accelerations of the mechanism are presented. The schematic of the mechanism is given in Fig. 3.1. The acceleration of a point X is derived by differentiating the vector OX twice with respect to time. The accelerations of interest are the angular accelerations of the links and the accelerations of the joints A and B. They are given by:

$$\begin{aligned}
 \ddot{q}_{t_1} &= 0 \\
 \ddot{q}_{Ax} &= -L_1\omega_1^2\cos(t_1) \\
 \ddot{q}_{Ay} &= -L_1\omega_1^2\sin(t_1) \\
 \ddot{q}_{t_2} &= \alpha_2 \\
 \ddot{q}_{Bx} &= -L_1\omega_1^2\cos(t_1) - L_2\omega_2^2\cos(t_2) - L_2\alpha_2\sin(t_1) \\
 \ddot{q}_{By} &= -L_1\omega_1^2\sin(t_1) - L_2\omega_2^2\sin(t_1) + L_2\alpha_2\cos(t_2) \\
 \ddot{q}_{t_3} &= \alpha_3
 \end{aligned} \tag{3.13}$$

3.9. CONCLUSION

In this chapter kinematic analysis was carried out in order to find the speeds and accelerations of the links of a four-bar mechanism running at a constant speed. The role of the transmission angle in the performance of the mechanism was discussed. The dynamic analysis provided the forces being applied at the joints of the links as well as the torque necessary to drive the mechanism at a constant speed.

Chapter 4

FINITE ELEMENT METHOD IN THE ANALYSIS OF A FOUR-BAR MECHANISM

4.1. INTRODUCTION

In this study it was decided not to use a commercial FE package but to develop the necessary routines as part of the research. The justification of this is:

- (i) that none of the packages readily available allows for rotating members
- (ii) developing the routines would allow a greater in-sight into the subject.

As a consequence of this it is appropriate to describe FE analysis in the context of this work. However, it is not intended that it should be an exhaustive treatment of the finite element method. Consistent with the scope of this chapter, the cases treated are limited to beam elements in bending and tension modes.

Basically, the FEM involves imagining the body to be an assembly of regular discrete pieces called elements with simple geometry and connected together at a finite number of points called nodes.

The FEM has been developed over many decades before it reached the level of sophistication of today. A brief outline of its history is presented herein to show the major steps in the development of this method. In the early 1940's, Courant (a mathematician) suggested a piece-wise Rayleigh-Ritz approach where the 2D structure investigated was divided into triangular sub-regions defined by polynomial interpolation to approximate a numerical solution. However the method was discarded due to the lack of digital computers capable of solving large systems of equations. The availability of computers and the need of the aerospace industry were largely responsible for the development of the matrix method in structural dynamics

between 1950 and 1960. Interest in the FEM increased a great deal in 1956 with a paper by Turner *et al.*. They defined a continuous 2D elastic body by an assembly of triangular elements in which the displacements are assumed to vary linearly. By the mid 1970's, the FEM was well established on solid theoretical grounds; the only limitation was the hardware available at that time. Computer resources were very limited in speed but most importantly in memory; programs developed were batch oriented and therefore tedious and time-consuming. In the late 1970's the 32-bit minicomputer was introduced and graphics terminals became available. The FEM was one of the biggest beneficiaries of this new technology. Also these changes in technology brought about new concepts in programming techniques. New programs were written to make use of the new interactive environment especially in pre- and post-processing of data. The programs were no longer batch oriented, the data was often introduced interactively in graphics mode using pointing devices such as mice and digitisers. Also the user had a wider choice of analysis tools enabling him to process the results (e.g. visualisation of the mode shapes, contour plotting, colour coded stress distribution, etc.). Today, powerful FE programs are no longer limited to mainframe computers, they are available on many platforms including desktop and personal computers.

The FEM may be viewed as a piece-wise Rayleigh-Ritz method. Some fundamental differences between the two methods exist, however. In the Rayleigh-Ritz method the admissible functions are global functions (i.e. defined over the entire domain of the system); they tend to be complicated and hard to work with. The use of global admissible functions makes the use of this method more suitable for systems with simple boundary geometry and easily specified mass and stiffness distributions. The coefficients of the series are generally abstract in nature, and they merely represent the contribution of a particular admissible function to the displacement distribution. In contrast, in the FEM the admissible functions are local (i.e. defined over small sub-domains of the system); they are very simple and easy to work with and

generally low-degree polynomials are chosen. Also, they are all the same for every element and because they overlap over consecutive elements only, the mass and stiffness matrices are banded. On the other hand, since the admissible functions are local this makes the FEM better able to handle systems with abrupt variations in mass or stiffness distributions. The coefficients of the series are nodal coordinates; therefore they have physical significance (displacements, slopes and curvatures) and can be easily interpreted. Finally in order to improve the accuracy of the computed solution of the eigenvalue problem (EVP) two approaches are possible: the mesh could be refined by reducing the size of the elements; or the degree of the polynomials over the elements could be increased. The first procedure is known as the h-version of the FEM and the second as the p-version. The latter version is similar to the Rayleigh-Ritz method in that the accuracy is improved by increasing the number of admissible functions. However, the differences between the two methods referred to earlier remain. The p-version provides a higher rate of convergence than the Rayleigh-Ritz method or the h-version.

Advantages of the FEM include the ability to deal with structures with arbitrary loading, including support conditions, and also the ability to model structures of arbitrary geometry. A further advantage of this method is the possibility of modelling composite structures comprising different structural components.

However, for the purpose of dynamic analysis, an alternative is to use the exact displacement functions arising from the solution of the governing differential equations for beam vibration. As will be seen in the next chapter, this approach offers certain advantages but has the disadvantage of leading to a non-linear EVP when computing the natural frequencies.

When the FEM is employed, two stages must be considered. The first requires study of the individual elements into which the system is divided, while the second

involves studying the assemblage of elements which represent the entire system. Thus, the outline of the FE process may be summarised into five essential steps which are as follows (Richards, 1977):

1 Definition of the finite element mesh: The first step involves the process of discretising the structure into appropriate sub-regions.

2 Selection of displacement models: In this process, a suitable displacement function must be selected for a typical element which would lead to a finite number of degrees of freedom and would satisfy the boundary conditions of the system. In order to retain the bounding and convergence properties inherent in the Ritz procedure, it is necessary that the element interpolation functions should include the rigid body displacements and uniform strain states, and that they maintain displacement compatibility along the inter element and exterior boundaries.

3 Formulating the discrete stiffness equation or equation of motion: The strains at any point within the element may be expressed in terms of the element nodal displacements. The static equations of equilibrium can be obtained by using the principle of stationary total potential energy whereas the dynamic equations of motion are obtained by using Hamilton's principle.

4 Solution of the stiffness equation or the equations of motion: The solution of stiffness equations lead to a set of simultaneous equations whereas the equations of motion in the free vibration case lead to an EVP.

5 Determination of the desired properties: Once the nodal displacements have been determined, strain and stress can be calculated from the strain-displacement relationship and by Hooke's law, respectively.

4.2. APPLICATION OF THE FEM TO THE ANALYSIS OF FOUR-BAR MECHANISMS

The application of the FEM in the analysis of four-bar mechanisms involves imagining the bars of the mechanism to be actually divided into a finite number of regular elements of finite (but not necessarily equal) length, and connected with each other through nodal points. The elements are in this case beam elements. At each instantaneous position, the mechanism is viewed as a structure upon which external loads and inertial forces are acting. The versatility of the method means that variations in the mechanism geometry can be taken into account easily without any additional difficulty.

4.2.1 Shape functions for a Beam Element.

In the analysis of the mechanism at a given position, it is assumed that it is a structure composed of discrete members, as shown in Fig. 4.1. In this respect, each of the constituent members is regarded as a beam, and so the beam theories of bending apply. The effects of shear deformation and rotary inertia are neglected.

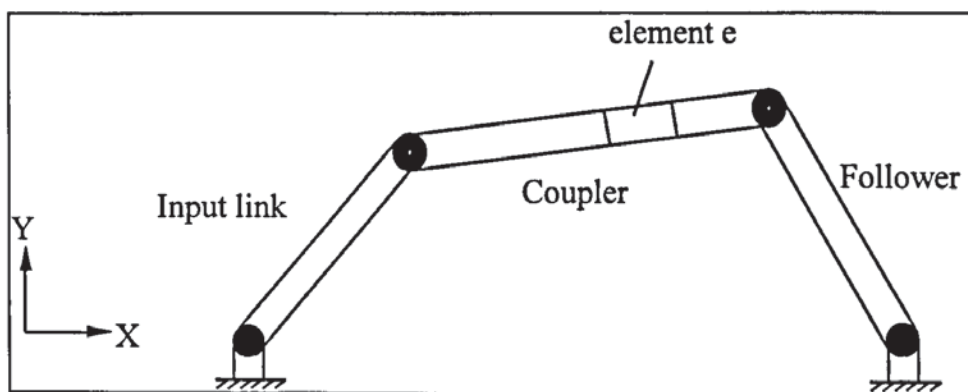


Fig. 4.1: Mechanism at a given position.

The simplest one-dimensional element is a uniform, straight beam. Such an element has been used when analysing the four-bar mechanism as shown in Fig. 4.2. For the

convenience of computation, the local coordinate axes are chosen to be coincident with the principal axes of the beam.

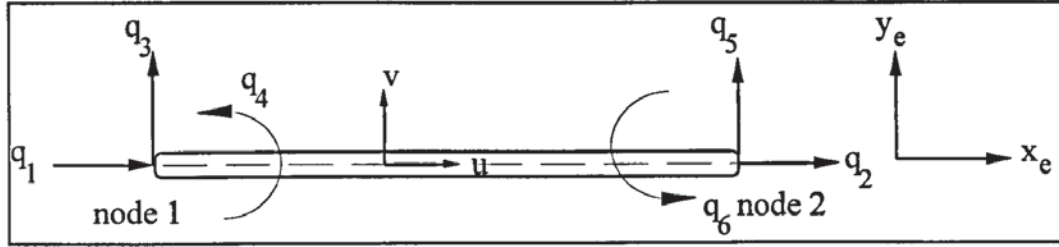


Fig. 4.2: Beam element with its nodal coordinates

When the mechanism vibrates mainly in one plane, two types of vibration must be considered: the flexural vibration and the longitudinal vibration. This is true in the mechanism considered because the links are flexible in the plane of motion and relatively stiffer in the plane perpendicular to the latter. The torsion effect is neglected. Thus, it is possible to construct stiffness and mass matrices for the beam element from the sub-matrices arising from the longitudinal and flexural vibration equations. In order to define the motion of the structure it is necessary to establish the nodal displacements associated with all these elements. The total number of these nodal displacements represents the number of degrees of freedom of the beam element which comprises two axial displacements, two transversal displacements and two rotations. The stiffness and mass matrices are therefore of order 6 by 6 for each element of the beam. Suitable polynomial displacement function for a one-dimensional element is of the form given by:

$$u(x) = \sum_{i=1}^n a_i x^{i-1} \quad (4.1)$$

where a_i are arbitrary constant coefficients and n the number of degrees of freedom of the element associated with the mode considered.

The procedure involved in finding the beam element stiffness and mass matrices in tension and bending is as follows:

1 Beam element in tension:

From (4.1), since the beam element in tension has two degrees of freedom, so the approximating function for the element displacement is represented by:

$$u(x) = a_1 + a_2 x \quad (4.2)$$

By substituting the boundary conditions, $x=0$ for node 1 and $x = L$ for node 2 in turn, into (4.2), $u(x)$ becomes:

$$\begin{aligned} u(x) &= \left(1 - \frac{x}{L}\right)q_1 + \frac{x}{L}q_2 = \begin{bmatrix} 1 - \frac{x}{L} & \frac{x}{L} \end{bmatrix} \{q_1 \quad q_2\}^T \\ &= [1 - \xi \quad \xi] \mathbf{q}_1 = \mathbf{N}_1(x) \mathbf{q}_1 \end{aligned} \quad (4.3)$$

where $\xi = \frac{x}{L}$ is a non dimensional parameter varying from 0 to 1.

$\mathbf{N}_1(x)$ is called the shape function. \mathbf{q}_1 is a vector of element nodal displacements.

The strain at any point within the element may be expressed in terms of the nodal displacements and can be found by a suitable differentiation of the displacements defined by (4.3), so that :

$$\varepsilon = [\partial] \mathbf{N}_1(x) \mathbf{q}_1 = \mathbf{B}_1 \mathbf{q}_1 \quad (4.4)$$

where ϵ is the element strain vector. In general, $[\partial]$ is a matrix of differential operators and in the present case B_1 contains the derivative of $N_1(x)$ and is given by:

$$B_1 = \frac{1}{L}[-1 \quad 1].$$

2- Beam element in bending mode

In this mode, the nodal displacements can undergo both transverse and rotational displacements at both ends. The element must therefore have four degrees of freedom, (see Fig. 4.2). Since the number of terms in the chosen displacement model must equal the total number of degrees of freedom a suitable function is :

$$v(x) = a_3 + a_4 x + a_5 x^2 + a_6 x^3 \quad (4.5)$$

Proceeding as before, $v(x)$ is given by:

$$v(x) = N_2(x) q_2 \quad (4.6)$$

where $q_{2T} = [q_3 \ q_4 \ q_5 \ q_6]$ and $N_2(x)$ is the shape function for beams in bending mode given by: $N_2(x) = [1 - 3\xi^2 + 2\xi^3 \quad L(\xi - 2\xi^2 + \xi^3) \quad 3\xi^2 - 2\xi^3 \quad L(-\xi^2 + \xi^3)]$

The interpolation functions in $N_2(x)$ are known as Hermite cubics. These functions are not unique and other choices are possible. They are chosen simply because they represent the lowest degree polynomials which describe a fourth-order problem.

4.2.2 The equations of motion of the mechanism

The equations of motion can be derived by several different methods. The most popular among researchers are Lagrange equations and Hamilton's principle. Both

methods lead to the same set of equations. In fact, it can be shown that the two methods are mathematically equivalent. Hamilton's principle stipulates that for a conservative system the real trajectory is the one which corresponds to a stationary

value of the integral $\int_{t_1}^{t_2} (T - U) dt$ with respect to any arbitrary compatible displacement δq between two instants t_1 and t_2 and in such a way that $\delta q = 0$ at t_1 and t_2 . Hence, the problem is formulated as:

$$\begin{aligned} \delta \int_{t_1}^{t_2} (T - U) dt &= 0 \\ \delta q(t_1) &= \delta q(t_2) = 0 \end{aligned} \quad (4.7)$$

where T is the kinetic energy and U the total potential energy (the potential energy of external forces + internal strain energy due to elastic deformations, U_{int}).

Note that in the special case of a static loading, Hamilton's principle becomes the well known principle of minimum energy.

The strain energy due to the flexural and bending deformations is given by:

$$U_{int} = \frac{1}{2} \int_0^L EA \left(\frac{\partial u}{\partial x} \right)^2 dx + \frac{1}{2} \int_0^L EI_z \left(\frac{\partial^2 v}{\partial x^2} \right)^2 dx \quad (4.8)$$

which leads to:

$$U_{int} = \frac{1}{2} \mathbf{q}_1^T \left(\int_0^L EA \mathbf{B}_1^T \mathbf{B}_1 dx \right) \mathbf{q}_1 + \frac{1}{2} \mathbf{q}_2^T \left(\int_0^L EI_z \mathbf{B}_2^T \mathbf{B}_2 dx \right) \mathbf{q}_2 \quad (4.9)$$

$$\text{where } \frac{\partial^2 v(x)}{\partial x^2} = \frac{d^2 N_2(x)}{dx^2} \mathbf{q}_2 = \mathbf{B}_2 \mathbf{q}_2 \quad (4.10)$$

A is the cross section area and E is Young's modulus of elasticity,

EA and EI_z are called the extentional and the flexural rigidity respectively.

The element stiffness matrices associated with the axial and transversal vibrations are therefore defined by:

$$\mathbf{K}_1 = \int_0^L EA \mathbf{B}_1^T \mathbf{B}_1 dx \text{ and } \mathbf{K}_2 = \int_0^L EI_z \mathbf{B}_2^T \mathbf{B}_2 dx \quad (4.11)$$

Replacing \mathbf{B}_1 and \mathbf{B}_2 by their expressions and integrating yields:

$$\mathbf{K}_1 = \frac{EA}{L} \begin{bmatrix} 1 & -1 \\ -1 & 1 \end{bmatrix} \quad (4.12)$$

and

$$\mathbf{K}_2 = \frac{EI_z}{L^3} \begin{bmatrix} 12 & 6L & -12 & 6L \\ & 4L^2 & -6L & 2L^2 \\ & \text{sym} & 12 & -6L \\ & & & 4L^2 \end{bmatrix} \quad (4.13)$$

The displacement models, the stiffness matrices associated with axial and bending loading of an element, have been presented separately. In plane motion analysis, the beam element will have 6 degrees of freedom as shown in Fig. 4.2. Consequently, the element stiffness matrix in a local coordinate system will be denoted by assembling the element sub-matrices \mathbf{K}_1 and \mathbf{K}_2 . The element stiffness matrix \mathbf{K} is given by:

$$\mathbf{K} = \begin{bmatrix} \mathbf{K}_1 & \\ & \mathbf{K}_2 \end{bmatrix} \quad (4.14)$$

In order to derive the mass matrices, the kinetic energy needs to be considered. To do this we must consider its expression with respect to the nodal coordinates. Fig. 4.3 shows an elemental mass in an element of the link and the coordinate systems used in the development of the equations of motion. The coordinate system (x_e, y_e) is fixed at a general point of the undeformed link, its origin is located by vector \mathbf{r}_0 . The

reference coordinate system (X,Y) is attached to the ground. Vector \mathbf{d} represents the displacement due to the elastic deformation of the link and it is measured in the (x_e, y_e) system. The general displacement of any point on the link in the reference coordinate system is measured by vector \mathbf{r} and can be expressed as:

$$\mathbf{r} = \mathbf{r}_0 + \mathbf{T}\mathbf{d} \quad (4.15)$$

where matrix \mathbf{T} is the transformation matrix between the local and the global coordinate system.

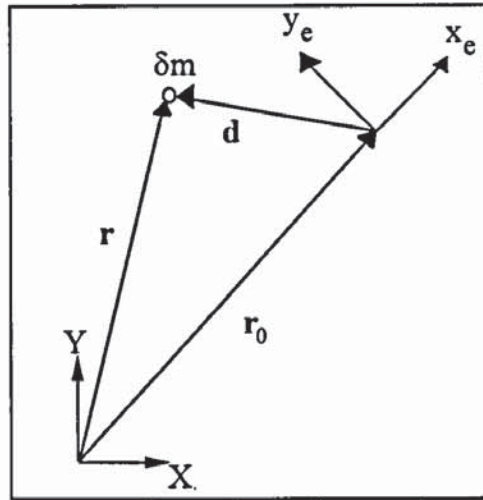


Fig. 4.3: Elemental mass displacement in local and global coordinate system.

The kinetic energy of the elemental mass δm is given by $\frac{1}{2} \dot{\mathbf{r}}^T \dot{\mathbf{r}} \delta m$. The velocity vector $\dot{\mathbf{r}}$ is obtained by differentiation of (4.15).

$$\dot{\mathbf{r}} = \dot{\mathbf{r}}_0 + \dot{\mathbf{T}}\mathbf{d} + \mathbf{T}\dot{\mathbf{d}} \quad (4.16)$$

The displacement \mathbf{d} and its derivative are related to the generalised nodal displacements by:

$$\begin{aligned} \mathbf{d} &= \mathbf{N}\mathbf{q} \\ \dot{\mathbf{d}} &= \mathbf{N}\dot{\mathbf{q}} \end{aligned} \quad (4.17)$$

Recalling that the shape functions must allow for rigid body displacement of the element, the expression of $\dot{\mathbf{r}}_0$ is similar to (4.17):

$$\dot{\mathbf{r}}_0 = \mathbf{T} \mathbf{N} \dot{\mathbf{q}}_r \quad (4.18)$$

where $\dot{\mathbf{q}}_r$ is the generalised rigid-body velocity vector.

Now, the kinetic energy of the element is given by:

$$T = \frac{1}{2} \int_0^L \rho A \dot{\mathbf{r}}^T \dot{\mathbf{r}} dx \quad (4.19)$$

Replacing the velocity vector by its expression in (4.19) gives:

$$\begin{aligned} T = \frac{1}{2} \int_0^L \rho A & (\dot{\mathbf{q}}_r^T \mathbf{N}^T \mathbf{N} \dot{\mathbf{q}}_r + 2 \dot{\mathbf{q}}_r^T \mathbf{N}^T \mathbf{T}^T \dot{\mathbf{T}} \mathbf{N} \mathbf{q} + \\ & 2 \dot{\mathbf{q}}_r^T \mathbf{N}^T \mathbf{N} \dot{\mathbf{q}} + \mathbf{q}^T \mathbf{N}^T \dot{\mathbf{T}}^T \dot{\mathbf{T}} \mathbf{N} \mathbf{q} + \\ & 2 \mathbf{q}^T \mathbf{N}^T \dot{\mathbf{T}}^T \mathbf{T} \mathbf{N} \dot{\mathbf{q}} + \dot{\mathbf{q}}^T \mathbf{N}^T \mathbf{N} \dot{\mathbf{q}}) dx \end{aligned} \quad (4.20)$$

After substituting the expressions of T , U_{int} and the potential energy due to external forces into (4.7) and after some manipulations, the equations of motion of one element are obtained.

$$\mathbf{M} \ddot{\mathbf{q}} + 2 \mathbf{M}_c \dot{\mathbf{q}} + (\mathbf{M}_a + \mathbf{K}) \mathbf{q} = \mathbf{p} - \mathbf{M} \ddot{\mathbf{q}}_r \quad (4.21)$$

where the different matrices are defined by:

$$\begin{aligned} \mathbf{M} &= \int_0^L \rho A \mathbf{N}^T \mathbf{N} dx \\ \mathbf{M}_c &= \int_0^L \rho A \mathbf{N}^T \mathbf{T}^T \dot{\mathbf{T}} \mathbf{N} dx \\ \mathbf{M}_a &= \int_0^L \rho A \mathbf{N}^T \mathbf{T}^T \ddot{\mathbf{T}} \mathbf{N} dx \end{aligned} \quad (4.22)$$

The external forces applied at the nodes and the one transmitted from adjacent elements or links are represented by the force vector \mathbf{p} , and $\mathbf{M}\ddot{\mathbf{q}}_r$ is the force vector due to the rigid-body motion. Furthermore, $2\mathbf{M}_c \dot{\mathbf{q}}$ represents the Coriolis type forces and $\mathbf{M}_a \mathbf{q}$ is the contribution of forces generated by normal and tangential accelerations. The matrix \mathbf{M} is given by:

$$\mathbf{M} = \begin{bmatrix} \mathbf{M}_1 & \\ & \mathbf{M}_2 \end{bmatrix} \quad (4.23)$$

where the mass matrices \mathbf{M}_1 and \mathbf{M}_2 are associated with the axial and the transversal modes respectively and given by:

$$\mathbf{M}_1 = \frac{\rho AL}{6} \begin{bmatrix} 2 & 1 \\ 1 & 2 \end{bmatrix}$$

$$\mathbf{M}_2 = \frac{\rho AL}{420} \begin{bmatrix} 156 & 22L & 54 & -13L \\ & 4L^2 & 13L & -3L^2 \\ & \text{sym} & 156 & -22L \\ & & & 4L^2 \end{bmatrix} \quad (4.24.a)$$

$$\mathbf{M}_c = \frac{\omega \rho AL}{60} \begin{bmatrix} 0 & 0 & -21 & -3L & -9 & 2L \\ & 0 & -9 & -2L & -21 & 3L \\ & & 0 & 0 & 0 & 0 \\ & & & 0 & 0 & 0 \\ & & & & 0 & 0 \\ & & & & & 0 \end{bmatrix} \quad (4.24.b)$$

$$\mathbf{M}_a = \alpha \mathbf{M}_c - \omega^2 \mathbf{M}$$

4.2.3 Transformation to global coordinates

The matrices developed in the previous section are expressed in the local or element coordinate system (x_e, y_e) . In practice, the mechanism, and structures in general, are made up of elements with different orientations. Therefore, expressing the

displacements in a coordinate system particular to each element will create difficulties in matching the displacements at a given node during the assembling process. The solution would be to express all matrices and vectors in the unified reference coordinate system (X,Y). The transformation matrix between the two coordinate systems is depicted in Fig. 4.4 and given by:

$$\begin{Bmatrix} x_e \\ y_e \end{Bmatrix} = \begin{bmatrix} \cos(\theta) & \sin(\theta) \\ -\sin(\theta) & \cos(\theta) \end{bmatrix} \begin{Bmatrix} X \\ Y \end{Bmatrix} \quad (4.25)$$

This transformation holds for displacements at both ends. If the displacements in the reference coordinate system are denoted q_g , they are related to the nodal displacements q by:

$$\begin{Bmatrix} q_1 \\ q_2 \\ q_3 \\ q_4 \\ q_5 \\ q_6 \end{Bmatrix} = \begin{bmatrix} \cos(\theta) & 0 & \sin(\theta) & 0 & 0 & 0 \\ 0 & \cos(\theta) & 0 & 0 & \sin(\theta) & 0 \\ -\sin(\theta) & 0 & \cos(\theta) & 0 & 0 & 0 \\ 0 & 0 & 0 & 1 & 0 & 0 \\ 0 & -\sin(\theta) & 0 & 0 & \cos(\theta) & 0 \\ 0 & 0 & 0 & 0 & 0 & 1 \end{bmatrix} \begin{Bmatrix} q_{g1} \\ q_{g2} \\ q_{g3} \\ q_{g4} \\ q_{g5} \\ q_{g6} \end{Bmatrix} = R q_g \quad (4.26)$$

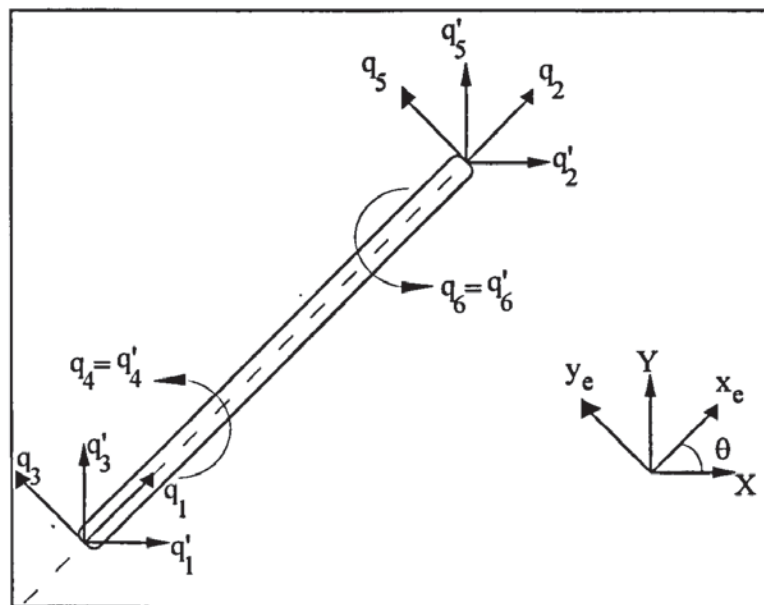


Fig. 4.4: Transformation between local and reference coordinate system.

In order to determine the stiffness and mass matrices in the reference coordinate system, equation (4.26) is differentiated twice and substituted into (4.21), after pre-multiplying by \mathbf{R}^T the equations of motion in a global coordinate system are obtained as:

$$\mathbf{M}_g \ddot{\mathbf{q}}_g + \mathbf{K}_g \mathbf{q}_g = \mathbf{p}_g - \mathbf{M}_g \ddot{\mathbf{q}}_{gr} - \mathbf{M}_{gc} \dot{\mathbf{q}}_g - \mathbf{M}_{ga} \mathbf{q}_g \quad (4.27)$$

The system matrices are as follows:

$$\begin{aligned} \mathbf{M}_g &= \mathbf{R}^T \mathbf{M} \mathbf{R} \\ \mathbf{K}_g &= \mathbf{R}^T \mathbf{K} \mathbf{R} \\ \mathbf{M}_{gc} &= 2(\mathbf{R}^T \mathbf{M}_c \mathbf{R} + \mathbf{R}^T \mathbf{M} \dot{\mathbf{R}}) \\ \mathbf{M}_{ga} &= \mathbf{R}^T \mathbf{M}_a \mathbf{R} + 2 \mathbf{R}^T \mathbf{M}_c \dot{\mathbf{R}} + \mathbf{R}^T \mathbf{M} \ddot{\mathbf{R}} \end{aligned} \quad (4.28)$$

The equations of motion are arranged in the form given by (4.27) because matrices \mathbf{M}_g and \mathbf{K}_g are symmetrical, a property which can be taken advantage of during the solution of the equations. The matrices \mathbf{M}_{gc} and \mathbf{M}_{ga} are not symmetrical and therefore they should be separated from \mathbf{M}_g and \mathbf{K}_g .

4.2.4 Assembly of the overall matrices.

So far the element matrices have been developed for each element in a local coordinate system and then transformed into a global system. The question to be answered in this section is how to extend the results obtained for the elements to the complete system. The next stage is therefore to assemble the stiffness and mass matrices and the generalised forces vector of the individual elements to form the overall matrices for the entire system. This is achieved by ensuring that the geometric compatibility is satisfied at all nodes i.e. the displacements at the nodes shared by many elements must be the same for each of these elements.

The quantities pertaining to individual elements will be identified by the subscript e . For convenience and since all matrices and vectors will be expressed in the reference coordinate system, the subscript g will be dropped in the remainder of this chapter. Then let \mathbf{q} be the vector of nodal displacements for the complete system. Introducing the matrix \mathbf{L}_e which relates the local nodal element displacements to the global ones, this relation can be written in the form:

$$\mathbf{q}_e = \mathbf{L}_e \mathbf{q} \quad (4.29)$$

\mathbf{L}_e consists of a matrix of zeros and ones. In each row there is at most one element equal to one. If all entries of a given row are zero, this would mean that the corresponding displacement is physically constrained. By replacing (4.29) and its derivatives in the equations of motion, the matrices corresponding to the whole system are identified. They are given by:

$$\begin{aligned} \mathbf{M} &= \sum_{e=1}^{n_e} \mathbf{L}_e^T \mathbf{M}_e \mathbf{L}_e \\ \mathbf{K} &= \sum_{e=1}^{n_e} \mathbf{L}_e^T \mathbf{K}_e \mathbf{L}_e \\ \mathbf{M}_c &= \sum_{e=1}^{n_e} \mathbf{L}_e^T \mathbf{M}_{ce} \mathbf{L}_e \\ \mathbf{M}_a &= \sum_{e=1}^{n_e} \mathbf{L}_e^T \mathbf{M}_{ae} \mathbf{L}_e \end{aligned} \quad (4.30)$$

where n_e is the number of elements

The equations of motion corresponding to the whole mechanism are:

$$\mathbf{M}\ddot{\mathbf{q}} + \mathbf{K}\mathbf{q} = \mathbf{p}_{\text{ext}} - \mathbf{M}\ddot{\mathbf{q}}_r - \mathbf{M}_c\dot{\mathbf{q}} - \mathbf{M}_a\mathbf{q} \quad (4.31)$$

In the assembly process, the forces transmitted from one element or link to the other become internal and they cancel each other. Therefore in (4.31), \mathbf{p}_{ext} is the force vector containing the external forces being applied to the whole mechanism.

Example: Fig. 4.5 shows a four bar mechanism modelled with one element per link.

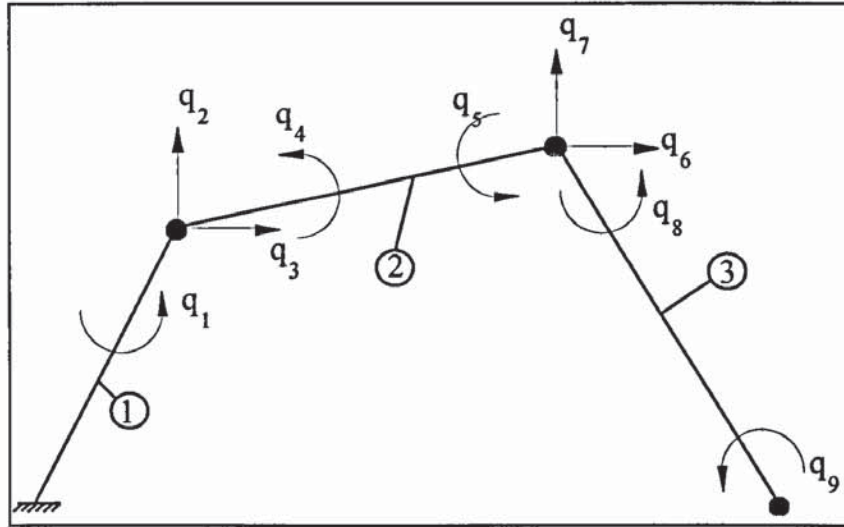


Fig. 4.5: Four bar mechanism modelled with 1 element per link.

In this example the matrices \mathbf{L}_e are:

$$\mathbf{L}_1 = \begin{bmatrix} 0 & 0 & 0 & 0 & 0 & 0 & 0 & 0 & 0 \\ 0 & 0 & 1 & 0 & 0 & 0 & 0 & 0 & 0 \\ 0 & 0 & 0 & 0 & 0 & 0 & 0 & 0 & 0 \\ 0 & 0 & 0 & 0 & 0 & 0 & 0 & 0 & 0 \\ 0 & 1 & 0 & 0 & 0 & 0 & 0 & 0 & 0 \\ 1 & 0 & 0 & 0 & 0 & 0 & 0 & 0 & 0 \end{bmatrix}, \mathbf{L}_2 = \begin{bmatrix} 0 & 0 & 1 & 0 & 0 & 0 & 0 & 0 & 0 \\ 0 & 0 & 0 & 0 & 0 & 1 & 0 & 0 & 0 \\ 0 & 1 & 0 & 0 & 0 & 0 & 0 & 0 & 0 \\ 0 & 0 & 0 & 1 & 0 & 0 & 0 & 0 & 0 \\ 0 & 0 & 0 & 0 & 0 & 0 & 1 & 0 & 0 \\ 0 & 0 & 0 & 0 & 1 & 0 & 0 & 0 & 0 \end{bmatrix}$$

$$\text{and } \mathbf{L}_3 = \begin{bmatrix} 0 & 0 & 0 & 0 & 0 & 1 & 0 & 0 & 0 \\ 0 & 0 & 0 & 0 & 0 & 0 & 0 & 0 & 0 \\ 0 & 0 & 0 & 0 & 0 & 0 & 1 & 0 & 0 \\ 0 & 0 & 0 & 0 & 0 & 0 & 0 & 1 & 0 \\ 0 & 0 & 0 & 0 & 0 & 0 & 0 & 0 & 0 \\ 0 & 0 & 0 & 0 & 0 & 0 & 0 & 0 & 1 \end{bmatrix}$$

It should be noted that the structural stiffness and mass matrices are symmetric, square and positive definite of an order equal to the number of degrees of freedom of the system. However, if the system is not constrained and possesses any rigid body degrees of freedom, the stiffness matrix becomes semi-definite.

4.2.5 Damping effect

In real mechanisms some energy dissipation is always present. Measurement and modelling of the material damping of a system generally proves to be a difficult problem that requires further research. It is therefore necessary to assume an approximate form for the material damping. A proportional viscous damping form is customarily assumed due to the ease in which it can be incorporated into the equations of motion, and also to ensure that the equations of motion can be uncoupled. If the system possesses viscous damping i.e. the damping forces are proportional to the generalised velocities, the equations of motion become:

$$\mathbf{M}\ddot{\mathbf{q}} + \mathbf{C}\dot{\mathbf{q}} + \mathbf{K}\mathbf{q} = \mathbf{f}' \quad (4.32)$$

where all terms on the r.h.s of (4.31) have been grouped in the vector forces \mathbf{f}' .

For the uncoupling procedure, the following coordinate transformation is made

$$\mathbf{q} = \Phi\boldsymbol{\eta} \quad (4.33)$$

where $\boldsymbol{\eta}$ represents the modal amplitude vector and Φ is the modal transformation matrix.

$$\text{Also } \dot{\mathbf{q}} = \Phi\dot{\boldsymbol{\eta}} \text{ and } \ddot{\mathbf{q}} = \Phi\ddot{\boldsymbol{\eta}} \quad (4.34)$$

Substituting (4.33) and (4.34) into (4.32), and pre-multiplying by Φ^T , the following equations hold when the eigenvectors are mass normalised:

$$\ddot{\eta} + \Phi^T C \Phi \dot{\eta} + [\omega^2] \eta = \Phi^T f' \quad (4.35)$$

where $[\omega^2]$ is a diagonal matrix containing the square of the natural frequencies.

In order that the orthogonality of the damping forces is secured, the following must be true:

$$\begin{aligned} \Phi_n^T C \Phi_m &= 0 \quad n \neq m \\ \Phi_n^T C \Phi_n &= \alpha_n \end{aligned} \quad (4.36)$$

A simplified damping form is often used. This is obtained by defining α_n in (4.36) as $2\zeta_n\omega_n$, where ζ_n is the damping ratio for the n th mode and ω_n is its frequency.

4.2.6 Stiffening effect

The strain was assumed to be a linear function of the displacement in (4.4). When the deformations are large, this relation becomes non-linear and rewritten in the form:

$$\varepsilon = B_1 q + \frac{1}{2} q^T B_n^T B_n q \quad (4.37)$$

where B_n is the non-linear strain-displacement matrix.

This leads to the definition of the non-linear stiffness matrix K_n as:

$$\mathbf{K}_n = \int_0^L \mathbf{f}_a \mathbf{B}_n^T \mathbf{B}_n dx \quad (4.38)$$

where \mathbf{f}_a is the axial force in the beam element.

The non-linear stiffness matrix accounts for the fact that a beam deflects more when an axial compression is added but less when a tension is added. The axial forces can be approximately obtained either by quasi-static analysis or when the time marching simulation is used in order to solve the equations of motion, it is derived from the deflections at the previous time step. For a beam element, \mathbf{K}_n is given by:

$$\mathbf{K}_n = \frac{EA(q_2 - q_1)}{L^2} \begin{bmatrix} 0 & 0 & 0 & 0 & 0 & 0 \\ & 0 & 0 & 0 & 0 & 0 \\ & & \frac{6}{5} & \frac{L}{10} & -\frac{6}{5} & \frac{L}{10} \\ & & & \frac{2L^2}{15} & -\frac{L}{10} & -\frac{L^2}{30} \\ \text{sym} & & & & \frac{6}{5} & -\frac{L}{10} \\ & & & & & \frac{2L^2}{15} \end{bmatrix} \quad (4.39)$$

4.3. NATURAL FREQUENCIES AND MODE SHAPES IN A STATIONARY MECHANISM

When the generalised forces vector \mathbf{f} is set to zero and the damping is neglected in (4.32), the harmonic free vibratory motion is described by:

$$(\mathbf{K} - \omega^2 \mathbf{M}) \mathbf{q} = 0 \quad (4.40)$$

The natural frequencies ω_i are found from the following equation called the characteristic equation:

$$\det[\mathbf{K} - \omega^2 \mathbf{M}] = 0 \quad (4.41)$$

If the structure is not constrained some solutions of (4.41) are zero. These frequencies correspond to the rigid body modes. In this case the stiffness matrix is singular. For a particular natural frequency ω_i the associated modal vector \mathbf{q}_i can be found from (4.40). If the system is of order n , i.e. n degrees of freedom, n natural frequencies can be obtained from (4.41). Although these frequencies can be obtained to any desired accuracy from standard computer programs for solving the EVP, one must remember that they are the frequencies of the approximate system. With a reasonable number of appropriate elements some lower fraction of these n frequencies should be good approximations of the frequencies of the real structure. In general the higher frequencies found from (4.41) have no physical significance.

Several methods of computing natural frequencies and modal vectors from (4.40) exist. They can be grouped in the following categories:

- Methods based on the expansion of the characteristic equation (4.41).
- Methods based on the evaluation of $d(\omega^2) = \det[\mathbf{K} - \omega^2 \mathbf{M}]$.
- Methods based on the application of successive transformations leading to a tri-diagonal form or upper (lower) Heissenberg form (for non symmetrical matrices).
- Iterative methods on the eigenvalues.
- Iterative methods on the eigenvectors.
- Subspace iteration methods.

The following factors affect their suitability and efficiency:

1. The size of the problem: It depends on the number of degrees of freedom included in the model.

2. The number of eigenvalues required: This depends on the application and the nature of analysis to be carried out on the model. In the vibration problems the lowest modes contribute most to the steady-state solution and therefore only the lowest natural frequencies are of interest. In contrast, the frequency band required might be wider in acoustic problems.

In most cases a limited number of frequencies is sufficient but in some cases the frequency range might be wider. This could be the case for structures with high modal density i.e. many natural frequencies are present in a certain range of frequencies; or when the calculated modes are used in a transient response analysis with high frequency content in the excitation using modal superposition technique.

3. The required frequency range: In many cases, the methods of solution of the EVP give the eigenvalues in a certain order. However, some methods enable the calculation of eigenvalues in a given interval without having to calculate the lower frequencies first.
4. Ability to calculate close eigenvalues: The problem of finding two eigenvalues close to each other is a delicate numerical problem. Close natural frequencies appear in structures, for example, with many symmetries or when a basic element is repeated many times in the structure. In such a situation the method of solution should be able to distinguish between the different frequencies.
5. Convergence ratio: This factor is linked to the previous one. The convergence of the method is affected a great deal by the existence of close solutions.
6. The cost: the cost of the solution includes the CPU time required to solve the problem, the programming cost which is a function of the complexity of the method and the computer resources available.

The mechanism was modelled with beam elements developed in this chapter. A computer program was written using Matlab to solve the EVP for a particular mechanism. First the number of elements per link was varied (h-version) and then

the degree of the polynomials used in the shape functions was increased (p-version). The latter could be achieved either by adding internal nodes or by increasing the number of nodal generalised coordinates in the model which, in this case was performed by adding curvatures as variables at both ends of one element. The shape functions are given in Appendix A as well as the different matrices used in the p-version of the FEM.

The data of the mechanism studied are given in Table 4.1.

	Input Link	Coupler	Follower	Ground
Length [m]	$L_1=0.170$	$L_2=0.328$	$L_3=0.525$	$L_4=0.547$
Cross Section Area [m ²]*10 ⁻⁶	157.5	85.5	78.75	
Second Moment of Area [m ⁴]*10 ⁻¹²	520.47	83.34	65.12	
The lumped masses of the joints : 0.174 kg				
Material: Steel, Density: 7.85 10 ³ kg/m ³ , Modulus of elasticity: 210 10 ⁹ N/m ²				

Table 4.1: Mechanism data.

Figs. 4.6.a to 4.6.d show a comparison between the h-version and the p-version of the FEM for the first four natural frequencies. They also show the influence of the number of elements per link on these frequencies. In these figures the p-version 1 corresponds to the element with an internal node whereas in the p-version 2, two curvatures have been added as nodal coordinates (see Fig. 4.7).

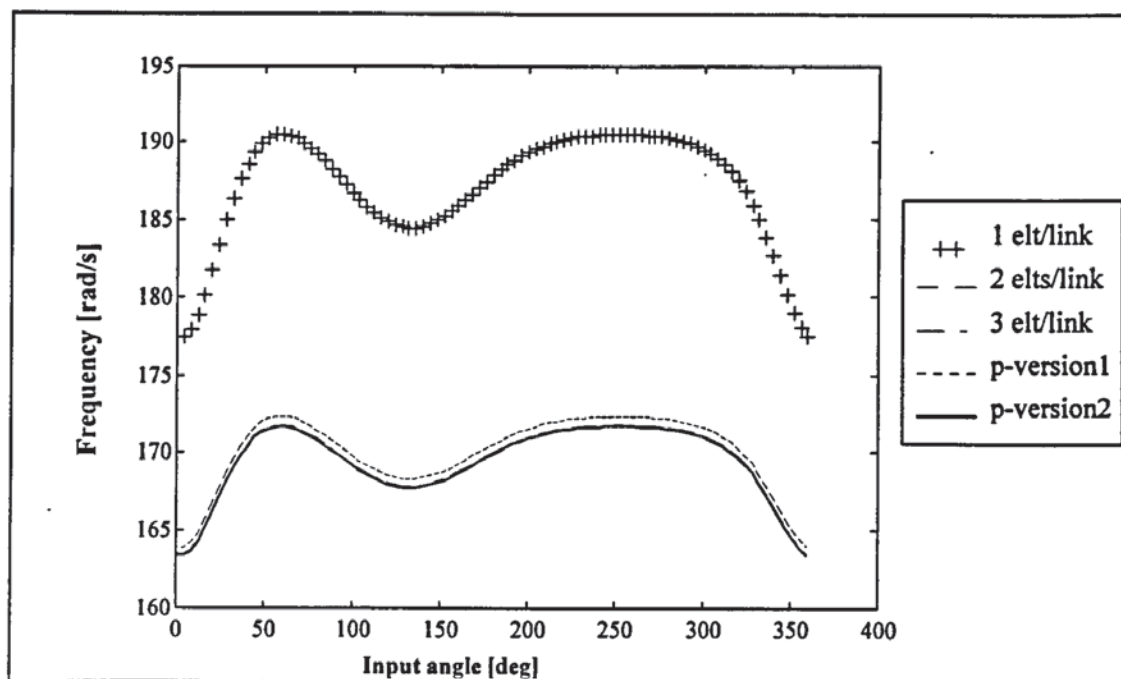


Fig. 4.6.a: First natural frequency.

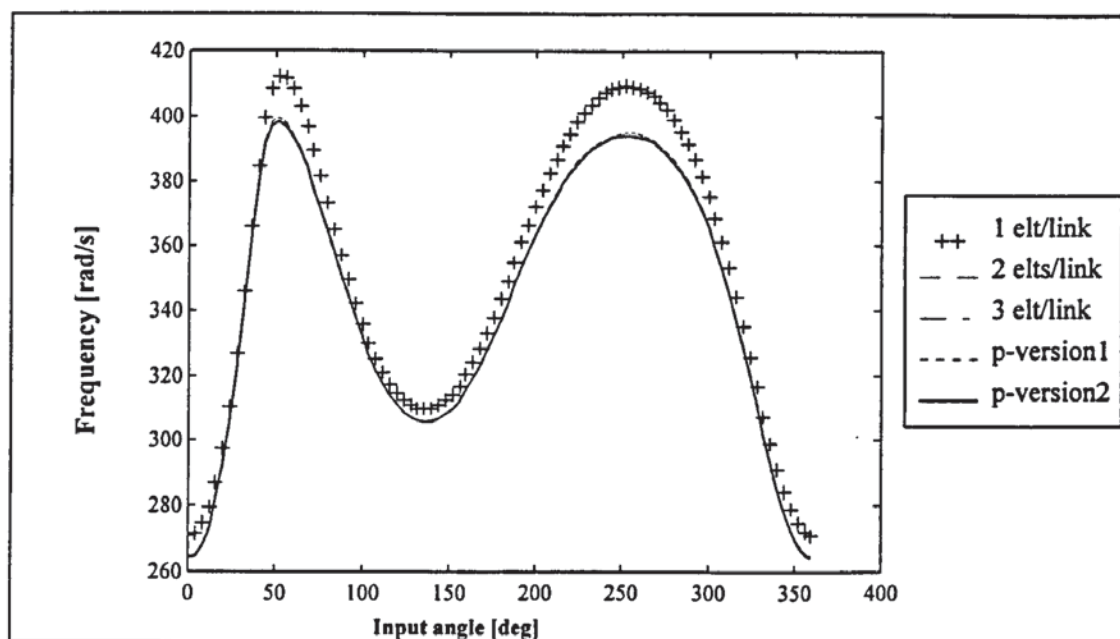


Fig. 4.6.b: Second natural frequency.

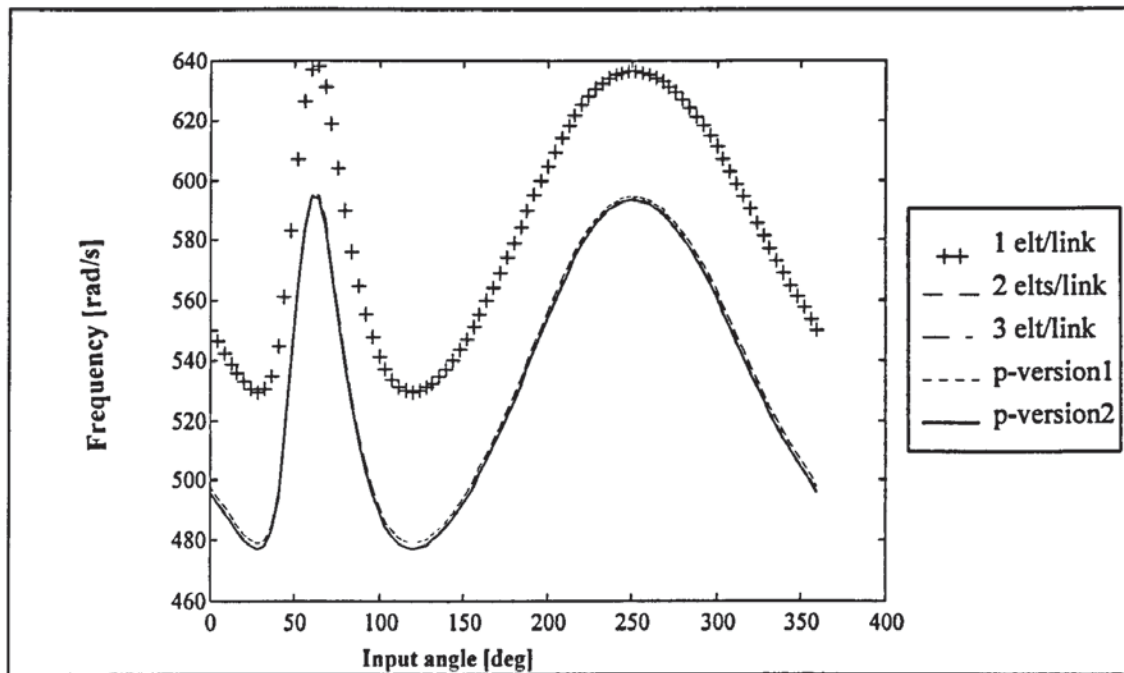


Fig. 4.6.c: Third natural frequency.

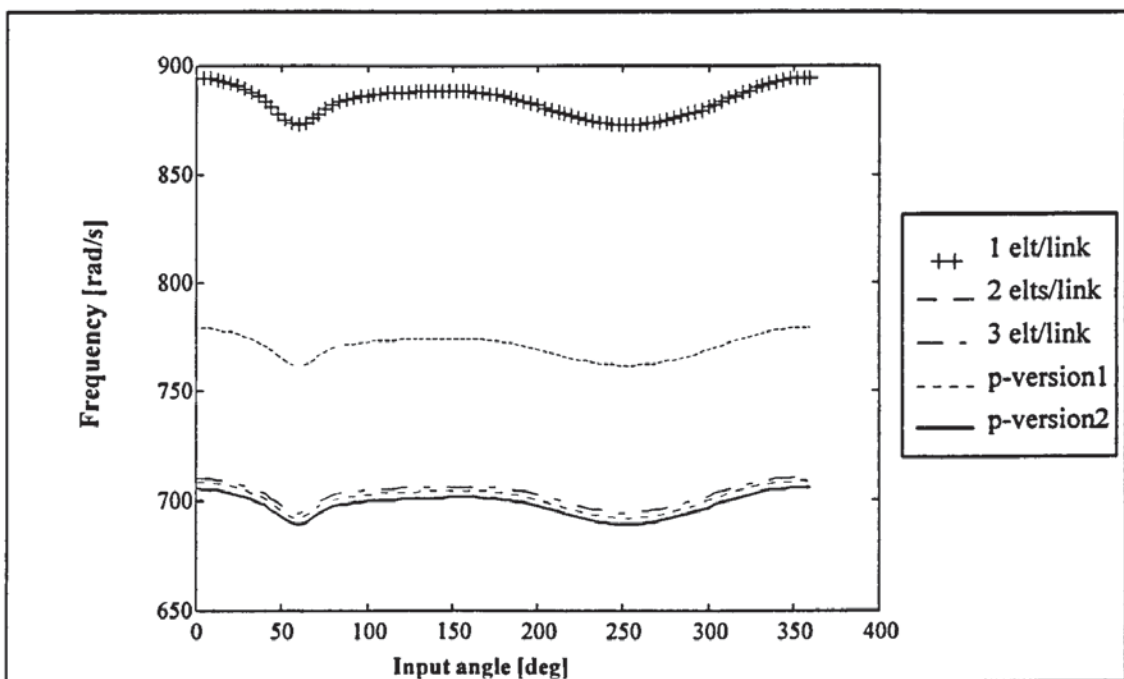


Fig. 4.6.d: Fourth natural frequency.

From these figures it can be concluded that:

- The model with 1 element per link over-estimates the natural frequencies. A mean difference of 10% for the first natural frequency and 26% for the fourth

one have been calculated with respect to the model with 3 elements per link. Therefore, multi-element idealisation should be used to model the mechanism.

- In the h-version the rate of convergence is quite high. A three elements model predicts the frequencies up to the fourth frequency accurately.
- In all cases, the p-version 2 gives better results. With only one element per link, the p-version 2 gives almost the same result as the h-version with 3 elements per link. Furthermore, the number of degrees of freedom in the latter case is 27 compared to 10 in the former.

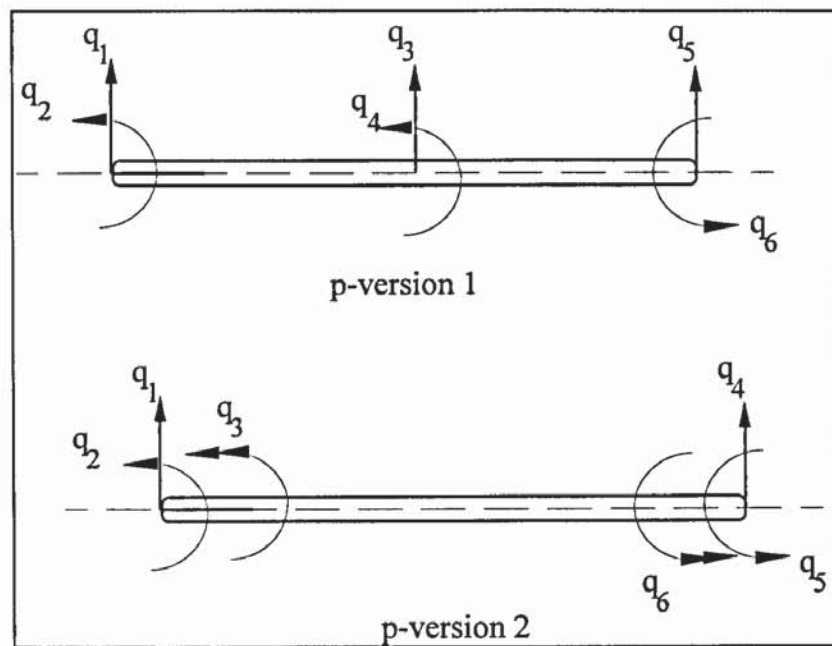


Fig. 4.7: Nodal coordinates in the p-version of the FEM.

4.4. CONCLUSION

The FEM has been presented and applied to investigate the elastodynamic vibration a four-bar mechanism. The equations of motion have been derived where all the effects of the rigid body motion on the elastic response have been taken into account. The stiffening effect due to the axial forces has also been included.

Moreover, the two classical versions of the FEM have been considered in order to solve the EVP, namely the h-version and the p-version. It has been shown that in general the latter is more accurate than the former for the same computing effort.

Chapter 5

DYNAMIC STIFFNESS METHOD

5.1. INTRODUCTION

The previous chapter was devoted exclusively to the vibration analysis of a four-bar mechanism using the FEM. The free undamped vibration of the mechanism led to a linear EVP. In this chapter a method of analysis based on the dynamic stiffness method will be presented. The dynamic stiffness matrix is usually a linear function of the frequency squared. This ceases to be true in the case of large systems which have been condensed or when exact rather than polynomial displacement functions are chosen. In the latter cases, usual methods of solution of the EVP are no longer valid and special algorithms are needed to solve the "non-linear" EVP which governs the free undamped vibration of the system. The success of the dynamic stiffness method resides in the fact that it can model beam elements very accurately based on the exact solutions of the elements in the modes considered. This makes the dynamic stiffness method impossibly difficult to use for general structures comprising elements other than beams.

An important requirement in the dynamic analysis of structures, and mechanisms in general, is to employ an adequate accuracy of computation to ensure that the natural frequencies and mode shapes are obtained with reasonable finite element discretisation, even for the higher modes. The size of the basic matrices depends on the number of unknown coefficients in the assumed deformation functions, and the size of the system matrices depends on the number of elements in the FE model. For reasons of economy, a desirable objective is the smallest overall system matrices with a given solution accuracy. The proper choice of the deformation functions is therefore the key to meeting this objective. This may be accomplished by the use of

exact rather than approximate displacement functions for the elements, obtained from the solution of the differential equations governing the free vibrational behaviour of structural components. A finite set of displacements of suitably localised joints of the structure is used to describe the total displacement. When applied to a structure, the resulting non-linear EVP is solved by a straightforward and infallible method which converges on as many of the natural frequencies as may be required.

The method was originally developed for rigidly jointed plane or space frames. Members of the structure are treated as being continuous and uniform rather than an approximately equivalent lumped mass system. It follows that each member of the structure, and hence the structure itself, has an infinite number of degrees of freedom so that there are an infinite number of natural frequencies for the structure. With this method it is possible to calculate the number of natural frequencies which lie below any chosen frequency without determining them and hence to converge on any required natural frequency to any specific accuracy.

The matrices for an exact solution are frequency-dependent and form a non-linear EVP. As the methods of solution which are presented for a linear eigen-system are inapplicable, the determinant method must be invoked. With the property of the Sturm sequence and the treatment of asymptotic poles, the determinant method has been proved to be efficient and reliable. The differential equation and general solution for the flexural and extensional vibrations of a uniform straight beam have been presented by many investigators, for example Wittrick and Williams (1970, 1971) and Richards and Leung (1977). Basci *et al* (1979) also reported that the influence of rotatory inertia on the frequencies of vibration is rather small, even for higher frequencies. In their application the effects of shear deformation and rotatory inertia were ignored. A comparison of the dynamic stiffness method, the FEM and the lumped mass approach was given by Henshell and Warburton (1969); the

examples treated were a free-free beam with one attached mass and a single storey two bay portal frame. In all cases, it was shown that the lumped mass method underestimated the natural frequencies, whereas the FEM overestimated them. When the computational time required was investigated it was found that the lumped mass required the least time; the exact method, in contrast, needed a long computational time. An important advance in the use of the dynamic stiffness method was made through the algorithm of Wittrick and Williams (1970) to automatically calculate natural frequencies to any degree of accuracy. Akesson (1976) developed a computer program for vibration analysis of planar frames by the dynamic stiffness method. Recently, a formulation of dynamic stiffness method was extended by Liu and Lin (1993) to the analysis of forced vibration of flexible body systems. In their paper, three applications were considered, namely a cantilever beam, a rotating beam and a slider crank mechanism.

5.2. APPLICATION OF THE DYNAMIC STIFFNESS METHOD TO THE ANALYSIS OF FOUR-BAR MECHANISMS

5.2.1 Exact displacement functions

Any link of the mechanism exhibits two basic modes of vibration: flexural and extensional modes. First, consider a beam in a flexural mode. The transverse displacement at any point x is a function of x and time t , denoted by $v(x,t)$. The governing differential equation of motion for a transverse vibration of a prismatic beam in the general form is given by:

$$EI \frac{\partial^4 v}{\partial x^4} + \rho A \frac{\partial^2 v}{\partial t^2} = 0 \quad (5.1)$$

where ρ is the material density, A is the cross section area, E is Young's modulus of elasticity and I the moment of inertia. Rotary inertia and shear have been ignored and the assumption that plane sections remain plane is implicitly made. Let

$$v(x,t) = V(x)\sin(\omega t + \phi) \quad (5.2)$$

where ϕ is the phase angle, $V(x)$ is a function of x only and ω is the angular frequency of harmonic motion.

Combining (5.1) and (5.2):

$$\frac{d^4 V(x)}{dx^4} - \lambda^4 V(x) = 0 \quad (5.3)$$

$$\text{where } \lambda^4 = \frac{\rho A}{EI} \omega^2 \quad (5.4)$$

It can be shown that the solution of (5.3) is in the form:

$$V(x) = c_1 \sin(\lambda x) + c_2 \cos(\lambda x) + c_3 \sinh(\lambda x) + c_4 \cosh(\lambda x) \quad (5.5)$$

Now, consider the beam in axial vibration mode; assuming that the axial displacement is $u(x,t)$, then the governing differential equation of motion for a uniform beam in this mode is given by:

$$EA \frac{\partial^2 u}{\partial x^2} = \rho A \frac{\partial^2 u}{\partial t^2} \quad (5.6)$$

As before, letting

$$u(x,t) = U(x)\sin(\omega t + \varphi) \quad (5.7)$$

and using separation of variables method, (5.6) reduces to:

$$\frac{d^2 U}{dx^2} + \beta^2 U = 0 \quad (5.8)$$

$$\text{where } \beta^2 = \frac{\rho}{E} \omega^2 \quad (5.9)$$

The general solution of (5.8) gives:

$$U(x) = c_5 \sin(\beta x) + c_6 \cos(\beta x) \quad (5.10)$$

In (5.5) and (5.10), c_i ($i = 1$ to 6) are arbitrary constants determined from boundary conditions. These equations represent the exact displacement functions in flexural and axial modes. One advantage of using such functions is that the results obtained from them will be independent of element subdivision. On the other hand, the shape functions satisfy both the boundary conditions and the equation of motion. An attempt to choose a displacement function which satisfies the equation of motion was made by Cohen and McCallion (1969). In their paper, the usual displacement polynomial functions were corrected so that they satisfy the equation of motion for a beam in bending. They found that this method leads to better results; a maximum error of 0.76% for the 12th eigenvalue was obtained compared to 11% for a beam modelled with 12 elements. It is therefore anticipated that the natural frequencies and mode shapes will be more accurate than the ones calculated from the FEM when exact functions are used.

Summarising, with the use of exact functions the displacement at any point x is evaluated in terms of circular and hyperbolic expressions. It may also be noted that

the transverse and longitudinal displacements are mutually independent of each other, but the relationship between the two frequency parameters is given by:

$$\beta = \lambda^2 \sqrt{\frac{I}{A}} \quad (5.11)$$

5.2.2 Stiffness and mass matrices

The procedure used for obtaining the stiffness and mass matrices in bending and in tension for a beam element using exact displacement functions is exactly the same as in the case of the displacement polynomial functions, already discussed in the previous chapter. The equations which link the nodal deflections q_i and the unknowns c_i are obtained using (5.5) and (5.10) and by substituting the boundary conditions respectively. Using the notations given in Fig. 4.2, the vector of element nodal displacements \mathbf{q} is given by:

$$\begin{Bmatrix} q_1 \\ q_2 \\ q_3 \\ q_4 \\ q_5 \\ q_6 \end{Bmatrix} = \begin{bmatrix} 0 & 1 & 0 & 0 & 0 & 0 \\ \sin(\beta L) & \cos(\beta L) & 0 & 0 & 0 & 0 \\ 0 & 0 & 0 & 1 & 0 & 1 \\ 0 & 0 & \lambda & 0 & \lambda & 0 \\ 0 & 0 & \sin(\lambda L) & \cos(\lambda L) & \sinh(\lambda L) & \cosh(\lambda L) \\ 0 & 0 & \lambda \cos(\lambda L) & -\lambda \sin(\lambda L) & \lambda \cosh(\lambda L) & \lambda \sinh(\lambda L) \end{bmatrix} \begin{Bmatrix} c_1 \\ c_2 \\ c_3 \\ c_4 \\ c_5 \\ c_6 \end{Bmatrix} \quad (5.12)$$

This may be written more concisely as:

$$\mathbf{q} = \mathbf{A} \mathbf{c} \quad (5.13)$$

In computing the mass and stiffness matrices, the methodology exposed in the previous chapter is still applicable. For structures, or more generally mechanisms for which instantaneous structure formulation have been adopted (i.e. the matrices due

to Coriolis forces, normal and tangential acceleration effects are neglected), it is more convenient to work with the dynamic stiffness matrix. In this case and noting \mathbf{D} the dynamic stiffness matrix, the equations of harmonic vibratory motion are simply:

$$\mathbf{D} \mathbf{q} = \mathbf{f} \quad (5.14)$$

where $\mathbf{D} = \mathbf{K} - \omega^2 \mathbf{M}$

The generalised forces vector \mathbf{f} associated with the nodal displacements vector \mathbf{q} for free-free beam element is given by:

$$\mathbf{f}^T = E \left[A \frac{dU(0)}{dx} \quad -A \frac{dU(L)}{dx} \quad I \frac{d^3V(0)}{dx^3} \quad -I \frac{d^2V(0)}{dx^2} \quad -I \frac{d^3V(L)}{dx^3} \quad I \frac{d^2V(L)}{dx^2} \right] \quad (5.15)$$

A theorem by Richards and Leung (1977) states that the mass matrix is obtained by differentiating the dynamic stiffness matrix with respect to the square of the frequency. Therefore:

$$\mathbf{M} = -\frac{\partial \mathbf{D}}{\partial \omega^2} \quad (5.16)$$

and

$$\mathbf{K} = \mathbf{D} + \omega^2 \mathbf{M} \quad (5.17)$$

Developing (5.15) and rearranging in the form of (5.14), the dynamic stiffness matrix is identified as:

$$\mathbf{D} = \begin{bmatrix} EA \begin{bmatrix} F_7 & F_8 \\ F_8 & F_7 \end{bmatrix} & \\ & EI \begin{bmatrix} F_6 & -F_4 & F_5 & F_3 \\ & F_2 & -F_3 & F_1 \\ \text{sym} & & F_6 & F_4 \\ & & & F_2 \end{bmatrix} \end{bmatrix} \quad (5.18)$$

The mass matrix is then obtained by applying (5.16).

$$\mathbf{M} = \begin{bmatrix} EA \begin{bmatrix} G_7 & G_8 \\ G_8 & G_7 \end{bmatrix} & \\ & \rho AL \begin{bmatrix} G_6 & -G_4 & G_5 & G_3 \\ & G_2 & -G_3 & G_1 \\ \text{sym} & & G_6 & G_4 \\ & & & G_2 \end{bmatrix} \end{bmatrix} \quad (5.19)$$

where the functions F_i and G_i are given in Appendix B.

Note that the displacement functions chosen in the FEM are solutions of (5.3) when λ and β are equal to zero. Therefore, one should expect that when ω is set to zero in (5.16) and (5.17), the same matrices given by the FEM are obtained. The difference between the two set of matrices can be considered as a correction to the matrices given by the FEM. Developing \mathbf{M} and \mathbf{K} as power series with respect to ω^2 , it is found:

$$\begin{aligned}
\mathbf{M} = & \rho A L \begin{bmatrix} \frac{1}{6} \begin{bmatrix} 2 & 1 \\ 1 & 2 \end{bmatrix} \\ & \frac{1}{420} \begin{bmatrix} 156 & 22L & 54 & -13L \\ & 4L^2 & 13L & -3L^2 \\ \text{sym} & & 156 & -22L \\ & & & 4L^2 \end{bmatrix} \end{bmatrix} + \\
& \rho A L \begin{bmatrix} \frac{L^2 \rho}{180E} \begin{bmatrix} 8 & 7 \\ 7 & 8 \end{bmatrix} \\ & \frac{L^4 \rho A}{80850EI} \begin{bmatrix} 59 & \frac{223}{18}L & \frac{1279}{24} & -\frac{1681}{144}L \\ & \frac{71}{27}L^2 & \frac{1681}{144}L & -\frac{1097}{432}L^2 \\ \text{sym} & & 59 & -\frac{223}{18}L \\ & & & \frac{71}{27}L^2 \end{bmatrix} \omega^2 + \\
& \rho A L \begin{bmatrix} \frac{L^4}{5040} \left(\frac{\rho}{E} \right)^2 \begin{bmatrix} 32 & 31 \\ 31 & 32 \end{bmatrix} \\ & \frac{L^8}{264864600} \left(\frac{\rho A}{EI} \right)^2 \begin{bmatrix} 551 & \frac{3547}{30}L & \frac{5801}{10.6} & -\frac{112631}{960}L \\ & \frac{127}{5}L^2 & \frac{112631}{960}L & -\frac{899}{35.5}L^2 \\ \text{sym} & & 551 & -\frac{3547}{30}L \\ & & & \frac{127}{5}L^2 \end{bmatrix} \omega^4 + \dots \end{bmatrix}
\end{aligned}$$

and

$$\begin{aligned}
\mathbf{K} = & \begin{bmatrix} \frac{EA}{L} \begin{bmatrix} 1 & -1 \\ -1 & 1 \end{bmatrix} \\ & \frac{EI}{L^3} \begin{bmatrix} 12 & 6L & -12 & 6L \\ & 4L^2 & -6L & 2L^2 \\ \text{sym} & & 12 & -6L \\ & & & 4L^2 \end{bmatrix} \end{bmatrix} + \\
& \begin{bmatrix} \frac{L^3 \rho^2 A}{360E} \begin{bmatrix} 8 & 7 \\ 7 & 8 \end{bmatrix} \\ & \frac{(\rho A L)^2 L^3}{161700EI} \begin{bmatrix} 59 & \frac{223}{18}L & \frac{1279}{24} & -\frac{1681}{144}L \\ & \frac{71}{27}L^2 & \frac{1681}{144}L & -\frac{1097}{432}L^2 \\ \text{sym} & & 59 & -\frac{223}{18}L \\ & & & \frac{71}{27}L^2 \end{bmatrix} \omega^4 + \dots \end{bmatrix}
\end{aligned}$$

5.3. WITTRICK-WILLIAMS ALGORITHM

Once the stiffness and mass matrices have been obtained, the procedure of transformation from local to global coordinate system and assemblage is carried out to yield the overall system matrices. This is done in a similar manner as in the conventional FEM. However, the matrices obtained are frequency dependent due to the presence of λ and β in the expressions of these matrices. Therefore, the free undamped vibration leads to the following non-linear EVP:

$$\mathbf{D}(\omega) \mathbf{q} = \mathbf{0} \quad (5.20)$$

In some exceptional circumstances, for some frequencies, (5.20) admits the solution $\mathbf{q} = \mathbf{0}$; at these frequencies \mathbf{q} is a vector of displacements at nodes of the corresponding natural modes of the system. One of the main advantages of the algorithm of Wittrick and Williams is that it accounts for these solutions as well as the solutions of the usual EVP, $\det(\mathbf{D}) = 0$.

Despite the fact that the exact displacement method for frames was developed in the early 1940's by Kolousek (1973), no reliable method of solution of the EVP was developed before 1970, the date of publication of the algorithm by Wittrick and Williams. Up till then, the natural frequencies had been calculated by a simple frequency scanning, where the determinant of the dynamic stiffness matrices was evaluated for various frequencies with constant step size. Once a sign change has been detected, the programme then activates a subroutine which calculates the trapped natural frequency using bisection or some other suitable algorithms. This procedure has some disadvantages, firstly the solutions of (5.20) corresponding to $\mathbf{q} = \mathbf{0}$ are not calculated with this method. Secondly if two or more natural frequencies are very close, some solutions may be missed by the programme. To

overcome the latter problem a very small step size is chosen in order to account for all solutions. However, a great deal of CPU time is unnecessarily consumed.

The algorithm developed by Wittrick and Williams is based on a theorem by Rayleigh which states that: "If one constraint is imposed upon a linearly elastic structure, whose natural frequencies of vibration, arranged in ascending order of magnitude, are ω_r , the natural frequencies ω'_r of the constrained structure are such that $\omega_r \leq \omega'_r \leq \omega_{r+1}$, $r = 1, 2, 3, \dots$ ". A corollary to this theorem would be: "If one constraint is removed from a structure, the number of natural frequencies which lie below some fixed chosen frequency either remains unchanged or increases by one". From this corollary it can be verified that, by extension, if k constraints are removed from a structure the number of natural frequencies which lie below a chosen frequency increases by a number s where $0 \leq s \leq k$. This represents the core of Wittrick-Williams algorithm.

The algorithm is valid for any linear finite or infinite elastic system with a dynamic stiffness matrix $\mathbf{D}(\omega)$. An infinite system is defined as a system which possesses an infinite number of natural frequencies through the use of exact shape functions. The algorithm calculates the number of natural frequencies which are less than some fixed chosen frequency ω_0 denoted by $J(\omega_0)$ and given by:

$$J(\omega_0) = J_0(\omega_0) + s\{\mathbf{D}(\omega_0)\} \quad (5.21)$$

where $J_0(\omega_0)$ is the number of natural frequencies which would still be exceeded by ω_0 if n constraints were imposed so as to make all displacements \mathbf{q} zero, and $s\{\mathbf{D}(\omega_0)\}$ is the sign-count of $\mathbf{D}(\omega_0)$ defined as the number of negative characteristic values of $\mathbf{D}(\omega_0)$. It is also equal to the number of negative elements on the diagonal of its upper triangular form as was suggested by the authors of the algorithm. In the present study, it has been evaluated as the number of negative eigenvalues of

$D(\omega_0)$. This came about because the package used for the development of the programs, Matlab, has a built-in function to calculate the eigenvalues.

Basically, the algorithm locates a frequency interval containing a root by an incremental method. The search is carried out in constant frequency steps supplied by the user of the program. At every step, the dynamic stiffness matrix is calculated and the number of its negative eigenvalues counted. Also, the sign count is corrected for the number of poles below the trial frequency. Hence the program needs to start by calculating and sorting all natural frequencies of the clamped-clamped beams of the structure in a given range. When the corrected sign count changes by one, the program activates a procedure which locates the root in the current interval between the present and the last trial frequencies. For reason of economy, the frequency step size should be quite large in order to avoid unnecessary calculations. However, if the step size is too large the program would "jump over" more than one natural frequency in one step and the corrected sign count would increase by the number of roots in the trial interval. The program scans backwards in order to locate an interval containing one root only. Once this is done, many methods are available to locate the root, the bisection procedure does this starting from an initial interval $[a_0, b_0]$ by reducing the width of the interval; after p iterations the interval is $[a_p, b_p]$ of width $(b_0 - a_0)2^{-p}$. Therefore the procedure converges upon the root to any required accuracy.

5.4. APPLICATIONS

In this section two applications are examined to show the superiority of the dynamic stiffness matrix method over the conventional FEM. The first application is a simple portal frame with its bars rigidly connected together, and clamped to the ground. The second application is the four-bar mechanism already treated in the previous chapter. In fact, the dynamic stiffness method was applied to investigate different structures

(portal frame with pinned joints, structures with inclined members, etc.); the reason for not considering the other applications is, first for brevity and second because in all cases the latter method gives better results.

5.4.1 Portal frame

The portal frame has been investigated by many researchers. Rieger and McCallions (1965) tabulated the first two eigenvalues of portal frames having identical members for two cases, namely for clamped and pinned footings. The entries in the tables are two dimensionless numbers. A linear interpolation was proposed when these numbers for a particular portal frame did not coincide with the entries given in the tables. The tabulated natural frequencies are calculated using the dynamic stiffness method. Chang (1978) considered more general frames with inclined members. He showed that the axial vibration in a portal frame could be neglected but for frames with inclined members this would lead to erroneous results. He also confirmed the results of previous studies in that the natural frequencies of frames may be close together or even coincident for some angles of inclination. Recently Jara-Almonte and Mitchell (1988a, 1988b) combined the dynamic stiffness method and the FEM in order to improve the extraction of high eigen-frequencies. The method was then formulated and applied to a portal frame and a Vierendeel truss. They showed, as expected, that the exact element model provides better results even for high frequencies than the standard FE model. They also showed that incorporating an exact element into a FE formulation reduces the number of finite elements required to obtain the same number of acceptable natural frequencies. In contrast with the papers by Rieger and McCallions (1965) and Chang (1978), Jara-Almonte and Mitchell accounted for all natural frequencies including the ones leading to $\mathbf{q} = \mathbf{0}$ in (5.20). Such frequencies exist in the case of the portal frame considered by Chang but he missed it due to the method of solution he used to obtain the EVP.

The solution proposed to overcome this problem is to add at least one fictitious joint in the middle of the bars (i.e. to model the bars with at least two "elements"). This would prevent the aforementioned frequencies becoming poles of the dynamic stiffness matrix, rather it would make its determinant vanish. Fig. 5.1 shows the variation of the determinant of the dynamic stiffness matrix against frequency for the portal frame considered for one and two elements per bar. It is seen that the fourth frequency missed by Chang which is a pole when the frame is modelled with one element per bar becomes an ordinary natural frequency for two elements per bar. The same problem occurs when the conventional FEM is applied; at least two elements per bar are needed to account for such frequencies. However a fundamental difference exists between the two methods, the natural frequencies do not change when the multi-element model combined with the dynamic stiffness method are considered whereas in the FEM they decrease when the number of finite elements increases.

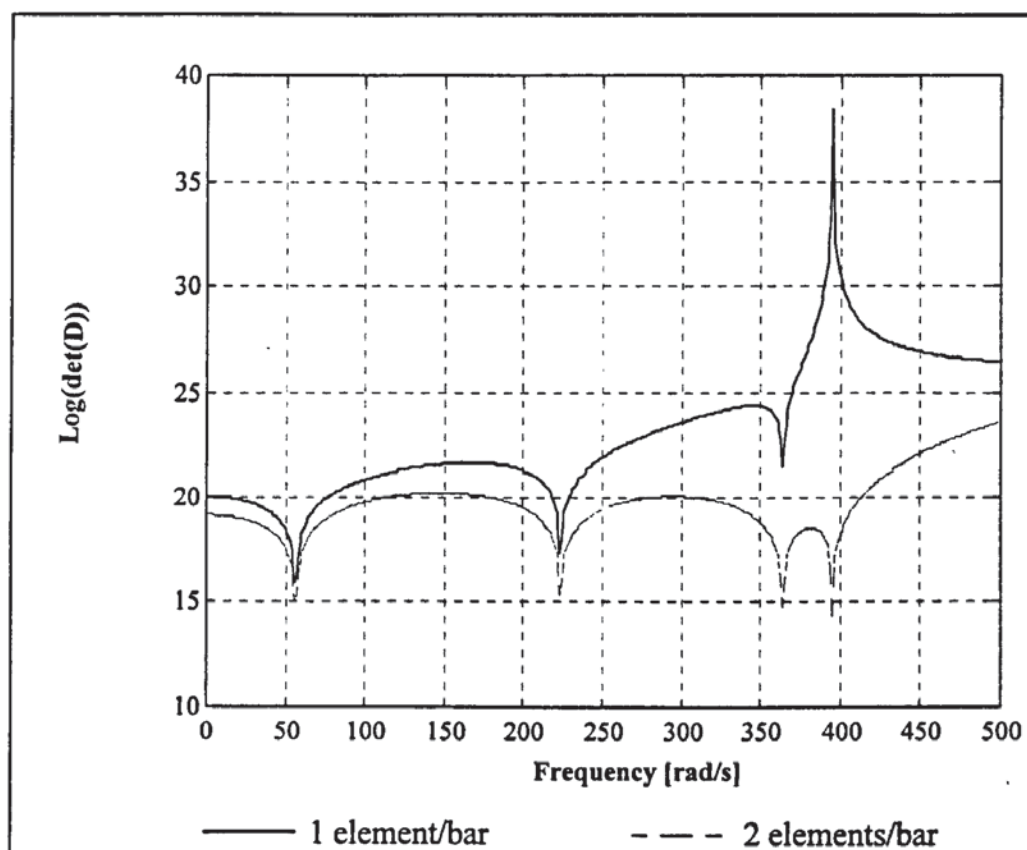


Fig. 5.1: Logarithm of the determinant of D for one and two elements/bar models.

The schematic and the data of the portal frame studied here are given in Fig. 5.2. The natural frequencies are given in Table 5.1.a and the relative error in Table 5.1.b. The mode shapes corresponding to different models are then given. The results obtained are in accordance with the results published by Chang (1978) except for the fourth frequency which leads to $q = 0$ as pointed out earlier and corresponds to one of the natural frequencies of clamped-clamped beam. From Table 5.1.b it is seen that the relative error is quite low for the first set of natural frequencies corresponding to half the number of frequencies provided by the model. The relative error for the higher modes shows that they are significantly inaccurate (relative error of up to 50%). Therefore a rule of thumb can be proposed in that if k frequencies are required it is necessary to model the system with a number of equal elements which provides at least $2k$ frequencies. This is only true for the h-version. For the p-version more calculations are needed to draw a similar conclusion.

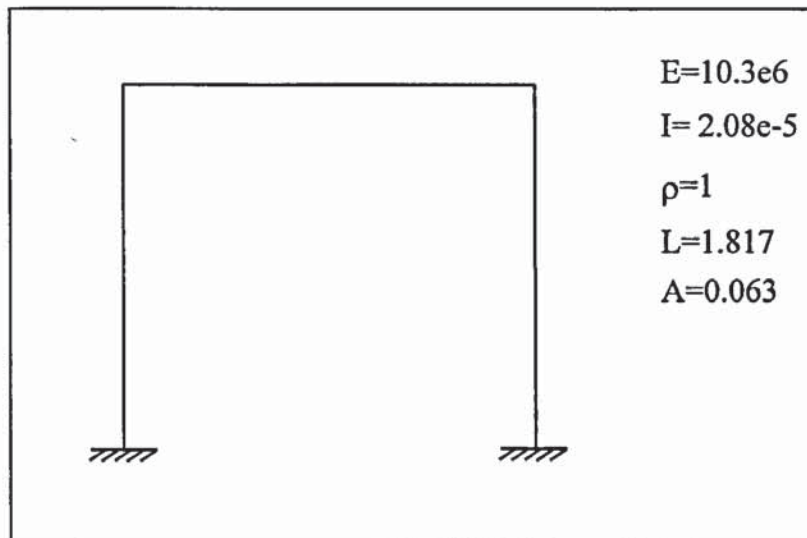


Fig. 5.2: Schematic of square portal frame and its data.

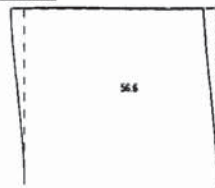
Exact solution	4 elements /bar 21 dof	3 elements /bar 15 dof	2 elements /bar 9 dof	1 element /bar 3 dof	p-version 1 9 dof
56.603	56.603	56.605	56.612	56.706	56.603
223.405	223.500	223.701	224.831	267.346	223.529
364.376	364.717	365.411	368.517	577.263	365.388
394.637	395.709	396.801	401.590		396.538
798.420	802.477	810.153	908.950		806.043
974.976	982.323	994.177	1186.629		994.282
1128.133	1138.522	1148.601	1490.239		1155.056
1713.310	1748.834	1919.682	2385.624		2724.169
2021.214	2065.320	2343.157	3195.329		3974.050
2135.532	2181.153	2584.211			
2984.904	3328.206	3670.536			
3321.571	3777.526	4431.450			
3572.354	4166.017	5172.888			
4596.701	5381.377	6614.060			
5067.413	6243.021	7635.244			
5273.455	6824.710				
6565.820	8597.032				
7062.693	9864.527				
7409.042	11024.125				
8874.718	12746.505				
9506.991	13849.266				

Table 5.1.a: Natural frequencies of portal frame.

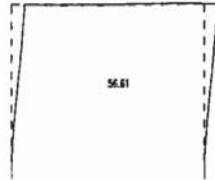
4 elements /bar	3 elements /bar	2 elements /bar	1 element /bar	p-version 1
0.001	0.003	0.016	0.182	0.000
0.042	0.132	0.638	19.668	0.055
0.093	0.284	1.136	58.425	0.277
0.271	0.548	1.761		0.481
0.508	1.469	13.843		0.954
0.753	1.969	21.708		1.980
0.920	1.814	32.097		2.386
2.07	12.045	39.240		59.000
2.18	15.928	58.089		96.616
2.13	21.010			
11.50	22.969			
13.72	33.414			
16.61	44.803			
17.070	43.887			
23.199	50.673			
29.416				
30.936				
39.670				
48.792				
43.627				
45.674				

Table 5.1.b: Relative error in %.

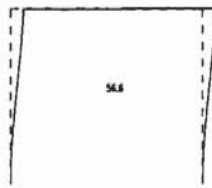
1st mode



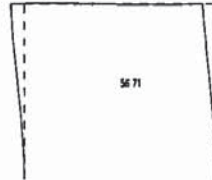
Exact solution



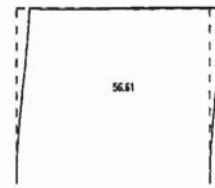
2 elements/bar



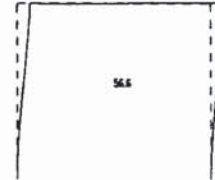
4 elements/bar



1 element/bar

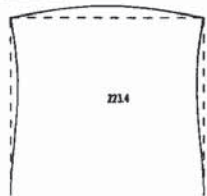


3 elements/bar

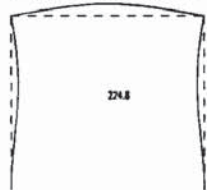


p-version 1

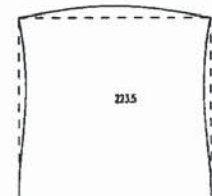
2nd mode



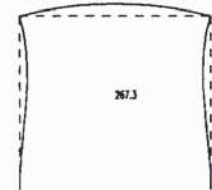
Exact solution



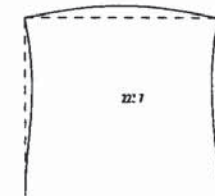
2 elements/bar



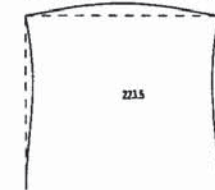
4 elements/bar



1 element/bar

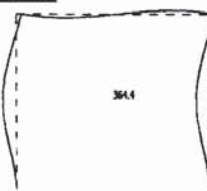


3 elements/bar

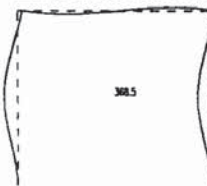


p-version 1

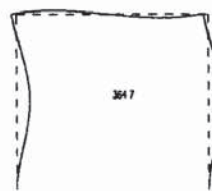
3rd mode



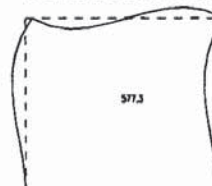
Exact solution



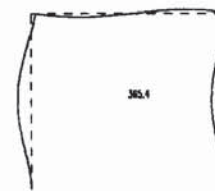
2 elements/bar



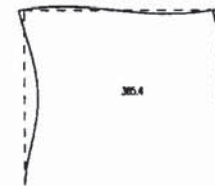
4 elements/bar



1 element/bar

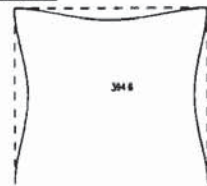


3 elements/bar

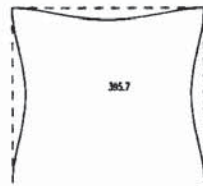


p-version 1

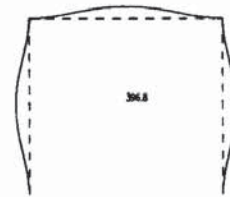
4th mode



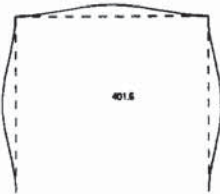
Exact solution



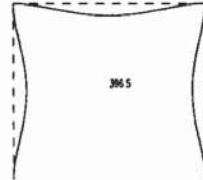
4 elements/bar



3 elements/bar

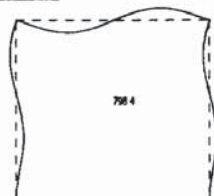


2 elements/bar

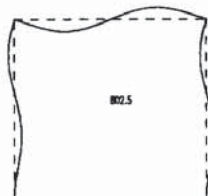


p-version 1

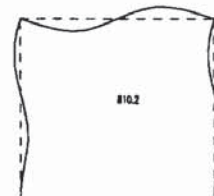
5th mode



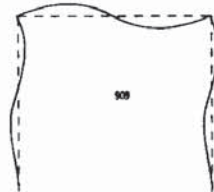
Exact solution



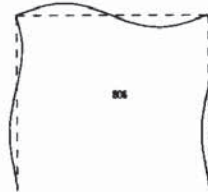
4 elements/bar



3 elements/bar

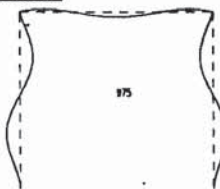


2 elements/bar

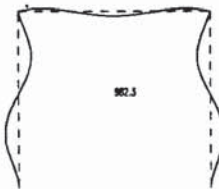


p-version 1

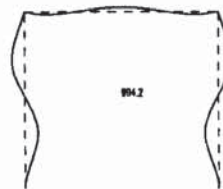
6th mode



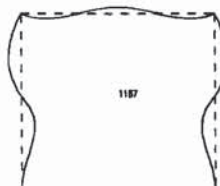
Exact solution



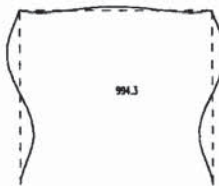
4 elements/bar



3 elements/bar

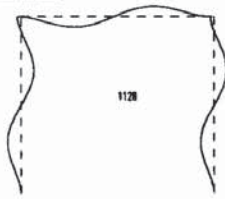


2 elements/bar

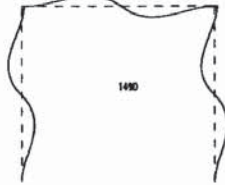


p-version 1

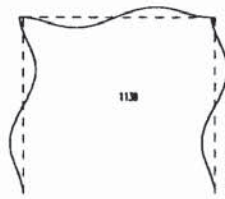
7th mode



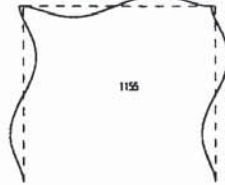
Exact solution



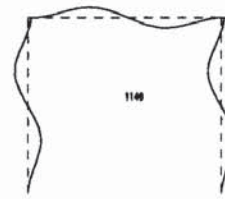
2 elements/bar



4 elements/bar

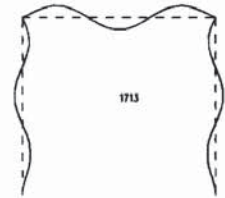


p-version 1

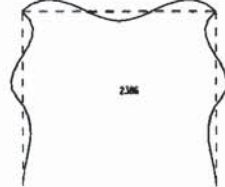


3 elements/bar

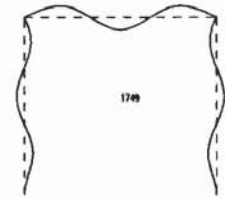
8th mode



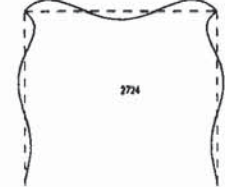
Exact solution



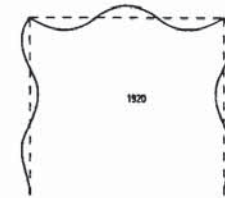
2 elements/bar



4 elements/bar

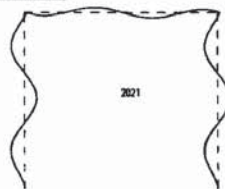


p-version 1

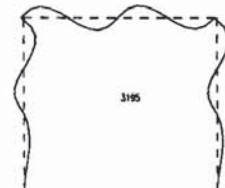


3 elements/bar

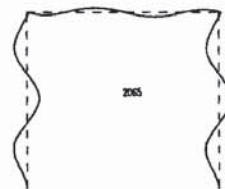
9th mode



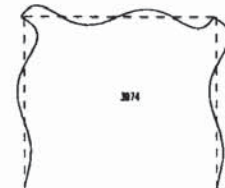
Exact solution



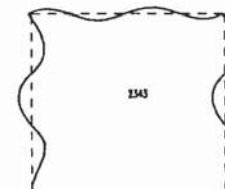
2 elements/bar



4 elements/bar

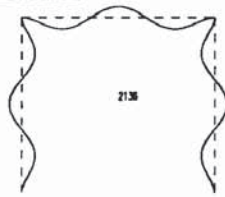


p-version 1

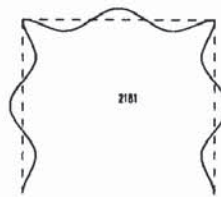


3 elements/bar

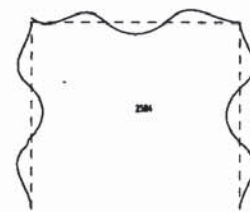
10th mode



Exact solution

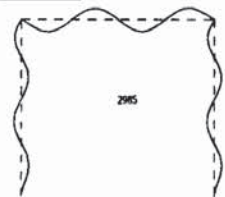


4 elements/bar

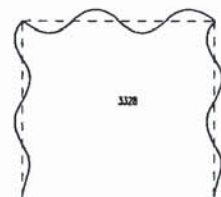


3 elements/bar

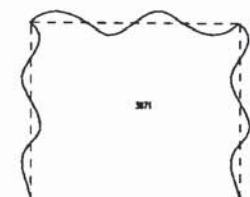
11th mode



Exact solution

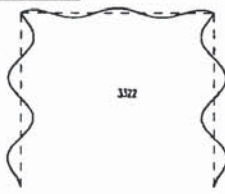


4 elements/bar

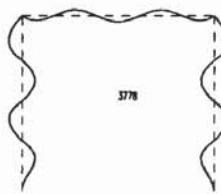


3 elements/bar

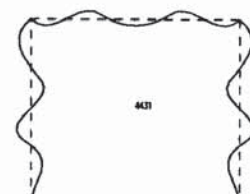
12th mode



Exact solution



4 elements/bar

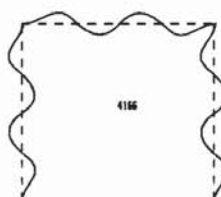


3 elements/bar

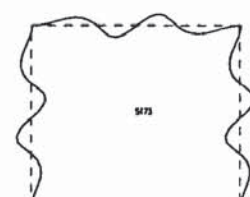
13th mode



Exact solution



4 elements/bar

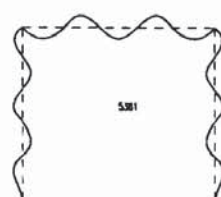


3 elements/bar

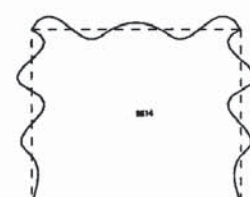
14th mode



Exact solution

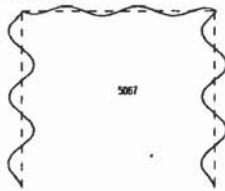


4 elements/bar

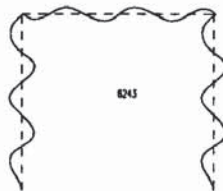


3 elements/bar

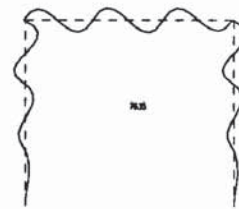
15th mode



Exact solution

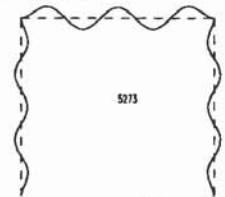


4 elements/bar

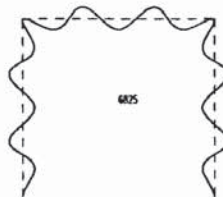


3 elements/bar

16th mode

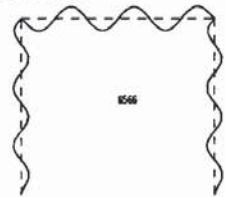


Exact solution

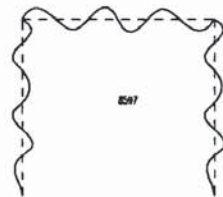


4 elements/bar

17th mode

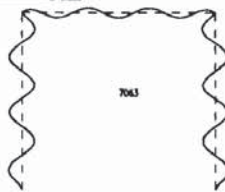


Exact solution

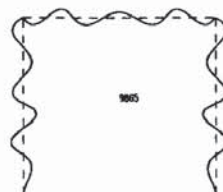


4 elements/bar

18th mode

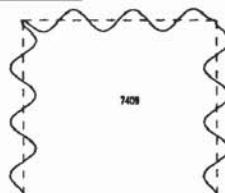


Exact solution

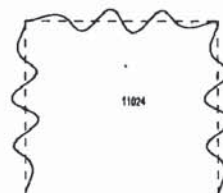


4 elements/bar

19th mode

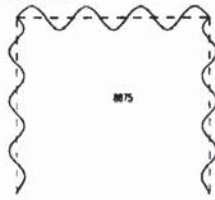


Exact solution

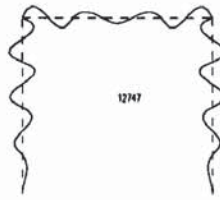


4 elements/bar

20th mode

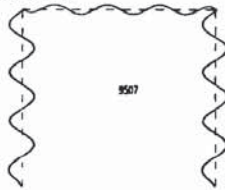


Exact solution

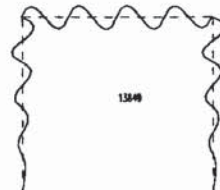


4 elements/bar

21st mode



Exact solution



4 elements/bar

5.4.2 Four-bar mechanism

The use of the dynamic stiffness method to investigate the modal characteristics of the four-bar mechanism serves two purposes. The first one is that it gives a practical answer on how many elements in conventional FE analysis are required to model the mechanism satisfactorily. The second, as will be seen in the next chapter, is that by a combination of this method and the conventional FEM the running four-bar mechanism can be modelled with relatively small number of elements, thus saving a great deal of CPU time. Since exact solutions are used in this method to solve the EVP, the natural frequencies do not change when the number of elements increases. Therefore only one element per link is used in the model. The results are compared to the FEM with 3 elements per link and are given in figures 5.3.a to 5.3.d. From these figures it can be concluded that, in this particular case, a model using 3 conventional elements per link is adequate up to the fourth mode with a maximum relative error of 1.18%. It has also been shown that this number of modes is enough to reconstruct the behaviour of a four-bar mechanism running at high-speed in the steady-state. The mode shapes from both methods, conventional FEM and the

dynamic stiffness method, were also investigated and compared. They are presented in chapter 8 where they are compared with the experimental results.

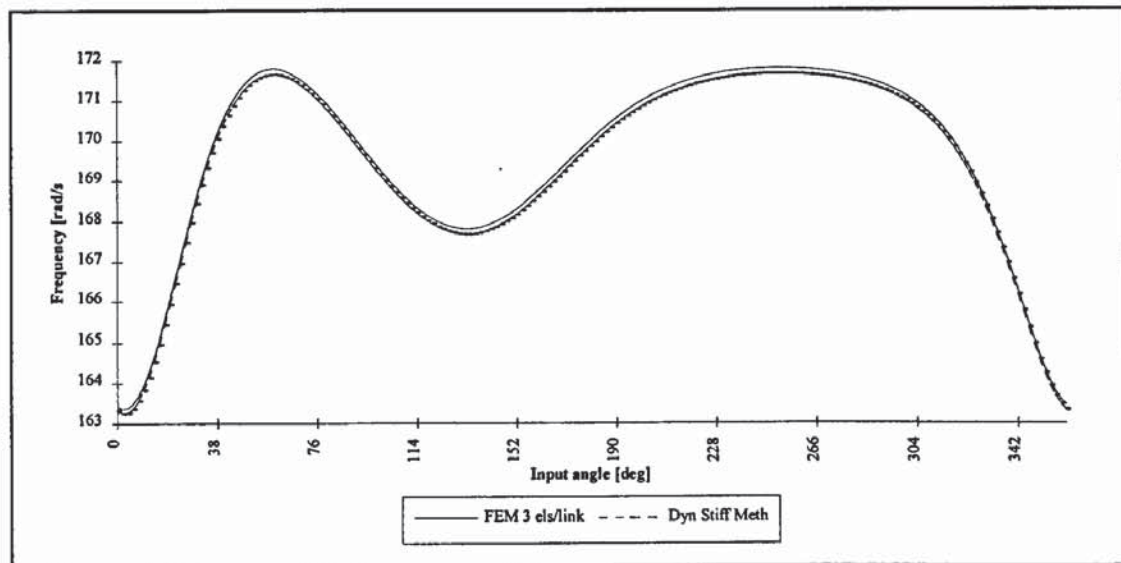


Fig. 5.3.a: First natural frequency.

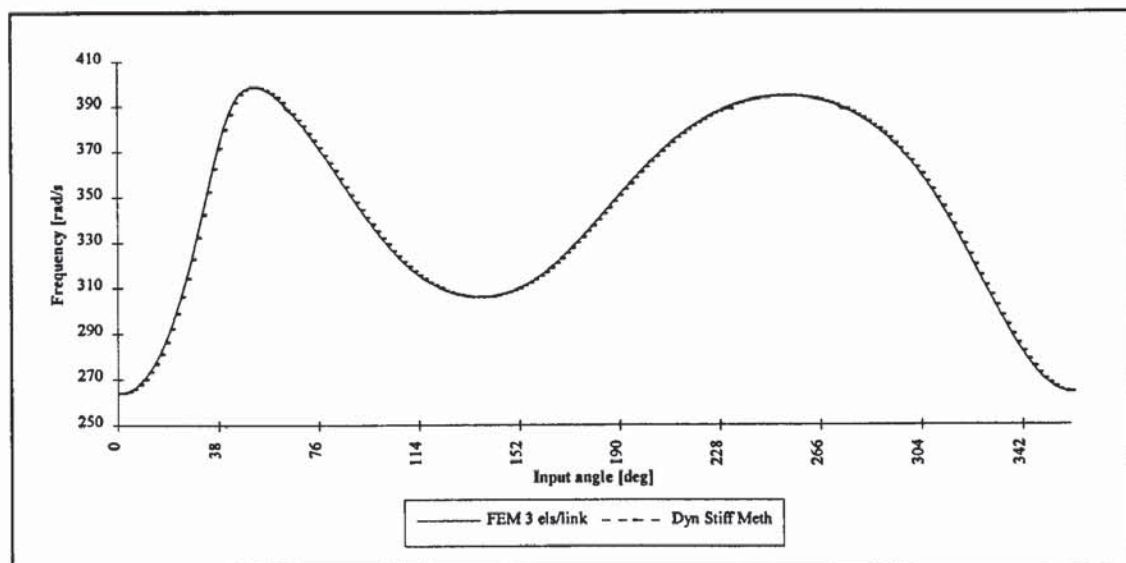


Fig. 5.3.b: Second natural frequency.

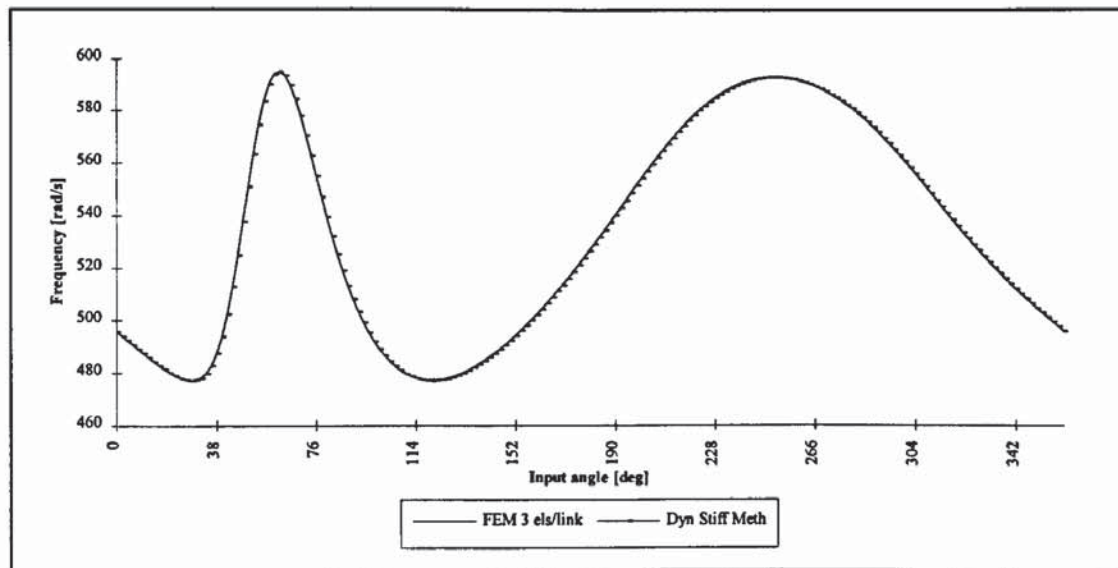


Fig. 5.3.c: Third natural frequency.

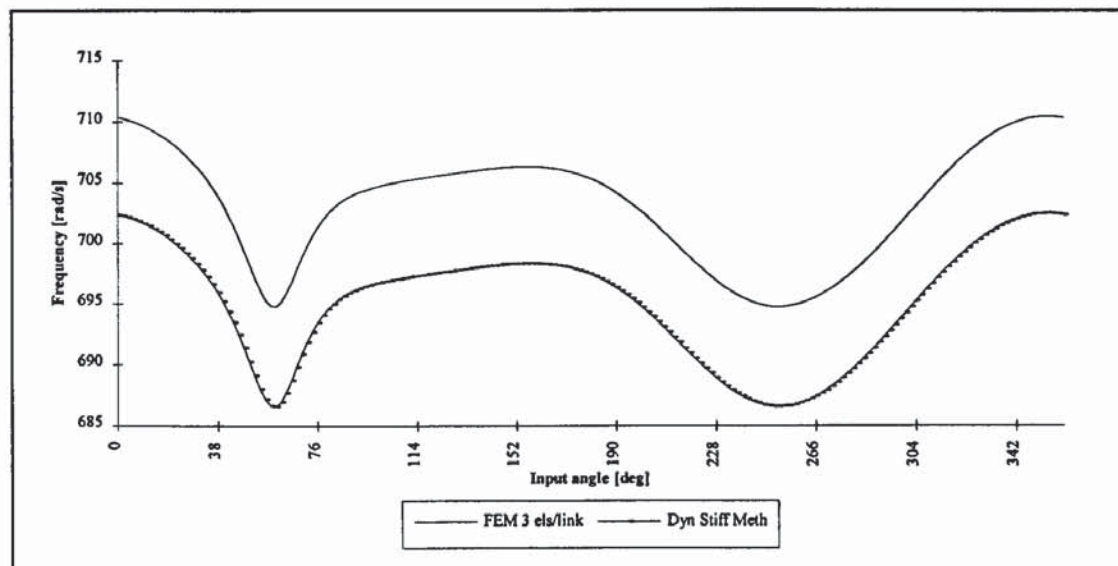


Fig. 5.3.d: Fourth natural frequency.

5.5. CONCLUSION

In this chapter the dynamic stiffness method has been developed. It has been shown that for frame structures this method is superior to the FEM. It has also been shown that in the case of the four-bar mechanism investigated, three elements per link were needed using the conventional FEM to deliver the same order of accuracy and up to the third mode when compared to the dynamic stiffness method. The main disadvantage, however, is that this method leads to a non-linear EVP and special

algorithms, such as the one developed by Wittrick and Williams, are needed to solve this EVP. Finally, it was shown that although the natural frequencies delivered by the dynamic stiffness method are independent of the number of subdivisions of the elements, in structures with rigid joints more than one element per bar might be needed to account for all natural frequencies.

Chapter 6

SOLUTION OF THE EQUATIONS OF MOTION FOR STEADY STATE

6.1. INTRODUCTION

The purpose of this chapter is to present some effective algorithms for solving the equations of motion of a four-bar mechanism to yield the steady-state solution. In the past, many methods have been applied successfully. However, even though the analysis of four-bar mechanism running at high-speed has been the subject of investigation for more than thirty years, little emphasis has been put on finding the steady-state solution directly. Apart from the methods which implicitly give the steady-state solution, such as the Fourier series analysis, most researchers used direct integration methods and kept on running the simulation until the steady-state solution was obtained. In this chapter, some established methods for solving the equations of motion will be discussed together with two efficient and new algorithms which give the steady-state solution very rapidly.

The methods most used thus far by researchers can be grouped as follows:

- Direct Integration methods.
- modal analysis,
- Fourier series analysis,

When the first method is used, a limited number of algorithms exist to provide the steady-state solution. The last two methods have the advantage of providing the steady-state solution without iteration.

6.2. DIRECT INTEGRATION METHOD

The problem of finding a solution which approaches the real solution is as important as deriving the governing equations of motion. Conceptually, the most straightforward method to obtain the steady-state solution is to use time marching simulation starting from any arbitrary initial conditions. The transients associated with the initial conditions die away naturally for stable systems leaving the steady-state solution after a number of cycles. This has been used in the past, but little emphasis has been placed on how to reach the steady-state solution quickly and efficiently. In many papers, the simulation is started from an arbitrary initial conditions (usually a zero state vector) and the steady-state solution is assumed to be obtained after the first cycle, this approach was taken for example by Liou and Erdman (1989b). In other papers, the solution was taken after a large number of cycles in order to be certain that the transient has died out completely (Midha *et al.*, 1979). Convergence to the steady-state can be very slow indeed for some input speeds, especially those near one of the critical speeds or when there is relatively low damping in the system.

The method described in this section as the "direct integration method" consists of integrating the equations of motion numerically. Unlike the modal analysis method, it is not limited to linear systems. However, there are potential problems with the direct integration method. Not least among them is the possibility that the step size could be chosen unwisely.

In general, multi-step methods are expressed as:
$$y_{k+1} = \sum_{j=1}^m a_j y_{k+1-j} - \Delta t \sum_{j=0}^m b_j \dot{y}_{k+1-j}$$

where $\Delta t = t_{k+1} - t_k$ is the time step size.

y_{k+1} is the state vector $[q_{k+1} \quad \dot{q}_{k+1}]^T$ at $t = t_{k+1}$ calculated from m previous state vectors and their derivatives. When $b_0 \neq 0$, the scheme is said to be implicit, in that in order to evaluate the state vector at $t = t_{k+1}$ its derivative is needed, whereas when $b_0 = 0$ the state vector y_{k+1} is readily calculated from the results already obtained from previous steps, and the scheme in this case is explicit. Finally when a_j and b_j are equal to zero for $j > 1$ the scheme becomes a one step scheme. The one step algorithm most used by researchers is the Newmark method. In general, any multi-step method of order m could be transformed into a one step method. This is done by creating a new vector containing the m state vectors at m successive time steps. The main disadvantage of this is that the size of the system is multiplied by m .

6.2.1 Newmark method

The Newmark method belongs to the family of one step methods when the state vector is considered. The state of the system at an instant $t_{k+1} = t_k + \Delta t$ could be determined with respect to the state at the instant t_k using Taylor expansion. For any function $f(t)$, Taylor's expansion gives:

$$f(t_k + \Delta t) = f(t_k) + \Delta t f'(t_k) + \frac{\Delta t^2}{2} f''(t_k) + \dots + \frac{\Delta t^s}{s!} f^{(s)}(t_k) + R_s \quad (6.1)$$

$$\text{where } R_s = \frac{1}{s!} \int_{t_k}^{t_{k+1}} f^{(s+1)}(\tau) [t_k + \Delta t - \tau]^s d\tau$$

Applying (6.1) to the displacement and velocity vectors, q and \dot{q} , yields:

$$\dot{q}_{k+1} = \dot{q}_k + \int_{t_k}^{t_{k+1}} \ddot{q}(\tau) d\tau \quad (6.2.a)$$

$$q_{k+1} = q_k + \Delta t \dot{q}_k + \int_{t_k}^{t_{k+1}} (t_{k+1} - \tau) \ddot{q}(\tau) d\tau \quad (6.2.b)$$

Then the integral in (6.2.a) is approximated by expressing the accelerations at $t = \tau$ as functions of the accelerations at instants $t = t_k$ and $t = t_{k+1}$ using (6.1). This gives:

$$\begin{aligned}\ddot{q}_k &= \ddot{q}(\tau) + q^{(3)}(t_k - \tau) + q^{(4)} \frac{(t_k - \tau)^2}{2} + \dots \\ \ddot{q}_{k+1} &= \ddot{q}(\tau) + q^{(3)}(t_{k+1} - \tau) + q^{(4)} \frac{(t_{k+1} - \tau)^2}{2} + \dots\end{aligned}\quad (6.3)$$

Multiplying both sides of the first equation by $(1 - \gamma)$ and the second by γ and summing, the integral in (6.2.a) is approximated by:

$$\int_{t_k}^{t_{k+1}} \ddot{q}(\tau) d\tau = (1 - \gamma) \Delta t \ddot{q}_k + \gamma \Delta t \ddot{q}_{k+1} + r_k \quad (6.4.a)$$

The integral in (6.2.b) is evaluated as before by expressing the velocities at $t = \tau$ as functions of the accelerations at instants $t = t_k$ and $t = t_{k+1}$. Then using β instead of γ , the integral in (6.2.b) is approximated by:

$$\int_{t_k}^{t_{k+1}} (t_{k+1} - \tau) \dot{q}(\tau) d\tau = \left(\frac{1}{2} - \beta \right) \Delta t^2 \ddot{q}_k + \beta \Delta t^2 \ddot{q}_{k+1} + r'_k \quad (6.4.b)$$

In (6.4.a) and (6.4.b):

$$\begin{aligned}r_k &= \left(\gamma - \frac{1}{2} \right) \Delta t^2 q^{(3)}(\zeta) + O(\Delta t^3 q^{(4)}) \quad t_k < \zeta < t_{k+1} \\ r'_k &= \left(\beta - \frac{1}{6} \right) \Delta t^3 q^{(3)}(\zeta) + O(\Delta t^4 q^{(4)})\end{aligned}$$

The constants γ and β are the parameters of the interpolation. For example the choice of $\gamma = 1/2$ and $\beta = 1/6$ leads to a linear interpolation of accelerations within the

interval of expression $\ddot{q}(\tau) = \ddot{q}_k + \frac{\tau}{\Delta t} (\ddot{q}_{k+1} - \ddot{q}_k)$; and, $\gamma = 1/2$ and $\beta = 1/4$ is equivalent to considering a mean value of the acceleration during the interval

$$\ddot{q}(\tau) = \frac{1}{2} (\ddot{q}_{k+1} + \ddot{q}_k)$$

By replacing (6.4) in (6.2), Newmark's scheme is obtained:

$$\begin{aligned}\dot{\mathbf{q}}_{k+1} &= \dot{\mathbf{q}}_k + (1-\gamma)\Delta t \ddot{\mathbf{q}}_k + \gamma\Delta t \ddot{\mathbf{q}}_{k+1} \\ \text{and} \\ \mathbf{q}_{k+1} &= \mathbf{q}_k + \Delta t \dot{\mathbf{q}}_k + \Delta t^2 \left(\frac{1}{2} - \beta \right) \ddot{\mathbf{q}}_k + \Delta t^2 \beta \ddot{\mathbf{q}}_{k+1}\end{aligned}\tag{6.5}$$

Combining (6.5) with the equations of motion and using straightforward algebra, the recurrence relation for the displacement \mathbf{q}_{k+1} at an instant t_{k+1} is obtained (Chan *et al.*, 1962):

$$\begin{aligned}\mathbf{D}\mathbf{q}_{k+1} &= \mathbf{B}\mathbf{q}_k - \mathbf{F}\mathbf{q}_{k-1} + \beta\Delta t^2 \left[\mathbf{f}_{k+1} + \left(\frac{1}{\beta} - 2 \right) \mathbf{f}_k + \mathbf{f}_{k-1} \right] \\ \text{where } \mathbf{D} &= \mathbf{M} + \frac{\Delta t}{2} \mathbf{C} + \beta\Delta t^2 \mathbf{K}, \\ \mathbf{B} &= 2\mathbf{M} - (1-2\beta)\Delta t^2 \mathbf{K}, \\ \mathbf{F} &= \mathbf{M} - \frac{\Delta t}{2} \mathbf{C} + \beta\Delta t^2 \mathbf{K}.\end{aligned}\tag{6.6.a}$$

The recurrence equation uses the displacements \mathbf{q} at t_k and t_{k-1} in order to find the displacement at t_{k+1} . In vibration problems, the initial state vector as well as the time history of applied forces are usually known. It is convenient to express another displacement equation in terms of initial displacement and initial velocity in order to start the procedure. In a similar manner as before, (6.6.b) is obtained:

$$\begin{aligned}\mathbf{D}\mathbf{q}_1 &= \mathbf{P}\mathbf{q}_0 + \mathbf{Q}\dot{\mathbf{q}}_0 + \beta\Delta t^2 \mathbf{f}_1 + \mathbf{R}\mathbf{f}_0 \\ \text{where } \mathbf{P} &= \mathbf{M} + \frac{\Delta t}{2} \mathbf{C} - \frac{1}{2}(1-2\beta)\Delta t^2 \mathbf{K} - \frac{1}{4}(1-4\beta)\Delta t^3 \mathbf{C}\mathbf{M}^{-1}\mathbf{K}, \\ \mathbf{Q} &= \left(\mathbf{M} - \frac{1}{4}(1-4\beta)\Delta t^2 \mathbf{C}\mathbf{M}^{-1}\mathbf{C} \right) \Delta t, \\ \mathbf{R} &= \left(\frac{1}{2}(1-2\beta)\mathbf{I} + \frac{1}{4}(1-4\beta)\Delta t \mathbf{C}\mathbf{M}^{-1} \right) \Delta t^2.\end{aligned}\tag{6.6.b}$$

6.2.2 Consistency of a scheme

The state vector \mathbf{y}_k describes completely the state of the system at an instant t_k . If the speed and the displacement are given, the acceleration could be calculated from the

equations of motion. A scheme is said to be consistent if $\lim_{\Delta t \rightarrow 0} \frac{y_{k+1} - y_k}{\Delta t} = \dot{y}(t)$.

This is a necessary condition for the convergence of the scheme and it means that for a small step size, the solution given by the scheme converges towards the exact solution. Applying this condition to Newmark method proves that it is a consistent scheme.

$$\lim_{\Delta t \rightarrow 0} \frac{y_{k+1} - y_k}{\Delta t} = \lim_{\Delta t \rightarrow 0} \left[\dot{q}_k + \left(\frac{1}{2} - \beta \right) \Delta t \ddot{q}_k + \beta \Delta t \ddot{q}_{k+1} \right] = \begin{bmatrix} \ddot{q}_k \\ \dot{q}_k \end{bmatrix} = \dot{y}_k \quad (6.7)$$

6.2.3 Stability of a scheme

A scheme of integration is said to be stable if there exists a step size $\Delta t_0 > 0$ so that for all $\Delta t \in [0, \Delta t_0]$, a finite perturbation of the state vector y_k at the instant t_k leads to only a bounded modification of the state vector y_{k+j} at later instant t_{k+j} . The scheme is unconditionally stable if the former property applies irrespective of the step size.

To check the stability of the Newmark method the state vectors at two consecutive instants are written in the form: $y_{k+1} = B(\Delta t)y_k + g_{k+1}(\Delta t)$, where $B(\Delta t)$ is the matrix amplification of the scheme. Now, consider a perturbation of the initial conditions $\delta y_0 = y'_0 - y_0$. The solutions at $t = t_{k+1}$ corresponding to y_0 and y'_0 are respectively

$$\begin{aligned} y_{k+1} &= B^{k+1}y_0 + \sum_{j=0}^{k+1} B^{k-j+1}g_j \\ y'_{k+1} &= B^{k+1}y'_0 + \sum_{j=0}^{k+1} B^{k-j+1}g_j \end{aligned} \quad (6.8)$$

Therefore the solution at $t = t_{k+1}$ varies with $B^{k+1}\delta y_0$. Hence, the stability of the system is conditioned by the eigenvalues of the matrix B . If one of its eigenvalues

has a modulus greater than one, the solution will be unbounded and the scheme unstable.

In order to assess the stability of the method for various parameters γ and β , the equation of an undamped vibration of a single degree of freedom is considered. The same reasoning applies for multi-degree-of-freedom systems when uncoupling via modal analysis is possible. The equation is then: $\ddot{\eta} + \omega^2 \eta = \phi$

The state vector is $\psi_k = [\eta_k \quad \dot{\eta}_k]^T$. The amplification matrix \mathbf{B} in this case can be shown to be:

$$\mathbf{B}(\Delta t) = \begin{bmatrix} 1 - \frac{1}{2} \frac{\omega^2 \Delta t^2}{1 + \beta \omega^2 \Delta t^2} & \frac{\Delta t}{1 + \beta \omega^2 \Delta t^2} \\ -\omega^2 \Delta t \left(1 - \frac{\gamma}{2} \frac{\omega^2 \Delta t^2}{1 + \beta \omega^2 \Delta t^2} \right) & 1 - \gamma \frac{\omega^2 \Delta t^2}{1 + \beta \omega^2 \Delta t^2} \end{bmatrix} \quad (6.9)$$

The EVP leads to the following characteristic equation:

$$\lambda^2 - \lambda \left(2 - \left(\gamma + \frac{1}{2} \right) \mu^2 \right) + 1 - \left(\gamma - \frac{1}{2} \right) \mu^2 = 0 \quad (6.10)$$

$$\text{where } \mu^2 = \frac{\omega^2 \Delta t^2}{1 + \beta \omega^2 \Delta t^2}$$

This equation admits two conjugate eigenvalues if the following relation holds:

$$\left(\gamma + \frac{1}{2} \right)^2 - 4\beta \leq \frac{4}{\omega^2 \Delta t^2} \quad (6.11)$$

The solutions are then written in the form $\lambda = \rho e^{\pm i\theta}$

$$\text{where } \rho = \sqrt{1 - \left(\gamma - \frac{1}{2} \right) \mu^2} \text{ and } \theta = \tan^{-1} \left(\frac{\mu \sqrt{1 - \frac{1}{4} \left(\gamma + \frac{1}{2} \right)^2 \mu^2}}{1 - \frac{1}{2} \left(\gamma + \frac{1}{2} \right) \mu^2} \right)$$

The scheme is stable if $\rho \leq 1$, this is verified if $\gamma \geq 1/2$. Furthermore, from (6.11) it is verified that if $\beta \geq \frac{1}{4} \left(\gamma + \frac{1}{2} \right)^2$ the stability is unconditional. The different regions of stability are plotted in Fig. 6.1 in (γ, β) space. Therefore, in the rest of the chapter the parameters γ and β are respectively chosen equal to 1/2 and 1/4. These values provide an unconditional stability to the scheme.

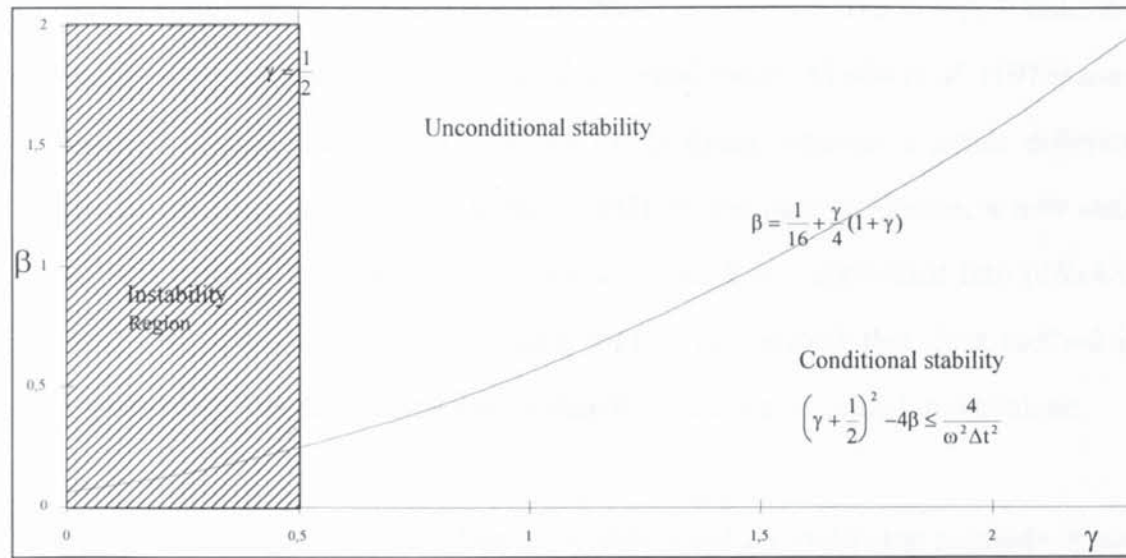


Fig. 6.1: Limits of stability of Newmark method.

Finally, it can be shown that structural damping has a stabilising effect on the method providing that the damping ratio is below a critical value (Géradin and Rixen, 1993).

6.3. MODAL ANALYSIS

Another technique determines a closed form steady-state solution of the equations of motion (Midha *et al.*, 1979 and, Yang and Sadler, 1993). This method utilises modal analysis to uncouple the equations of motion. The advantage of the modal analysis approach is that it allows modes thought not to contribute significantly to the solution to be discarded. Ordinarily, the size of the problem is dictated by the number of intervals and the number of degrees of freedom in the model. The use of

modal analysis enables a substantial reduction in the size of the problem by using a limited number of "degrees of freedom" to completely represent the system state at any instant. The cycle is divided into N intervals and the equations are uncoupled in each interval, assuming that the coefficients of the equations remain constant during the interval. A solution is found analytically for every mode and by imposing continuity constraints between two consecutive intervals and using the periodicity of the modal coordinates a matrix \mathbf{P} of order $2N \times 2N$ is obtained. The matrix \mathbf{P} links the N modal vector states and the corresponding modal forces. Midha *et al.* (1979) used a Gaussian elimination method to solve the problem whereas a rather different approach was used by Yang and Sadler (1993). In the latter reference, a new state vector was defined with two extra elements so that \mathbf{P} is transformed into $(4N \times 4N)$ matrix having an almost block diagonal form. They argued that their method is computationally less expensive to solve than the Gaussian elimination technique.

Xiaochun *et al.* (1988) developed an algorithm based on multi-step methods. Since the authors used second order differential equations of motion with the displacements as unknowns, the Newmark method was applied and in this case it can be cast into a two step method because the displacement at any instant is related to the displacements at the two previous instants. Then in dealing with the steady-state solution the periodicity of the displacement is considered. A large algebraic system is obtained which relates the N vector displacements to their equivalent forces. However, the system is highly sparse, only three diagonals are non zero (the leading diagonal and two diagonals below it) and a block in the upper right corner as shown in Fig. 6.2. The latter is due to the periodicity condition on the vector displacement. Xiaochun *et al.* proposed to solve the system by elimination and the back-substitution method. Some examples were given to show the efficiency of the algorithm. In their comparison, the authors used the Fourier series method to show the superiority of their method. However, the Fourier series method they used to generate graphs was not the same as the method referred to in their text. When this

Fourier series method is correctly used it provides identical solution to the method they proposed. It is thought that the method by which they obtained the graphs is the same as the method published by Bahgat and Willmert (1976) whereby the force and displacement vectors were developed in Fourier series but the system matrices **K**, **M** and **C** were assumed to be independent of the input angle. This limitation had a repercussion on the solution obtained, in that only the quasi-static response was predicted by this method.

$$\begin{bmatrix} X & & & & & X & X \\ X & X & & & & & X \\ X & X & X & & & & \\ & X & X & \dots & & & \\ & & & & X & X & X \\ & & & & & X & X & X \\ & & & & & & X & X & X \end{bmatrix}$$

Fig. 6.2: Form of the equation system obtained by Xiaochun *et al.* (1988)

The modal analysis method is based on the results of linear modal analysis and consists of expressing the dynamic response in the form of mode series in order to uncouple the equations of motion. The method is very efficient provided that the fundamental modes are dominant in the response. In cases where the frequency content of the excitation is such that many modes have to be included before the problem converges adequately, the direct integration is preferred to the modal analysis. Such cases are encountered when the excitation is in the form of a shock for example. Another limitation is that the modal analysis is limited to linear systems.

For any angular position of the input link, a coordinate transformation can be effected in order to obtain a set of uncoupled equations which leads to a system of second order ordinary differential equations. The modal transformation matrix is a

function of the angular position of the input link and this substantially reduces the benefits of the uncoupling.

The matrices are written in the modal coordinate system :

$$\begin{aligned} \mathbf{K} &= \Phi^{-T} [\Lambda] \Phi^{-1} \\ \mathbf{M} &= \Phi^{-T} \mathbf{I} \Phi^{-1} \\ \mathbf{C} &\approx \Phi^{-T} [\delta] \Phi^{-1} \end{aligned} \tag{6.12}$$

where $[\Lambda]$ and $[\delta]$ are diagonal matrices.

Because the matrices \mathbf{K} , \mathbf{M} and \mathbf{C} are functions of the input angle t_1 , the matrix Φ (the modal matrix) and $[\Lambda]$ (the spectral matrix) also depend on t_1 . In many cases, the eigenvectors (columns of Φ) are only weakly dependent on t_1 . Under these circumstances, Φ may be calculated at a specific position and the same Φ used for all other positions. The equations are then no longer uncoupled and the following conditions apply for the general t_1 .

$$\begin{aligned} \Phi^T \mathbf{K}(t_1) \Phi &\text{ non diagonal} \\ \Phi^T \mathbf{M}(t_1) \Phi &\neq \text{Identity} \\ \Phi^T \mathbf{C}(t_1) \Phi &\text{ non diagonal} \end{aligned}$$

However the off-diagonal entries may be relatively small. If the off-diagonal entries are ignored completely then the equations of motion reduce to a system of uncoupled equations which can be solved independently. A numerical integration procedure must still be used to solve these equations but the requisite computation time is dramatically reduced.

If the off-diagonal entries cannot be ignored, it may still be advantageous to carry out the coordinate transformation. The advantage is that solution of the set of simultaneous equations necessary at each step of the time marching simulation may

be more efficient if it becomes possible to use iterative solution methods in place of direct methods.

In the present study, an approach similar to the one developed by Midha *et al.* (1979) was taken to obtain the large system **P** described earlier. A different method of solution was developed, however. One of the new algorithms developed in this chapter was combined with the modal analysis concept in order to obtain the steady-state solution. In figures 6.3.a and 6.3.b a comparison is made between the latter method and a method where no uncoupling of the equations of motion is performed. The two methods are compared by calculating the deflection at the midpoint of the coupler and the follower at a specific speed. It is noticed that while the method which uses the modal analysis technique yields a good result for the follower, it is quite inaccurate when calculating the deflection of the coupler midpoint. In figures 6.4.a and 6.4.b, the contribution of each mode to the global deflection of the coupler and the follower midpoints are presented up to the fourth mode. From these figures it can be seen that these contributions vary along the cycle and that the first mode is dominant in the follower case, but more modes contribute to the deflection of the coupler.

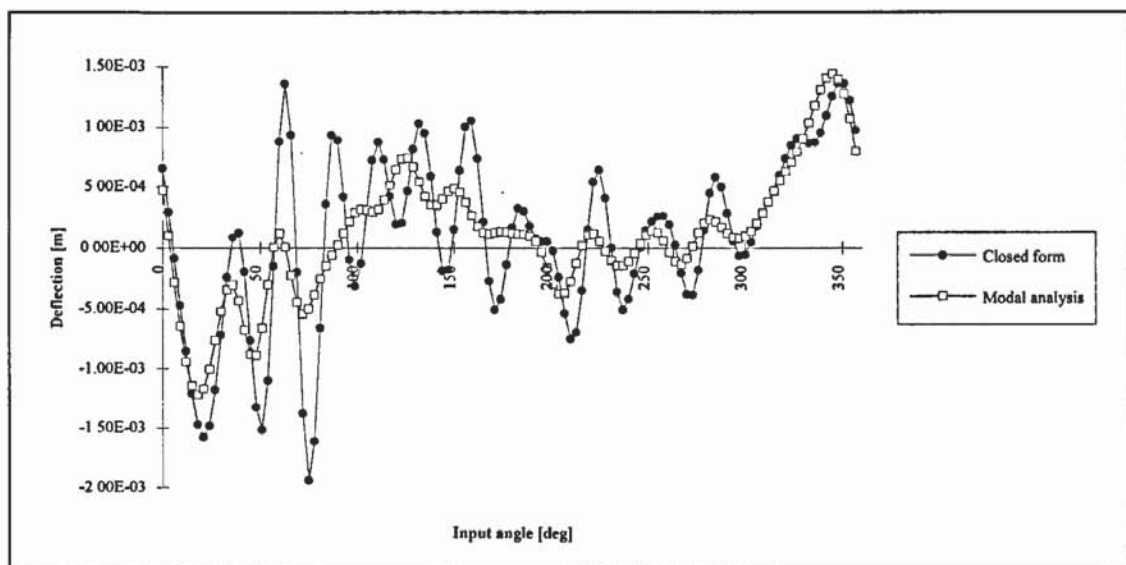


Fig. 6.3.a: Displacement of the coupler midpoint for $\omega=35$ rad/s and $\zeta=0.02$.

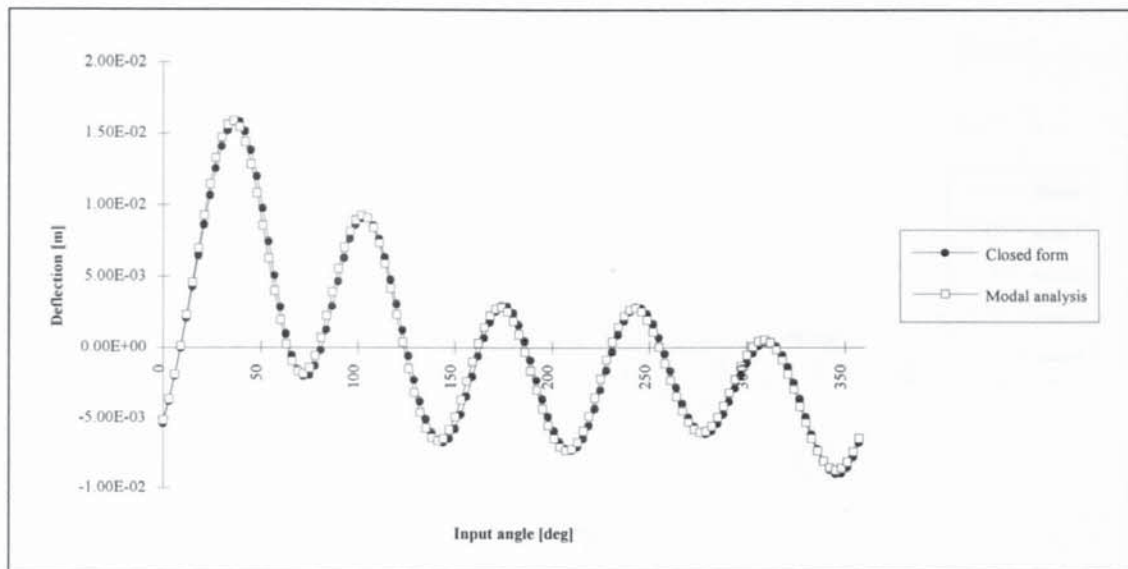


Fig. 6.3.b: Displacement of the follower midpoint for $\omega=35$ rad/s and $\zeta=0.02$.

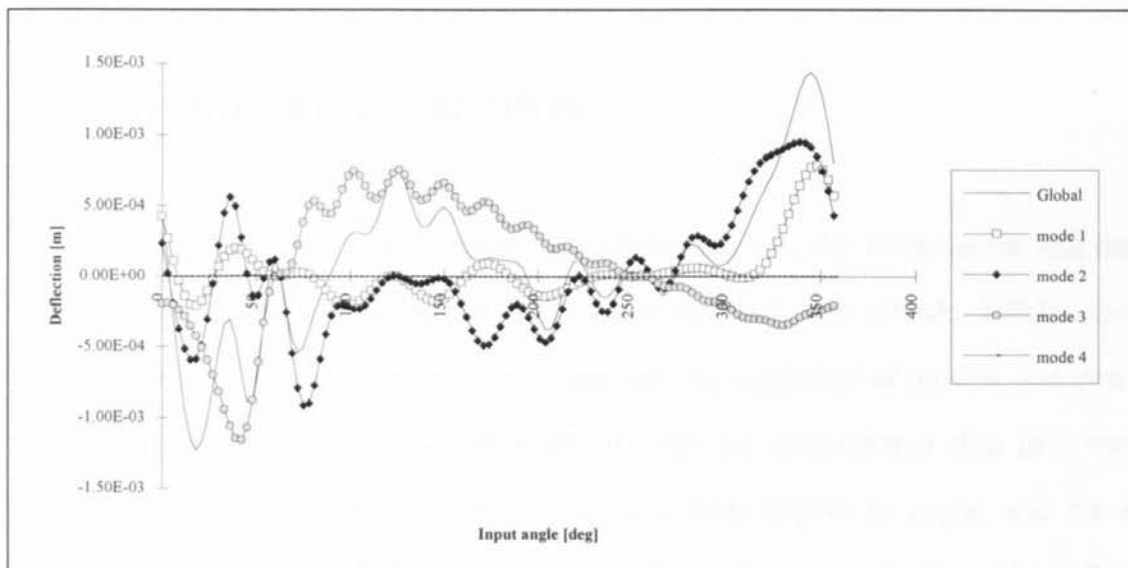


Fig. 6.4.a: Contributions of different modes to the global deflection at the coupler mid-point for $\omega=35$ rad/s and $\zeta=0.02$.

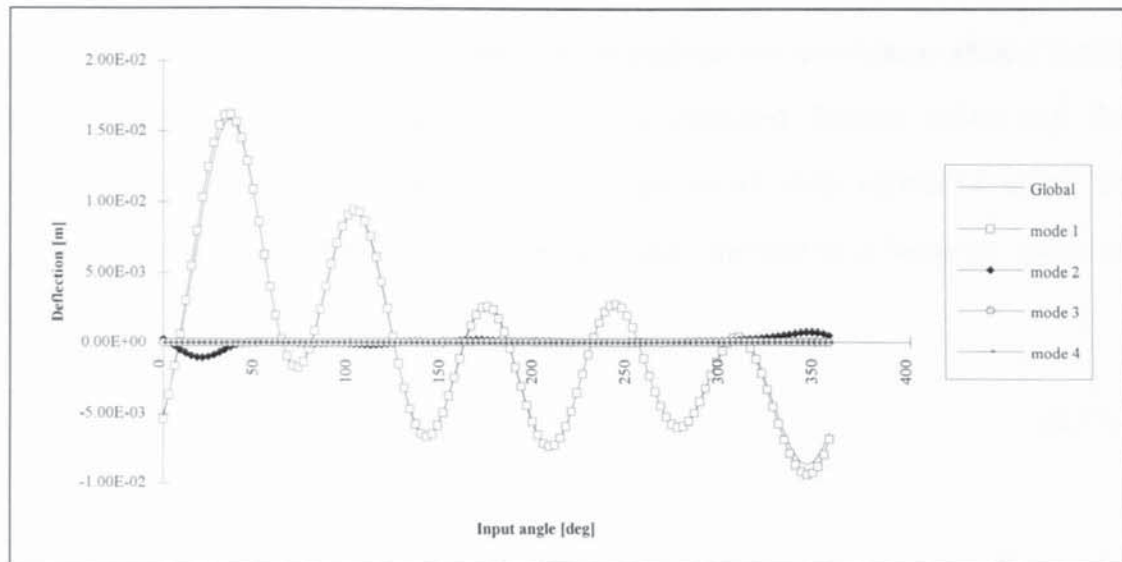


Fig. 6.4.b: Contributions of different modes to the global deflection at the follower mid-point for $\omega=35$ rad/s and $\zeta=0.02$.

6.4. FOURIER SERIES METHOD

An alternative approach is to develop the system matrices, the force vector and the displacement vector into truncated Fourier series (Nath and Ghosh, 1980b, and Cleghorn *et al.*, 1984a). By substituting these into the equations of motion, a system of linear algebraic equations is obtained. It must be remembered that this was possible because the above entities are periodic with respect to angle, and for a constant speed of rotation they become periodic with respect to time also. This method has the advantage of addressing the computation of the steady-state solution directly and the rotational speed of the mechanism has no effect on the amount of computation required. Against this, however, is the fact that the system of equations produced can be extremely large, depending on the number of terms retained in the series and the number of degrees of freedom in the model.

The Fourier series analysis is only valid for the steady-state solution. The system matrices in the equations of motion are position-dependent, and therefore are periodic functions of time for a constant rotational speed. The period of these

functions is the time taken by the input link to perform one revolution. Hence in this method the matrices are approximated by a truncated Fourier series and the equations of motion are transformed into a larger set of linear equations which are independent of time. First the force vector \mathbf{f} is approximated by a harmonic series of the form:

$$\mathbf{f}(t) \cong \sum_{j=0}^{N/2} (\mathbf{f}_{cj} \cos(j\omega t)) + \sum_{j=1}^{N/2} (\mathbf{f}_{sj} \sin(j\omega t)) \quad (6.13)$$

where \mathbf{f}_{cj} and \mathbf{f}_{sj} are constants, ω is the angular speed of the input link and N is the number of equal time intervals per revolution of the same link. The coefficients \mathbf{f}_{cj} and \mathbf{f}_{sj} can be calculated by expressing \mathbf{f} for N instants of time and solving the set of N linear algebraic equations in which the unknowns are \mathbf{f}_{cj} and \mathbf{f}_{sj} .

Bahgat and Willmert (1976) used Fourier series analysis of the force vector to predict the behaviour of the mechanism. Since the displacement vector \mathbf{q} is also a periodic function of time once the steady-state has been achieved, it too can be approximated by a harmonic series:

$$\mathbf{q}(t) \cong \sum_{j=0}^{N/2} (\mathbf{q}_{cj} \cos(j\omega t)) + \sum_{j=1}^{N/2} (\mathbf{q}_{sj} \sin(j\omega t)) \quad (6.14)$$

Bahgat and Willmert assumed initially that the system matrices \mathbf{K} , \mathbf{M} and \mathbf{C} are independent of the input link angle, t_1 , and derived an expression relating \mathbf{q}_{cj} and \mathbf{q}_{sj} to \mathbf{K} , \mathbf{M} , \mathbf{C} , \mathbf{f}_{cj} and \mathbf{f}_{sj} . The dependence of the system matrices on t_1 is then partially restored by evaluating $\mathbf{q}(t)$ at each instant in the cycle using the instantaneous values of \mathbf{K} , \mathbf{M} and \mathbf{C} . Their method is computationally efficient but quite inaccurate at high-speeds where the inertial forces associated with elastic deflections are significant.

For an accurate analysis, all the periodic terms in the equations of motion including \mathbf{K} , \mathbf{M} and \mathbf{C} should be expressed in a Fourier series. In other words, the mass, the stiffness and the damping matrices are all approximated by a series as in (6.13) and substituted together with the expressions for \mathbf{q} and \mathbf{f} into the equations of motion. This leads to a system of $(N + 1)n$ linear equations in terms of the unknown deflection vector coefficient components, n being the number of elastic degrees of freedom of the mechanism. Cleghorn *et al.* (1984a) used the latter method which gave better results in predicting the behaviour of the mechanism than those given in the former reference.

6.5. NEW ALGORITHM 1: USING THE TRANSITION MATRIX TO CALCULATE THE STEADY-STATE SOLUTION

A method is now presented for calculating the steady-state after just two cycles. The response of a linear dynamic system is the sum of two components: the steady-state response and the transient response which, for stable systems, vanishes after a certain number of cycles. If the simulation is started from a state vector corresponding to the steady-state solution then the transient solution should never appear. Therefore in the method presented here, the response after one cycle is separated into the transient and the steady-state contributions. The latter is then used as the starting point for a new cycle. The solution within the second cycle is the periodic steady-state solution.

First, the equations of motion are transformed into a set of first order differential equations expressed as:

$$\dot{\mathbf{y}}(t) = \mathbf{A}(t)\mathbf{y}(t) + \mathbf{h}(t) \quad (6.15)$$

In this equation

$$\mathbf{A} = \begin{bmatrix} \mathbf{0} & \mathbf{I} \\ -\mathbf{M}^{-1}\mathbf{K} & -\mathbf{M}^{-1}\mathbf{C} \end{bmatrix} \text{ and } \mathbf{h} = \begin{Bmatrix} \mathbf{0} \\ \ddot{\mathbf{q}}_r \end{Bmatrix}$$

In (6.15), Coriolis and other acceleration effects are either assumed to be negligible or the matrices corresponding to these effects are combined with \mathbf{C} and \mathbf{K} . If the stiffening effect is taken into account, the axial forces in the links should be calculated from the quasi-static deflections otherwise the problem becomes non-linear.

The transition matrix, \mathbf{R} , is defined as the system of solutions, $\mathbf{Y}(T)$, of the homogeneous part of (6.15) where $\mathbf{Y}(0) = \mathbf{I}$. Hence a column k of \mathbf{R} is obtained by integrating (6.15) without the forcing term for the initial vector $\mathbf{y}(0)$ in which all elements are zero except the k th element which is equal to 1. The transition matrix will be studied in more detail in the next chapter, and in particular its role in assessing the stability of the system will be explored.

If the simulation starts from the zero state vector, $\mathbf{y}(0) = \mathbf{0}$, and $\mathbf{y}_c(T)$ is the total response after the first cycle then:

$$\text{at } t = 0 \quad \mathbf{0} = \mathbf{y}_t(0) + \mathbf{y}_s(0) \quad (6.16)$$

$$\text{and at } t = T \quad \mathbf{y}_c(T) = \mathbf{y}_t(T) + \mathbf{y}_s(T) \quad (6.17)$$

Here, $\mathbf{y}_t(t)$ is the transient response and $\mathbf{y}_s(t)$ is the steady-state response. Since $\mathbf{y}_s(t)$ is periodic, the following relation is obtained by use of the transition matrix \mathbf{R} and (6.16):

$$\begin{aligned} \mathbf{y}_c(T) &= \mathbf{R} \mathbf{y}_t(0) + \mathbf{y}_s(0) \Rightarrow \mathbf{y}_c(T) = -\mathbf{R} \mathbf{y}_s(0) + \mathbf{y}_s(0) \\ &\Rightarrow \mathbf{y}_s(0) = (\mathbf{I} - \mathbf{R})^{-1} \mathbf{y}_c(T) \end{aligned} \quad (6.18)$$

If the simulation is begun with a non-zero state vector, y_i , the steady-state solution can be computed according to (6.19).

$$y_s(0) = (\mathbf{I} - \mathbf{R})^{-1} (y_c(T) - \mathbf{R} y_i) \quad (6.19)$$

Note that since all the eigenvalues of \mathbf{R} are less than 1 in magnitude (for a stable system), all of the eigenvalues of $(\mathbf{I} - \mathbf{R})$ are greater than 0. It is possible that the condition number of $(\mathbf{I} - \mathbf{R})$ could be very poor in the case of a system which is very marginally stable. This could affect the accuracy of $y_s(0)$ but has no effect on the speed of computation. Moreover, many cases of marginally stable systems will nevertheless produce a well-conditioned $(\mathbf{I} - \mathbf{R})$ since two complex eigenvalues (in a conjugate pair) may each have modulus ≈ 1 but the size of the imaginary parts might not be small.

Thus, one procedure for determining the steady-state solution is as follows:

- Calculate the transition matrix by integrating the homogeneous part of (6.15) over one period of time starting from the identity matrix.
- Run the simulation with a zero initial state vector. The simulation is carried out by integrating either (6.15) or its initial form whichever is suitable.
- Run the simulation with an initial state vector given by (6.18). The result of this simulation during this cycle is the steady-state solution.

6.6. NEW ALGORITHM 2: VARIATION ON THE ESTABLISHED "CLOSED-FORM" ALGORITHMS

As an alternative to the procedure given in the preceding section, a method is presented which has some similarities to the "closed-form" procedure described in section 6.3. In the following development, modal analysis is not used because this would limit the applicability to systems with proportional damping. Where

proportional damping can be assumed, modal analysis can be combined with the algorithm presented here to achieve some additional economy.

If the equations of motion are integrated over one time-step using the Newmark method, then:

$$\mathbf{y}_{k+1} + \mathbf{G}_k \mathbf{y}_k = \mathbf{f}_k \quad k = 1 \text{ to } N \quad (6.20)$$

where \mathbf{y} is the state vector, k denotes the time step and, \mathbf{G} (2nx2n) and \mathbf{f} emerge from Newmark integration scheme.

Because \mathbf{q} and $\dot{\mathbf{q}}$ are both periodic functions of time, \mathbf{y} must satisfy (6.21):

$$\mathbf{y}_{N+1} = \mathbf{y}_1 \quad (6.21)$$

Grouping (6.20) for all intervals and using (6.21), the following system is obtained:

$$\begin{bmatrix} \mathbf{G}_1 & \mathbf{I} & & & \\ & \mathbf{G}_2 & \mathbf{I} & & \\ & & & \dots & \\ & & & & \mathbf{G}_{N-1} & \mathbf{I} \\ \mathbf{I} & & & & & \mathbf{G}_N \end{bmatrix} \begin{bmatrix} \mathbf{y}_1 \\ \mathbf{y}_2 \\ \vdots \\ \mathbf{y}_{N-1} \\ \mathbf{y}_N \end{bmatrix} = \begin{bmatrix} \mathbf{f}_1 \\ \mathbf{f}_2 \\ \vdots \\ \mathbf{f}_{N-1} \\ \mathbf{f}_N \end{bmatrix} \quad (6.22)$$

The unknowns of the problem are the N state vectors \mathbf{y}_k .

From (6.22) it is clear that if the initial state vector (i.e. \mathbf{y}_1) is known then all others can readily be determined. Therefore finding \mathbf{y}_1 is the key to solving the problem. The following general formula allows any \mathbf{y}_k to be calculated in terms of \mathbf{G}_k , \mathbf{f}_k and \mathbf{y}_1 :

$$y_{N-k} = \left[\sum_{j=0}^k (-1)^{j+k} \left(\prod_{i=N-k}^{N-j} G_i^{-1} \right) f_{N-j} \right] + (-1)^{k+1} \left(\prod_{j=k}^0 G_{N-j}^{-1} \right) y_1$$

$k = 0 \text{ to } N-1$

(6.23)

Substituting $k = N-1$ in (6.23) and rearranging gives the following equation:

$$y_1 = \left[I - (-1)^N \left(\prod_{j=N-1}^0 G_{N-j}^{-1} \right) \right]^{-1} \left[\sum_{j=0}^{N-1} (-1)^{j+N-1} \left(\prod_{i=1}^{N-j} G_i^{-1} \right) f_{N-j} \right]$$
(6.24)

The following recursive formula can then be used to determine y_2, y_3, \dots, y_N ,

$$y_{N-k} = G_{N-k}^{-1} (f_{N-k} - y_{N-k+1})$$

$k = 0 \text{ to } N-2$

(6.25)

Some difficulties may arise when computing y_1 from (6.24) if the matrix

$\left[I - (-1)^N \left(\prod_{j=N-1}^0 G_{N-j}^{-1} \right) \right]$ is ill-conditioned. Since this matrix equals $[I - R](-R^{-1})$ the comments made earlier about the condition of $[I - R]$ also hold.

If the model includes many degrees of freedom, then using even a modest number of intervals causes the square matrix in (6.22) to become large and difficulties may arise in handling the matrix in memory unless the sparse nature of this matrix is recognised.

In (6.24) the sequence of operations is of extreme importance. If the solution is evaluated as (6.24) implies the number of operations involved is considerable. In contrast if the summation is carried out in reverse order the computation is much more efficient.

6.7. EQUIVALENCE BETWEEN THE TWO ALGORITHMS

It will now be shown that the two approaches presented in sections 6.5 and 6.6 are mathematically equivalent. Using the definition of the transition matrix \mathbf{R} , and assuming that all of the forcing terms, \mathbf{f}_k , in (6.22) are all zero, it can be shown that:

$$\mathbf{R} = (-1)^N \prod_{k=N}^1 \mathbf{G}_k \text{ and hence } \mathbf{R}^{-1} = (-1)^N \prod_{k=1}^N \mathbf{G}_k^{-1} \quad (6.26)$$

Combining (6.20) (with $k = N$) and (6.23), proves that if $\mathbf{y}_1 = \mathbf{0}$, then \mathbf{y}_{N+1} is given by:

$$\mathbf{y}_{N+1} = \sum_{k=1}^{N-1} (-1)^{k+N} \left(\prod_{k=N}^{k+1} \mathbf{G}_k \right) \mathbf{f}_k + \mathbf{f}_N \quad (6.27)$$

Using the transition matrix, \mathbf{y}_1 is given by:

$$\begin{aligned} \mathbf{y}_1 &= [\mathbf{I} - \mathbf{R}]^{-1} \mathbf{y}_{N+1} \\ &= [\mathbf{I} - \mathbf{R}^{-1}]^{-1} (-\mathbf{R}^{-1}) \mathbf{y}_{N+1} \end{aligned} \quad (6.28)$$

replacing (6.27) and (6.26) into (6.28) gives:

$$\begin{aligned} \mathbf{y}_1 &= [\mathbf{I} - \mathbf{R}^{-1}]^{-1} \left[\sum_{k=1}^{N-1} (-1)^{k+1} \prod_{i=1}^N \mathbf{G}_i^{-1} \prod_{i=N}^{k+1} \mathbf{G}_i \mathbf{f}_k + (-1)^{N+1} \prod_{i=1}^N \mathbf{G}_i^{-1} \mathbf{f}_N \right] \\ \mathbf{y}_1 &= [\mathbf{I} - \mathbf{R}^{-1}]^{-1} \left[\sum_{k=1}^N (-1)^{k+1} \prod_{i=1}^k \mathbf{G}_i^{-1} \mathbf{f}_k \right] \end{aligned} \quad (6.29)$$

Comparing (6.24) and (6.29) it can be concluded that the two algorithms are mathematically equivalent.

6.8. COMPARISON OF EFFICIENCY OF DIFFERENT ALGORITHMS

In this section a comparison is made between different algorithms in terms of the number of flops required to obtain a steady-state solution. Since the matrices \mathbf{M} , \mathbf{C} ,

\mathbf{K} and \mathbf{f} depend on the problem being treated, it is assumed that they are calculated separately and stored and therefore in the following formula the number of flops required to determine these matrices was not taken into account. The storage of the intermediate matrices \mathbf{G}_k 's and \mathbf{f}_k 's allows substantial saving in terms of time and flops, but in some situations this is not possible and therefore the above matrices are calculated whenever they are needed. The limitation of computer memory, number of intervals, N , and number of degrees of freedom, n , are the major causes for these situations. The algorithm which uses the transition matrix will be referred to as algorithm 1, and algorithm 2 is the algorithm which solves the problem in closed form. TMS is the method which uses the time marching simulation. In the following table, comparison between different algorithms is made for the two cases.

	Storage	No storage
TMS	$N(22n^3+(29+4n_c)n^2+(3+2n_c)n)$	$Nn_c(22n^3+33n^2+5n)$
Algorithm 1	$N(38n^3+37n^2+7n)+16n^3+8n^2$	$N(78n^3+77n^2+10n)-14n^3-21n^2-3n$
Algorithm 2	$N(62n^3+37n^2+9n)+8n^3+8n^2+2n$	$N(102n^3+87n^2+10n)-14n^3-21n^2-n$

Table 6.1: Number of Flops for different algorithms.

In the time-marching simulation n_c is the number of cycles necessary for the solution to converge. This obviously depends on the rotational speed and the damping ratio in the case of mechanisms. A general formula which gives the initial state vector after m cycles can be derived easily: $\mathbf{y}_1 = [\mathbf{I} - \mathbf{R}^{-1}]^{-1} [\mathbf{I} - \mathbf{R}^{m+1}] \left[\sum_{k=1}^N (-1)^{k+1} \prod_{i=1}^k \mathbf{G}_i^{-1} \mathbf{f}_k \right]$. This formula shows again that if the modulus of all eigenvalues of \mathbf{R} is less than one, \mathbf{y}_1 converges towards the value given by algorithm 1.

The method based on the transition matrix involves the inversion of the products of N matrices whereas the method based on the closed form involves the product of the inverses of the same N matrices, it is clear that using the transition matrix will always be computationally more efficient. The time marching simulation is more

advantageous when the storage is considered for n_c below a critical value. This drops if n decreases. If no storage is adopted the critical value is very low and in this case the time marching simulation is to be avoided.

			Storage			No storage		
N	n	n_c	T M S	Algorithm 1	Algorithm 2	T M S	Algorithm 1	Algorithm 2
90	10	5	2.43	3.78	5.93	11.4	7.71	9.96
90	10	100	6.02	3.78	5.93	228	7.71	9.96
90	50	5	259	438	707	1270	893	1170
90	50	100	345	438	707	25500	893	1170
720	10	5	19.5	30.1	47.4	91.3	61.8	79.8
720	10	100	48.2	30.1	47.4	1830	61.8	79.8
720	50	5	2070	3490	5650	10200	7160	9340
720	50	100	2760	3490	5650	204000	7160	9340

Table 6.2: Comparison of number of flops (in million) between different algorithms.

The number of flops required using the Fourier series expansion method is:

$$N_h^3(8n^3+32n^2)+N_h^2(12n^3-120n^2+8n+32)+N_h(6n^3+270n^2+10n+4nN)+n^3-135n^2+4n$$

where N_h is the number of harmonics.

In Table 6.3, a comparison is made between the Fourier series analysis method and Algorithm 1 when the intermediate matrices are stored. It can be seen that a critical number of harmonics exists below which the Fourier series analysis is better. This changes with the number of intervals, it increases when the latter increases.

N	N_h	n	Fourier Series Analysis	Algorithm 1
90	6	10	2.50	3.78
90	6	50	277	438
90	10	10	11.6	3.78
90	10	50	1200	438
720	6	10	2.59	30.1
720	6	50	277	3490
720	10	10	11.8	30.1
720	10	50	1200	3490
720	15	10	39.7	30.1
720	15	50	3920	3490

Table 6.3: Comparison between algorithm 1 and the Fourier Series analysis.

Various speeds and numbers of intervals were used to compare the two new algorithms in the analysis of four-bar mechanism modelled with one finite element per link and whose data is given in Table 4.1. Both algorithms deliver the maximum computational advantage near one of the critical speeds where the time taken by the transient solution to vanish is quite large. A method which will be discussed in the next chapter shows that $\omega = 62 \text{ rad/s}$ is one of these critical speeds for the mechanism considered modelled with 1 element per link. In Fig. 6.5 the convergence of the solution is shown starting from a zero state vector. It was found that 31 cycles were necessary for the solution to converge with a relative error of 10^{-4} and a damping ratio of 2%, whereas the same result is obtained using algorithm 1 after just two cycles.

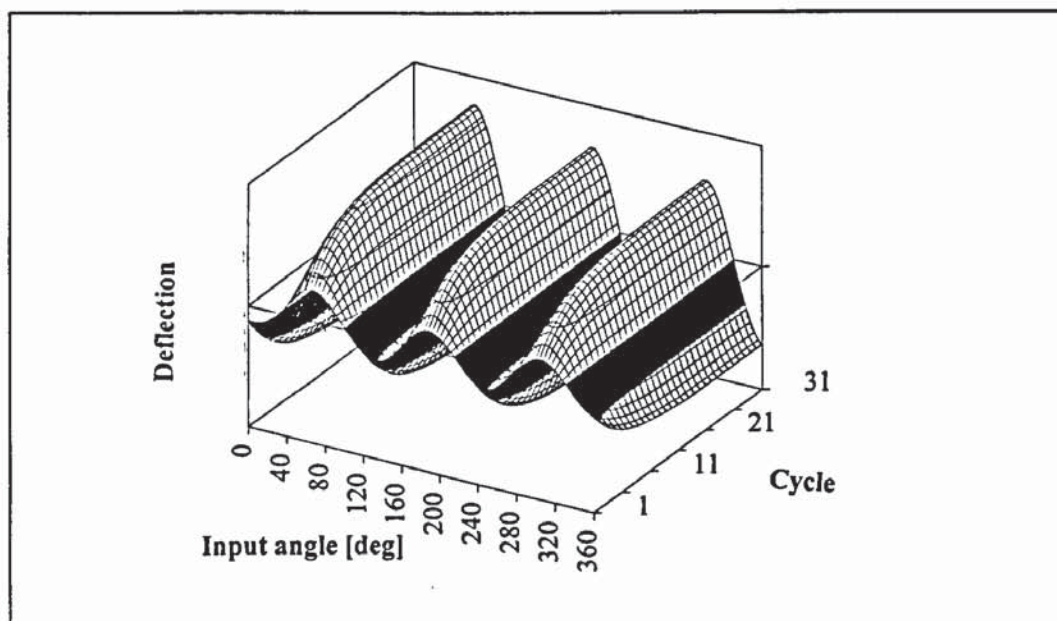


Fig. 6.5: Convergence of the deflection at the midpoint of the follower, $\omega=62 \text{ rad/s}$.

Further comparison was made between the two algorithms. One of the important features of an algorithm is the CPU time consumed or the number of floating point operations. In Fig. 6.6 a comparison between algorithm 1 and 2 is made with regard to the number of floating point operations involved. The difference between the two algorithms is due to the extra operations needed in algorithm 2 to evaluate the inverse of matrices G_k . Finally the CPU time is linear with respect to the number of

intervals. The results from the straightforward method in which the simulation is started from an arbitrary initial condition and the transient solution is let to die out over the cycles have been included in Fig. 6.6. at a speed of 62 rad/s and for two damping ratios.

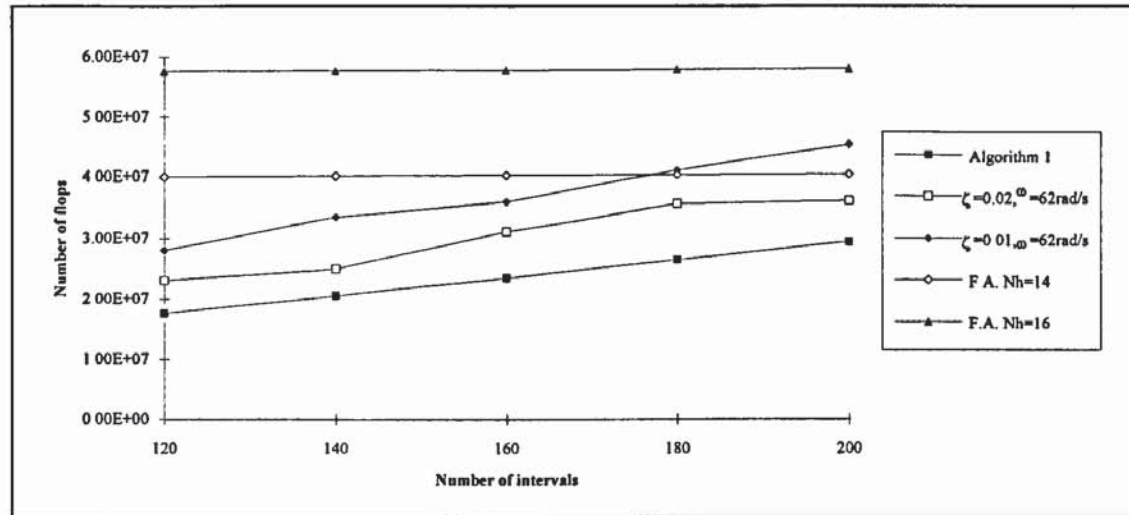


Fig. 6.6: Comparison of the number of flops between different algorithms.

6.9. CONCLUSION

In this chapter an outline of the methods available to calculate the steady-state solution of a four-bar mechanism running at constant high-speeds has been presented. Two new algorithms have been discussed which give the steady-state solution quickly and efficiently. It has been shown that the difference between the two algorithms is purely procedural and that one of them is always more advantageous than the other. In many situations the new algorithms have been proven to be superior to the existing algorithms. The algorithms developed could be used to solve the steady-state of any second order equations with periodic coefficients and therefore they could be applied to many other mechanisms and to manipulators performing repetitive tasks.

Chapter 7

A METHOD OF RUNNING THE MECHANISM ABOVE SEVERAL CRITICAL SPEEDS

7.1. INTRODUCTION

The response of a mechanism running at high-speed is made up of two components, namely the quasi-static and the dynamic response. Both responses depend on the rotational speed. However, when the quasi-static response is plotted versus speed, no peaks are encountered. In contrast, when the "responsiveness" of the system is at a local maximum for a given speed, the dynamic response peaks at this speed called a critical speed. Dynamic analysis of a four-bar mechanism shows that it has many critical speeds where the response of the system is large compared to the response at neighbouring speeds. In the literature these critical speeds have been linked by some researchers to the natural frequencies of the individual links (Lawrence and Alexander, 1975; Sanders and Tesar, 1978; Turcic *et al.*, 1984; and Liao *et al.*, 1985) and to the mean value of the natural frequencies of the mechanism by others (Stamps and Bagci, 1983). In this study critical speeds are related to the mean value of the natural frequencies over the cycle. Some of these speeds are *limiting* critical speeds defined as speeds which cannot be exceeded because stresses in one of the links would become greater than the safe working stress. This chapter deals with the location of the critical speeds, assesses the stability of the system and proposes a method of running the mechanism safely above one or more limiting critical speeds. The role of damping in governing the vibration levels of the mechanism is also discussed.

The equations of motion of a four-bar mechanism rotating at a constant speed form a system of ordinary differential equations with periodic coefficients. Such systems are encountered in many fields of engineering, for example helicopter rotor blades (Peters and Hohenemser, 1971), wind turbines (Friedmann and Silverthorn, 1974), rotor dynamics and elastic structures under parametric excitation (Bolotin, 1964). For such systems, stability is an important issue. Instability exists, under certain conditions, for excitation frequencies significantly lower than the first natural frequency. For many years the stability of mechanisms has been a subject of thorough investigation. The studies have concentrated on two basic mechanisms, namely the four-bar mechanism and the slider crank mechanism. Initially only one link was considered to be flexible (Smith and Maunder, 1971; Jasinski *et al.*, 1971; Masurekard and Gupta, 1988a; Lee and Beale, 1992). The resulting equation of motion was then transformed into a Mathieu-Hill type for which stability charts exist and methods of solution are readily available. In the sections that follow the stability of a four-bar mechanism with all links flexible will be studied.

7.2. TRANSITION MATRIX AND STABILITY ANALYSIS

Time domain simulation of a four-bar mechanism can absorb a significant amount of computer time. In particular, near a critical speed or when the damping in the system is low, the time needed for the solution to converge may become quite long. In order to reduce the time required for simulations it is essential to use a method to predict the critical speeds over the range of speeds of interest. Nagarajan and Turcic (1990c) developed an approximate theoretical method to predict what they referred to as critical speeds for elastic linkage systems without performing time marching simulations. Their method predicts only the critical speeds for one "mode" at a time and implicitly, they assume that there is no transfer of energy between different modes of vibration throughout the cycle. This is not true in general. However, it

does suggest an accurate approach for the computation of critical speeds and unstable bands which is not based purely on numerical integration.

The equations of motion for a mechanism, when instantaneous structure formulation is adopted, are of the form:

$$\mathbf{M} \ddot{\mathbf{q}} + \mathbf{C} \dot{\mathbf{q}} + \mathbf{K} \mathbf{q} = -\mathbf{M} \ddot{\mathbf{q}}_r \quad (7.1)$$

The behaviour of a system governed by (7.1) is determined by its transient response starting from any set of initial conditions. For stability analysis purposes only the homogeneous part of the equations of motion is considered. The system is unstable if the transient response is unbounded, marginally stable if the transient part is neither decaying nor growing, and finally it is stable if the transient response is bounded and tends towards zero. One way of checking if the transient response is bounded is by calculating the *transition matrix* which will now be defined. First the homogeneous part of (7.1) is transformed into a first order differential form as:

$$\dot{\mathbf{y}}(t) = \mathbf{A}(t)\mathbf{y}(t) \quad (7.2)$$

In this equation \mathbf{y} is the state vector and $\mathbf{A} = \begin{bmatrix} \mathbf{0} & \mathbf{I} \\ -\mathbf{M}^{-1}\mathbf{K} & -\mathbf{M}^{-1}\mathbf{C} \end{bmatrix}$

Since the operating speed is held constant and since all matrices are periodic, then the matrix $\mathbf{A}(t)$ is time periodic with a period T . Equation (7.2) is therefore a linear differential equation with periodic coefficients. A paper by Floquet (1883) was a landmark in the study of this type of problems. In fact Floquet presented two separate theorems; one dealt with the form of the solution, and the other gave a practical method to assess the stability of the system.

7.2.1 Floquet Theorem for Analysing Periodic Systems

A theorem by Floquet (1883) states that the fundamental system of solutions of (7.2) is of the form:

$$\mathbf{Y}(t) = \Phi(t)\exp(\mathbf{B}t) \quad (7.3)$$

Where $\Phi(t)$ is a periodic matrix with period T and \mathbf{B} is a constant matrix. $\mathbf{Y}(t)$ is a square matrix where each column represents one possible solution of (7.2).

Although Floquet's theorem does not yield the exact solution to the problem, it yields valuable information regarding the form and the properties of the solution. It is interesting to learn under what circumstances (7.1) has a stable solution.

If $\mathbf{y}(t)$ is a solution of (7.2) then it is always possible to find a vector \mathbf{z} so that $\mathbf{y}(t) = \mathbf{Y}(t) \mathbf{z}$, i.e. \mathbf{y} is a linear combination of the fundamental solutions. Then using (7.3) it is found that $\mathbf{y}(t) = \Phi(t)\exp(\mathbf{B}t) \mathbf{z}$. In particular, when \mathbf{z} is an eigenvector of $\exp(\mathbf{B}T)$ it is found that:

$$\mathbf{y}(t + T) = \rho \mathbf{y}(t) \quad (7.4)$$

where ρ is the corresponding eigenvalue of $\exp(\mathbf{B}T)$, and is called a *characteristic multiplier*.

From (7.4) it can be concluded that the system will be stable if all the eigenvalues of $\exp(\mathbf{B}T)$ have a modulus less than or equal to 1 and will be unstable if any of the eigenvalues have modulus greater than 1. The stable ranges are each bounded by two speeds. One corresponds to $\rho = 1$ and the other corresponds to $\rho = -1$ (the solutions of (7.2) in this case are periodic with period T and $2T$ respectively). Some methods

for assessing stability of the system are based on the latter property. Such methods include the *infinite determinant* method. Since the regions of stability and instability are separated by boundaries corresponding to the solution being T periodic or $2T$ periodic, in the infinite determinant method the state vector is expanded as Fourier series for both cases and replaced in the equations of motion. Then, by equating to zero the total coefficient of linearly independent trigonometric functions, a set of linear, homogenous algebraic equations is obtained where the unknowns are the coefficients of the Fourier series. For the system to have non-trivial solutions, the determinant of the system is set equal to zero. Strictly, the size of the matrix whose determinant is sought is initially infinite. However by truncating the Fourier series an approximate solution is found for the parameter which makes the determinant zero. In the present case the independent parameter is rotational speed. Usually the level of truncation is varied starting from a small number of terms and continuing until the solution adequately converges.

7.2.2 Definition of the Transition Matrix and its use for Assessing Stability.

The transition matrix \mathbf{R} (also called the *monodromy* matrix) is defined by:

$$\mathbf{R} = \mathbf{Y}(T) \text{ when } \mathbf{Y}(0) = \mathbf{I} \quad (7.5)$$

\mathbf{I} is the identity matrix.

There are two main methods by which the transition matrix can be obtained numerically.

Method 1: a column k is obtained by integrating (7.2) for the initial conditions where the k th element of $\mathbf{y}(0)$ equals 1 and all remaining elements are zero. Therefore it follows from the definition that the transition matrix is $\mathbf{R} = \exp(\mathbf{B}T)$.

Method 2 was first presented by Pipes (1953) and later refined by Hsu (1974). Hsu divided the fundamental period into N sub-intervals over which $A(t)$ is approximated by some set of simple continuous functions for which a closed form analytical solution is known. Pipes (1953) and Hsu (1974) presented several functions which can be used to form a piece-wise continuous approximation of $A(t)$, each of which resulted in a different form of the solution. The simplest of these was the constant step function where the matrix A is considered constant over each sub-interval. The latter approach was used by Nagarajan and Turcic (1990c), the difference being that they used the original second order differential equation (the homogenous part of (7.1)).

Let $\psi(t, t_0)$ be a fundamental solution, t_0 indicates the time at which the matrix was initialised (usually $t_0 = 0$). Let $z(t)$ be defined by: $z(t) = \psi(t, t_0) y(t_0)$. Since $\psi(t_0, t_0) = I$, $z(t_0) = y(t_0)$. Also, z satisfies (7.2): $\dot{z} = \dot{\psi} y(t_0) = A(t)\psi y(t_0) = A(t)z$. Clearly, z is the solution to the problem described by (7.2).

Some interesting relations hold for ψ (group properties):

$$\begin{aligned}\psi(t_3, t_1) &= \psi(t_3, t_2) \psi(t_2, t_1) \quad \forall t_1, t_2, t_3 \in [0, T] \\ \psi(t_2, t_1) &= \psi^{-1}(t_1, t_2)\end{aligned}\tag{7.6}$$

In the particular case where matrix A is constant, $\psi(t, t_0)$ is given by $\exp(A(t - t_0))$. Meirovitch (1986) gave some alternative recursive algorithms to compute ψ based on the series development of the exponential function of a matrix.

When the non-homogenous term $h(t)$ is considered (in this case $h(t) = [0 \ \ddot{q}_r]^T$), the general solution is given by:

$$y(t) = \psi(t, t_0) y(t_0) + \int_{t_0}^t \psi(t, \tau) h(\tau) d\tau\tag{7.7}$$

If the integration is started from $t_0 = 0$, the steady-state solution would be obtained for a particular value of $y(0)$. This value is found by expressing the periodicity of the system i.e. $y(T) = y(0)$. This leads to the expression:

$$y(0) = [I - \psi(T, 0)]^{-1} \int_0^T \psi(T, \tau) h(\tau) d\tau \quad (7.8)$$

$\psi(T, 0)$ is the transition matrix **R** introduced in the previous section. Furthermore it can be shown that (7.8) leads to the same initial state vector given by algorithm 2 from the previous chapter.

7.2.3 Use of the Transition Matrix to Compute Critical Speeds.

Instability is more of an academic concern than a practical one for mechanism designers. This is because the stresses in the links generally will exceed safe working levels at speeds well below those where unstable speed bands are encountered. Fig. 7.1 shows that critical speeds as defined in this chapter are a real concern for the mechanism designer and efficient computation of these is therefore important. It is proposed here that an efficient computation method for finding critical speeds is possible based only on the eigenvalues of the transition matrix.

It is intuitively obvious that the "responsiveness" of the mechanism is characterised by the values of the eigenvalues of the transition matrix. Thus, it is to be expected that since the forcing pattern (the r.h.s. of the equations of motion) has no local maxima with respect to speed, a local maximum of displacements can arise when the "responsiveness" of the mechanism is at, or near, a local maximum. Fig. 7.1 shows clearly that every critical speed coincides, or nearly coincides, with a local maximum of the real part of one of the eigenvalues of the transition matrix. This observation can account for very substantial savings in computational effort for finding critical speeds because in the region of most critical speeds, the transient

vibrations in the numerical integration for the mechanism takes many cycles to decay. The same trend was obtained for the solution of an equation similar to (7.2) where y is: (i) a scalar and (ii) a two elements vector with arbitrary periodic coefficients.

Nagarajan and Turcic (1990c) proposed an approximate method whereby the ranges of speeds where instability occurs can be determined. Their method involved the determination of the monodromy matrix at each speed. The eigenvalues of this matrix indicated whether the mechanism was stable or unstable at each speed. The presence of one or more eigenvalues of the monodromy matrix which exceeded 1 in magnitude indicated that the mechanism was unstable at that speed. A variation of their method has been used in the present study to find those speeds which are defined in this study as "critical speeds" (i.e. local maxima in the plots of r.m.s. stress or displacement versus rotational speed). In their method, if damping is considered some critical speeds "disappear" in that no numerical instability occurs at those speeds. However as witnessed by Fig. 7.1, despite this there are still local maxima in the strain curves at these speeds.

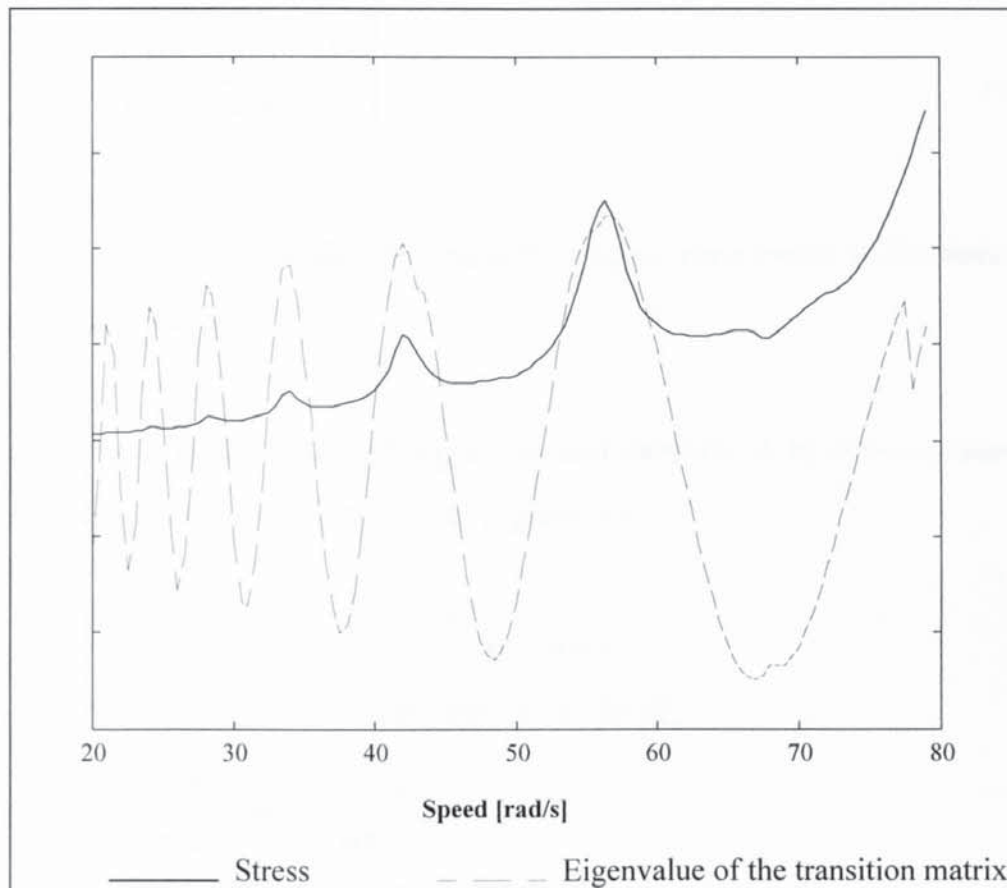


Fig. 7.1: Local maxima of stress and the real part of the maximum eigenvalue of transition matrix (The vertical axis is different for the two graphs)

When modal analysis is employed and each mode is treated separately as Nagarajan and Turcic (1990c) did, it is shown that the critical speeds coincide with the maxima of the real part of one of the eigenvalues of the transition matrix. Furthermore these critical speeds occur at integer divisions of the mean value of the eigenvalue over one cycle. This has also been verified using the data published by Nagarajan and Turcic. In fact, this can be proven analytically if the natural frequencies of the mechanism are assumed to be constant over one cycle.

If the natural frequencies during the cycle are approximated by their average value ω , the basic transition matrix during the time Δt is (Nagarajan and Turcic, 1990c):

$$A = \begin{bmatrix} \cos(\varpi\Delta t) & \frac{1}{\varpi}\sin(\varpi\Delta t) \\ -\varpi\sin(\varpi\Delta t) & \cos(\varpi\Delta t) \end{bmatrix} \quad (7.9)$$

The damping was not included because zero damping corresponds to the worst case with regard to stability.

When the cycle is divided into N equally spaced intervals, A becomes constant for all sub-intervals. After two intervals A^2 is given by:

$$\begin{aligned} A^2 &= \begin{bmatrix} \cos^2(\varpi\Delta t) - \sin^2(\varpi\Delta t) & \frac{1}{\varpi}\sin^2(\varpi\Delta t) \\ -2\varpi\cos(\varpi\Delta t)\sin(\varpi\Delta t) & \cos^2(\varpi\Delta t) - \sin^2(\varpi\Delta t) \end{bmatrix} \\ &= \begin{bmatrix} \cos(2\varpi\Delta t) & \frac{1}{\varpi}\sin(2\varpi\Delta t) \\ -\varpi\sin(2\varpi\Delta t) & \cos(2\varpi\Delta t) \end{bmatrix} \end{aligned}$$

and after N intervals ($N\Delta t = T$) the monodromy matrix is:

$$A^N = \begin{bmatrix} \cos(N\varpi\Delta t) & \frac{1}{\varpi}\sin(N\varpi\Delta t) \\ -\varpi\sin(N\varpi\Delta t) & \cos(N\varpi\Delta t) \end{bmatrix} = \begin{bmatrix} \cos(\varpi T) & \frac{1}{\varpi}\sin(\varpi T) \\ -\varpi\sin(\varpi T) & \cos(\varpi T) \end{bmatrix}$$

The eigenvalues of the monodromy matrix are solutions of the characteristic equation: $\lambda^2 - 2\lambda\cos(\varpi T) + 1 = 0$. The solutions are $\lambda = \cos(2\pi\frac{\varpi}{\omega}) \pm i\sin(2\pi\frac{\varpi}{\omega})$ where $\omega = 2\pi/T$.

When the speed is an integer division of the mean natural frequency the eigenvalues become real and the transient solution is periodic with period T . Although the natural frequencies are not constant, the eigenvalues of the transition matrix exhibit the same variation as when the natural frequency was assumed constant, and for the mechanism considered the above approximate equation holds.

Stability of systems governed by differential equations with periodic coefficients has been the subject of investigation for a long time. Meissner (1918) investigated the Hill type equation:

$$\frac{d^2y}{d\theta^2} + T^2 q(\theta)y = 0 \quad (7.10)$$

where $q(\theta)$ assumes a finite number of different values in the interval $[0, 2\pi]$ and is periodic with period 2π .

Meissner divided the interval into N parts of length θ_i , $i = 1$ to N with $\theta_1 + \dots + \theta_N = 2\pi$. He then assumed that $q(\theta) = v_i^2 / 4\pi^2$ during the i th interval; he also assumed that the solution, $y(\theta)$, during this interval was of the form: $a_1 \cos\left(\frac{Tv_i\theta}{2\pi}\right) + a_2 \sin\left(\frac{Tv_i\theta}{2\pi}\right)$, where a_1 and a_2 are different for each interval and are unknowns. A system of equations was obtained by ensuring the continuity of the state vector solution across the sub-intervals. Moreover, at the end of one complete cycle, the state vector must be λ times the state vector at the start of the cycle thereby providing an extra two equations. The condition for these equations to give non-trivial solutions led to an algebraic system. Meissner then derived a procedure to assess the stability of (7.10).

$$\text{First he defined } C_i = \cos\left(\frac{Tv_i\theta_i}{2\pi}\right), \quad S_i = \sin\left(\frac{Tv_i\theta_i}{2\pi}\right) \quad \text{and} \quad V_{ik} = \frac{1}{2}\left(\frac{v_i}{v_k} + \frac{v_k}{v_i}\right)$$

($i, k = 1$ to N)

In the cases where the interval was divided into 2 and 3 sub-intervals, Meissner defined J_2 and J_3 respectively by:

$$J_2 = C_1C_2 - V_{12}S_1S_2, \text{ and} \quad (7.11)$$

$$J_3 = C_1C_2C_3 - V_{12}S_1S_2C_3 - V_{13}S_1S_3C_2 - V_{23}S_2S_3C_1$$

In the two interval case, by drawing J_2 in the plane $\left(x_1 = \frac{T v_1}{2}, x_2 = \frac{T v_2}{2}\right)$, the author drew the curves $J_2 = \pm 1$ and found that they consisted of infinitely many separate branches bounding the regions of stability as shown in Fig. 7.2. Therefore, given T, v_1 and v_2 the stability of the system governed by (7.10) could be assessed.

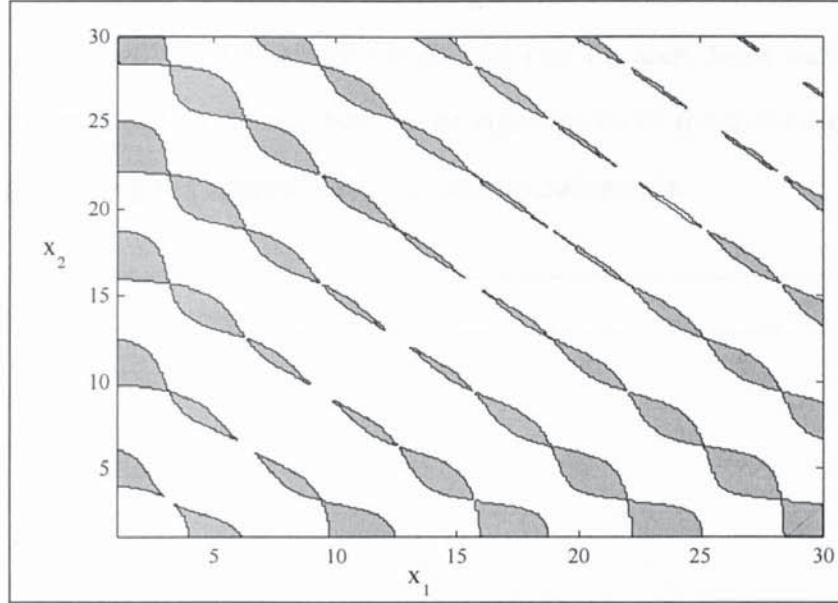


Fig. 7.2: Instability regions corresponding to $J_2 = \pm 1$.

A closer examination of the procedure reveals that it is equivalent to calculating the eigenvalues of the monodromy matrix as developed by Nagarajan and Turcic. The advantage of the Nagarajan and Turcic method is its compact form. As the number of sub-intervals grows, Meissner's method becomes cumbersome as it leads to a bigger system (of order $2N$). Also, in the latter case, an analytical method is necessary to assess the stability of the system. Surprisingly, however the method converges quite rapidly. On the other hand the natural frequencies used in the functions J could be obtained experimentally.

When modal analysis is used, the homogenous part of (7.1) is transformed into a set

of uncoupled equations of form (7.10). $\frac{d^2 y}{d\theta^2} + \frac{\omega_{mi}^2(\theta)}{\omega^2} y = 0, \theta \in [0, 2\pi]$, where ω_{mi} is

the instantaneous natural frequency of mode m and ω is the rotational speed of the input link. From this, it is seen that ω is analogous to $2\pi/T$ and ω_{mi} is analogous to v_i in (7.10).

In Fig. 7.3, the functions J for $N = 2, 3$ and 4 are compared to the real part of one of the eigenvalues of the monodromy matrix for different speeds. The monodromy matrix was obtained for 180 sub-intervals. As can be seen from this figure, the functions J correspond to the real part of the eigenvalues of the monodromy matrix, and they can give a good approximation of the critical speeds.

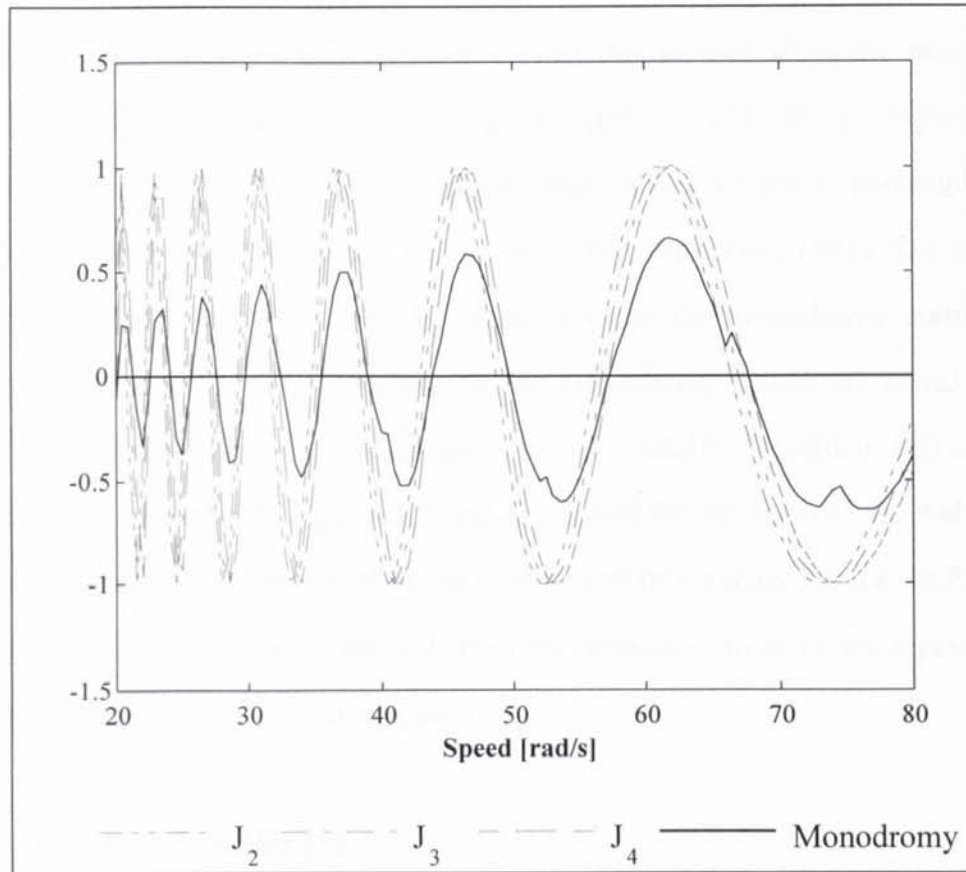


Fig. 7.3: Comparison between the functions J and the real part of one of the eigenvalues of the monodromy matrix.

Another equation which gained considerable attention and which appears in many engineering applications is Mathieu's equation: $\ddot{y} + (d + \epsilon \cos(2t))y = 0$. Mathieu (1886) himself derived this equation while dealing with vibrational modes of a

stretched membrane having an elliptical boundary. There are many similarities between the problem in hand and the stability charts resulting from the solution of the Mathieu equation. When $\epsilon = 0$, there is an infinite number of values of d where the solution is unstable. These values are $d = i^2$ where i is an integer. In the same way the parameter d corresponds to $(\bar{\omega}_m / \omega)^2$ and therefore when the speed ω is an integer division of the mean value of the natural frequency $\bar{\omega}_m$ corresponding to mode m , the system becomes unstable. Furthermore when the parameter d increases (for a constant value of ϵ) the regions of instability become narrower. When the speed decreases the regions of instability also become narrower. Finally the damping has greater effect when d is bigger. In the case of the four-bar mechanism, damping has more effect when the speed is low. In fact this is why when the mechanism rotates at low speeds no critical speed appears, and many experimental investigations failed to observe any critical speed below a certain rotational speed (Lawrence and Alexander, 1975; Turcic *et al.*, 1984; Hao *et al.*, 1986). The stability chart of Mathieu's equation could be obtained using the monodromy matrix. For each value of d and ϵ , the eigenvalues of the monodromy matrix are calculated. If either one exceeds unity in modulus, the system is unstable. Results of this analysis are shown in Appendix E. Figures E.1 and E.2 shows the variation of the real part of the first and second eigenvalue of the monodromy matrix versus d and ϵ . In Fig. E.3, the stability of the system is derived from the absolute values of the eigenvalues; dark areas correspond to unstable system.

7.3. CRITICAL SPEEDS

The simulation of the four-bar mechanism was run for a variety of different angular speeds and lengths L_4 (distance between the ground pivots). The mechanism was modelled using instantaneous structure formulation with one finite element per link. The steady-state deflection of the follower midpoint was calculated at different speeds and Fig. 7.4 shows its r.m.s. value plotted against operating speed. Fig. 7.5

shows the maximum stress in the input link for different values of speed and L_4 and Fig. 7.6 shows the peak strain energy for the input speed and for various values of the geometrical parameter L_4 . Clearly, the plots exhibit some local maxima with respect to speed where the r.m.s. steady-state deflection of the follower midpoint, the maximum stress on the input link and the stored energy of the complete mechanism is larger than at neighbouring speeds. These speeds are called critical speeds and have been verified experimentally by many authors especially for higher speed mechanisms; For example Alexander and Lawrence (1974), Cleghorn *et al.* (1984), and Nagarajan and Turcic (1990d). It is interesting to note that the critical speeds themselves are only very weakly dependent on L_4 . The natural frequencies of the mechanism were equally verified to be very weakly dependent on L_4 . By contrast, the peak displacements and stresses at the critical speeds depend very strongly on L_4 .

After a certain number of critical speeds the mechanism begins to have unstable bands where the equations of motion have one or more unstable solutions. That is to say, at least one mode of the transient solution keeps growing indefinitely. The width of these unstable regions increases when the speed is increased. In general it is found that these unstable regions occur at higher speeds than those at which the mechanism can operate due to the level of stress induced.

The deflections, stresses and strain energy depend strongly on L_4 . Fig. 7.4, 7.5 and 7.6 show plots for six different values of L_4 . In this particular case, it transpires that when L_4 decreases, the deflections are greater and the peaks are more pronounced. The usefulness of knowing the relationship between L_4 , the input speed and the maximum stress is demonstrated in section 7.4.

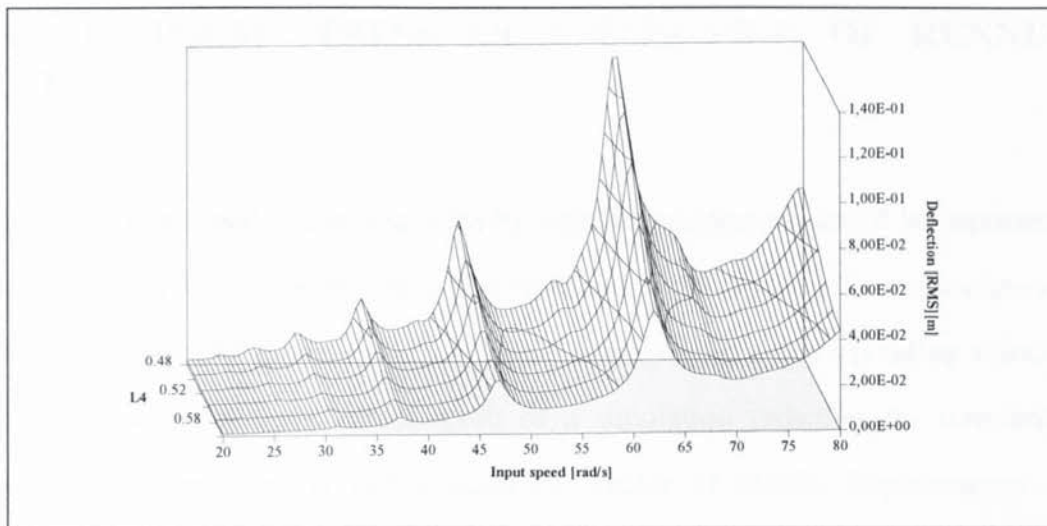


Fig. 7.4: Predicted response of follower midpoint.

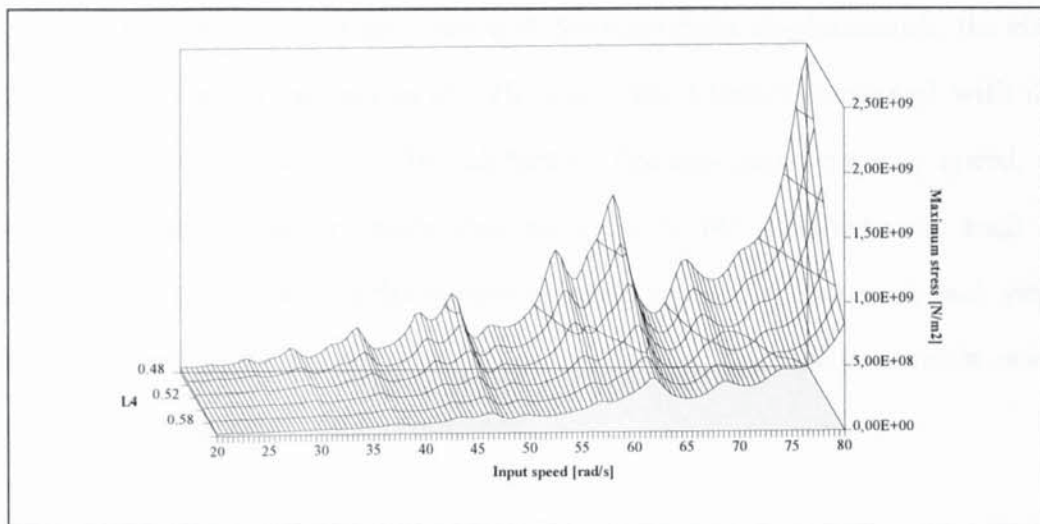


Fig. 7.5: Predicted maximum stress on the input link.

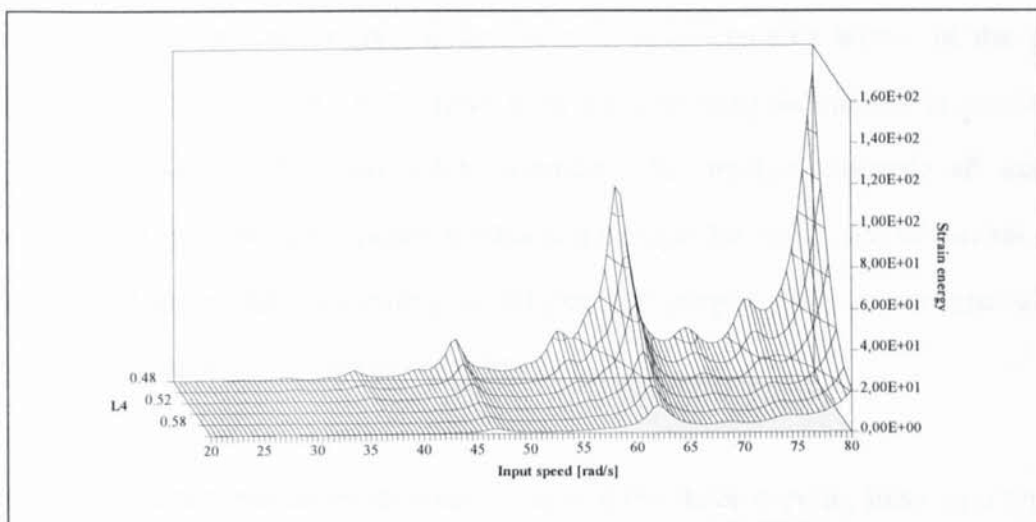


Fig. 7.6: Predicted strain energy of the system.

7.4. MAXIMUM STRESS AS A FUNCTION OF RUNNING SPEED

In Chapter 6, methods were discussed by which a mechanism could be represented in matrix form and its steady-state solution found. A FE model of a mechanism uses displacements as the fundamental variables - along with the corresponding velocities in some cases. The most direct result of a simulation (whether for transient or steady-state behaviour) is that a complete vector of elastic displacements and velocities is obtained for each one of many steps taken during the simulation. The displacements computed are relative to the instantaneous undeformed (rigid-body) position of the mechanism. Compared with the rigid-body displacements, the elastic displacements tend to be very small. However, the stresses associated with these displacements can nevertheless be substantial. For any given running speed, it is sensible to examine the complete state of stress of the mechanism at each step through one cycle and to plot the maximum stress in the mechanism at each step. If several different materials are used in the mechanism, then the maximum ratio of stress to allowable stress can be computed.

Because, in general, stresses are ultimately the most important result of the simulation, it is sometimes necessary to use more finite elements in the model than might be considered necessary for determining displacements alone. In the past, some authors (Midha *et al.*, 1979) have used a modal analysis method to accelerate the determination of the steady-state solution. This method discards all natural modes except the lowest frequency modes and though the nodal displacements may be computed sufficiently accurately for all practical purposes, cases can arise where the computed stresses are significantly inaccurate.

Fig. 7.7 shows the maximum stresses in each of the three moving links in a typical four-bar mechanism as a function of speed. The stresses in this figure have been

determined for a mechanism whose data are given in table 4.1 from a simulation in which 3 beam elements were used for each link in order that the stresses would be determined accurately.

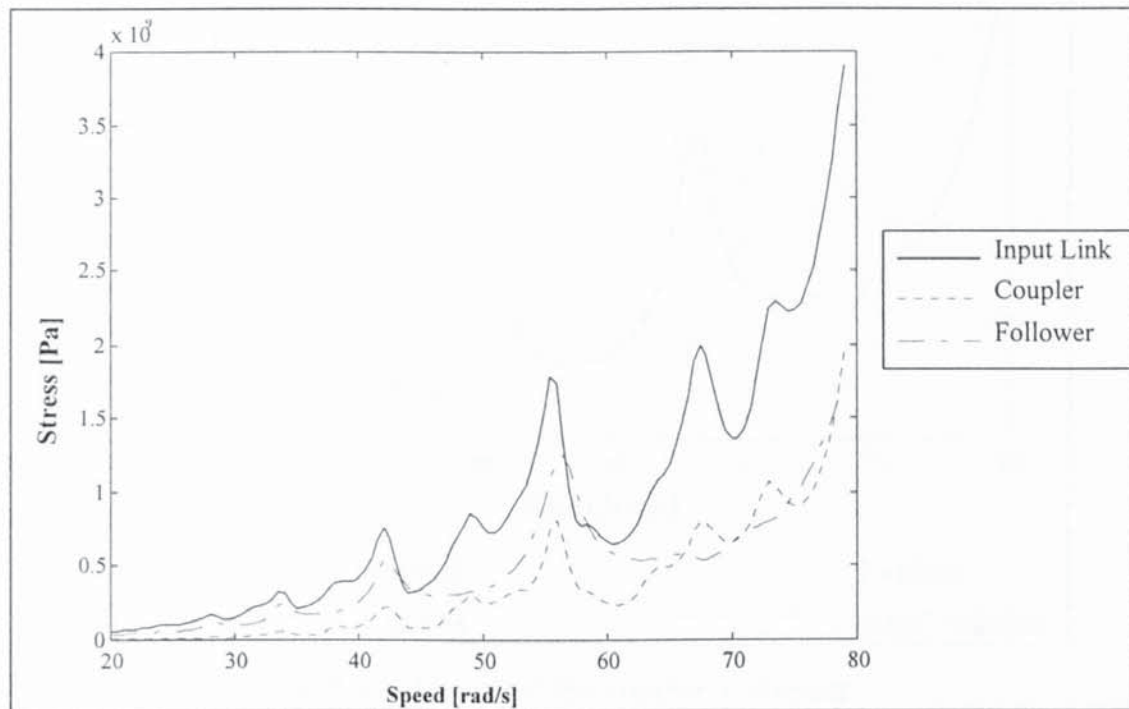


Fig. 7.7: Maximum stress for a damping ratio of 0.02.

7.4.1 Influence of the number of elements

When the FEM is used to model a system, the natural frequencies decrease when the number of elements is increased. Since the critical speeds are related to the natural frequencies, one expects to obtain a decreasing estimations for these critical speeds as the number of elements is increased. Consistent with this, Fig. 7.8 shows the maximum stress versus speed for different numbers of elements per link. From this figure, it is seen that one element per link overestimates the critical speeds noticeably. However, the solution converges quite rapidly as the number of elements increases.

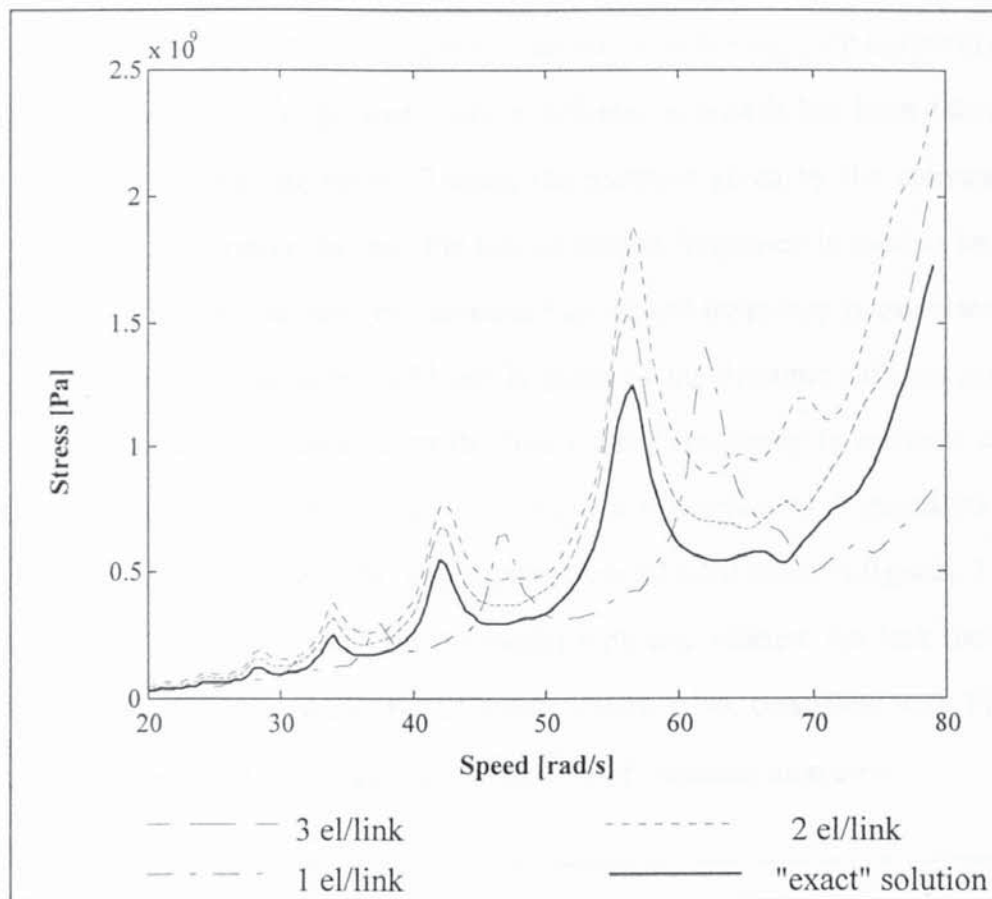


Fig. 7.8: Influence of the number of elements.

Also Fig. 7.9 shows the variation of the stress at the midpoint of the follower for a single speed and for various conditions.

As the number of elements grows, the size of the problem and the CPU time required to solve the problem increases. However, one can achieve an accurate solution by using just one finite element per link and the dynamic stiffness method. Liu and Lin (1993) used the dynamic stiffness method to find the solution of forced flexible systems. They used the principle of virtual work to establish the equations of motion. In their analysis were included: the stiffening effect due to the axial deformation, the effect of Coriolis and the effect of normal accelerations. Then the authors used modal analysis to uncouple the equations of motion. Because these are non-linear, the Wittrick and Williams algorithm (1971) could not be used in order to obtain the natural frequencies and mode shapes needed to uncouple the equations of

motion, instead they used Newton-Raphson method to solve the EVP iteratively, and solved the problem. In the present study a different approach has been taken; the procedure starts by solving the EVP using the matrices given by the conventional FEM. Then by an iterative process, the lowest natural frequency is used to improve the matrices of the system: at every iteration this natural frequency is calculated and then used to calculate the matrices \mathbf{M} and \mathbf{K} given by the dynamic stiffness method. This is repeated until the change on the first natural frequency is within a certain band. The number of iterations was quite low (a maximum of 5 iterations for a relative error of 10^{-3} was needed). This method was labelled exact in figures. 7.8 and 7.9. Fig. 7.9 shows that apart from the model with one element per link there is a good phase agreement between the different models. Also, consistent with Fig. 7.8 the maximum amplitude decreases as the number of elements increases.

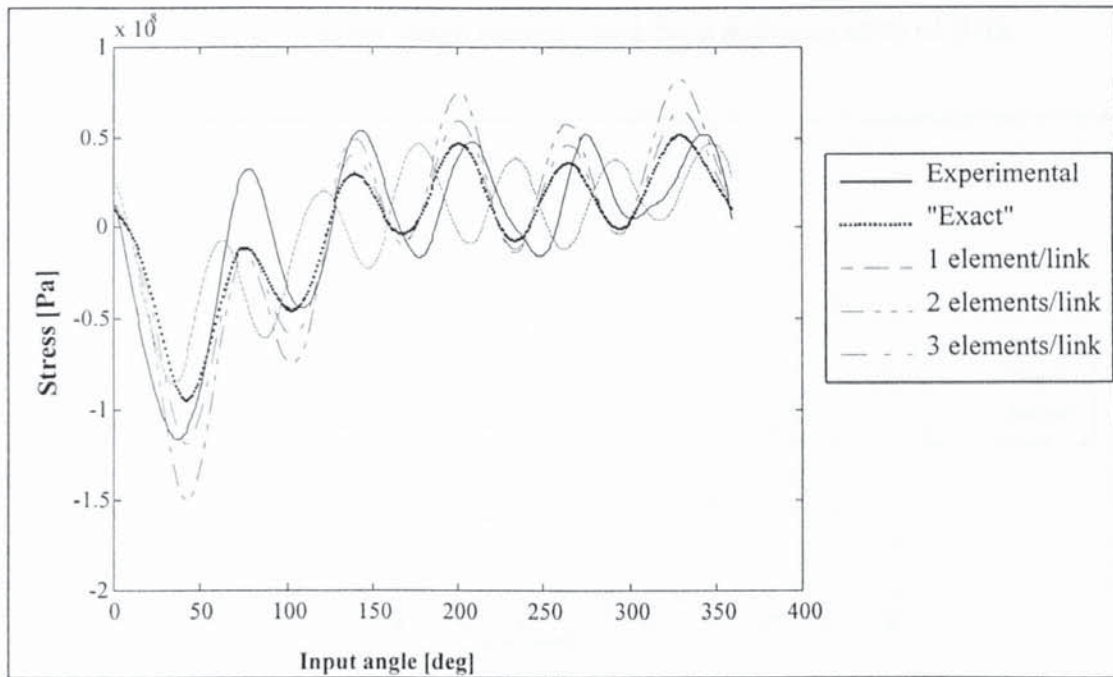


Fig. 7.9: Stress at the follower midpoint for different models at $\omega = 30$ rad/s

7.4.2 The role of damping

The simulation was run for a range of speeds and different damping ratios. For each speed, the steady-state stress was computed over one cycle of rotation. The

maximum stress was then recorded. Figures. 7.10 and 7.11 give a comparison of the maximum stress on the linkages against the rotational speed for different damping ratios.

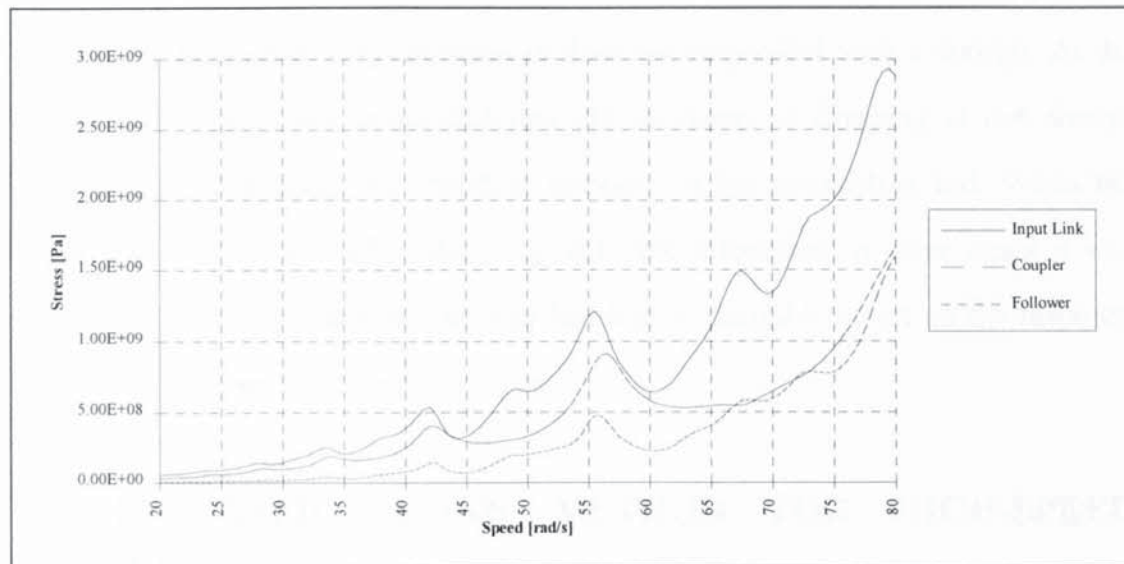


Fig. 7.10: Maximum stress versus speed for a damping ratio of 0.03.

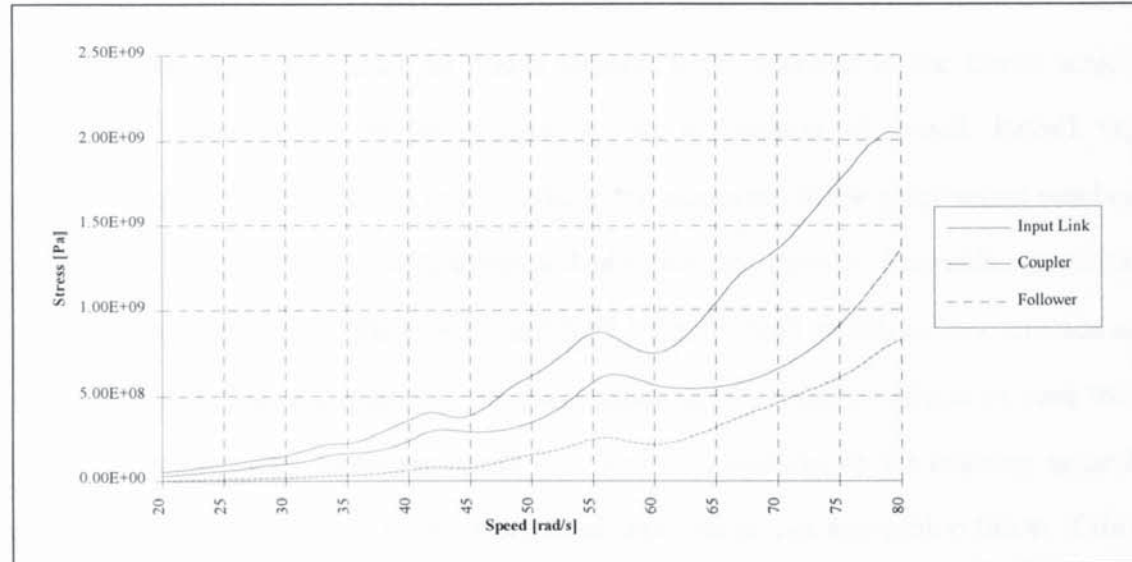


Fig. 7.11: Maximum stress versus speed for a damping ratio of 0.06.

From figures. 7.7, 7.10 and 7.11 it can be concluded that at the critical speeds the damping has a substantial and desirable effect by reducing the maximum stress. However, for the "quiet" speeds it is counterproductive for some links. Therefore, in order to run the mechanism above certain critical speeds, adding more damping to

the system might not be the appropriate solution. A similar result was found by Badlani and Midha (1983) for a different situation. The problem treated then was the effect of internal material damping on the dynamics of a slider-crank mechanism. The connecting rod was assumed to be made of a linear viscoelastic material which they model by Kelvin-Voigt material (a dash pot in parallel with a spring). At the end of their study they concluded that the inclusion of damping is not always beneficial in attenuating the vibration response of the connecting rod. When the speed was in a stable region, damping had little effect and in some cases it was counterproductive, in contrast damping had a most desirable effect on the response when the speed was in an unstable region.

7.5. PROPOSED DESIGN METHOD FOR HIGH-SPEED OPERATION

Most mechanisms run normally above several "critical" speeds in the sense that their normal operating speed may lie above several local maxima in the curve which expresses highest stress in the mechanism as a function of speed. Recall the definition of critical speeds as speeds where the response of the mechanism reaches a local maximum but the deflections and stresses may remain tolerable. At some point in the speed range, there is a "limiting" critical speed which causes stresses to become higher than acceptable if the mechanism is run continuously at or near this speed. In many cases, however, there is a "quiet" speed above the limiting critical speed at which the stresses in the mechanism may be within acceptable limits if this speed can be achieved. This phenomenon is not limited to planar four-bar mechanism, it has been reported by Stamps and Bagci (1983) while investigating a high-speed mechanism with 3 dimensional offsets. The authors reported the existence for these mechanisms of critical speeds and quiet speeds which they called in-between efficiency speeds. Stamps and Bagci linked the critical speeds to the average values of the natural frequencies of the mechanism and concluded that this

effect exists in planar mechanisms also and that it is evident from the experimental work carried out by Alexander and Lawrence (1974).

To reach a "quiet" speed above a limiting critical speed, one approach is to ensure that the system runs for an absolute minimum of time at or near any limiting critical speed. Thus the mechanism is accelerated to its operating speed as quickly as possible by using a high torque driving motor. This is not a practical solution because the torque required to run the mechanism is quite low.

An alternative approach is suggested in this study. From figures. 7.4 to 7.6, it is seen that the amplitude of the stresses induced in a four-bar mechanism reduces if L_4 is increased. By making this distance adjustable, it is possible to run the mechanism up to speed with a large distance between the ground pivots, thereby minimising the amplitude of the induced stresses. Once the operating speed is reached the follower pivot is returned to its original position in order that the mechanism can perform its designed function. It is recognised that the context of some mechanisms is such that changing L_4 would be impractical. In these circumstances it may be possible to achieve the same effect by changing another attribute of the mechanism dynamics - such as the support stiffness for the follower pivot but such a solution has not been pursued.

Increasing L_4 by too much causes the transmission angle to increase beyond the acceptable range, thus affecting the behaviour of the mechanism. Recall that the response of the mechanism is made up of two responses; namely the quasi-static and the dynamic response. The former depends very much on the accelerations of the links. Any change to these accelerations during the cycle, is reflected on the full vibration response of the mechanism. The acceleration curve in Fig. 3.8 is a typical one for a normally proportioned four-bar mechanism; once during each cycle, at a certain angle, the mechanism is subjected to a sudden variation of the inertial forces.

At this angle, the stress becomes maximum. However when L_4 is increased, a second inertia pulse appears at another angle of the cycle; its effect increases with L_4 progressively until the stress at the latter angle becomes dominant. This is shown clearly in Fig. 7.12 and 7.13. This also has been proven experimentally and the results will be presented in the following chapter. Therefore, L_4 should be increased only in a certain range in order to run the mechanism above certain critical speeds. The criterion to determine this range would be the transmission angle below a certain value. Beyond certain value of L_4 the transmission angle becomes too big and the maximum stress begins to increase again.

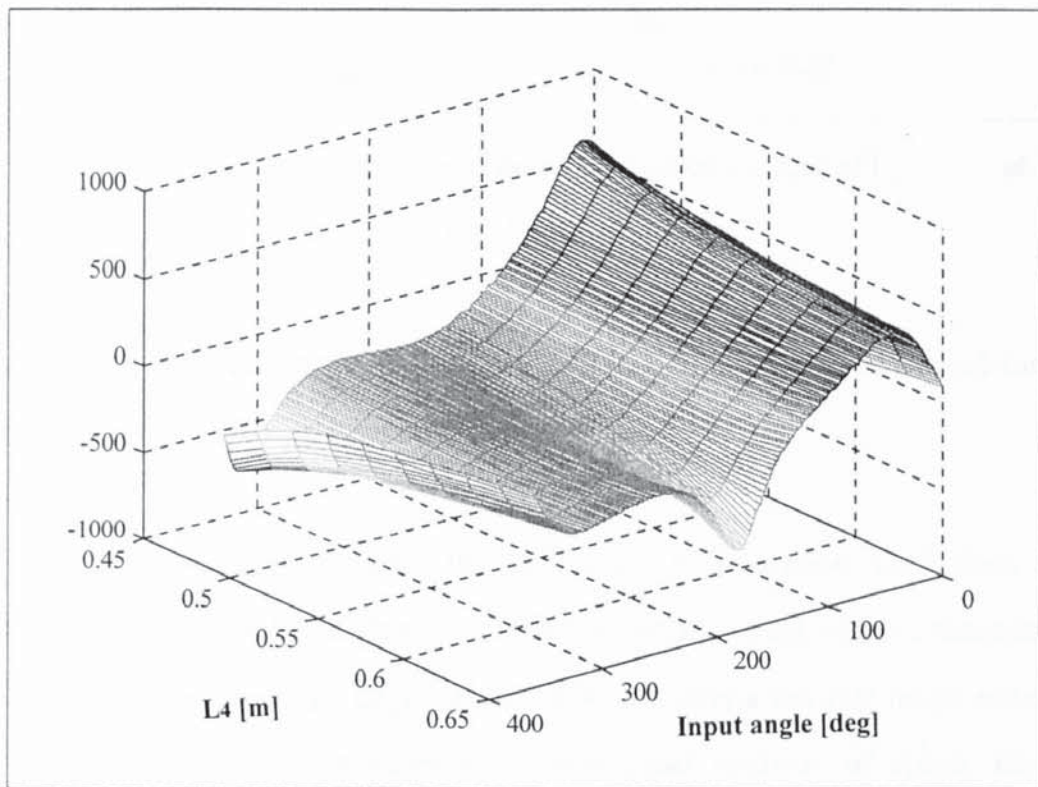


Fig. 7.12: Acceleration of the follower for various transmission angles at $\omega=30$ rad/s.

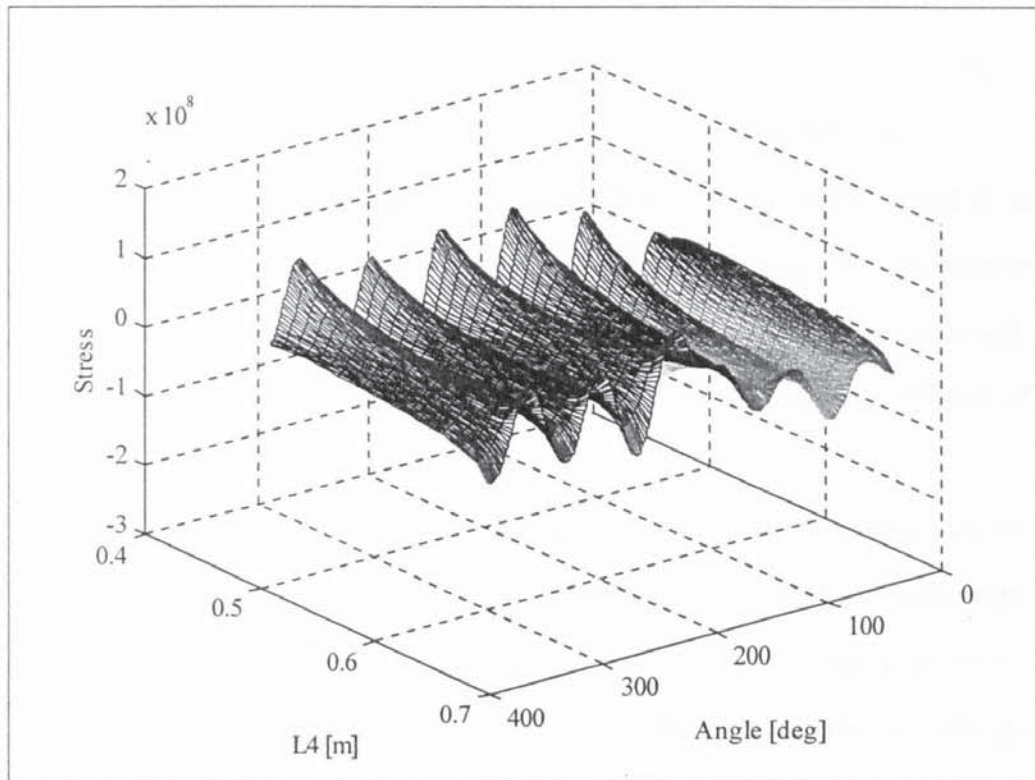


Fig. 7.13: Stress at the follower midpoint for various values of L_4 at $\omega = 30 \text{ rad/s}$.

From the above discussions it becomes evident that the highest steady speed for any given mechanism can be improved the most as follows :

1. Run dynamic simulations for the mechanism to determine the highest ratio between stress in the mechanism and the acceptable stress of the corresponding mechanism element at a large number of speeds over a sensible range assuming low damping. It is not necessary to use equal intervals of speed. Instead, investigate only those speeds which are integer divisions of the average natural frequencies corresponding to the dominant modes.
2. From 1., identify the first limiting critical speed and determine whether there is a "quiet" speed above this at which the stresses could be acceptable.
3. If the answer to 2 is "yes", run the dynamic simulation for the selected "quiet" speed for a slightly increased level of damping to determine whether increasing the damping from the initial low value has the effect of reducing the maximum

stress in the mechanism. (Experience suggests that in some cases at least, the maximum stress in one link reduces while that in another link increases).

4. If increasing the damping appears to be beneficial at the "quiet" speed in terms of reducing the maximum stress in the mechanism, determine the optimum value for the damping by multiple simulations. So long as this value is small, the damping can be introduced without substantially influencing the stiffness of the mechanism elements.
5. Having determined the damping and the desired "quiet" running speed, the minimum change in the mechanism attributes is determined such that the mechanism can be run up to the "quiet" speed without disintegrating. This change of attributes will usually be a change in the distance between the ground pivots.

7.6. CONCLUSION

In this chapter a method to locate critical speeds has been presented based on the mean values of the natural frequencies of the mechanism. Also the stability of the mechanism at certain speeds has been assessed. It has been shown that the response curve presents many critical speeds where the response of the mechanism reaches a local maximum. Some of these speeds are limiting critical speeds. Furthermore, above certain of these speeds there might be a range of speeds where the mechanism can be run safely. In the latter case a method has been presented whereby one of the characteristics of the mechanism is changed temporarily so that, during the run-up, the stresses at the previously limiting critical speeds become acceptable. One characteristic which has been shown to permit this is the distance between the ground pivots. The effect of damping was also discussed and it was shown that increasing damping invariably reduces stresses in links at the critical speeds but that it can have the effect of increasing stresses in some links at quiet speeds. In these cases, the addition of damping can be counterproductive.

Chapter 8

EXPERIMENTAL INVESTIGATION

8.1. INTRODUCTION

In engineering analysis, complex systems are modelled and approximated using simplified mathematical models. These models are based on the physical data of the system (geometrical data and its properties) and a set of rules and principles governed by theoretical models (strength of material, heat transfer, CFD, etc.). Once the mathematical model has been built, results are obtained. These results however are of little value unless corroborated by experimental data or compared to other results obtained from other models which have been validated for a similar problem. Discrepancies are then interpreted, and corrections are made to the model in order to improve its validity. The process is repeated until a satisfactory model is obtained.

In this chapter, the experimental work is conducted in order to validate the theoretical model. The results reported include the path generated by the mid-point of the coupler, the natural frequencies and mode shapes at static configurations and finally the dynamic behaviour of the mechanism running at high-speed.

8.2. DESIGN OF THE TEST RIG

A photograph of the four-bar mechanism used in the present study is presented in Fig. 8.1. The mechanism was designed to have certain characteristics including:

- A good transmission angle throughout the cycle,
- Flexibility at relatively low speed,

- The facility to test different combinations of linkages (length ratios and thicknesses).

The data of the selected mechanism is given in Table 8.1. A split crank and follower design was adopted to ensure that motion would be predominantly in-plane.

	Input Link	Coupler	Follower	Ground
Length [m]	$L_1 = 0.170$	$L_2 = 0.328$	$L_3 = 0.525$	$L_4 = 0.547$
Width [mm]	24.8	25	25	
Thickness [mm]	6.35	3.42	3.15	
The lumped masses of the joints : 0.174 kg				
Material : Steel, Density : $7.85 \cdot 10^3 \text{ kg/m}^3$, Modulus of elasticity : $210 \cdot 10^9 \text{ N/m}^2$				

Table 8.1: Dimensions of the mechanism.

As in any model, some assumptions were made. In order to be able to compare objectively the experimental and the theoretical results, the assumptions made in the model must be reasonably valid in the experimental set-up. One of the assumptions is zero clearance in the joints. The presence of clearance in the joints leads to a discontinuous response, due to the loss of contact which is difficult to model. To ensure smooth power transmission through the joints, the use of small ball bearings was preferred to journal bearings where the clearance is inherent. Also the bearings used had twin races and were pre-loaded. Another assumption made by most researchers relates to the speed of operation. This was assumed to remain constant so that the coefficients of the equations of motion are time periodic. This has been achieved by some researchers using a motor driving the mechanism fitted with a controller. In the present study speed was held constant simply by using two large flywheels at the input shaft, one on each side of the split input links. The flywheels, by virtue of their large inertia, keep the angular speed constant. In reality the angular

speed at the input link will fluctuate due to the dynamic response of the mechanism. In the model, however, the input link was assumed to be a cantilever beam and therefore no dynamic deflection was allowed at the end connected to the flywheel.

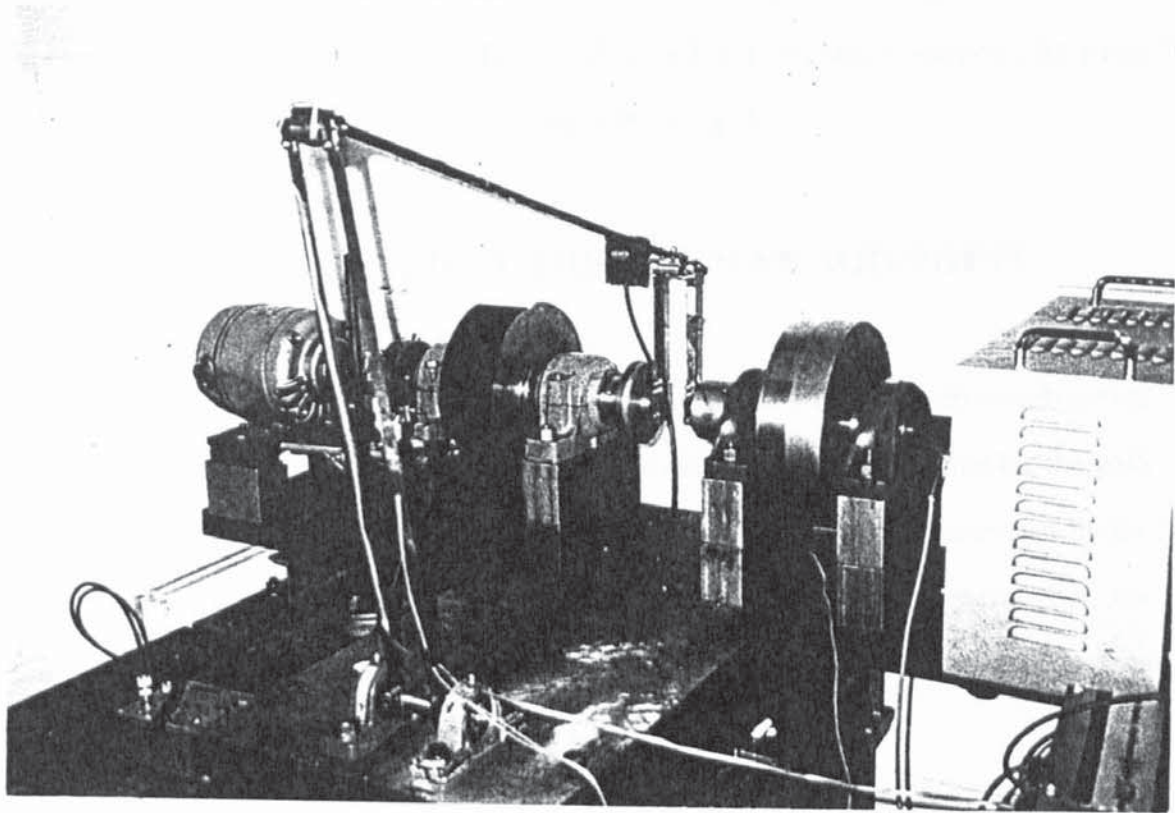


Fig. 8.1 Photograph of the test-rig.

The mechanism was driven by an 0.75 hp DC motor. The speed was adjusted by varying the voltage applied to the motor. An optical tachometer was used to provide an accurate location of the start of the cycle and to calculate the rotational speed. One of the flywheels was fitted with a stripe (the stripe is visible on the flywheel painted in black in Fig. 8.1). At the start of every cycle, a beam of light is reflected from the stripe to a detector and an output spike is generated which could be used to trigger a data acquisition device, or to check if the average speed over the cycles is constant by taking averaged sweeps and checking that the spikes occur at the same position during the sweeps. Finally, the mechanism was mounted on a large cast-iron test bed which isolates the mechanism from any external vibration source. Strain gauges were mounted on the upper and lower surfaces of the coupler, the follower

and the input link. Measuring strain in the input link presented some difficulties. The mechanism being investigated is of a crank rocker type, and therefore unlike the other links which oscillate between two extreme angles, the input link rotates completely. In order to transmit the signal in and out the strain gauges, slip rings were used (these are clearly visible on the right in Fig. 8.1).

8.3. PATH GENERATED BY THE COUPLER MID-POINT

One application of the four-bar mechanism is to generate a certain path which serves some specific purpose. The set of equations developed in Chapter 3 enables the path generated by any point on the coupler to be determined. The paths generated by the input link of the mechanism considered here are circles and those generated by the follower are either circles or arcs depending on the type of the mechanism (see the classification of four-bar mechanisms in Chapter 3).

The purpose of visualising the path generated by any point of the coupler is first to check the validity of the model for various operation speeds and then to see the effect of rotational speed on the path generated. A literature search revealed that only a few researchers have experimentally verified the paths predicted by the model. In a series of papers by Liou and Erdman (1987, 1989), the authors used a photogrammetry technique to analyse the motion of a four-bar mechanism running at high-speed. To achieve this, the background of the experimental set-up was painted in black and special reflectors (precision reflector targets shaped as solid circles) were attached to different points of the linkages. The high-speed camera used was capable of delivering high quality pictures at frame rates between 16 and 500 frames per second. The pictures were then digitised and processed on the computer. The result of this operation could either be a printout of the deflection state at any configuration, or an animation showing the mechanism in motion. The

system could also give the path followed by any point of the mechanism, in particular the coupler. Although the paths generated by the input link were circles this method enabled Liou and Erdman to show that use of a controller to keep the speed constant was not successful. The points on the circle generated by a point of the input link were not equally spaced and therefore it can be concluded that although the average speed over the cycles could be constant, the speed during the cycle did change.

The advantage of the photogrammetry technique in giving the exact deflection shape compared to the method where a series of strain gauges are mounted to the link of interest lies in its accuracy. Also photogrammetry does not cause any change of the characteristics of the system unlike the use of strain gauges. The many wires used with the strain gauges could have an effect on the response of the system. Alexander and Lawrence (1975) recommended that the mass densities of the coupler and output links should be increased by 8% to account for the additional mass of the wires and strain gauges attached to these links in the experimental set-up. The main disadvantages of the photogrammetry method are that the technique is expensive and that the speeds up to which the mechanism could be analysed depend on the speed of the camera. The digitising process is tedious and time-consuming.

Zou *et al.* (1992) used a different technique; a fibre optic cable was attached to the coupler and a laser beam was used as a source of light to generate the path followed by the point where the tip of the fibre optic cable was attached. The speed was kept constant while the pictures were taken. The shutter was kept open long enough for the mechanism to perform some cycles. The path generated was clearly visible from the dark background.

In this study a similar technique was employed but using more accessible devices. The same results were achieved using a LED and a camera. The LED was attached

to the coupler and powered by an external power supply. Different colours were tested and it was found that a green LED had the best effect. The LED was powered then the mechanism was run at a constant speed. A standard manual camera was mounted on its tripod in order to avoid any movement while the pictures were taken. The speed of the shutter was chosen so that several cycles were captured while the shutter was open. Graph paper was placed in the background of the test rig to facilitate digitising the pictures. The following figures show the paths generated for two speeds, a low speed which corresponds to a quasi-static motion and a relatively high speed where the dynamic vibration starts to appear. The high-speed trace is superimposed on the quasi-static one. Also, these figures show that the movement of the mechanism is periodic.

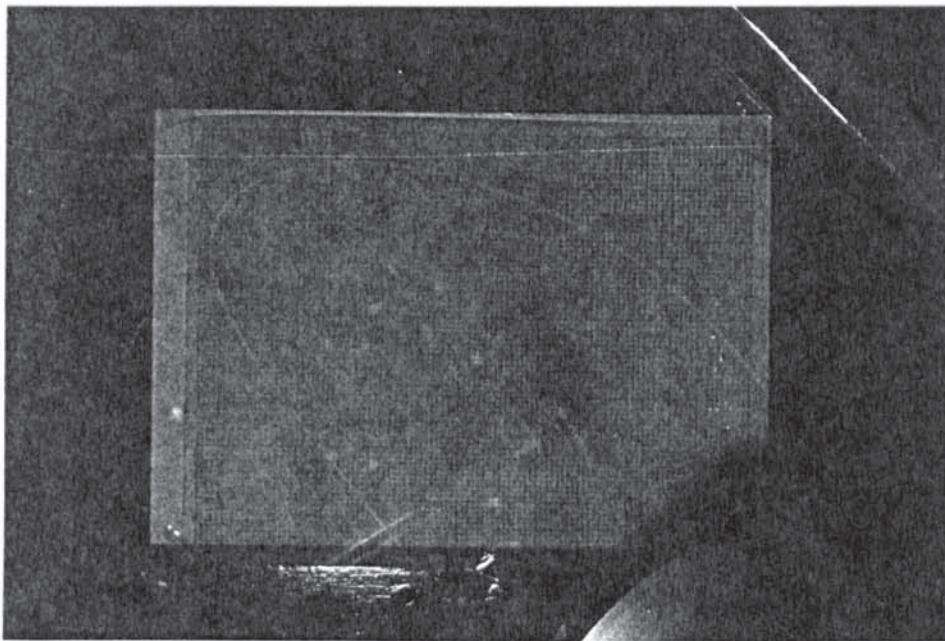


Fig. 8.2.a: Path generated at a low speed.

In the present study the pictures were digitised manually and the results are shown in figures 8.3 and 8.4, whereby the experimental and the theoretical paths are given. The process of digitising was tedious and could have been improved by writing software to facilitate calculating the coordinates of the points on the curve. In figures

8.3 and 8.4 the path obtained experimentally is incomplete because the flywheel seen in Fig 8.2.a masks the lower part of the path.

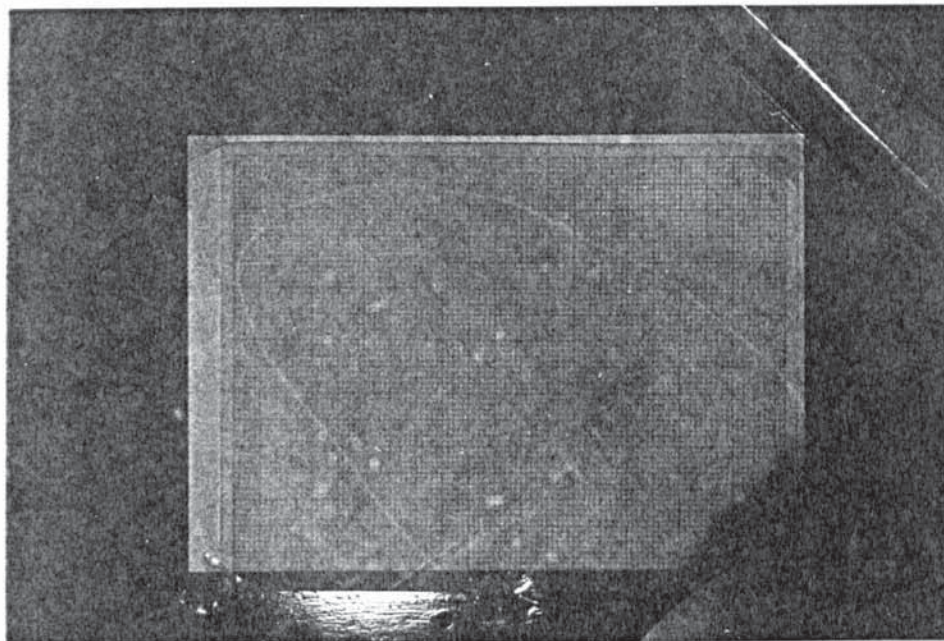


Fig. 8.2.b: Path generated at higher speed.

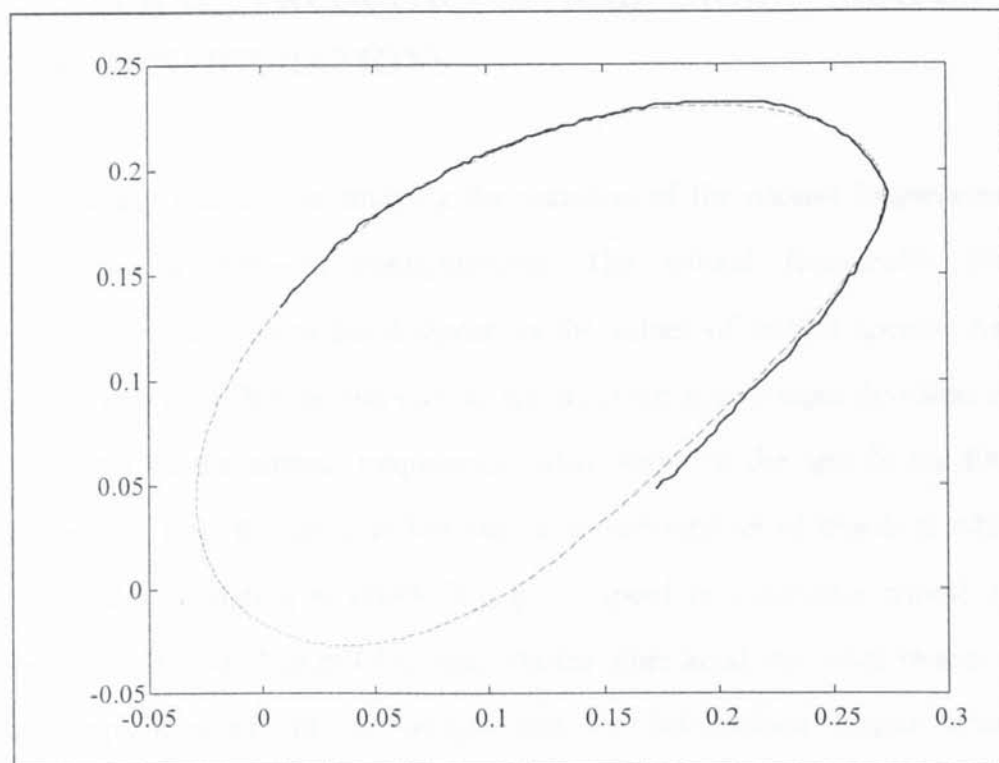


Fig. 8.3: Comparison between the path generated experimentally and theoretically.

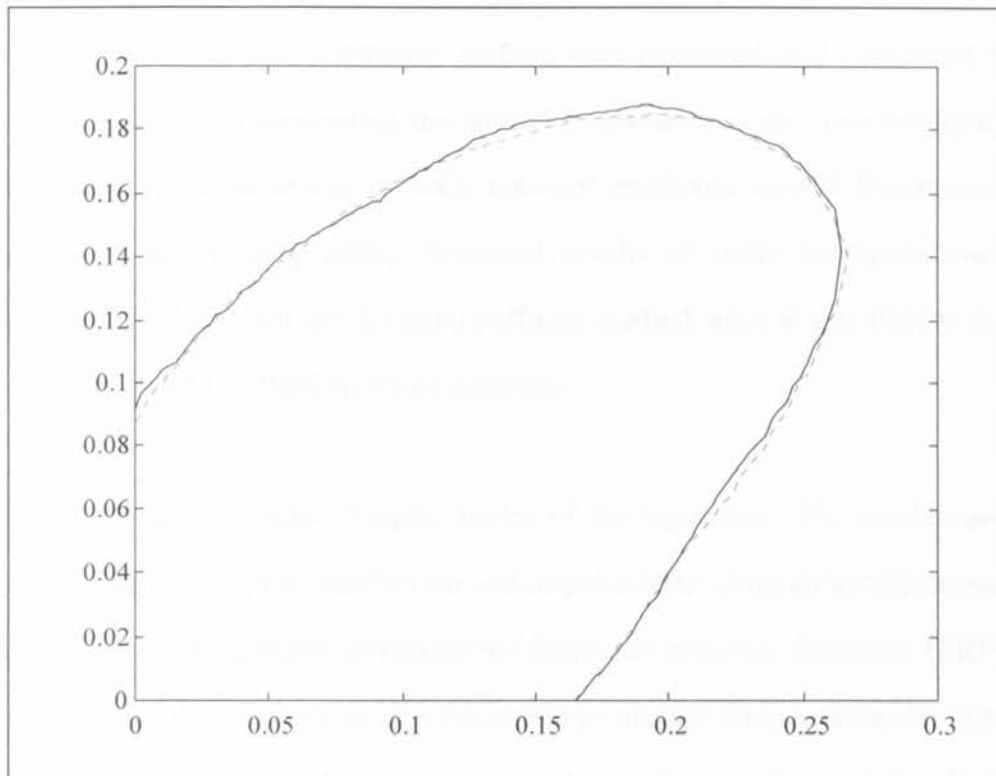


Fig 8.4: Comparison between the path generated experimentally at a low speed (---) and at a higher speed(—).

8.4. NATURAL FREQUENCIES AND MODE SHAPES AT STATIC CONFIGURATIONS

There are many reasons for studying the variation of the natural frequencies and mode shapes at different configurations. The natural frequencies provide approximate information to the designer on the values of critical speeds. As was seen in the previous chapter, the critical speeds occur near integer divisions of the average value of the natural frequencies. Also, some of the speeds are limiting critical speeds. Thus the designer has only a limited number of speeds at which to run the costly simulation to check if a given speed is a limiting critical speed, thereby saving a great deal of CPU time. On the other hand, the mode shapes at the natural frequencies provide an insight into the deformation shapes when the mechanism is excited at those frequencies. The designer visualises which linkage undergoes the worst deformation for a given mode.

In Chapter 5, the dynamic stiffness method was presented and compared to the conventional FEM for computing the natural frequencies at any one configuration. In this chapter, a comparison is made between predicted natural frequencies and mode shapes and corresponding measured results at static configurations. The predictions were based on the dynamic stiffness method since it was proven that the results given by this method are most accurate.

The cycle was divided into 10 equal angles of the input link. The mechanism was held at each of the ten positions in turn and impulse tests using an accelerometer and a hammer were conducted to determine the frequency response functions (FRF). For each position of the mechanism, the excitation point was varied along the links and the measurement point was kept fixed for each set of tests. Once all data had been collected from the measurement and excitation points, the natural frequencies, damping ratios and mode shapes were extracted using modal analysis software (SMS-STAR). Fig. 8.5 shows a schematic of the experimental set-up.

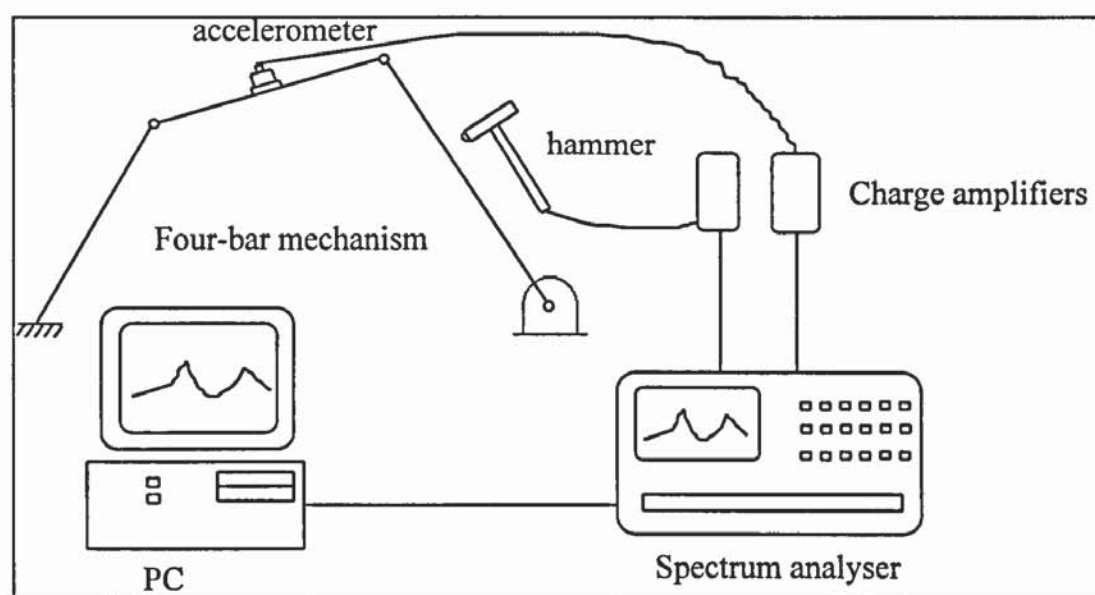


Fig. 8.5: Experimental modal analysis using a hammer and an accelerometer.

The SMS-STAR modules are shown in Fig. 8.6. The structure is described as a series of numbered points. The points are linked with lines so that a wire frame

representation can be created. The coordinates are expressed with respect to a Cartesian frame. A wire frame representation of four-bar mechanism at a given configuration is shown in Fig. 8.7. The module labelled "acquire measurements" in Fig. 8.6 deals with the acquisition of data. Once enough measurements are taken on the spectrum analyser i.e. no change is noticed on the average spectrum, the user activates this module and measurements are downloaded from the analyser to the PC as transfer functions between two points, the excitation and the measurement points. The PC and the spectrum analyser are linked via a GPIB card. This is done for every set of measurements where the position of the accelerometer is kept unchanged and the excitation point is varied along the links. Once all the FRFs are stored in the PC, the identification of modes procedure is started. The natural frequencies, the mode shapes and the damping ratios are determined from the set of measurements. Prior to proceeding with the identification process, a module in the package calculates the modal peaks and helps to locate the natural frequencies. Then, bands are specified together with the number of modes contained in each band and a choice of curve fitting method is made. The curve fitting routine chooses the best possible modal parameter estimate from the FRFs. Different accelerometer locations had to be chosen because the quality of the response depends on the mode being investigated. The response at a point may be at maximum for some modes and at a node for others. An example of an FRF corresponding to the accelerometer placed at the midpoint of the follower is given in Fig. 8.8.

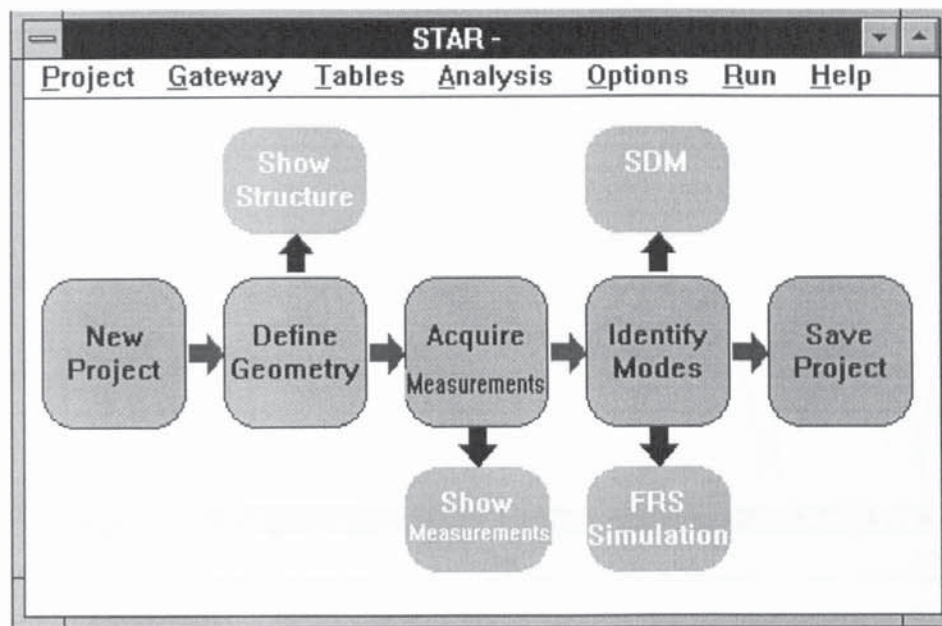


Fig. 8.6: Modules of SMS-STAR package.

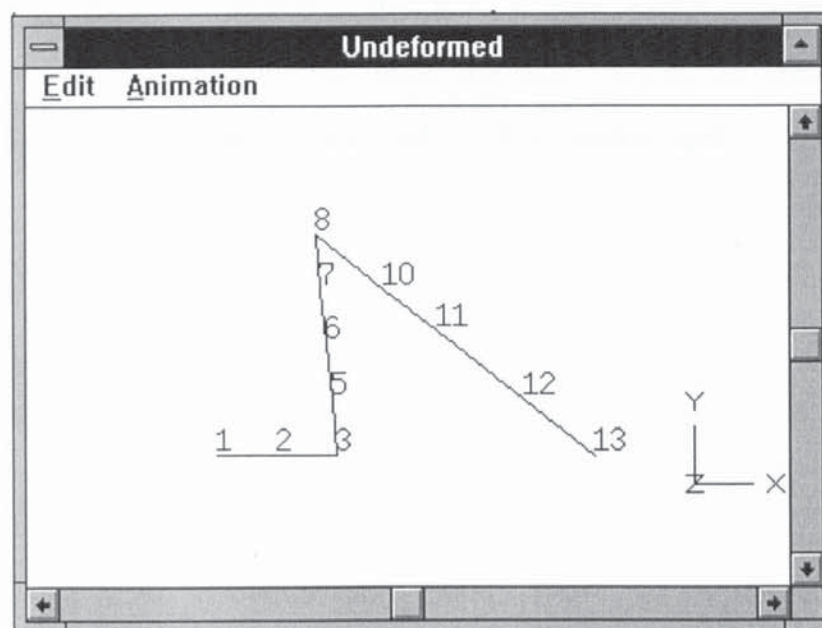


Fig. 8.7: Wire frame representation of the mechanism at $t_1=0^\circ$.

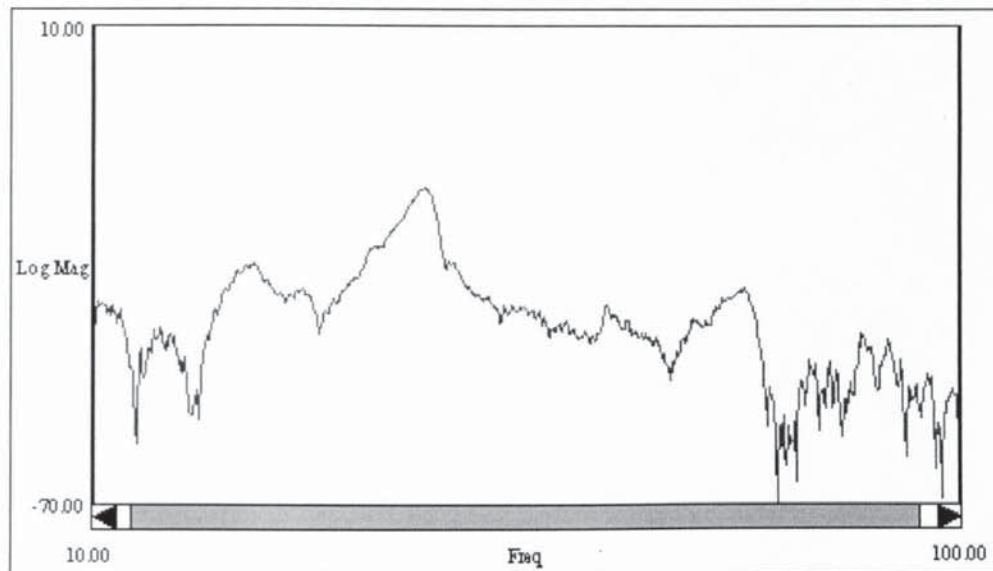


Fig. 8.8: FRF corresponding to the accelerometer at the midpoint of the follower.

The frequency range was chosen so that three distinct modes were captured. The measured frequencies, the damping ratios and mode shapes are presented in the following figures where they are compared to the theoretical ones.

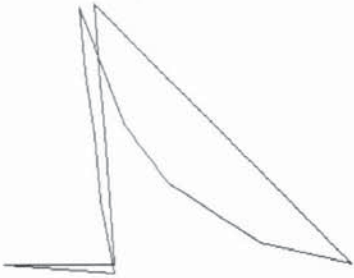

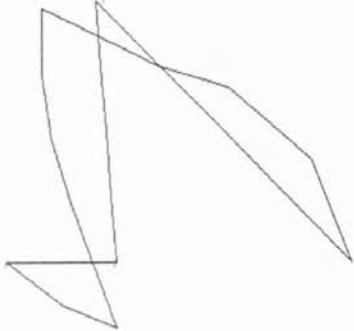
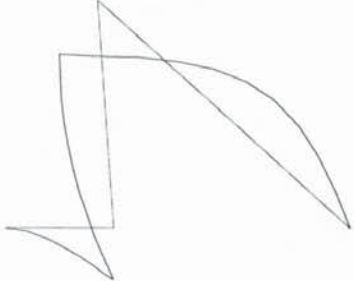
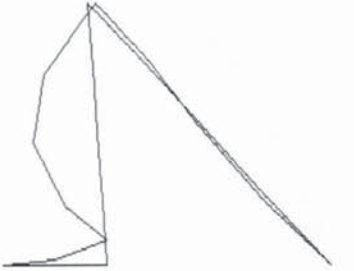
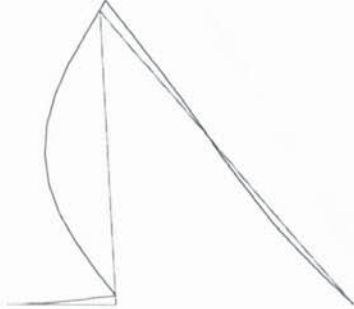
	Experimental	Model
Mode 1	 <p>24.99 Hz, 5.38 %</p>	 <p>26.08 Hz</p>
Mode 2	 <p>43.59 Hz, 2.53 %</p>	 <p>42.63 Hz</p>
Mode 3	 <p>75.18 Hz, 2.74 %</p>	 <p>78.55 Hz</p>

Fig. 8.9: Mode shapes and frequencies for $t_1=0^\circ$.

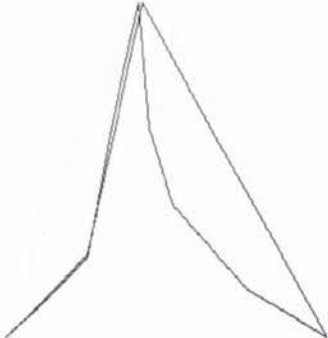
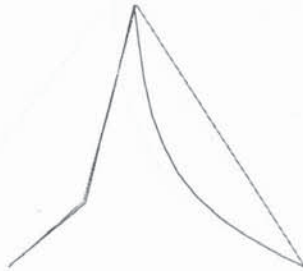
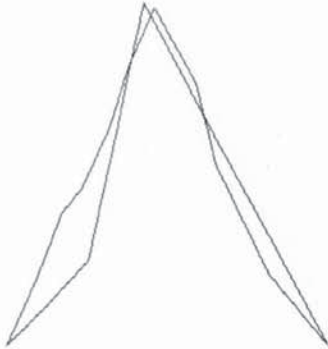

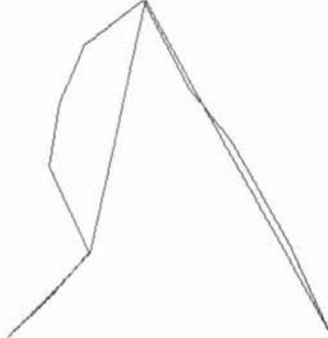
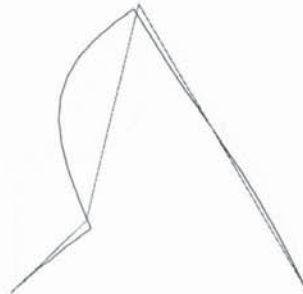
	Experimental	Model
Mode 1	 <p>26.52 Hz, 5.54%</p>	 <p>27.04 Hz</p>
Mode 2	 <p>55.85 Hz, 2.0 %</p>	 <p>57.67 Hz</p>
Mode 3	 <p>68.99 Hz, 2.95 %</p>	 <p>77.27 Hz</p>

Fig. 8.10: Mode shapes and frequencies for $t_1=36^\circ$.

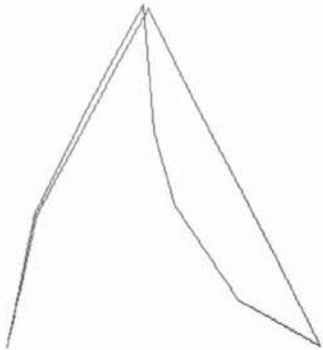
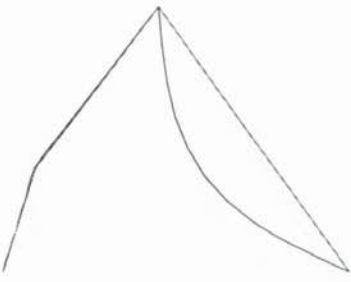
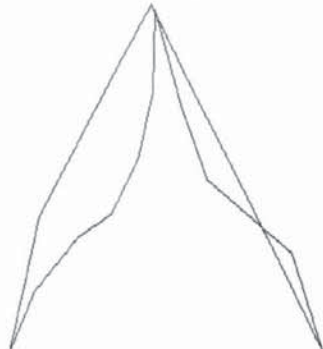

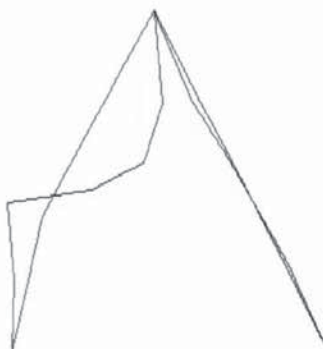
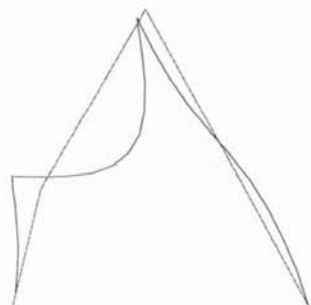
	Experimental	Model
Mode 1	 <p>27.68 Hz, 4.62 %</p>	 <p>27.26 Hz</p>
Mode 2	 <p>56.11 Hz, 0.46 %</p>	 <p>60.10 Hz</p>
Mode 3	 <p>91.18 Hz, 1.36 %</p>	 <p>90.20 Hz</p>

Fig. 8.11: Mode shapes and frequencies for $t_1=72^\circ$.

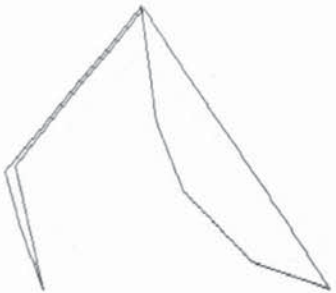


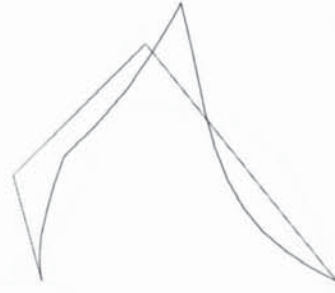


	Experimental	Model
Mode 1	 <p>27.30 Hz, 4.36 %</p>	 <p>26.82 Hz</p>
Mode 2	 <p>49.18 Hz, 1.65 %</p>	 <p>51.08 Hz</p>
Mode 3	 <p>78.40 Hz, 1.24 %</p>	 <p>76.36 Hz</p>

Fig. 8.12: Mode shapes and frequencies for $t_1=108^\circ$.

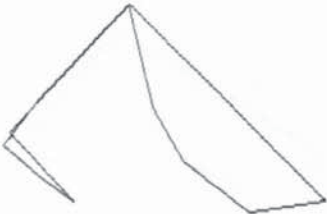
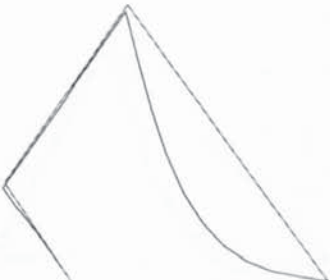



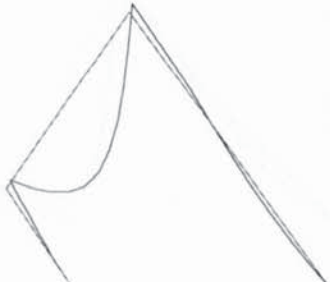
	Experimental	Model
Mode 1	 <p>28.07 Hz, 4.79 %</p>	 <p>26.70 Hz</p>
Mode 2	 <p>47.00 Hz, 1.36 %</p>	 <p>48.59 Hz</p>
Mode 3	 <p>75.31 Hz, 2.65 %</p>	 <p>77.92 Hz</p>

Fig. 8.13: Mode shapes and frequencies for $t_1=144^\circ$.







	Experimental	Model
Mode 1	 <p>28.83 Hz, 5.2 %</p>	 <p>27.04 Hz</p>
Mode 2	 <p>51.61 Hz, 1.37 %</p>	 <p>53.70 Hz</p>
Mode 3	 <p>77.36 Hz, 1.98 %</p>	 <p>84.57 Hz</p>

Fig. 8.14: Mode shapes and frequencies for $t_1=180^\circ$.


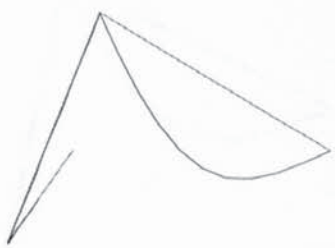

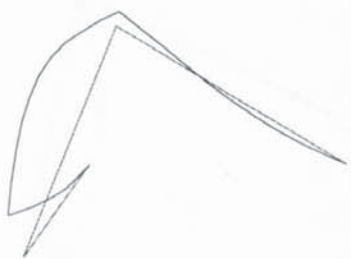


	Experimental	Model
Mode 1	 <p>28.91 Hz, 4.76 %</p>	 <p>27.28 Hz</p>
Mode 2	 <p>58.79 Hz, 1.28 %</p>	 <p>60.56 Hz</p>
Mode 3	 <p>82.55 Hz, 1.91 %</p>	 <p>92.20 Hz</p>

Fig. 8.15: Mode shapes and frequencies for $t_1=216^\circ$.

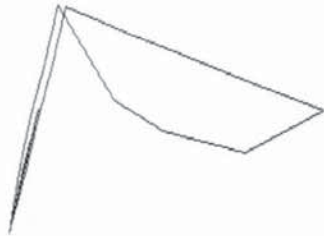
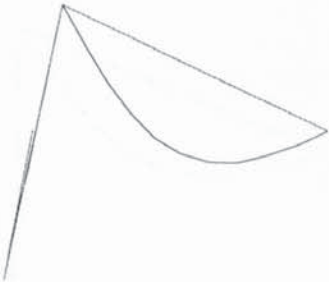

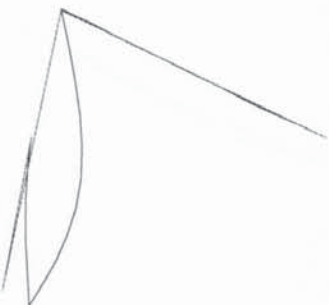
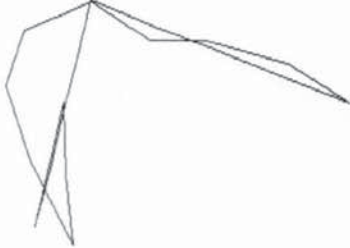

	Experimental	Model
Mode 1	 <p>28.66 Hz, 4.25 %</p>	 <p>27.32 Hz</p>
Mode 2	 <p>60.26 Hz, 1.67 %</p>	 <p>62.78 Hz</p>
Mode 3	 <p>86.95 Hz, 1.14 %</p>	 <p>94.27 Hz</p>

Fig. 8.16: Mode shapes and frequencies for $t_1=252^\circ$.

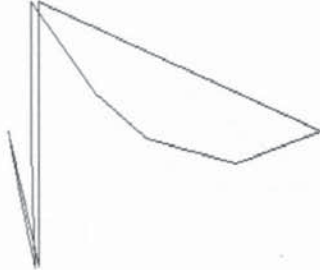
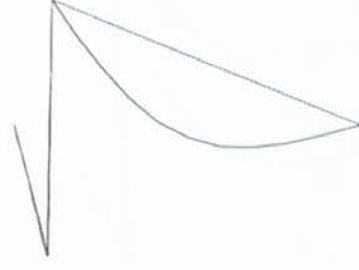

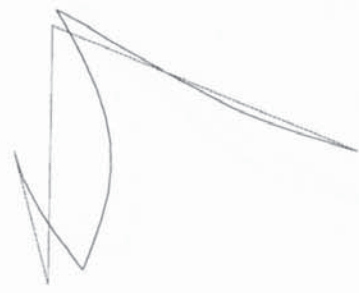
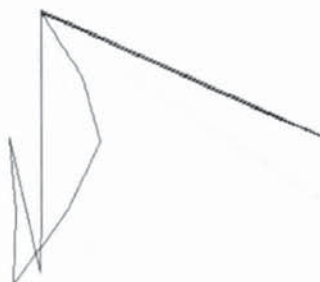
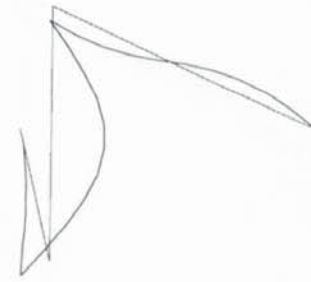
	Experimental	Model
Mode 1	 <p>27.72 Hz, 4.67 %</p>	 <p>27.26 Hz</p>
Mode 2	 <p>57 Hz, 1.27 %</p>	 <p>60.23 Hz</p>
Mode 3	 <p>87.97 Hz, 1.62 %</p>	 <p>90.45 Hz</p>

Fig. 8.17: Mode shapes and frequencies for $t_1=288^\circ$.

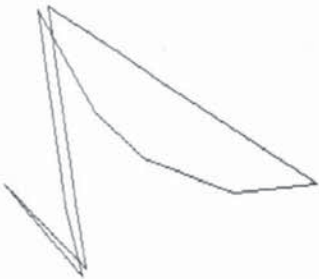




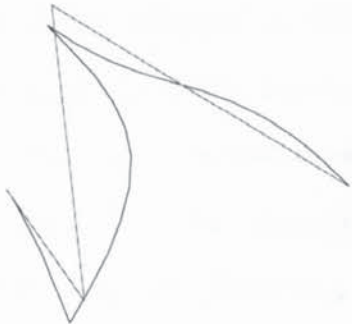
	Experimental	Model
Mode 1	 <p>26.66 Hz, 4.52 %</p>	 <p>26.91 Hz</p>
Mode 2	 <p>48.50 Hz, 2.45 %</p>	 <p>50.82 Hz</p>
Mode 3	 <p>82.70 Hz, 1.75 %</p>	 <p>83.84 Hz</p>

Fig. 8.18: Mode shapes and frequencies for $t_1=316^\circ$.

From these figures it is evident that there is a good agreement between the theoretical and the experimental results. Nevertheless such discrepancies as there are can be explained since there are many potential sources of error. The input link was assumed to be a cantilever beam in the model; however this link is attached to a flywheel with a finite stiffness. The length of the links in the numerical model are bigger than those in the physical model, in reality a part of the theoretical length pertain to the joint blocks which are stiffer and also, short length leads to higher natural frequencies. This explains the fact that the experimental frequencies are higher than the computed ones. In order to minimise the effect of the length of the joints, the linkages were chosen long enough so that the length of joints are negligible compared to the beam proper.

8.5. MECHANISM RUNNING AT HIGH-SPEED

When the mechanism was run at a high-speed the strain responses were measured. The measurements were taken using strain gauges placed at the midpoint of the coupler and the follower and at the end of the input link connected to the flywheel. The gauges were then calibrated in order that voltages provided by the strain gauge amplifiers to be related to the measured stresses and thereby furnish response data for comparison with the predictions from the model. This was accomplished by supporting the coupler and the follower at their ends and deflecting them by suspending different loads and recording the voltages delivered by the amplifiers. The same procedure was applied to the input link with one end clamped. The relation between the voltage and the weights was linear for a wide range of loads. The data acquisition device used was the CED 1401+ manufactured by Cambridge Electronic Design Ltd. The device has 16 ADC input channels, 4 output channels and a series of control inputs which include 5 event channels for external triggers. The CED 1401+ was controlled from a PC using interactive menu driven software.

The signal from the optical tachometer mentioned earlier on was used to trigger the measurements and was also fed to one of the analogue input channels. The data were acquired in sweeps whose duration were set such that two cycles of rotation were captured in every case. The purpose of this was to provide a visual means for verifying that the rotational speed was constant during the test. Once the speed was stabilised, the different signals were sampled at a rate of 1 kHz (which is well above the highest expected frequency) and were averaged over 10 samples. Data for each test were saved into individual files. These files were then processed. First the speed was calculated from the duration between the two spikes captured from the optical tachometer. Then for each test, a file which contains the values of the voltage provided by the strain gauge amplifiers, was generated.

The model was then run at the same speed and the results were compared. The comparisons between the experimental stresses and the stresses given by the model are given for different speeds in Appendix C. The method used in the model was the method introduced earlier in section 7.4.1 and labelled the "exact" solution.

8.5.1. Effect of L_4

The mechanism was tested for different values of L_4 (see Fig. 3.1) in order to show the effect of this parameter on the maximum stresses in the mechanism. The plate on which the two ground pivots were bolted was extended by adding an extension with two oblong holes in which the output pivot could slide. Once the desired value of L_4 was reached, the output pivot was secured at this position by tightening two pairs of bolts. The following figure shows the variation of the maximum stress against speed for different values of L_4 .

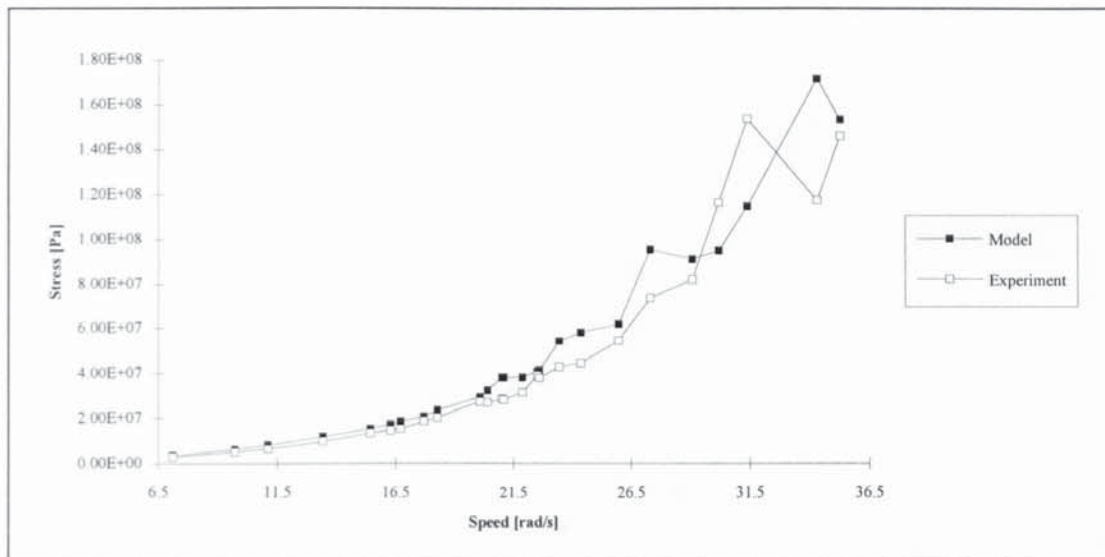


Fig. 8.19: Maximum stress at follower midpoint for $L_4 = 0.547$ m.

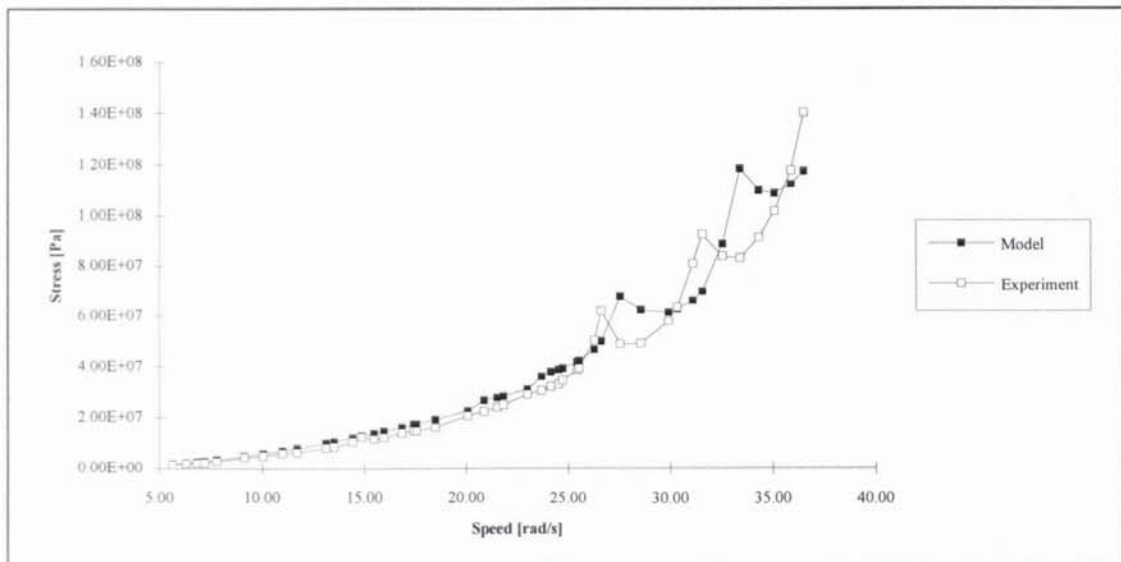


Fig. 8.20: Maximum stress at follower midpoint for $L_4 = 0.632$ m.

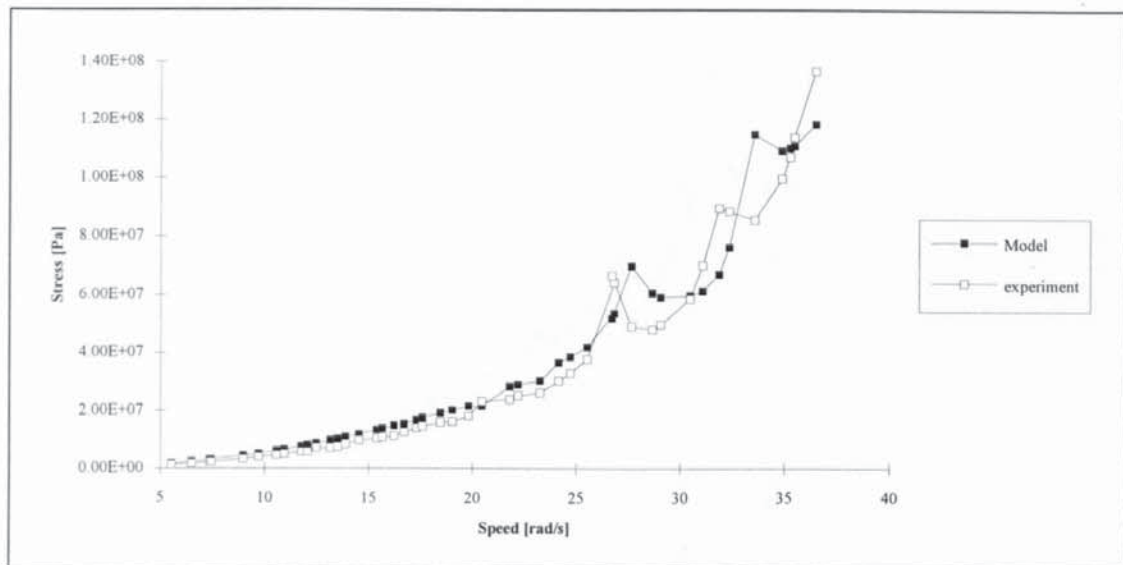


Fig. 8.21: Maximum stress at follower midpoint for $L_4 = 0.642$ m.

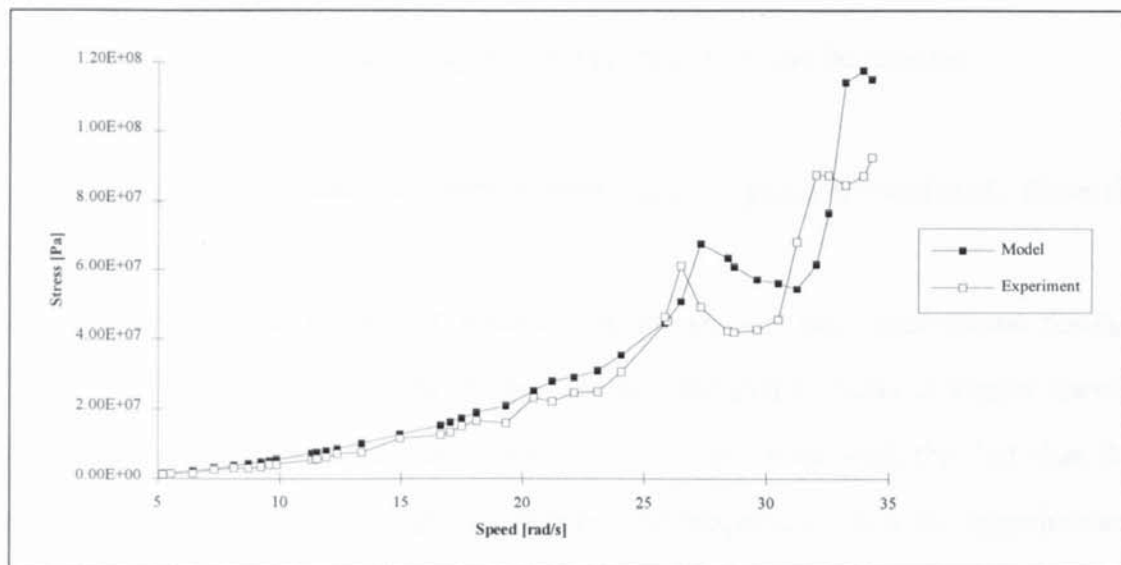


Fig. 8.22: Maximum stress at follower midpoint for $L_4 = 0.652$ m.

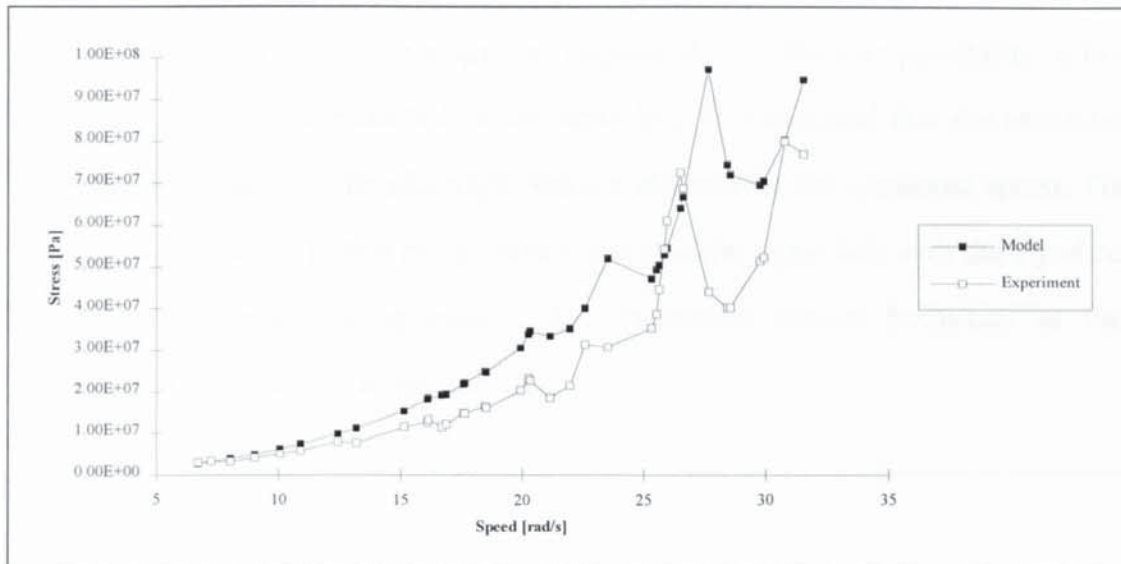


Fig. 8.23: Maximum stress at follower midpoint for $L_4 = 0.662$ m.

From the above figures and the figures in Appendix C, it can be seen that:

- The experimental stress exhibits as many critical speeds as predicted. These do vary when L_4 is changed.
- There is a good agreement between the model and the experimental results. However the critical speeds on the experimental graphs occur at higher speeds than those on the theoretical graphs. This is consistent with the fact that the numerical model gives slightly lower natural frequencies than the experimental ones.
- When L_4 increases, the maximum stresses experienced by the links decrease. However above a certain limit ($L_4 = 0.66$ m) the trend is reversed, when L_4 is increased, the stresses start increasing again. The effect of the transmission angle is clearly visible in the next figure where the stress becomes maximum for an input angle of 180° , the angle at which the maximum transmission angle occurs.
- When the speed was low, the measured stress on the input link shows unexpected response at a fixed frequency (13.67 Hz) with relatively high amplitude superimposed on the original response. It was found that the frequency of this signal was independent of L_4 and L_2 . Initially, it was suspected

that the friction in the slip rings was responsible. To test this possibility, a low voltage battery was mounted on the input link. It was found that the measured output voltage from the slip rings was not affected by the rotational speed. The likely explanation of this phenomenon was that the input link with the flywheel constituted an oscillating system. The theoretical natural frequency of this system was calculated to be 11.31 Hz.

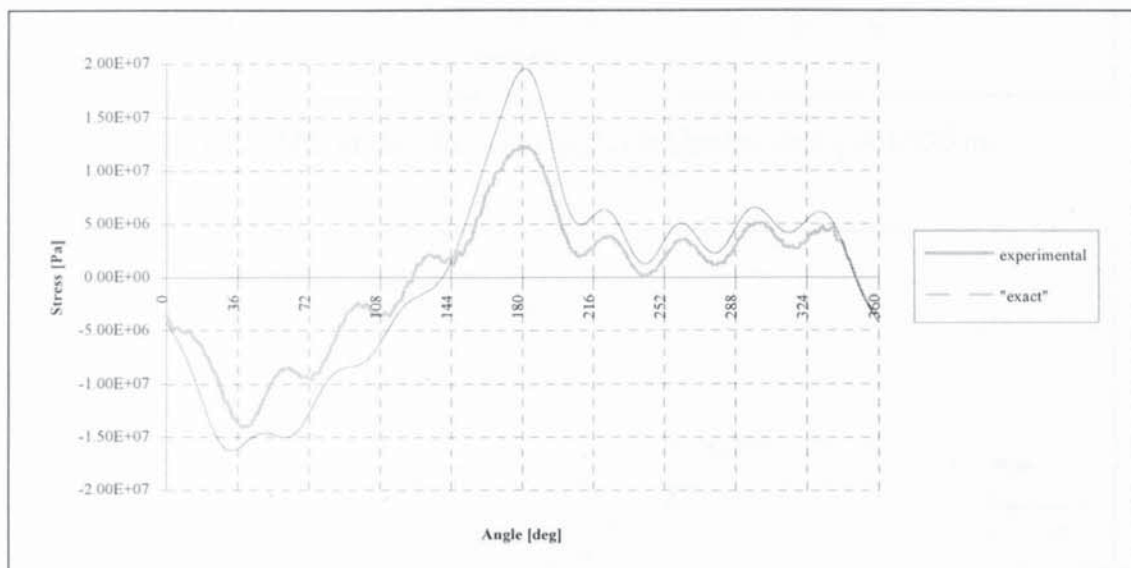


Fig. 8.24: Stress at the midpoint of the follower for $\omega=17$ rad/s and $L_4 = 0.662$ m.

8.5.2. Effect of L_2

In the previous set of tests, the follower was the most flexible element of the mechanism, and the other links were relatively stiff. A new set of measurements was carried out on a mechanism where both the coupler and the follower were flexible elements. This was done by replacing the initially short coupler with a longer one (636 mm in place of 328 mm). The experimental results are presented in Appendix D. The maximum stresses at the coupler and the follower midpoints are presented in figures 8.25 and 8.26.

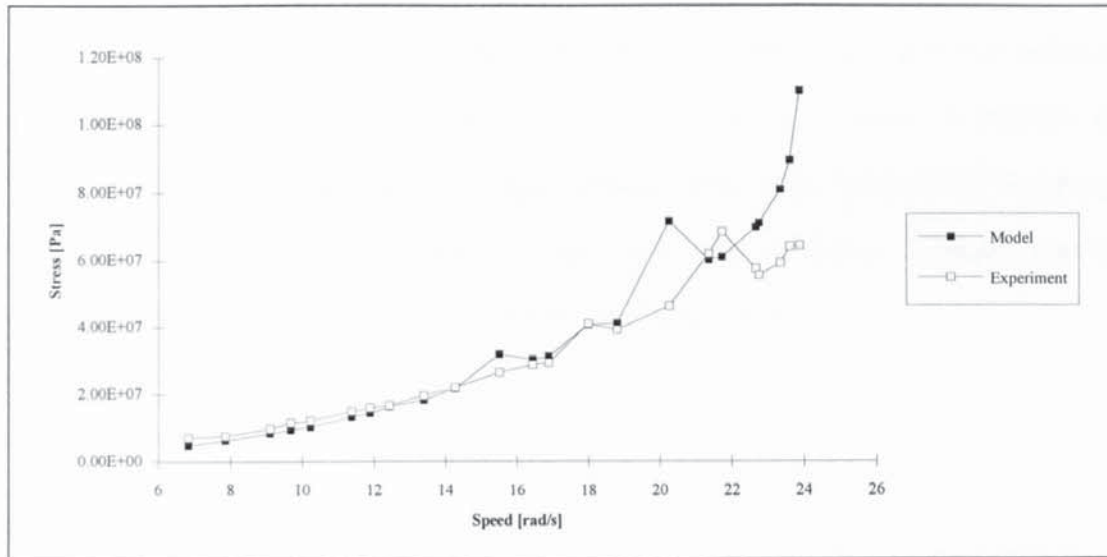


Fig. 8.25: Maximum stress at coupler midpoint for $L_2 = 0.636$ m.

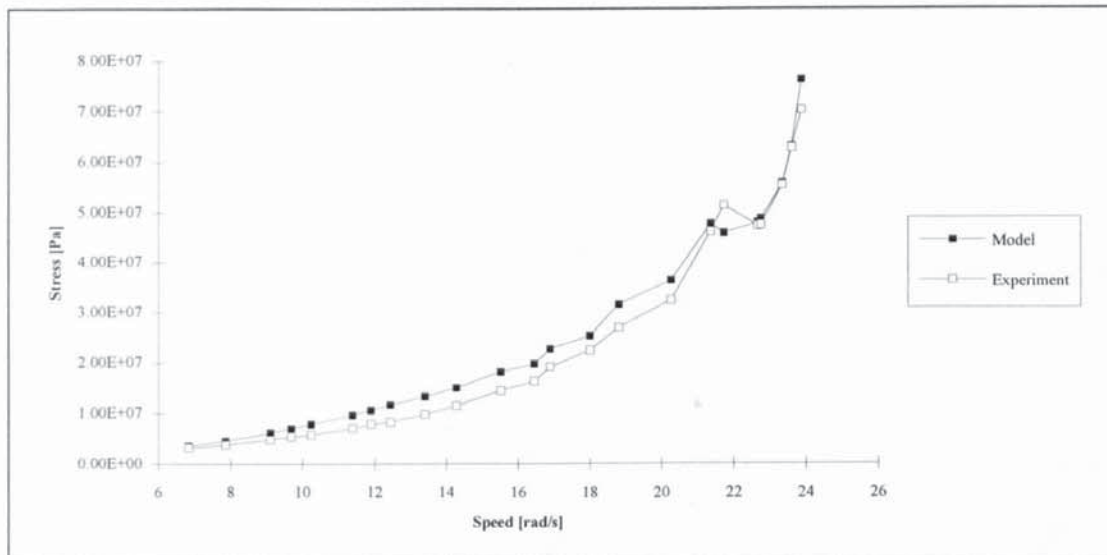


Fig. 8.26: Maximum stress at follower midpoint for $L_2 = 0.636$ m.

8.6. CONCLUSION

In this chapter, results have been reported from a series of experimental tests carried out on a four-bar mechanism. Firstly, a very simple method was presented for investigating the experimental path generated by any point of the coupler. Then, modal tests were carried out to determine the natural frequencies and mode shapes of the mechanism where it has been considered as a structure at different static configurations. Finally, the mechanism was run at different speeds and the results

were compared with the results from model. In the last test series, different values of L_4 (the distance between the ground pivots) were tested in order to confirm the prediction from the model that the maximum stresses in the mechanism do change with L_4 . Also two different couplers were tested, the parameter changed was the length of the latter which leads to a stiff or flexible coupler.

Chapter 9

CONCLUSIONS AND SUGGESTIONS FOR FURTHER WORK

9.1. CONCLUSIONS

The main goal of this study has been the modelling of a flexible four-bar mechanism running at high-speed. Although this problem has been addressed for many years, there were, and indeed are still, areas where more research is needed.

The first purpose of this study was to develop a set of routines to deliver the steady-state solution quickly and efficiently. The first problem addressed was how to obtain an accurate result using the FEM with the minimum number of elements per link. An iterative method was then developed whereby the conventional FEM was used conjointly with the dynamic stiffness method to provide the same results as a model using the conventional FEM with many elements per link. This resulted in a drastic saving in CPU time. Two new algorithms have been developed to determine the steady-state solution and in many situations these have proved to be superior to the existing algorithms. It has also been shown that these two algorithms are mathematically equivalent but conceptually different and also it was demonstrated that one of them is more advantageous than the other.

It is known that the mechanism exhibits many critical speeds where the stresses in the links are greater than those at neighbouring speeds. Some of these critical speeds, called limiting critical speeds, cannot be exceeded without damaging the mechanism. However, above certain limiting critical speeds there might be a speed band where the mechanism could run safely and there is a need for a method to

allow a mechanism to accelerate up to this speed band. The problem addressed was therefore how to run the mechanism up to that safe speed without damaging it. The dynamic response of the mechanism depends on many geometrical parameters, the only one which could be varied while the mechanism is rotating is the distance between the ground pivots L_4 . Hence, the variation of the maximum stresses in the linkages against speed for different values of L_4 has been investigated. It was found that when L_4 increases within a certain interval, the maximum stresses decrease. Furthermore, the critical speeds are not affected by L_4 . The solution to drive the mechanism above a limiting critical speed, if there is a safe speed band above it, is therefore to start the mechanism with a large value of L_4 and then, once the safe speed is reached, return the ground pivot to its normal position. The effect of changing L_4 has been confirmed experimentally. However, above a certain value of L_4 , the transmission angle becomes unsatisfactory and the maximum stresses during the cycle start increasing again. The maximum stresses occur at an input angle of 180° , the angle at which the maximum transmission angle occurs. This effect has also been proven experimentally.

A possibility which might be considered is to add more damping in the mechanism in order to reduce the amplitude of the stresses and to run the mechanism through the critical speeds up to the target safe speed band. When the effect of the damping on the maximum stresses against speed was considered, it was found that the amplitudes of the stresses are indeed reduced at the critical speeds. However, at speeds between critical speeds, increasing damping is counterproductive; instead of being reduced, the amplitudes of the maximum stresses are increased. Therefore, adding more damping to run the mechanism above several critical speeds, in general, may not be a solution.

A system excited at a certain frequency is said to be unstable if its response grows indefinitely. For mechanisms, the source of excitation is due to the rigid-body

motion. Unlike static structures, resonance occurs in mechanisms at excitation frequencies (speeds) quite below the fundamental natural frequency at any position of the mechanism. At these speeds, if no damping is included in the model, the stresses and deflections become unbounded. In reality the physical system has always some damping present. Also, when the deflections are large the linkages start behaving in a non-linear manner. The deflections, in this case, become bounded but still they are larger than at neighbouring speeds. These speeds are called critical speeds. In the past, a method to locate these was developed based on the eigenvalues of the monodromy matrix. The critical speeds correspond to these eigenvalues greater than unity. However, it has been shown that when the damping was included, at many low speeds the system became stable but nevertheless these speeds remained critical. Also it was found that by calculating the monodromy matrix for each mode the critical speeds occur at integer divisions of the mean value of the natural frequencies. In this study, a method has been developed based on the transition matrix without performing the modal uncoupling. It has been found that the critical speeds coincide with the maximum of one of the real parts of the eigenvalues of the transition matrix and the predominant ones still occur near integer divisions of the mean values of the corresponding natural frequency over the cycle.

The experimental work achieved three main objectives. First, a practical method has been used to show the coupler curves. To do this, a LED was placed at the desired point and the mechanism was run at a series of constant speeds. Photographs were then taken at different speeds, digitised and the coupler curves were compared to the theoretical ones. The second objective was to carry out the modal analysis of the mechanism at static configurations. The natural frequencies, the mode shapes and the damping ratios were determined experimentally for ten positions of the mechanism. It was found that the measured characteristics were in good agreement with the predicted ones. The third objective was to run the mechanism at different speeds and to measure the stresses on the linkages. It was found that there was a

good agreement between the experimental results and the theoretical predictions for both amplitude and phase. The effect of L_4 was also experimentally investigated. The results from the model were confirmed in that the stresses were reduced when L_4 was increased. Also it was confirmed that when the transmission angle was beyond a certain limit, the stresses become critical at an input angle of 180° , the angle at which the maximum transmission angle occurs and the effect of increasing L_4 is reversed.

9.2. FURTHER WORK

The method developed in this study to run the mechanism above several critical speeds requires the distance between the ground pivots to be adjusted while the mechanism is rotating. Sometimes this is not possible for technical reasons. Another method which could be pursued is to have an elastic support at the follower ground pivot. Basically, this would change the characteristics of the mechanism at the limiting critical speed and the system would be arranged in such a way that the maximum vibration is at the support. Once the safe speed is attained, the support could be locked.

The effect of damping on the maximum stresses experienced by the linkages has been investigated theoretically. A method which could be used to dissipate energy and therefore to increase damping is, for example, a laminated viscoelastic beam where a viscoelastic layer is confined between two elastic layers. Studying the characteristics of laminated viscoelastic beams would have two purposes, firstly to quantify the variation of damping for different combinations of the layer thicknesses, and secondly to investigate the influence of this solution on the critical speeds.

In the past, two papers have been published in which an expert system was proposed as an intelligent front to design software for a four-bar mechanism (Liou *et al.*, 1988; Patra and Liou, 1992). From the set of geometrical data of the mechanism, the system estimates the maximum deflection, maximum stress, etc. without the need for simulation. The set of rules and the basic equations were derived from a simple cantilever beam. The results obtained are quite accurate for speeds outside the critical speed bands. However, at or near critical speeds the results will underestimate the responses since the resonance phenomenon was not taken into account. To improve the system a more refined model should be developed where the model accounts for the critical speeds of the system.

It is intuitive that the natural frequencies of a structure depend on the natural frequencies of its individual members. Published results showed that critical speeds have been linked by some researchers to the natural frequencies of the links, and to the average values of the natural frequencies of the whole mechanism by others. For some configurations of the mechanism these two can be considered equal but for others they are quite different as witnessed by Fig. 9.1. The variation of the different frequencies against the coupler length is shown.

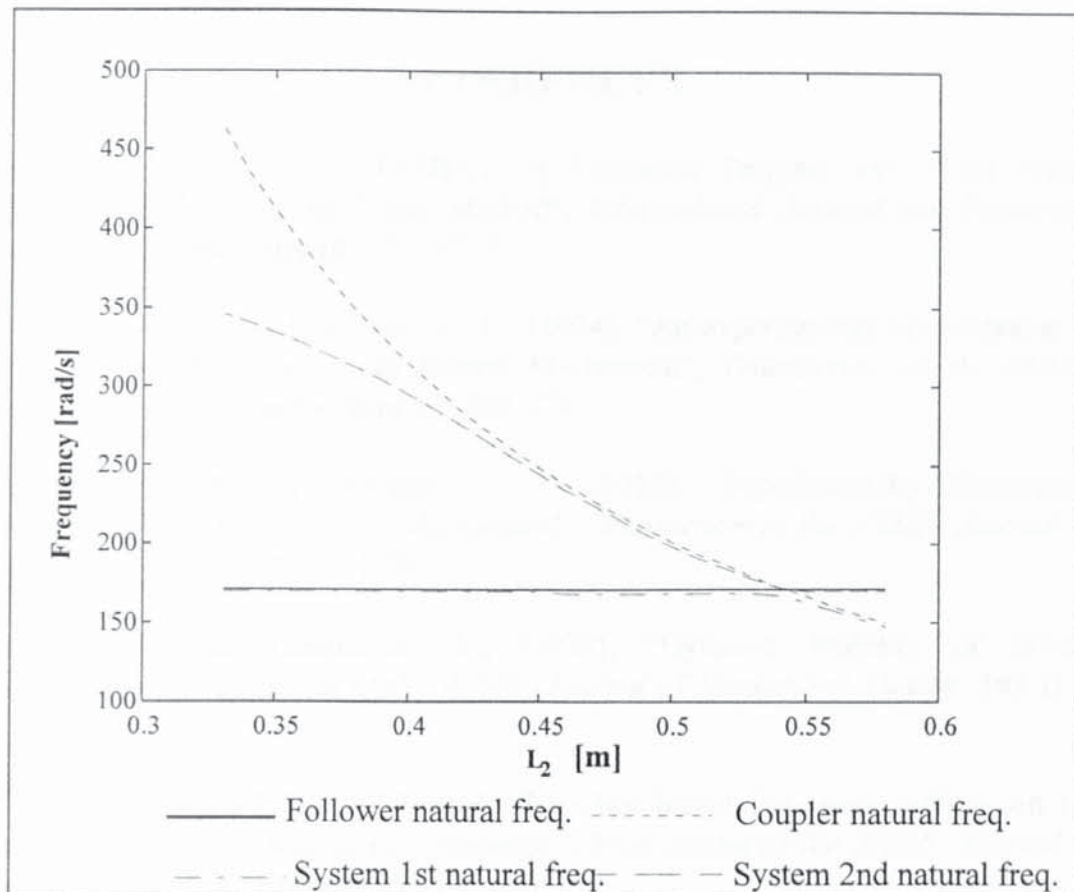


Fig. 9.1: Variation of natural frequencies with L_2 .

From this figure it is seen that the average of the first natural frequency could be approximated by the natural frequency of the most flexible link assumed to be pinned-pinned. In this particular case, for $L_2 < 0.547$ m, the first natural frequency of the mechanism is determined from the natural frequency of the follower; and when $L_2 > 0.547$ m, the coupler determines the first natural frequency of the mechanism. A systematic investigation of the variation of the effect of the natural frequencies of the links on the natural frequency of the mechanism is needed.

Finally, the fatigue phenomenon has not been taken into account in this study. The definition of the limiting critical speeds was based on the maximum stress in the links. It is desirable to include the fatigue so that not only can the mechanism withstand the stresses at a certain speed, but it can also run at this speed for a reasonable length of time.

REFERENCES

- Akesson, B. A., (1976), "PFVIBAT- A Computer Program For Plane Frame Vibration Analysis by an Exact Method", *International Journal for Numerical Methods In Engineering*, **10**, 1221-1231.
- Alexander, R. M. and Lawrence, K. L., (1974), "An experimental Investigation of the Dynamic Response of an Elastic Mechanism", *Transaction of the ASME, Journal of Engineering for Industry*, 268-274.
- Alexander, R. M. and Lawrence, K. L., (1975), "Experimentally Determined Dynamic Strains in an Elastic Mechanism", *Transaction of the ASME, Journal of Engineering for Industry*, 791-794.
- Badlani, M. and Klieinhenz, W., (1979), "Dynamic Stability of Elastic Mechanisms", *Transaction of the ASME, Journal of Mechanical Design*, **101** (1) , 149-153.
- Badlani, M., and Midha, A., (1982), "Member Initial Curvature Effects on the Elastic Slider-Crank Mechanism Response", *Transaction of the ASME, Journal of Mechanical Design*, **104**, (1), 159-167.
- Badlani, M. and Midha, A., (1983), "Effect of Internal Material Damping on the Dynamics of a Slider-Crank Mechanism", *Transaction of the ASME, Journal of Mechanisms, Transmission and Automation in Design*, **105**, 452-459.
- Bagci, C. and Kalaycioglu, S., (1979), "Elastodynamic of Planar Mechanisms Using Planar Actual Finite Elements, Lumped Mass Systems, Matrix-Exponential Method, and The Method of Critical-Geometry Kineto Elasto Static (CGKS)", *Transaction of the ASME, Journal of Mechanical Design*, **101**, 417-427.
- Bahgat, B. M. and Willmert, K. D., (1976), "Finite Element Vibrational Analysis of Planar Mechanisms", *Mechanism and machine Theory*, **11** (1), 47-71.
- Barker, C. R., (1985), "A complete Classification of Planar Four-Bar" *Mechanism and machine Theory*, **20** (6), 535-554.
- Basci, M. I., Toridis, T. G. and Khozeimeh, K., (1979), "Improved Method of Free Vibration Analysis of Frame Structures", *Computers and Structures*, **10**, 255-301.
- Bolotin, V. V., (1964), "*The Dynamic Stability of Elastic Systems*", Holden-Day Inc., San Francisco.
- Boutaghou, Z. E. and Erdman, A. G., (1989), "Design Methodology for High-Speed Elastic Four-Bar Linkages", *Vibration analysis- Techniques and Applications, ASME 12th Biennial Conference on Mechanical Vibration and noise 17-21 Sep*, **18** (4), 85-92.

Chan, S. P., Cox, H. L. and Benfield, W. A., (1962), "Transient Analysis of Forced Vibrations of Complex Structural Mechanical Systems", *Journal of The Royal Aeronautical Society*, 457-460.

Chang, C. H., (1978), "Vibrations of Frames With Inclined Members", *Journal of Sound and Vibration*, **56**, 201-214.

Chang, R. and Chen, L., (1987), "Finite Element Vibration Analysis of a Composite Material Planar Mechanisms", *Finite Element in Analysis and Design*, **3**, 241-252.

Chu, S. C. and Pan, K. C., (1975), "Dynamic Response of a High-Speed Slider Crank Mechanism with an Elastic Connecting Rod", *Transaction of the ASME, Journal of Engineering for Industry*, **97** (2), 542-549.

Cleghorn, W. L., Fenton, R. G. and Tabarrok, B., (1981), "Finite Element Analysis of High speed flexible Mechanisms", *Mechanism and machine Theory*, **16** (4), 407-424.

Cleghorn, W. L., Fenton, R. G. and Tabarrok, B., (1981), "Optimum Design of High-Speed Flexible Mechanisms", *Mechanism and machine Theory*, **16** (4), 399-406.

Cleghorn, W. L., Fenton, R. G. and Tabarrok, B., (1984a), "Steady-State Vibrational Response of High-Speed Flexible Mechanisms", *Mechanism and machine Theory*, **19** (4/5), 417-423.

Cleghorn, W. L., Tabarrok, B. and Fenton, R. G., (1984b), "Critical Running Speeds and Stability of High-Speed Flexible Mechanisms", *Mechanism and machine Theory*, **19** (3), 307-317.

Cohen, E. and McCallion, H., (1969), "Improved Deformation functions for the Finite Element Analysis of Beam Systems", *International Journal of Numerical Methods en Engineering*, **1**, 163-167.

Courant, R., (1943), "Variational Methods for the Solutions of Problems of Equilibrium and Vibrations" *Bulletin of the American Mathematical Society*, **49**, 1-23.

Diaz, J. C., Fairweather, G. and Keast, P., (1983), "FORTRAN Packages for Solving Certain Almost Block Diagonal Linear Systems by Modified Alternate Row and Column Elimination", *ACM Transactions on Mathematical Software*, **9** (3), 358-375.

Erdman, A. G. and Sandor, G. N., (1972), "Kineto-Elastodynamics- A review of the state of the art and Trends", *Mechanism and machine Theory*, **7**, 19-33.

Erdman, A. G., Sandor, G. N. and Oakberg, R. G., (1972), "A General Method for Kineto-Elastodynamic Analysis and Synthesis of Mechanisms", *Transaction of the ASME, Journal of Engineering for Industry*, 1193-1205.

Erdman, A. G. and Sandor, G. N., (1984), "*Mechanism Design: Analysis and Synthesis*", Prentice Hall.

Fallahi, B., Lai, S. H. Y. and Gupta, R., (1994), "Full Beam Formulation of a Rotating Beam-Mass System", *Transaction of the ASME, Journal of Vibration and Acoustics*, **116**, 93-99.

Floquet, G., (1883), "Sur les Equations Différentielles Linéaires a Coefficients Périodiques", *Annales de l' Ecole Normale Supérieure, Paris*, **2** (12), 47-89.

Francis, P. H., (1968), "Parametric Excitation of a Non-Homogenous Bernoulli-Euler Beam", *Journal of Mechanical Engineering Science*, **10** (3), 205-211.

Freudeinstein, F., (1955), "Approximate Synthesis of Four-Bar linkages", *Transactions of the ASME*, **77** (6), 853-861.

Friedmann P., Hammond, C. E. and Woo, T., (1977), "Efficient Numerical Treatment of Periodic Systems with Application to Stability Problems", *International Journal for Numerical Methods in Engineering*, **11**, 1117-1136.

Friedmann, P. and Silverthorn, L. J., (1974), "Aeroelastic Stability of Periodic Systems with Application to rotor Blade Flutter", *AIAA Journal*, **12**, 1559-1564.

Gamache, D. and Thompson, B. S., (1981), "The Finite Element Design of Linkages- A comparison of Timoshenko and Euler Bernoulli Elements", *ASME Paper No 81-DET-109*, 1-9.

Gao, X., King, Z. and Zhang, Q., (1988), "A closed-Form Linear Multi-step Algorithm for the Steady state Response of high-speed Flexible Mechanisms", *Mechanism and Machine Theory*, **23** (5), 361-366.

Gao, X., King, Z. and Zhang, Q., (1989), "A Hybrid Beam Element For Mathematical Modelling Of High-Speed Flexible Linkages", *Mechanism and machine Theory*, **24** (1), 29-36.

Gérardin, M. and Rixen, D., (1993), "*Théorie des Vibrations; Application à la dynamique des structures*", Editions Masson.

Grashof, F., (1883), "*Theoretische Mashinenlehre*", Leipzig.

Hensell, R. D. and Warburton, G. B., (1969), "Transmission of Vibrations in Beam Systems", *International Journal for Numerical Methods in Engineering*, **1** (1), 47-66.

Hrones, J. A. and Nelson, G. L., (1951), "*Analysis of the Four-Bar Linkage*", M.I.T., Wiley, New York.

Hsu, C. S., (1974), "On Approximating a General Linear Periodic Systems", *Journal of Mathematical Analysis and Applications*, **45**, 234-251.

Hsu, C. S. and Cheng, W. H., (1973), "Applications of the Theory of Impulsive Parametric Excitation and New Treatments of General Parametric Excitation Problems", *Journal of Applied Mechanics*, **40**, 78-86.

Imam, I., Sandor, G. N. and Kramer, S. N., (1973a), "Deflection and Stress Analysis in High-speed Planar Mechanisms with Elastic Links", *Transaction of the ASME, Journal of Engineering for Industry*, 541-548.

Imam, I., Sandor, G. N. and Kramer, S. N., (1973b), "A General Method of Kineto-Elastodynamic Design of High speed Mechanisms", *Mechanism and machine Theory*, **8**, 497-516.

Imam, I. and Sandor, G. N., (1975), "High-Speed Mechanism Design -A General Analytical Approach", *Transaction of the ASME, Journal of Engineering for Industry*, **97B**, 609-628.

Jandarists, W. G. and Lowen, G. C., (1979), "The Elastic Dynamic Behaviour of a Counter-Weighted Rocker Link with an Overhanging Endmass in a Four-bar Linkage, Part I: Theory; Part II: Application and Experiment", *Transaction of the ASME, Journal of Mechanical Design*, **101** (1), 77-98.

Jara-Almonte, J. and Mitchell, L. D., (1988a), "A proposed Method for Enhanced Eigen-Pair Extraction Using Finite Element Methods; Part I: Theory", *7th International Modal Analysis Conference, Las Vegas NV*, 213-219.

Jara-Almonte, J. and Mitchell, L. D., (1988b), "A proposed Method for Enhanced Eigen-Pair Extraction Using Finite Element Methods; Part I: Applications", *7th International Modal Analysis Conference, Las Vegas NV*, 220-226.

Jasinski, P. W., Lee, H. C. and Sandor, G. N., (1971), "Vibration of Elastic Connecting Rod of a High-Speed Slider-Crank Mechanism", *Transaction of the ASME, Journal of Engineering for Industry*, **93** (2), 636-644.

Kalaycioglu, S. and Bagci, C., (1979), "Determination of the Critical Operating Speeds of Planar Mechanisms by the Finite Element Method Using Planar Actual Line Elements and Lumped Mass Systems", *Transaction of the ASME, Journal of Mechanical Design*, **101** (2), 210-223.

Karkoub, M. and Erdman, A. G., (1990), "Experimental Structural Damping Analysis in High speed Elastic Mechanisms", *21st Biennial Mechanism Conference Sep 16-19*, 251-258.

Khan, M. R., Thornton, W. A., and Willmert, K. D., (1978), "Optimality Criterion Techniques Applied to Mechanism Design", *Transaction of the ASME, Journal of Mechanical Design*, **100**, 319-327.

Kohli, D., Hunter, D. and Sandor, G. N., (1977), "Elastodynamic Analysis of a Completely Elastic System", *Transaction of the ASME, Journal of Engineering for Industry*, 604-609.

Kolousek, V., (1973), "*Dynamics in Engineering Structures*", Butterworths.

Lee, S. W. and Beale, D. G., (1992), "Periodic Response and Stability of Flexible Rod Slider Crank Mechanism", *DE-Vol 47, Flexible Mechanisms, Dynamics, and Analysis ASME*, 317-325.

Liao, C. Y. and Sung, C. K., (1993), "Elastodynamic Analysis and Control of Flexible Linkages Using Piezoceramic Sensors and Actuators", *Transaction of the ASME, Journal of Mechanical Design*, **115** (3), 658-665.

Liao, D. X., Sung, C. K., Thompson, B. S. and Soong, K., (1986), "A Note on the Quasi-Static Responses, Dynamic Responses and the Super-Harmonic Resonance of Flexible Linkages: Some Experimental Results", *ASME Paper 86-DE-146*, 1-7.

Lindh, K. G. and Likins, P. W., (1970), "Infinite Determinant Methods for Stability Analysis of Periodic Coefficient Differential Equations" *AIAA Journal*, **8** (4), 680-686.

Liou, F. W. and Erdman, A. G., (1987), "Experimental Motion Analysis of Flexible Mechanism and Drive System Using High-Speed Camera and Digital Imaging Technique", Oklahoma State University's 10th Applied Mechanisms Conference, **III**, session 8c-4.

Liou, F. W., Erdman, A. G. and Stelson, K. A., (1988), "General Design Rules for High-Speed Flexible Mechanisms", *Trends and Development in Mechanisms, Machines and robotics 20 th Biennial Mechanisms Conference 25-28 Sept*, 423-431.

Liou, F. W. and Erdman, A. G., (1989a), "Analysis of a High-Speed Flexible Four-Bar Linkage: Part I- Formulation and Solution", *Transaction of the ASME, Journal of Vibration, Acoustic, Stress and Reliability in Design*, **111**, 35-41.

Liou, F. W. and Erdman, A. G., (1989b), "Analysis of a High-Speed Flexible Four-Bar Linkage: Part II- Analytical and Experimental Results from the Apollo", *Transaction of the ASME, Journal of Vibration, Acoustic, Stress and Reliability in Design*, **111**, 42-47.

Liu, T. S. and Lin, J. C., (1993), "Forced Vibration of Flexible Body Systems: A Dynamic Stiffness Method", *Transaction of the ASME, Journal of Vibration and Acoustics*, **115**, 468-476.

- Lowen, G. C. and Chassapis, C., (1986), "The Elastic Behaviour of Linkages: An Update", *Mechanism and machine Theory*, **21**, 33-42.
- Lowen, G. G. and Jandrasits, W. G., (1972), "Survey of investigations into the Dynamic Behaviour of Mechanisms Containing Links With Distributed Mass and Elasticity", *Mechanism and machine Theory*, **7** (1), 3-17.
- Mahalingam, S., (1966), "Small Amplitude Vibrations of a Four Bar Mechanisms", *Journal of Mechanical Engineering Science*, **8** (4), 456-458.
- Masurekar, V. and Gupta, K. N., (1988a), "Stability Analysis of Four Bar Mechanism. Part I-With the Assumption that Damping is Absent", *Mechanism and machine Theory*, **23** (5), 367-375.
- Masurekar, V. and Gupta, K. N., (1988b), "Stability Analysis of Four Bar Mechanism. Part II-Taking Damping into Consideration", *Mechanism and Machine Theory*, **23** (5), 377-382.
- Meirovitch, L., (1986), "*Elements of Vibration Analysis*", Mc GrawHill
- Meissner, E., (1918), "Ueber Schüttelerscheinungen in Systemen mit periodisch veränderlicher", *Elastizität Schweizer Bauzeitung*, **72** (10), 95-98.
- Midha, A., Badlani, M. L. and Erdman, A. G., (1977), "A Note of the Effects of Multi-Element Idealisation of Planar Elastic Linkage Members", *Proceeding of the 5th OSU Applied Mechanics Conference Nov*, **27**, 1-11.
- Midha, A., Erdman, A. G. and Frohrib, D. A., (1978), "Finite Element Approach to Mathematical Modelling of High-speed Elastic linkages", *Mechanism and machine Theory*, **13**, 603-618.
- Midha, A., Erdman, A. G. and Frohrib, D. A., (1979a), "A closed Form Numerical Algorithm for The Periodic Response of High-Speed elastic Linkages", *Transaction of the ASME, Journal of Mechanical Design*, **101**, 154-162.
- Midha, A., Erdman, A. G. and Frohrib, D. A., (1979b), "A Computationally Efficient Numerical Algorithm For the Transient Response of High-Speed Elastic Linkages", *Transaction of the ASME, Journal of Mechanical Design*, **101**, 138-148.
- Midha, A., Karam, D. and Thompson B. S., (1992), "The Elastic Slider-Crank Mechanism: A Study of the Intrinsic Configuration-Dependent Modal Properties", *DE-Vol 47, Flexible Mechanisms, Dynamics, and Analysis ASME*, 337-346.
- Nagarajan, S. and Turcic, D. A., (1990a), "Lagrangian Formulation of the Equations of Motion for Elastic Mechanisms with mutual Dependence Between Rigid Body and Elastic Motion Part I: Element level Equations", *Transaction of the ASME, Journal of Dynamic Systems, Measurements and Control*, **112**, 203-214.

Nagarajan, S. and Turcic, D. A., (1990b), "Lagrangian Formulation of the Equations of Motion for Elastic Mechanisms with mutual Dependence Between Rigid Body and Elastic Motion Part II: System Equations", *Transaction of the ASME, Journal of Dynamic Systems, Measurements and Control*, **112**, 215-224.

Nagarajan, S. and Turcic, D. A., (1990c), "Dynamic Stability Considerations in Elastic Closed Loop Linkage Systems", *Flexible mechanisms, Dynamics and Robot trajectories, 21st Biennial mechanisms Conference, 16-19 Sept, Chicago ASME*, **24**, 1-8.

Nagarajan, S. and Turcic, D. A., (1990d), "Experimental Verification of Critical Speed ranges for Elastic, Closed Loop Linkage Systems", *Flexible mechanisms, Dynamics and Robot trajectories, 21st Biennial mechanisms Conference, 16-19 Sept, Chicago ASME*, **24**, 9-14.

Nath, P. K. and Ghosh, A., (1980a), "Kineto-Elastodynamic Analysis of Mechanisms by Finite Element Method", *Mechanism and machine Theory*, **15**, 179-197.

Nath, P. K. and Ghosh, A., (1980b), "Steady State Response of Mechanisms with Elastic Links by Finite Element Method", *Mechanism and machine Theory*, **15**, 199-211.

Oliver, J. H., Wysock, D. A. and Thompson, B. S., (1985), "The Synthesis of Flexible Linkages by Balancing the Tracer Point Quasi-Static Deflections Using Microprocessor and Advanced Materials Technologies", *Mechanism and machine Theory*, **20** (2), 103-114.

Patra, A. K. and Liou, F. W., (1992), "An Advisory Expert System for Preliminary Design and Finite Element Modelling of High-Speed Mechanisms", *Flexible mechanisms, Dynamics and Robot trajectories, 21st Biennial mechanisms Conference, 16-19 Sept, Chicago ASME*, 153-160.

Peng, K. C. and Liou, F. W., (1992), "A Survey of the Experimental Studies of flexible Mechanisms", *Flexible mechanisms, Dynamics and Robot trajectories, 21st Biennial mechanisms Conference, 16-19 Sept, Chicago ASME*, 161-168.

Peters, D. A. and Hohenemser, K. H., (1971), "Application of the Floquet transition Matrix to Problems of Lifting Rotor Stability", *Journal of American Helicopter Society*, **16**, 25-33.

Pipes, L. A., (1953), "Matrix Solution of the Equations of the Mathieu-Hill Type", *Journal of Applied Physics*, **24** (7), 902-910.

Raghu, E. and Balasubramonian, A., (1990), "Experimental Study on the Elastodynamic Behaviour of the Unbalanced and the Counterweighted Four Bar Mechanisms", *Transaction of the ASME, Journal of Mechanical Design*, **112**, 271-277.

Reuleaux, F., (1875), "*Theoretische Kinematik: Grundzuge einer Theorie des maschinenwesens*", Vieweg, Brunswick, Deutschland. Translated by Kennedy, A. B. W., (1876), "*Reuleaux Kinematics of Machinery*", Macmillan, London, republished by Doven, New York, 1963.

Richards, T. H., (1977), "*Energy Methods in Stress Analysis*", Ellis Harwood Ltd.

Richards, T. H. and Leung, Y. T., (1977), "An accurate Method in structural Vibration Analysis", *Journal of Sound and Vibration*, **55** (3), 363-376.

Rieger and McCallions, (1965), "The Natural Frequencies of Portal Frames", *International Journal of Mechanical Science*, **7**, 253-261.

Sadler, J. P. and Sandor, G. N., (1973), "A lumped Approach to Vibration and Stress Analysis of Elastic Linkages", *Transaction of the ASME, Journal of Engineering for Industry*, **95** (2), 549-557.

Sadler, J. P. and Sandor, G. N., (1974), "Non linear Vibration Analysis of Elastic four-bar linkages", *Transaction of the ASME, Journal of Engineering for industry*, 411-419.

Sadler, J. P. and Sandor, G. N., (1975), "On the Analytical Lumped-Mass model of an Elastic 4-bar Mechanism", *Transaction of the ASME, Journal of Engineering for industry*, 561-565.

Sanders, J. R. and Tesar, D., (1978), "The Analytical and Experimental Evaluation of Vibratory Oscillations in Realistically Proportioned Mechanisms", *Transaction of the ASME, Journal of Mechanical Design*, **103** (3), 762-768.

Sandor, G. N. and Erdman, A. G., (1984), "*Advanced Mechanic Design, Vol I*", Prentice Hall.

Sandor, G. N. and Zhuang, X., (1985), "A linearized Lumped Parameter Approach to Vibration and Stress Analysis of elastic Linkages", *Mechanism and machine Theory*, **20** (5), 427-437.

Shigley, J. E., (1969), "*Kinematic Analysis of Mechanisms*", McGraw-Hill.

Smith, M. R. and Maunder, L., (1967), "Inertia Forces in a Four-Bar Linkage", *Journal of Mechanical Engineering Science*, **9** (3), 218-225.

Smith, M. R. and Maunder, L., (1971), "Stability of a Four-Bar Linkage With Flexible Coupler", *Journal of Mechanical Engineering Science*, **13** (4), 237-342.

Soni, A. H., (1974), "*Mechanism Synthesis and Analysis*", McGraw-Hill.

Soong, K., Sunappan, D. and Thompson, B. S., (1989a), "The Elastodynamic Response of a Class of Intelligent Machinery, Part I: Theory", *Transaction of the*

ASME, Journal of Vibration, Acoustic, Stress and Reliability in Design, **111**, 430-436.

Soong, K., Sunappan, D. and Thompson, B. S., (1989b), "The Elastodynamic Response of a Class of Intelligent Machinery, Part II: Computational and Experimental Results", *Transaction of the ASME, Journal of Vibration, Acoustic, Stress and Reliability in Design*, **111**, 437-442.

Stamps, F. R. and Bagci, C., (1983), "Dynamics of Planar, Elastic, High-Speed Mechanisms Considering Three-Dimensional Offset Geometry: Analytical and Experimental Investigations", *Transaction of the ASME, Journal of Mechanisms, Transmission and Automation in Design*, **105**, 498-510.

Sung, C. K. and Thompson, B. S., (1982), "A Note on the Effect of Foundation Motion Upon the Response of Flexible Linkages", *ASME Paper No 82-DET-26*, 1-7.

Sung, C. K. and Thompson, B. S., (1984), "Material Selection: An Important Parameter In the Design of High-Speed Linkages", *Mechanism and machine Theory*, **19** (4/5), 389-396.

Sung, C. K., Thompson, B. S. and Crowley, P., (1986), "An Experimental Study to Demonstrate the Superior Response Characteristics of Mechanisms Constructed with Laminates", *Mechanism and Machine theory*, **21** (2), 103-119.

Sung, C. K., Thompson, B. S., Xing, T. M. and Wang, C. H., (1986), "An Experimental Study on the Non-linear Elastodynamic Response of Linkage Mechanisms", *Mechanism and Machine theory*, **21** (2), 121-133.

Sung, C. K. and Chen, Y. C., (1991), "Vibration Control of the Elastodynamic Response of High-Speed Flexible Linkage Mechanisms", *Transaction of the ASME, Journal Of Vibration and Acoustics*, **113**, 14-21.

Sutherland, G. H., (1975), "Analytical and Experimental Study of a High-Speed Elastic Mechanism", *I. Mech. E, Fourth world Congress on The theory of Machines and Mechanisms*, 533-536.

Sutherland, G. H., (1976), "Analytical and Experimental Investigation of a High-speed Elastic Member Linkage", *Transaction of the ASME, Journal of Engineering for Industry*, 788-793.

Tadjbakhsh, I. G., (1982), "Stability of Motion of Elastic Planar Linkages with Application to Slider-Crank Mechanisms", *Transaction of the ASME, Journal of Mechanical Design*, **104**, 698-703.

Tadjbakhsh, I. G. and Younes, G. J., (1986), "Dynamic Stability of the Flexible Connecting Rod of a Slider Crank Mechanism", *Transaction of the ASME, Journal of Mechanisms, Transmission and Automation in Design*, Paper No 86-DET-4.

- Thompson, B. S. and Barr, A. D. S., (1975) "A Variational Principle for the Motion of Components of Elastic Mechanisms", *Proceedings of the IV World Congress on the Theory of Machines and Mechanisms, University of Newcastle-Upon-Tyne, England, Institution of Mechanical Engineers*, 235-239.
- Thompson, B. S. and Sung, C. K., (1984), "A Variational Formulation for the Non-Linear Finite Element Analysis of Flexible Linkages: Theory, Implementation and Experimental Results", *Transaction of the ASME, Journal of Mechanisms, Transmission and Automation in Design*, **106**, 482-488.
- Thompson, B. S. and Sung, C. K., (1986a), "An Analytical and Experimental Investigation of High-Speed Mechanisms Fabricated with Composite Laminates", *Journal of Sound and Vibration*, **111**, (3), 399-428.
- Thompson, B. S. and Sung, C. K., (1986b), "A Survey of Finite Element Techniques for Mechanism Design", *Mechanism and Machine Theory*, **21** (4), 351-359.
- Thompson, B. S. and Sung, C. K., (1986c), "A survey of Finite Element technique for Mechanism Design", *Mechanism and machine Theory*, **21** (4), 351-359.
- Thompson, B. S., Zuccaro, D., Gamache, D. and Gandhi, M. V., (1983a), "An Experimental and Analytical Study of a Four-Bar Mechanism With Links Fabricated from Fibre reinforced Composite Material", *Mechanism and machine Theory*, **18**, 165-171.
- Thompson, B. S., Zuccaro, D., Gamache, D. and Gandhi, M. V., (1983b), "An Experimental and Analytical Study of the Dynamic Response of a Linkage Fabricated From a Unidirectional Fibre-Reinforced Composite Laminate", *Transaction of the ASME, Journal of Mechanisms, Transmission and Automation in Design*, **105**, 526-533.
- Turcic, D. A. and Midha, A., (1984a), "Generalised Equations of Motion for the Dynamic Analysis of Elastic Mechanism Systems", *Transaction of the ASME, Journal of Dynamic Systems, Measurements and Control*, **106** (4), 243-248.
- Turcic, D. A. and Midha, A., (1984b), "Dynamic Analysis of Elastic Mechanism Systems Part I: Applications", *Transaction of the ASME, Journal of Dynamic Systems, Measurements and Control*, **106**, 249-254.
- Turcic, D. A., Midha, A. and Bosnik, J. R., (1984), "Dynamic Analysis of Elastic Mechanism Systems Part II: Experimental Results", *Transaction of the ASME, Journal of Dynamic Systems, Measurements and Control*, **106**, 255-260.
- Turner, M. J., Clough, R. W., Martin, H. C. and Topp, L. J., (1956), "Stiffness and Deflection Analysis of Complex Structures", *Journal of Aeronautical Sciences*, **23**, 805-824.

Tyc, G., Cleghorn, W. L. and Rimrott, F. P. J., (1990), "Infinite Eigenvalue Method for Stability Analyses of Canonical Linear Systems with Periodic Coefficients", *AIAA Journal*, **28** (5), 869-876.

Xu, T. and Lowen, G. G., (1992), "A New Analytical Approach For the Determination of the Transient Response in Elastic Mechanisms", *DE-Vol 47, Flexible Mechanisms, Dynamics, and Analysis ASME*, 347-352.

Yang, Z. and Sadler, J. P., (1990), "Large Displacement Finite Element Analysis of Flexible Linkages", *Transaction of the ASME, Journal of Mechanical Design*, **112**, 175-182.

Yang, Z. and Sadler, J. P., (1993), "A Numerically Efficient Algorithm for Steady State Response of Flexible Mechanism Systems", *Transaction of the ASME, Journal of Mechanical Design*, **115**, 848-855.

Zadoks, R. I. and Midha, A., (1987a), "Parametric Stability of a Two Degree-of-Freedom Machine System: Part I-Equations of Motion and Stability", *Transaction of the ASME, Journal of Vibration, Acoustic, Stress and Reliability in Design*, **109**, 210-215.

Zadoks, R. I. and Midha, A., (1987b), "Parametric Stability of a Two Degree-of-Freedom Machine System: Part II-Stability Analysis", *Transaction of the ASME, Journal of Vibration, Acoustic, Stress and Reliability in Design*, **109**, 216-223.

Zou, H.; Wang, L., Kovacevic, R., (1992), "Measurement and Theoretical Analysis of Elastic Locus of High-Speed Mechanism", *DE-Vol 47, Flexible Mechanisms, Dynamics, and Analysis ASME*, 593-597.

Winfrey, R. C., (1971), "Elastic Link Mechanism Dynamics", *Transaction of the ASME, Journal of Engineering for industry*, 268-272.

Winfrey, R. C., (1972), "Dynamic Analysis of Elastic link Mechanisms by Reduction of coordinates", *Transaction of the ASME, Journal of Engineering for industry*, 577-582.

Wittrick, W. H. and Williams, F. W., (1970), "An automatic Computation procedure for calculating natural frequencies of skeletal structures", *International Journal of Mechanical Science*, **12**, 781-791.

Wittrick, W. H. and Williams, F. W., (1971), "A General Algorithm for Computing Natural Frequencies Of Elastic Structures", *Quarterly Journal of Mechanics and Applied Mathematics*, **XXIV** (3), 263-284.

Wu, W. T., Wickert, J. A. and Griffin, J. H., (1993), "Modal Analysis of the Steady State Response of Driven Periodic Linear System", *Journal of Sound and Vibration*, **183** (2), 297-308.

Appendix A

MATRIX ELEMENTS FOR THE p-VERSION

A.1. BEAM ELEMENT WITH 1 INTERNAL NODE

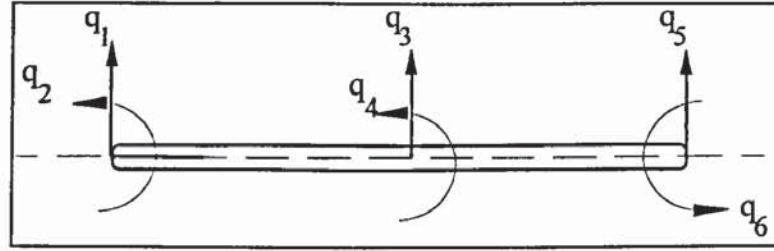


Fig. A.1: Schematic of the element with 1 internal node.

In order to derive the element stiffness and mass matrices, the method followed was outlined in chapter 4. The shape functions $N(x)$ for this particular case are quintic polynomials. Its coefficients are determined by equating the coordinates q_i 's to the displacements (and the rotations) at the respective position. Then the shape functions are differentiated twice with respect to the space coordinate x to yield $B(x)$ used to calculate the stiffness matrix.

It is found that:

$$N(x)^T = \begin{bmatrix} 1 - 23\zeta^2 + 66\zeta^3 - 68\zeta^4 + 24\zeta^5 \\ L(\zeta - 6\zeta^2 + 13\zeta^3 - 12\zeta^4 + 4\zeta^5) \\ 16\zeta^2 - 32\zeta^3 + 16\zeta^4 \\ L(-8\zeta^2 + 32\zeta^3 - 40\zeta^4 + 16\zeta^5) \\ 7\zeta^2 - 34\zeta^3 + 52\zeta^4 - 24\zeta^5 \\ L(-\zeta^2 + 5\zeta^3 - 8\zeta^4 + 4\zeta^5) \end{bmatrix} \quad (A.1)$$

$$\mathbf{B}(x)^T = \begin{bmatrix} -46 + 396\zeta - 816\zeta^2 + 480\zeta^3 \\ L(-12 + 78\zeta - 144\zeta^2 + 80\zeta^3) \\ 32 - 192\zeta + 192\zeta^2 \\ L(-16 + 192\zeta - 480\zeta^2 + 320\zeta^3) \\ 14 - 204\zeta + 624\zeta^2 - 480\zeta^3 \\ L(-2 + 30\zeta - 96\zeta^2 + 80\zeta^3) \end{bmatrix} \quad (\text{A.2})$$

$$\mathbf{M} = \rho A L \begin{bmatrix} \frac{523}{3465} & \frac{19L}{2310} & \frac{4}{63} & \frac{-8L}{693} & \frac{131}{6930} & \frac{-29L}{13860} \\ & \frac{2L^2}{2L} & \frac{2L}{2L} & \frac{-L^2}{-L^2} & \frac{29L}{29L} & \frac{-L^2}{-L^2} \\ & \frac{3465}{3465} & \frac{315}{128} & \frac{1155}{1155} & \frac{13860}{4} & \frac{4620}{-2L} \\ & & \frac{315}{315} & 0 & \frac{63}{63} & \frac{315}{315} \\ & & & \frac{32L^2}{3465} & \frac{8L}{8L} & \frac{-L^2}{-L^2} \\ & & & & \frac{693}{523} & \frac{1155}{-19L} \\ & & & & \frac{3465}{3465} & \frac{2310}{2L^2} \\ & & & & & \frac{2L^2}{3465} \end{bmatrix} \quad (\text{A.3})$$

$$\mathbf{K} = \frac{EI}{L^3} \begin{bmatrix} \frac{5092}{35} & \frac{1138L}{35} & \frac{-512}{5} & \frac{384L}{7} & \frac{-1508}{35} & \frac{242L}{35} \\ & \frac{322L^2}{35} & \frac{-128L}{5} & \frac{64L^2}{7} & \frac{-242L}{35} & \frac{38L^2}{35} \\ & & \frac{1024}{5} & 0 & \frac{-512}{5} & \frac{128L}{5} \\ & & & \frac{256L^2}{7} & \frac{-384L}{7} & \frac{64L^2}{7} \\ & & & & \frac{5092}{35} & \frac{-1138L}{35} \\ & & & & & \frac{332L^2}{35} \end{bmatrix} \quad (\text{A.4})$$

A.2. BEAM ELEMENT WITH CURVATURES

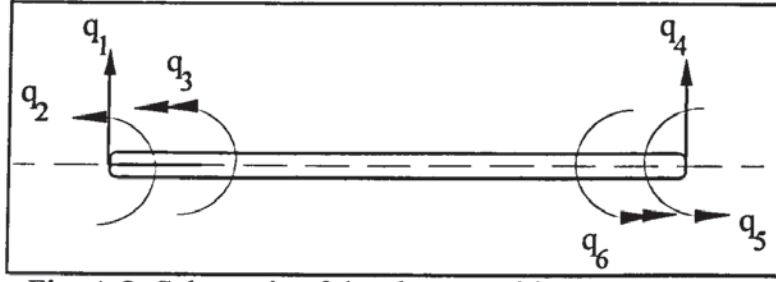


Fig. A.2: Schematic of the element with two curvatures.

$$\mathbf{N}(\mathbf{x})^T = \begin{bmatrix} 1 - 23\zeta^2 + 66\zeta^3 - 68\zeta^4 + 24\zeta^5 \\ L(\zeta - 6\zeta^2 + 13\zeta^3 - 12\zeta^4 + 4\zeta^5) \\ 16\zeta^2 - 32\zeta^3 + 16\zeta^4 \\ L(-8\zeta^2 + 32\zeta^3 - 40\zeta^4 + 16\zeta^5) \\ 7\zeta^2 - 34\zeta^3 + 52\zeta^4 - 24\zeta^5 \\ L(-\zeta^2 + 5\zeta^3 - 8\zeta^4 + 4\zeta^5) \end{bmatrix} \quad (\text{A.5})$$

$$\mathbf{B}(\mathbf{x})^T = \begin{bmatrix} -46 + 396\zeta - 816\zeta^2 + 480\zeta^3 \\ L(-12 + 78\zeta - 144\zeta^2 + 80\zeta^3) \\ 32 - 192\zeta + 192\zeta^2 \\ L(-16 + 192\zeta - 480\zeta^2 + 320\zeta^3) \\ 14 - 204\zeta + 624\zeta^2 - 480\zeta^3 \\ L(-2 + 30\zeta - 96\zeta^2 + 80\zeta^3) \end{bmatrix} \quad (\text{A.6})$$

$$\mathbf{M} = \rho A L \begin{bmatrix} \frac{523}{3465} & \frac{19L}{2310} & \frac{4}{63} & \frac{-8L}{693} & \frac{131}{6930} & \frac{-29L}{13860} \\ & \frac{2L^2}{3465} & \frac{2L}{315} & \frac{-L^2}{1155} & \frac{29L}{13860} & \frac{-L^2}{4620} \\ & & \frac{128}{315} & 0 & \frac{4}{63} & \frac{-2L}{315} \\ & & & \frac{32L^2}{3465} & \frac{8L}{693} & \frac{-L^2}{1155} \\ & & & & \frac{523}{3465} & \frac{-19L}{2310} \\ & & & & & \frac{2L^2}{3465} \end{bmatrix} \quad (\text{A.7})$$

$$\mathbf{K} = \frac{EI}{L^3} \begin{bmatrix} \frac{5092}{35} & \frac{1138L}{35} & \frac{-512}{5} & \frac{384L}{7} & \frac{-1508}{35} & \frac{242L}{35} \\ & \frac{322L^2}{35} & \frac{-128L}{5} & \frac{64L^2}{7} & \frac{-242L}{35} & \frac{38L^2}{35} \\ & & \frac{1024}{5} & 0 & \frac{-512}{5} & \frac{128L}{5} \\ & & & \frac{256L^2}{7} & \frac{-384L}{7} & \frac{64L^2}{7} \\ & & & & \frac{5092}{35} & \frac{-1138L}{35} \\ & & & & & \frac{332L^2}{35} \end{bmatrix} \quad (A.8)$$

Appendix B

FREQUENCY FUNCTIONS F_i and G_i

$$F_1 = -\frac{\lambda}{\delta}(\sinh l - \sin l) \quad (B.1)$$

$$F_2 = -\frac{\lambda}{\delta}(\cosh \lambda \sin \lambda - \sinh \lambda \cos \lambda) \quad (B.2)$$

$$F_3 = -\frac{\lambda^2}{\delta}(\cosh \lambda - \cos \lambda) \quad (B.3)$$

$$F_4 = \frac{\lambda^2}{\delta}(\sinh \lambda \sin \lambda) \quad (B.4)$$

$$F_5 = \frac{\lambda^3}{\delta}(\sinh \lambda + \sin \lambda) \quad (B.5)$$

$$F_6 = -\frac{\lambda^3}{\delta}(\cosh \lambda \sin \lambda + \sinh \lambda \cos \lambda) \quad (B.6)$$

$$F_7 = -\beta \cot(\beta L) \quad (B.7)$$

$$F_8 = \frac{\beta}{\sin(\beta L)} \quad (B.8)$$

$$\delta = \cosh \lambda \cos \lambda - 1 \quad (B.9)$$

$$G_1 = \frac{1}{4\lambda^4}(F_1 F_2 - F_3 - F_1) \quad (B.10)$$

$$G_2 = \frac{1}{4\lambda^4}(F_1^2 - F_2) \quad (B.11)$$

$$G_3 = -\frac{1}{4\lambda^4}(F_1 F_4 + 2F_3) \quad (B.12)$$

$$G_4 = -\frac{1}{4\lambda^4}(F_1 F_3 + 2F_4) \quad (B.13)$$

$$G_5 = \frac{1}{4\lambda^4}(F_3 F_4 - 3F_5) \quad (B.14)$$

$$G_6 = \frac{1}{4\lambda^4}(F_3^2 - 3F_6) \quad (B.15)$$

$$G_7 = \frac{\beta}{2\sin^2(\beta L)} - \frac{1}{2}\cot(\beta L) \quad (B.16)$$

$$G_8 = \frac{-\beta^2 \cos(\beta L)}{2 \sin^2(\beta L)} + \frac{1}{2 \sin(\beta L)} \quad (\text{B.17})$$

Appendix C

EXPERIMENTAL RESULTS FOR $L_2 = 0.328$ m

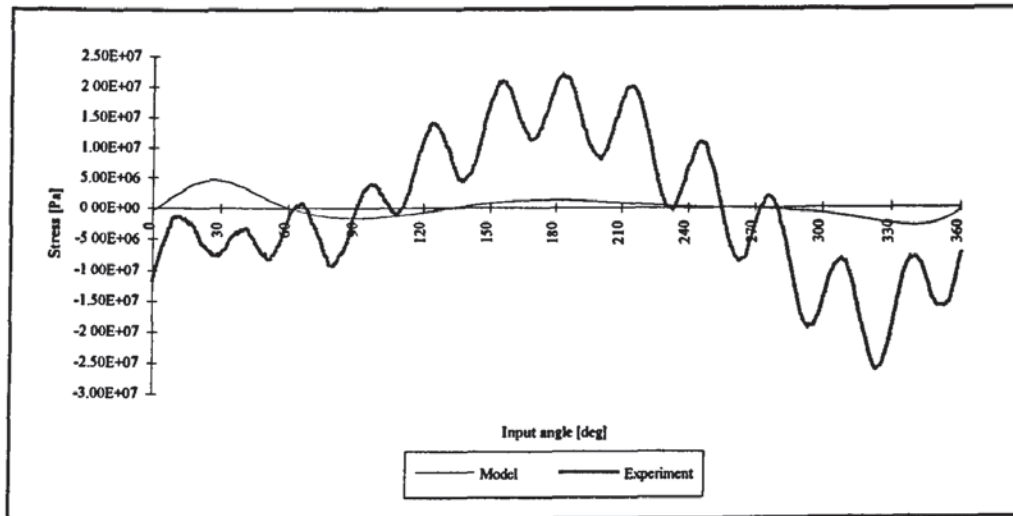


Fig. C.1.a: Stress at the input link midpoint for $\omega=7.11$ rad/s

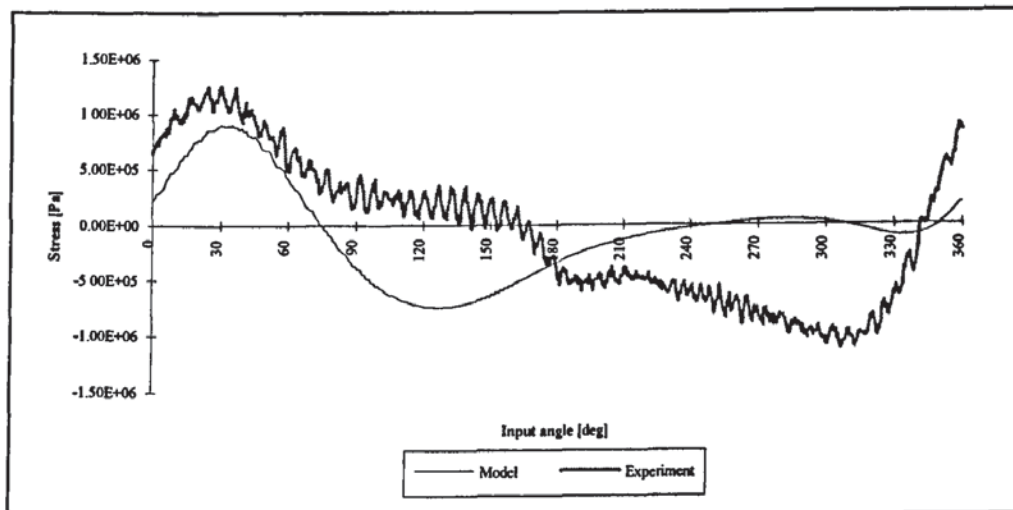


Fig. C.1.b: Stress at the coupler midpoint for $\omega=7.11$ rad/s

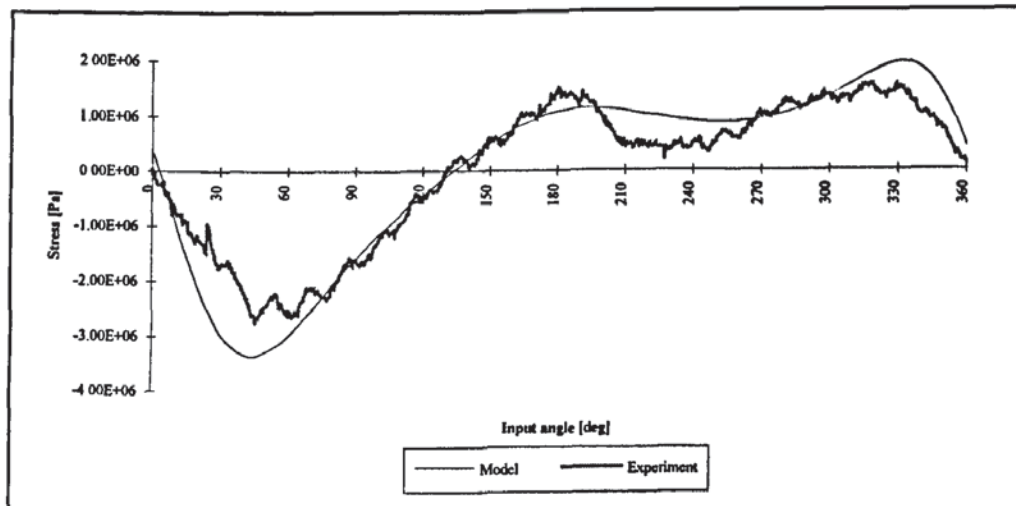


Fig. C.1.c: Stress at the follower midpoint for $\omega=7.11$ rad/s

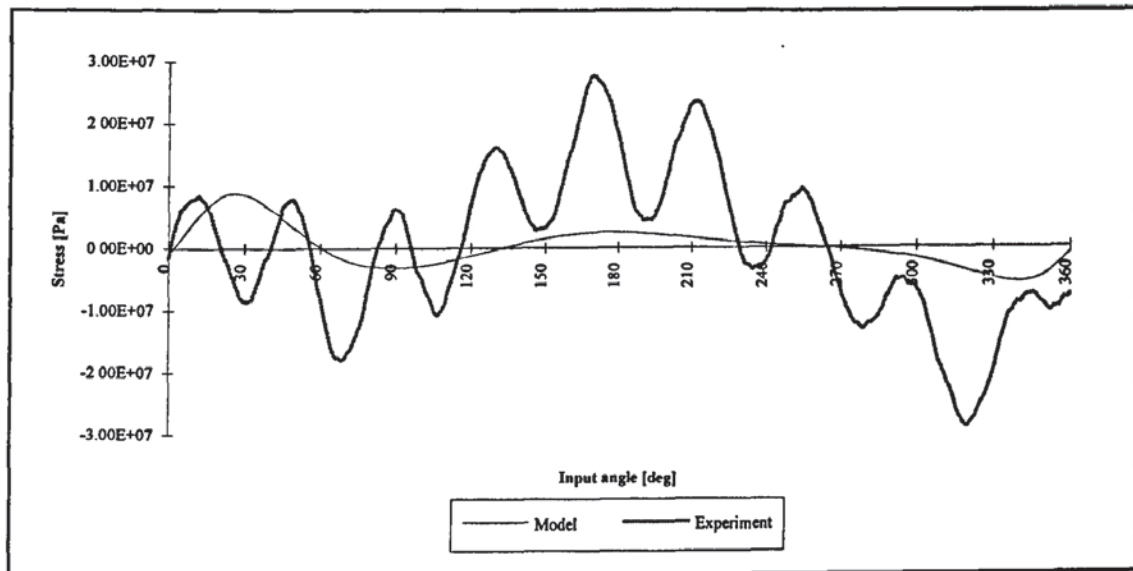


Fig. C.2.a: Stress at the input link midpoint for $\omega = 9.71$ rad/s

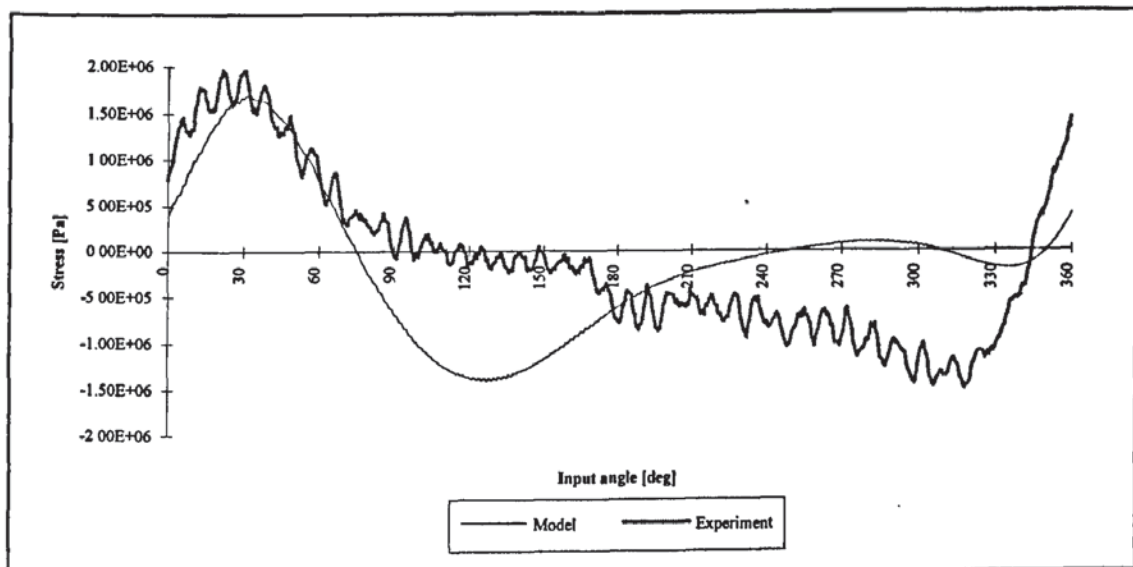


Fig. C.2.b: Stress at the coupler midpoint for $\omega = 9.71$ rad/s

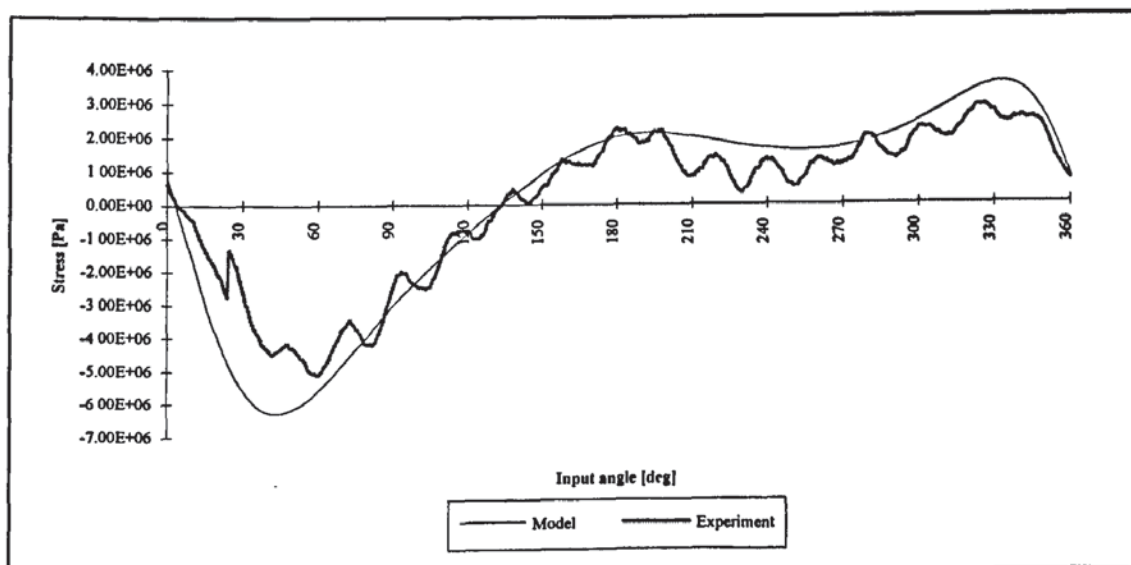


Fig. C.2.c: Stress at the follower midpoint for $\omega = 9.71$ rad/s

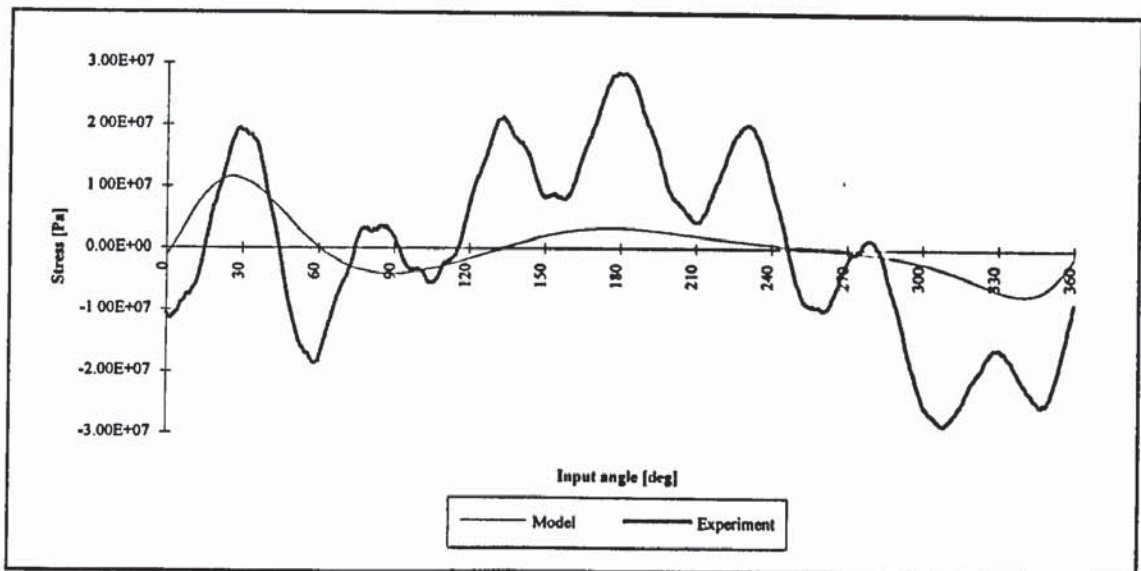


Fig. C.3.a: Stress at the input link midpoint for $\omega = 11.1$ rad/s

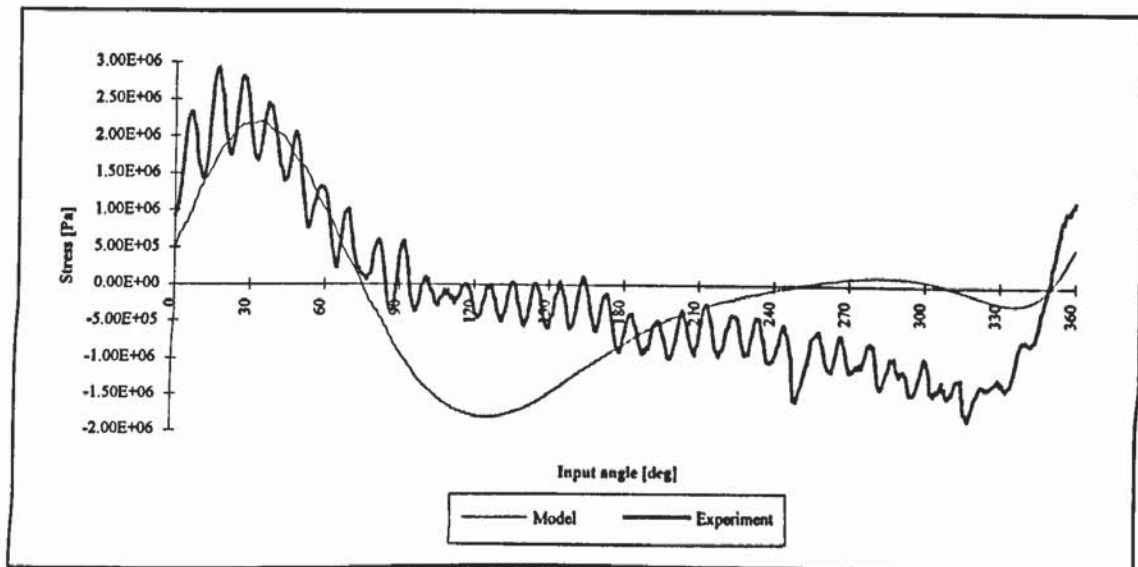


Fig. C.3.b: Stress at the coupler midpoint for $\omega = 11.1$ rad/s

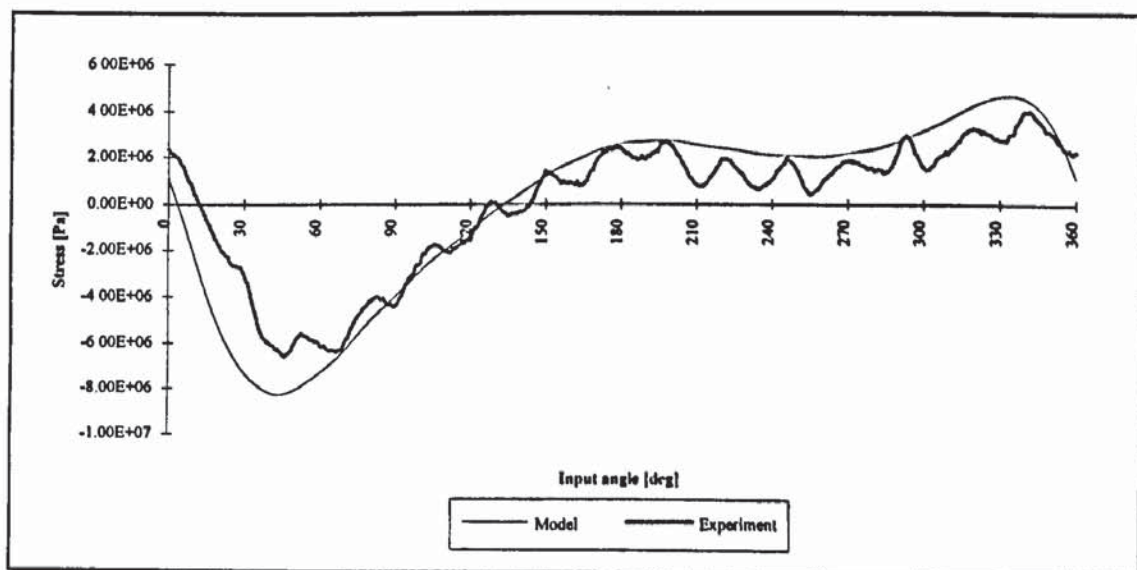


Fig. C.3.c: Stress at the follower midpoint for $\omega = 11.1$ rad/s

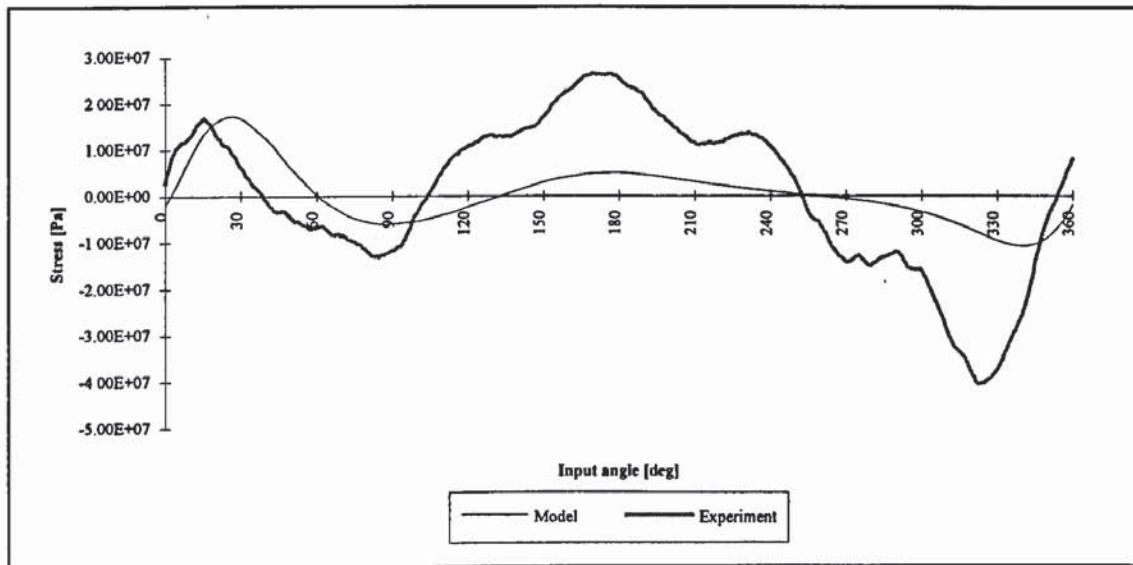


Fig. C.4.a: Stress at the input link midpoint for $\omega = 13.43$ rad/s

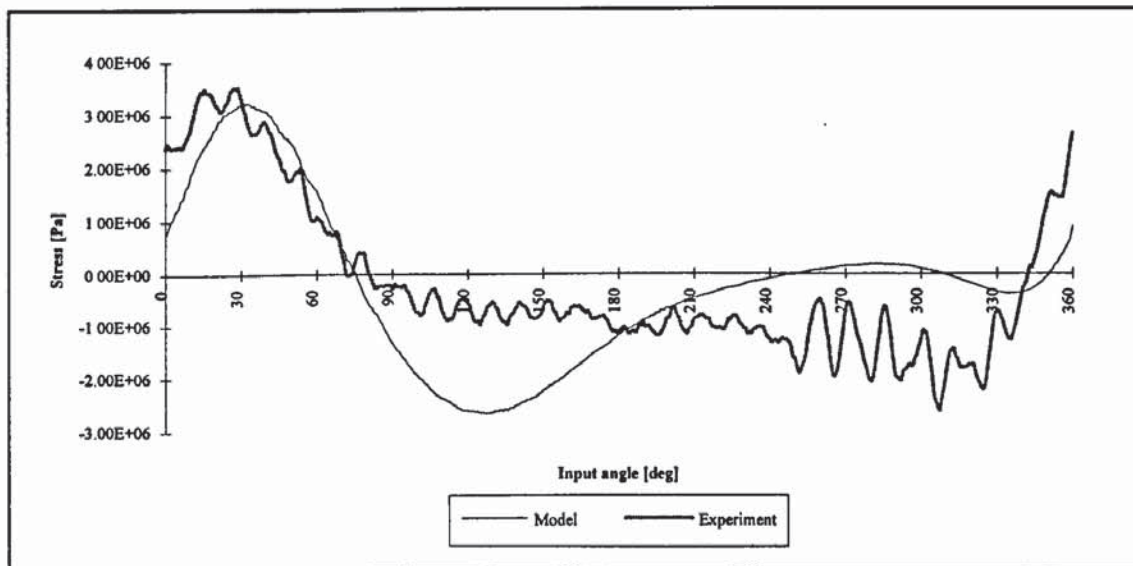


Fig. C.4.b: Stress at the coupler midpoint for $\omega = 13.43$ rad/s

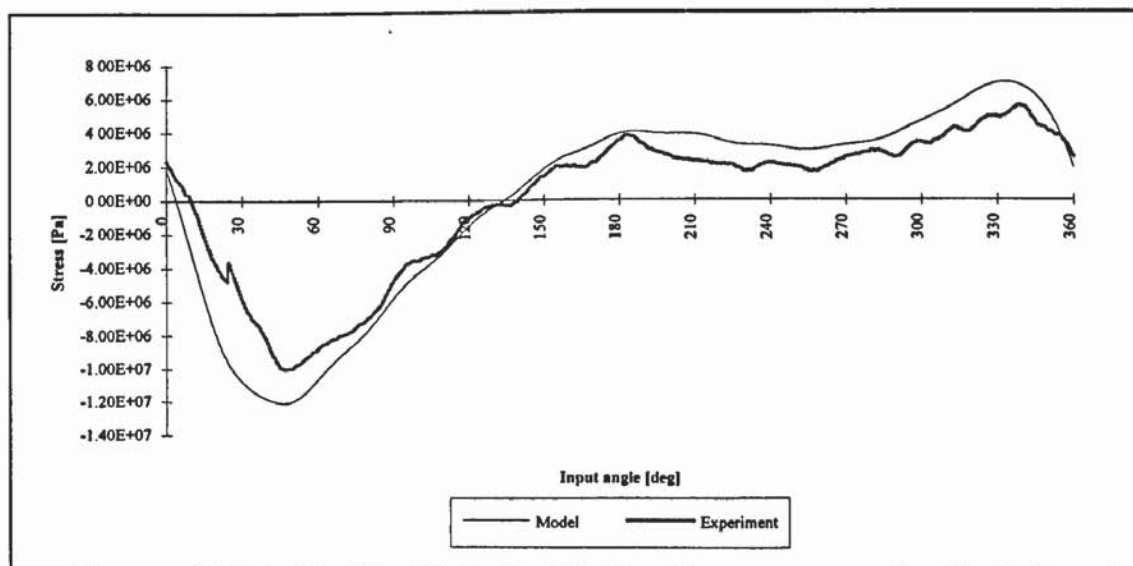


Fig. C.4.c: Stress at the follower midpoint for $\omega = 13.43$ rad/s

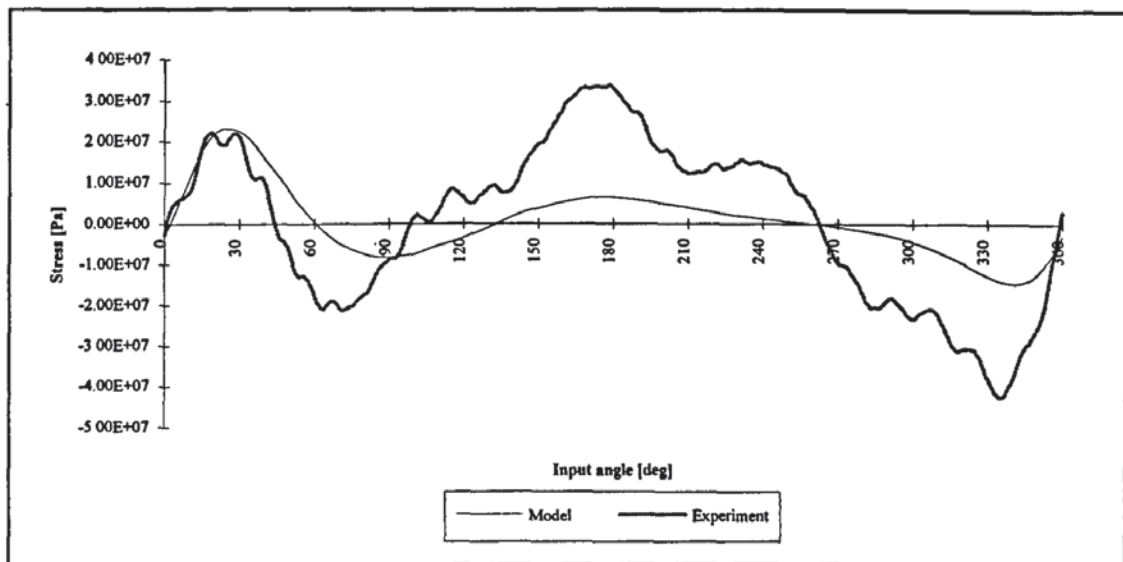


Fig. C.5.a: Stress at the input link midpoint for $\omega = 15.44$ rad/s

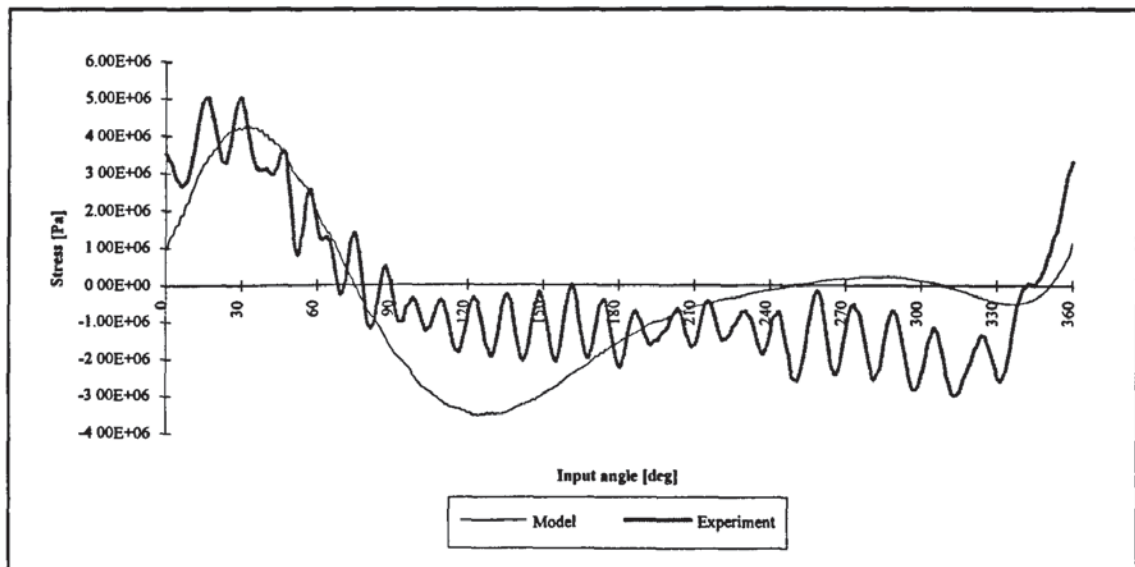


Fig. C.5.b: Stress at the coupler midpoint for $\omega = 15.44$ rad/s

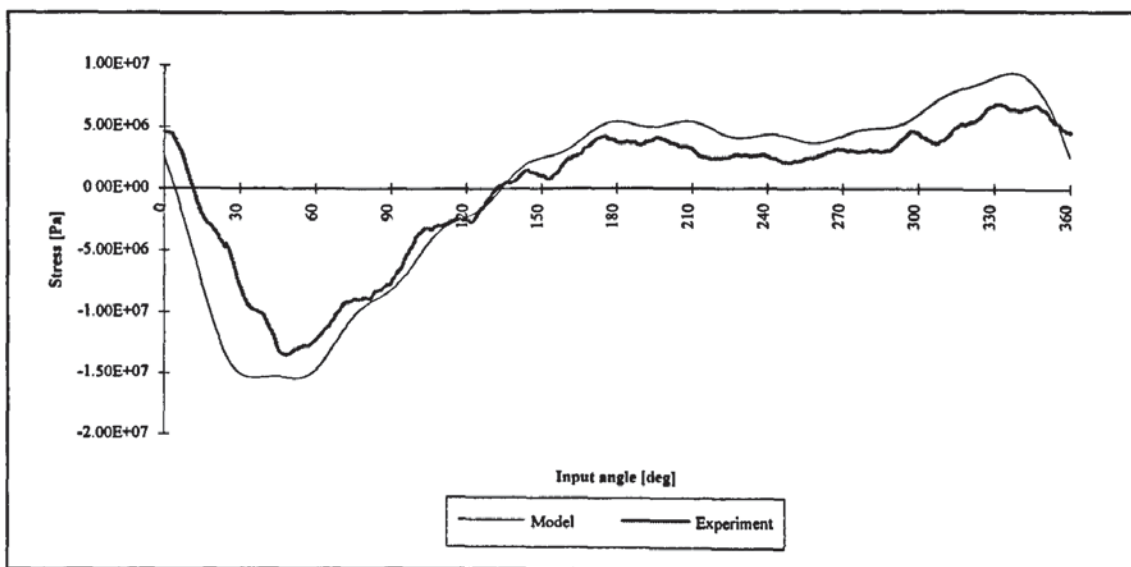


Fig. C.5.c: Stress at the follower midpoint for $\omega = 15.44$ rad/s

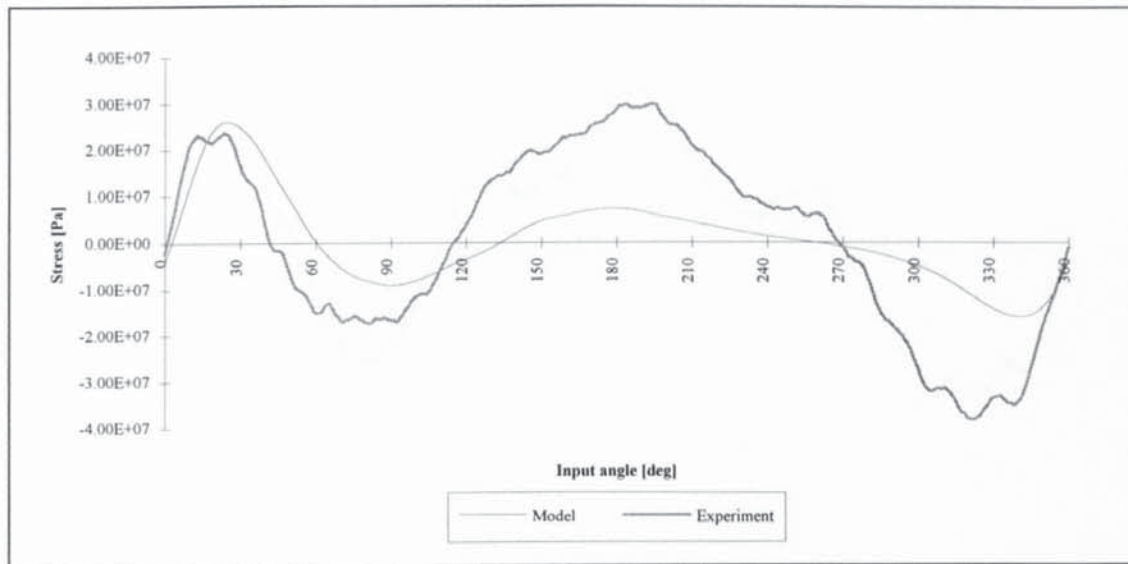


Fig. C.6.a: Stress at the input link midpoint for $\omega = 16.28$ rad/s

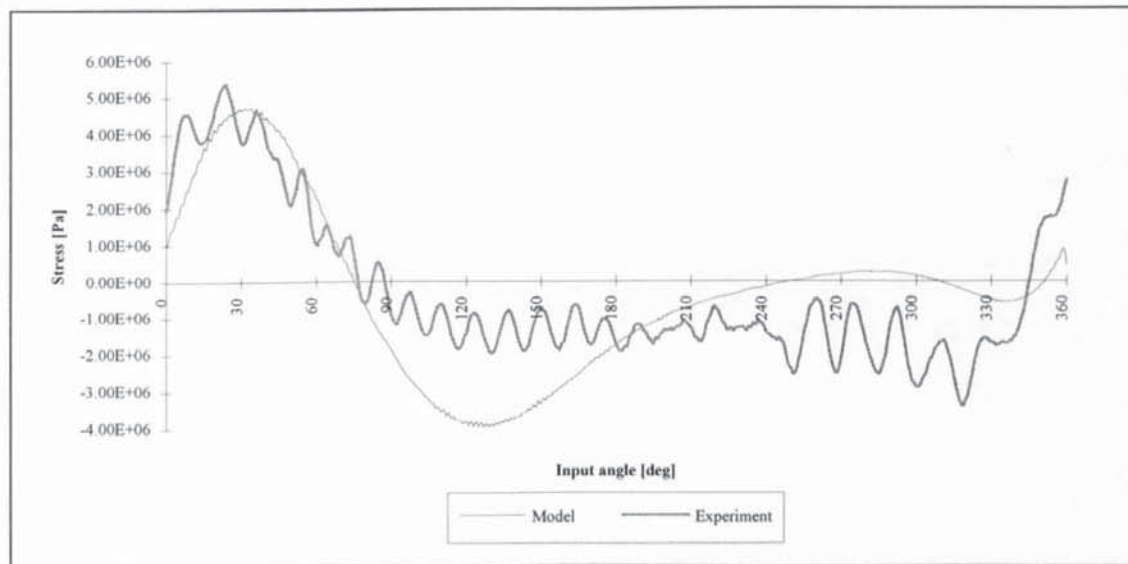


Fig. C.6.b: Stress at the coupler midpoint for $\omega = 16.28$ rad/s

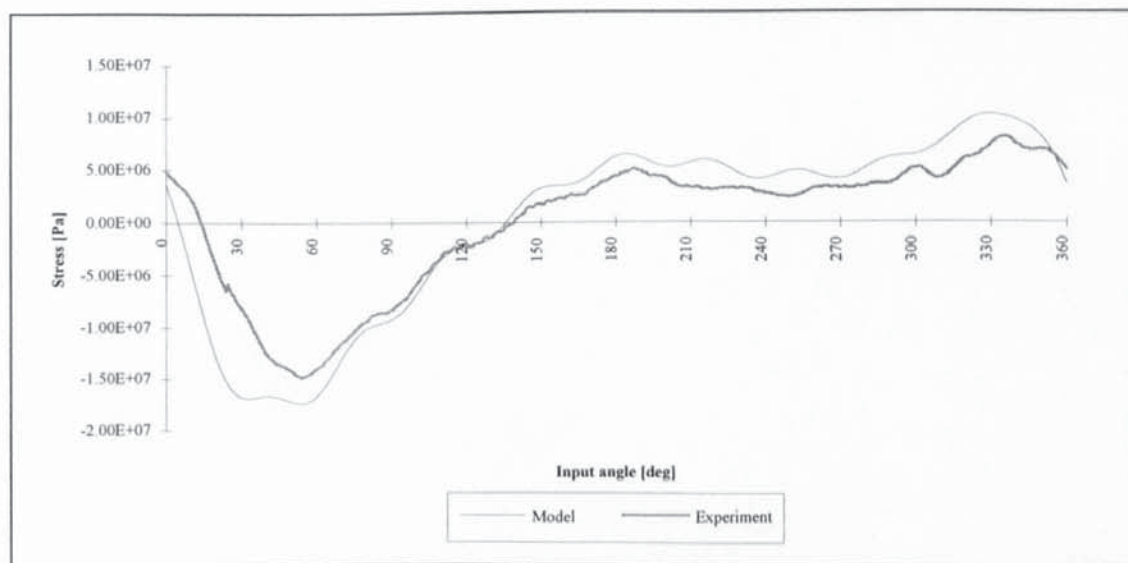


Fig. C.6.c: Stress at the follower midpoint for $\omega = 16.28$ rad/s

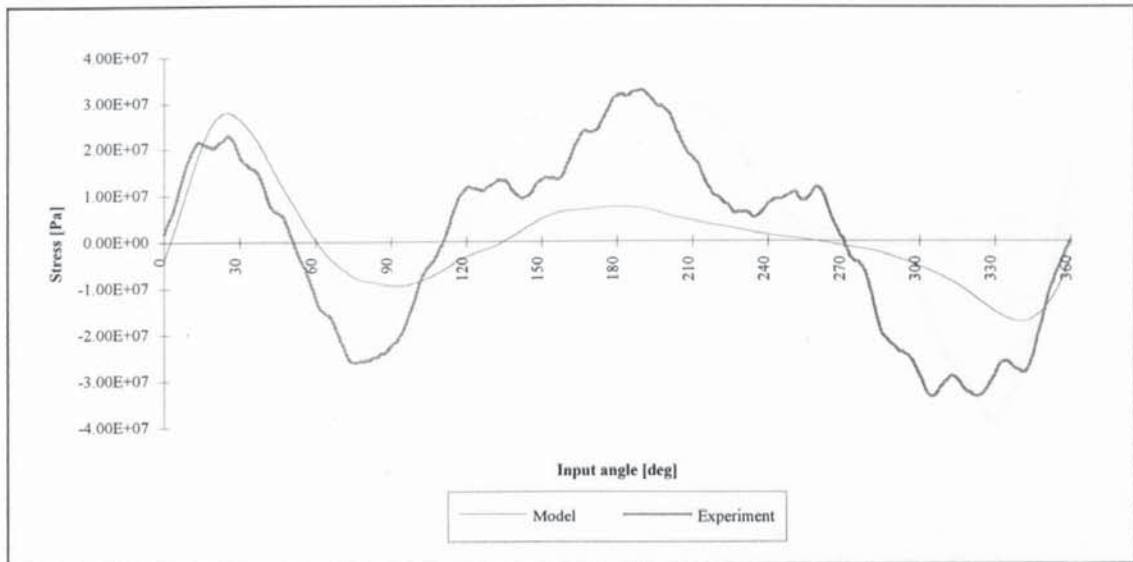


Fig. C.7.a: Stress at the input link midpoint for $\omega = 16.71$ rad/s

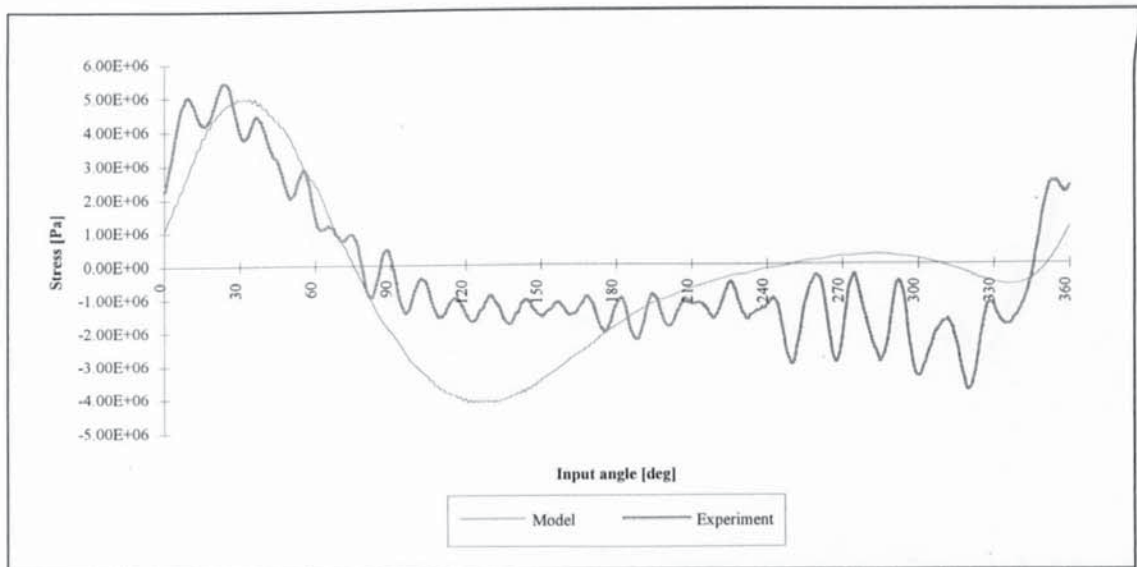


Fig. C.7.b: Stress at the coupler midpoint for $\omega = 16.71$ rad/s

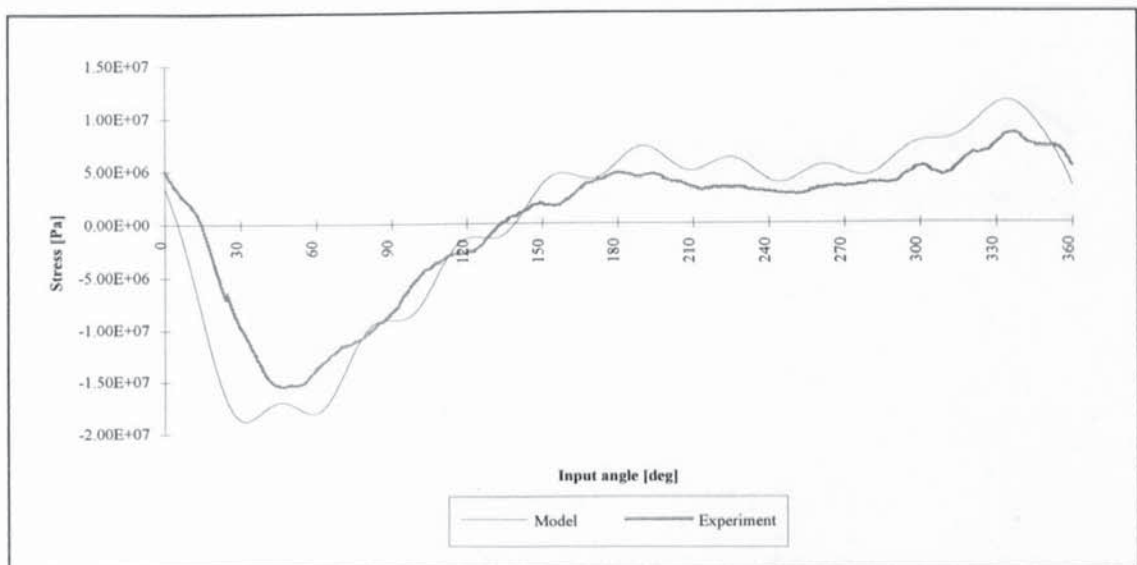


Fig. C.7.c: Stress at the follower midpoint for $\omega = 16.71$ rad/s

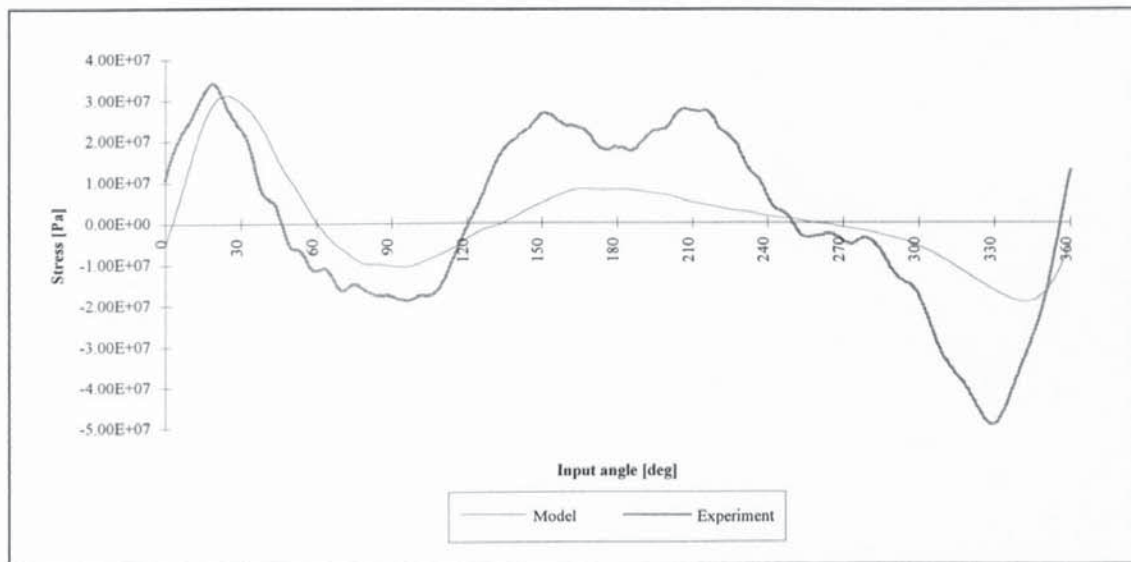


Fig. C.8.a: Stress at the input link midpoint for $\omega = 17.70$ rad/s

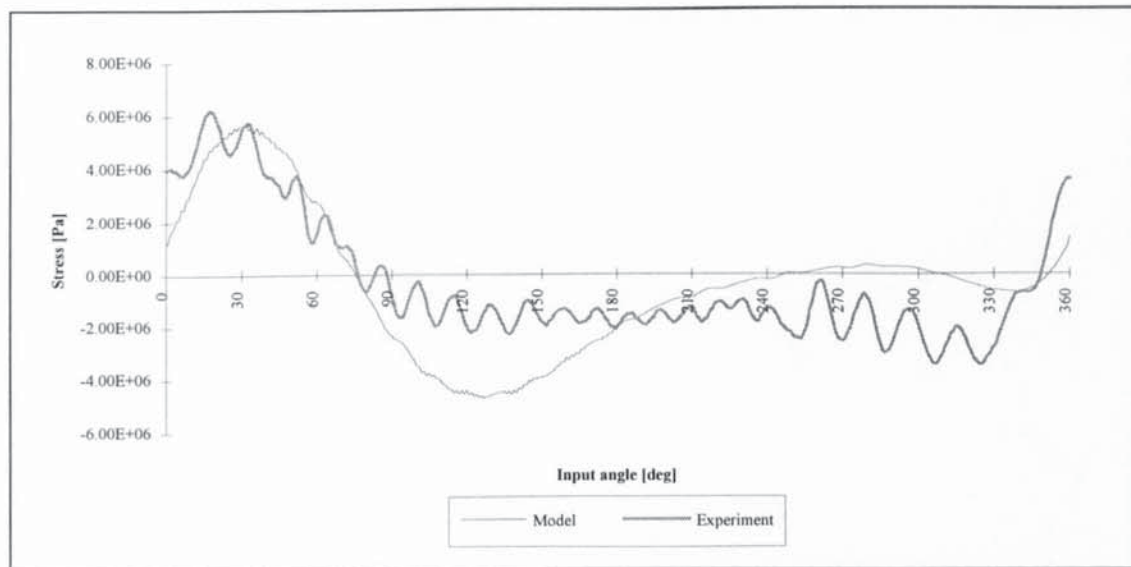


Fig. C.8.b: Stress at the coupler midpoint for $\omega = 17.70$ rad/s

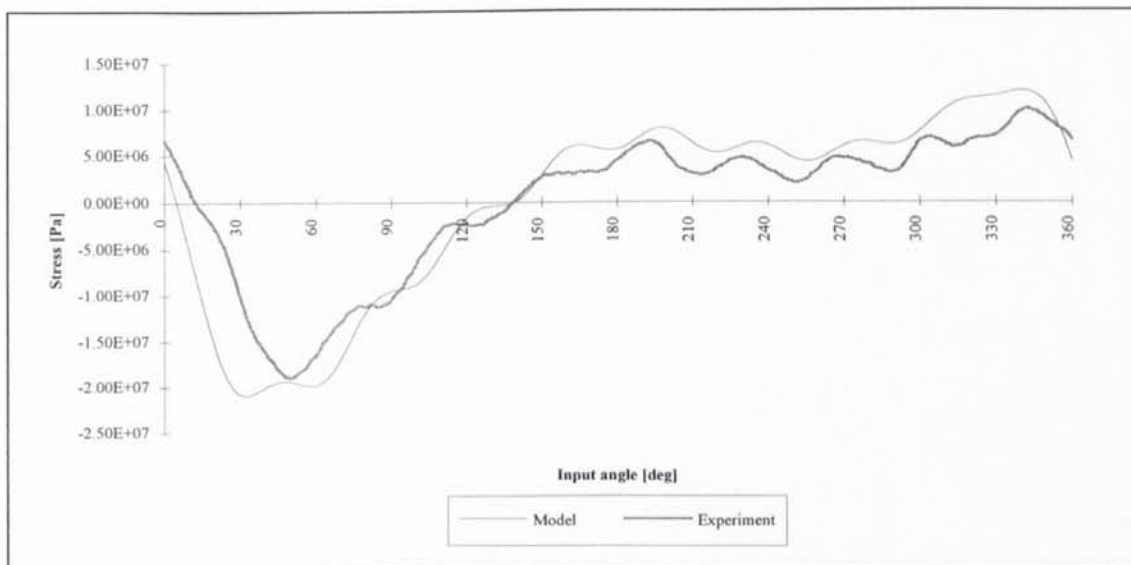


Fig. C.8.c: Stress at the follower midpoint for $\omega = 17.70$ rad/s

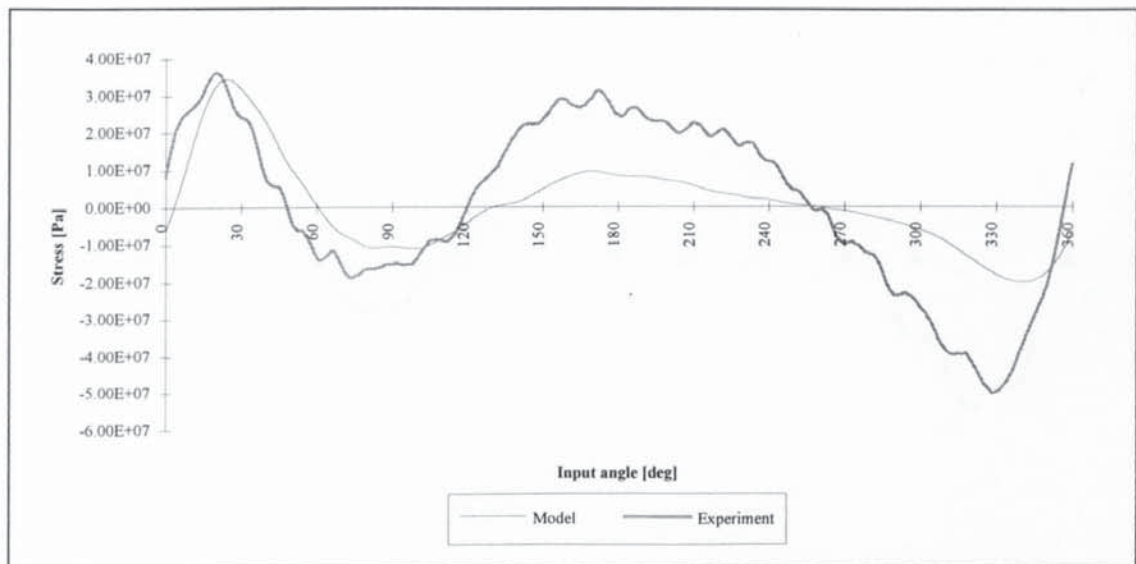


Fig. C.9.a: Stress at the input link midpoint for $\omega = 18.27$ rad/s

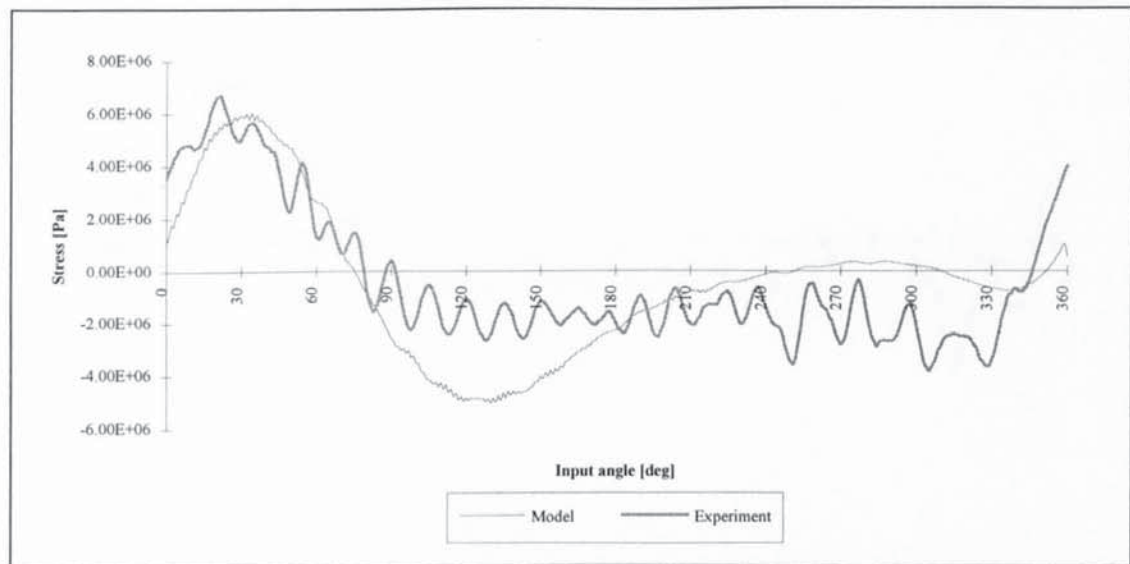


Fig. C.9.b: Stress at the coupler midpoint for $\omega = 18.27$ rad/s

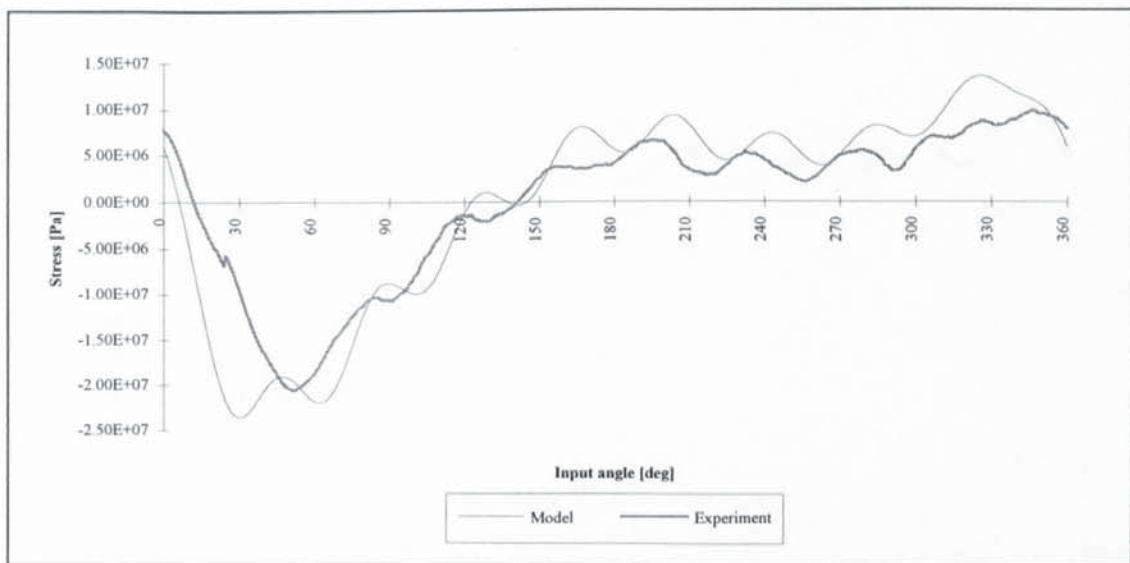


Fig. C.9.c: Stress at the follower midpoint for $\omega = 18.27$ rad/s

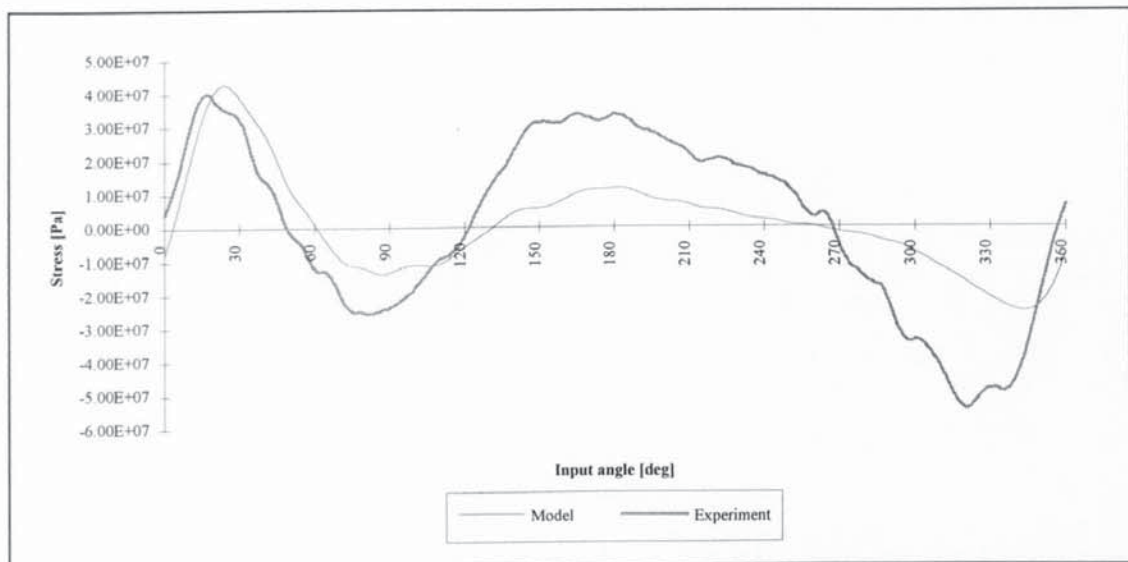


Fig. C.10.a: Stress at the input link midpoint for $\omega = 20.07$ rad/s

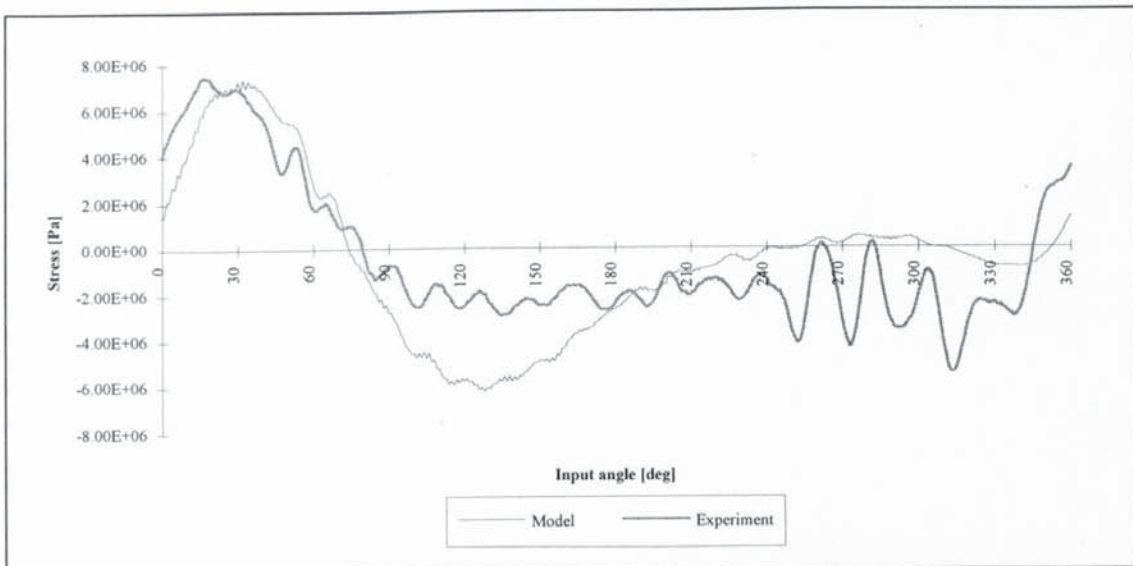


Fig. C.10.b: Stress at the coupler midpoint for $\omega = 20.07$ rad/s

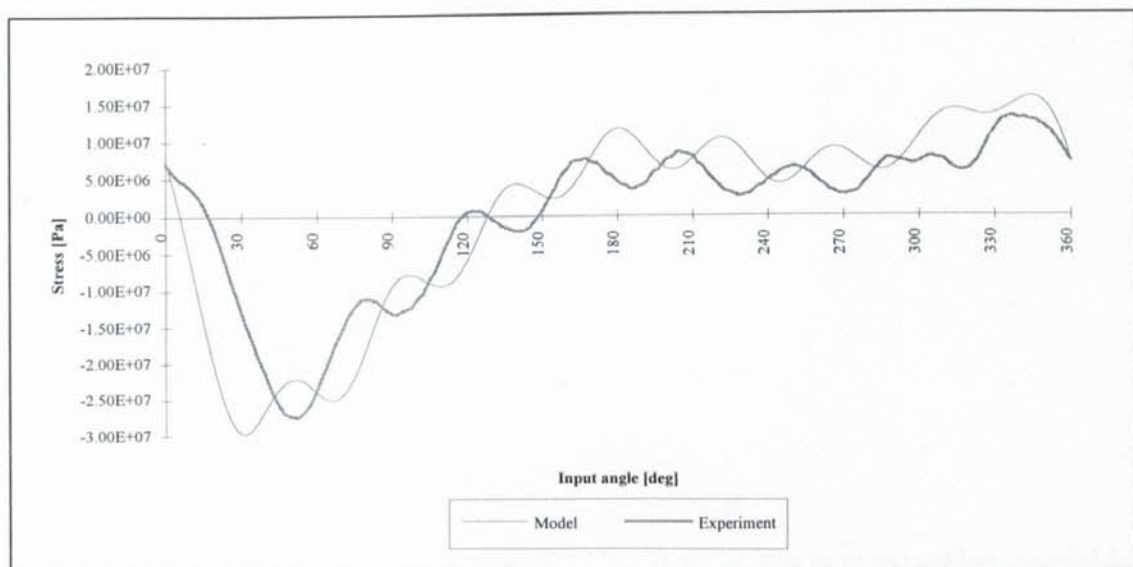


Fig. C.10.c: Stress at the follower midpoint for $\omega = 20.07$ rad/s

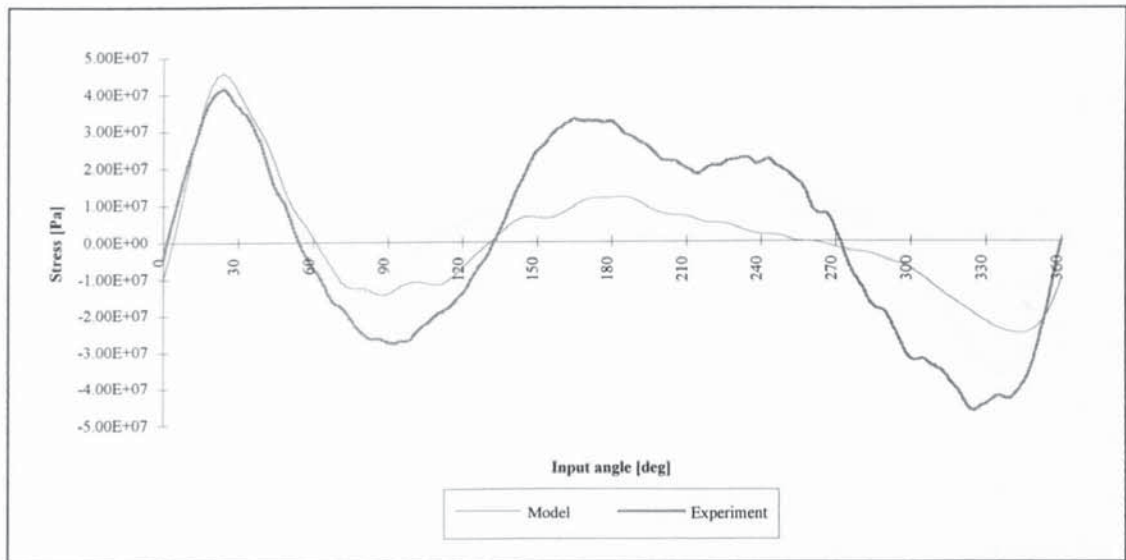


Fig. C.11.a: Stress at the input link midpoint for $\omega = 20.40$ rad/s

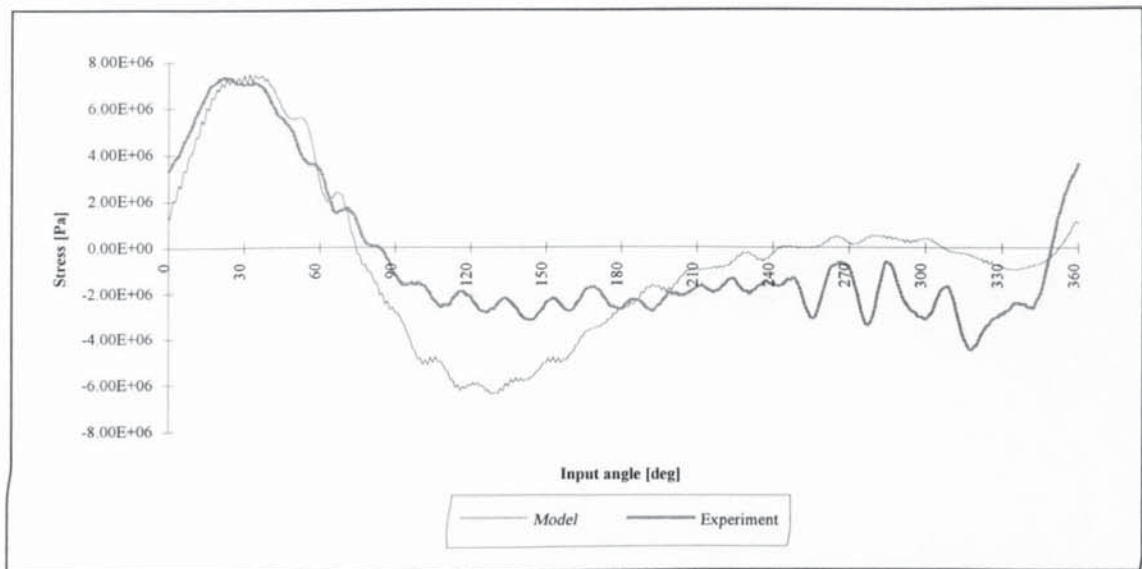


Fig. C.11.b: Stress at the coupler midpoint for $\omega = 20.40$ rad/s

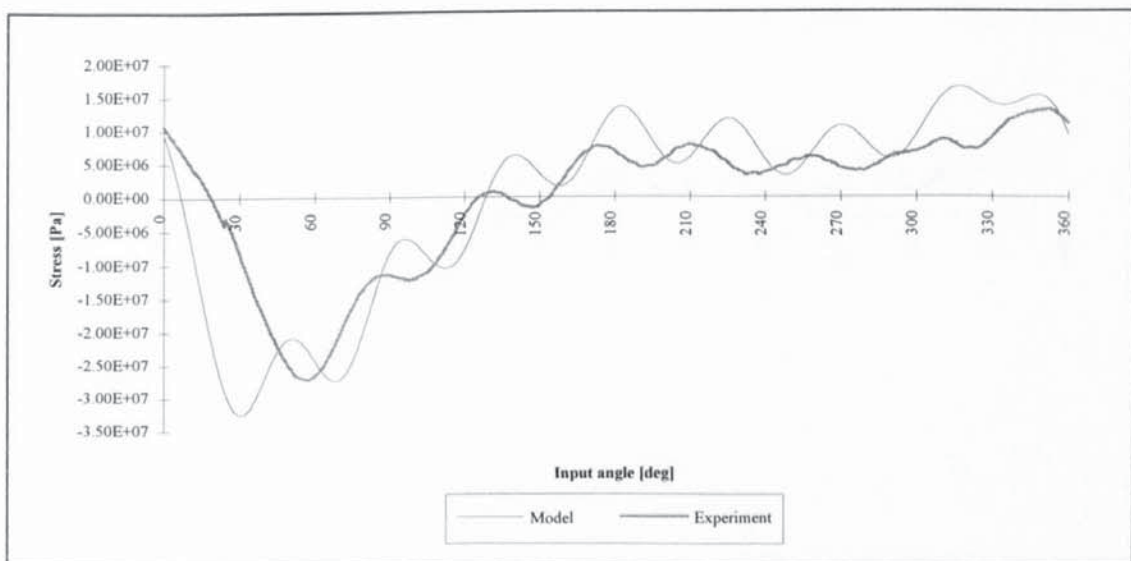


Fig. C.11.c: Stress at the follower midpoint for $\omega = 20.40$ rad/s

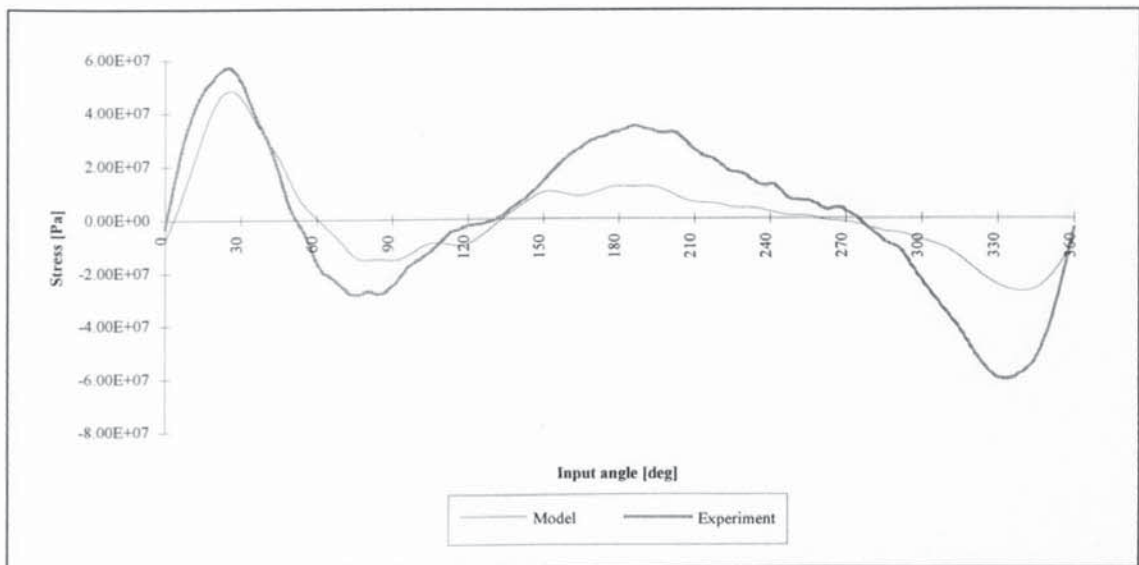


Fig. C.12.a: Stress at the input link midpoint for $\omega = 21.01$ rad/s

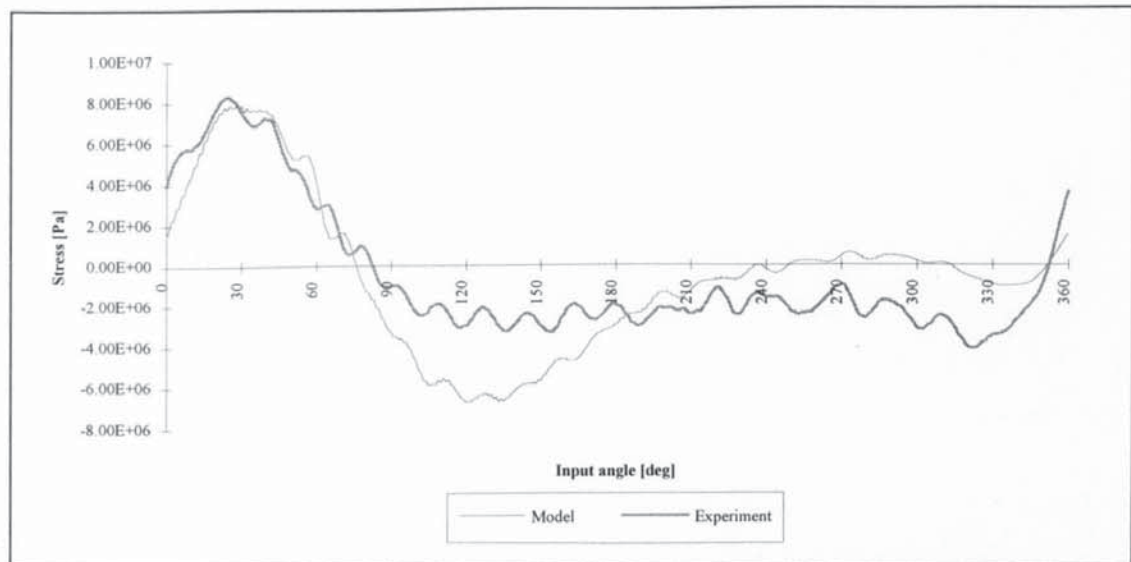


Fig. C.12.b: Stress at the coupler midpoint for $\omega = 21.01$ rad/s

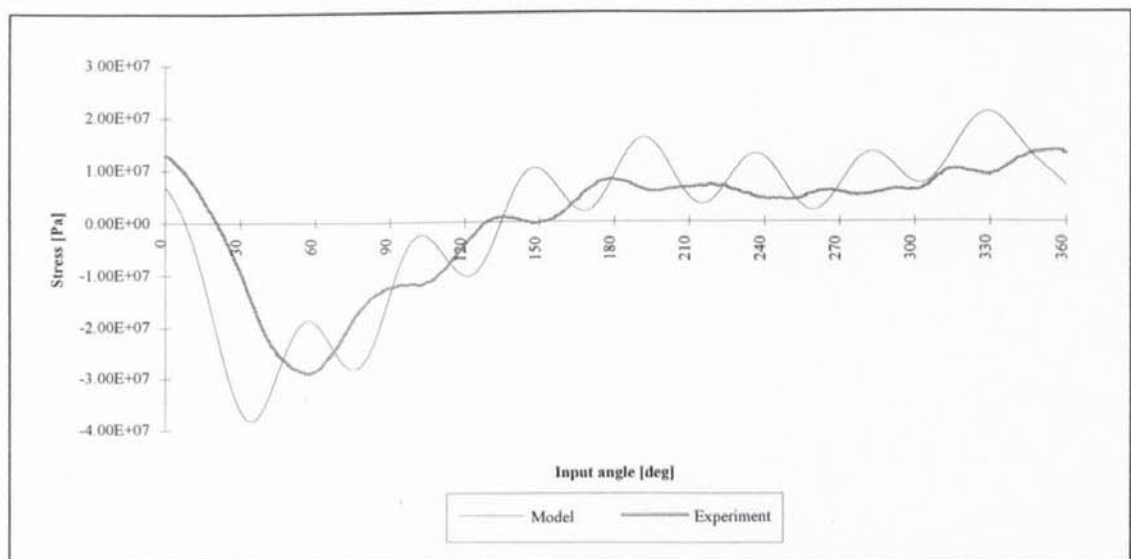


Fig. C.12.c: Stress at the follower midpoint for $\omega = 21.01$ rad/s

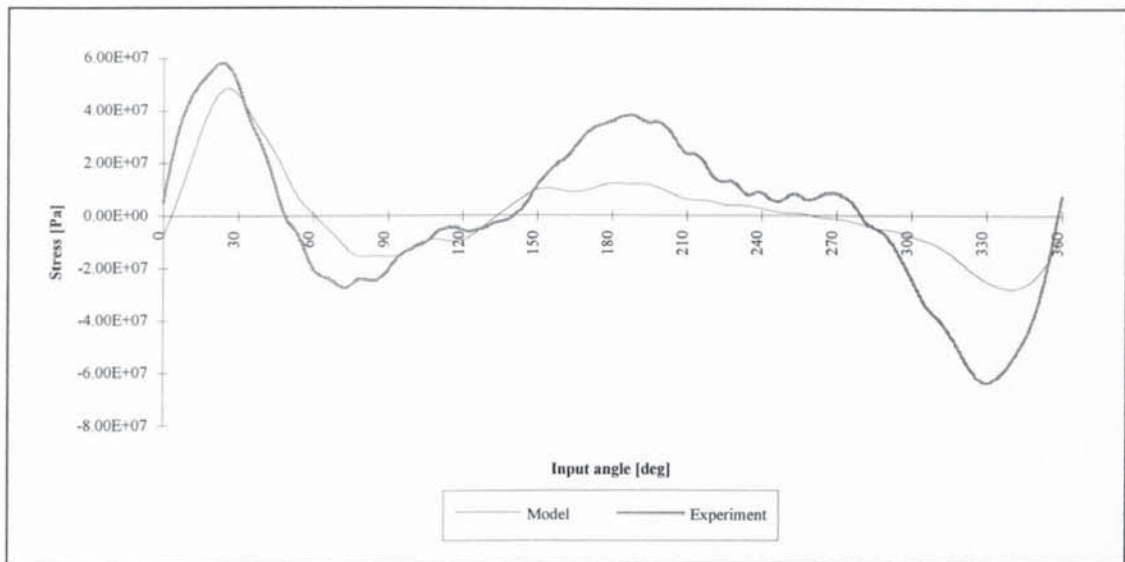


Fig. C.13.a: Stress at the input link midpoint for $\omega = 21.08$ rad/s

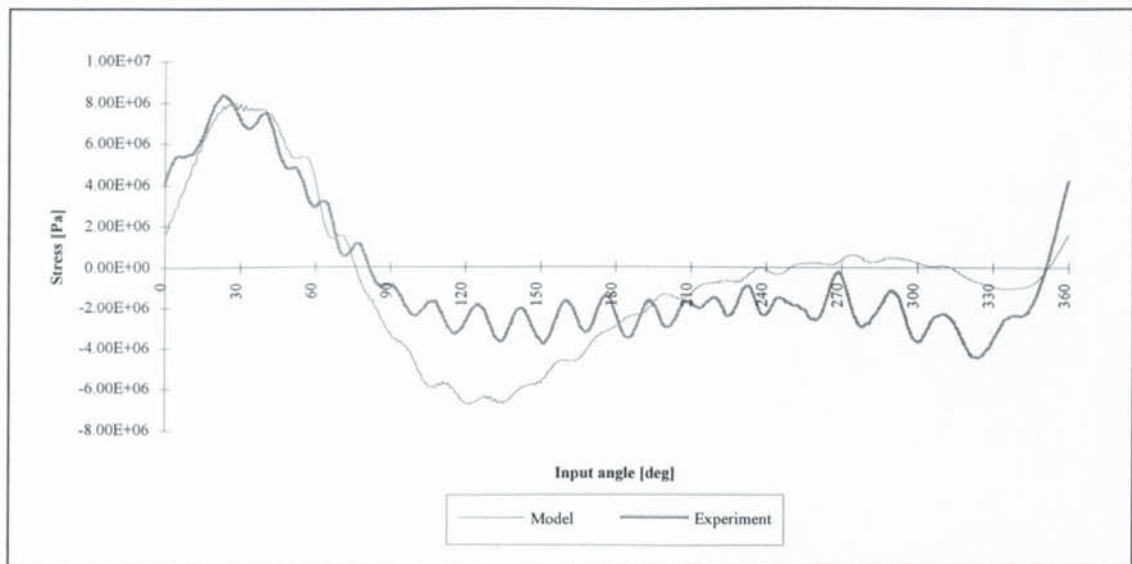


Fig. C.13.b: Stress at the coupler midpoint for $\omega = 21.08$ rad/s

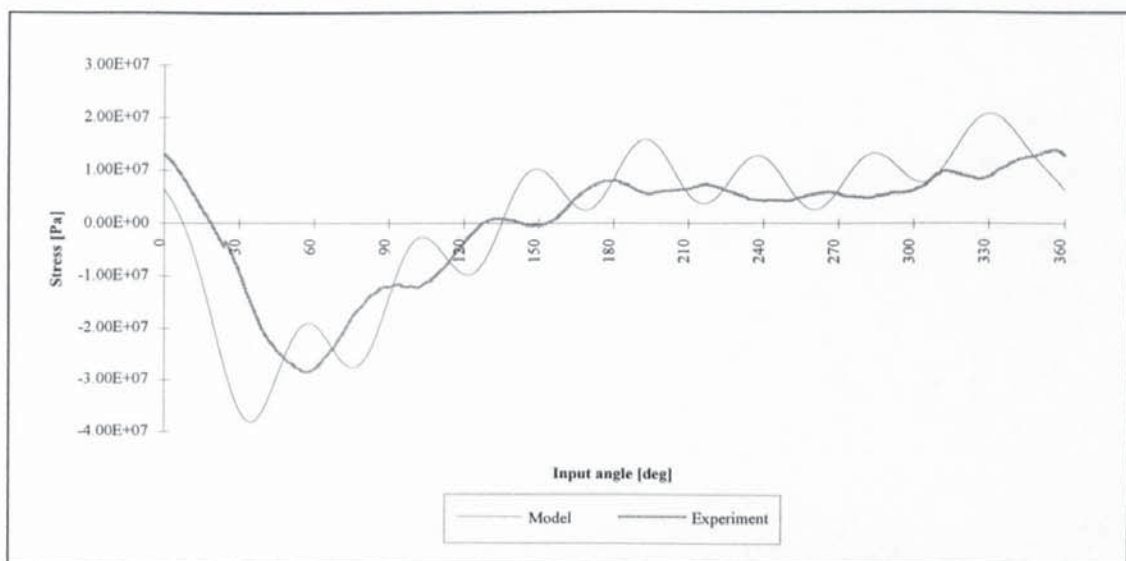


Fig. C.13.c: Stress at the follower midpoint for $\omega = 21.08$ rad/s

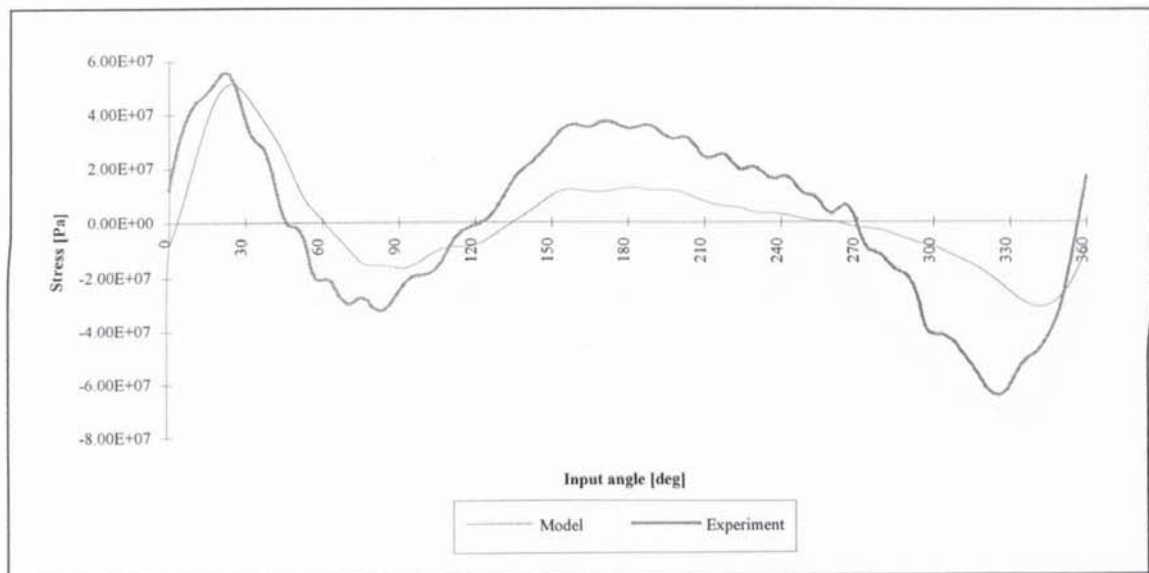


Fig. C.14.a: Stress at the input link midpoint for $\omega = 21.89$ rad/s

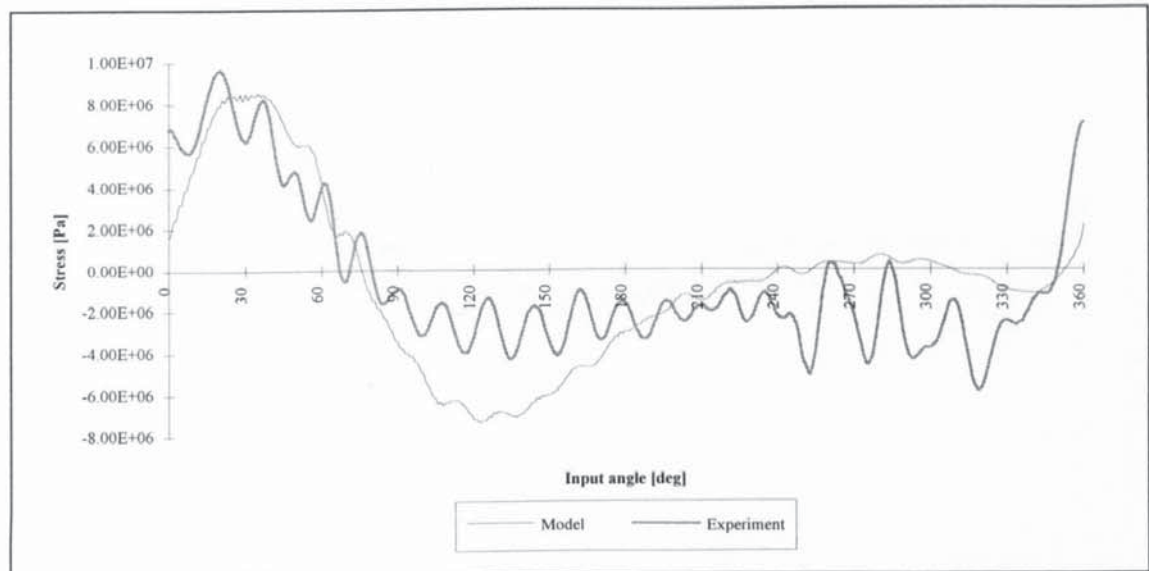


Fig. C.14.b: Stress at the coupler midpoint for $\omega = 21.89$ rad/s

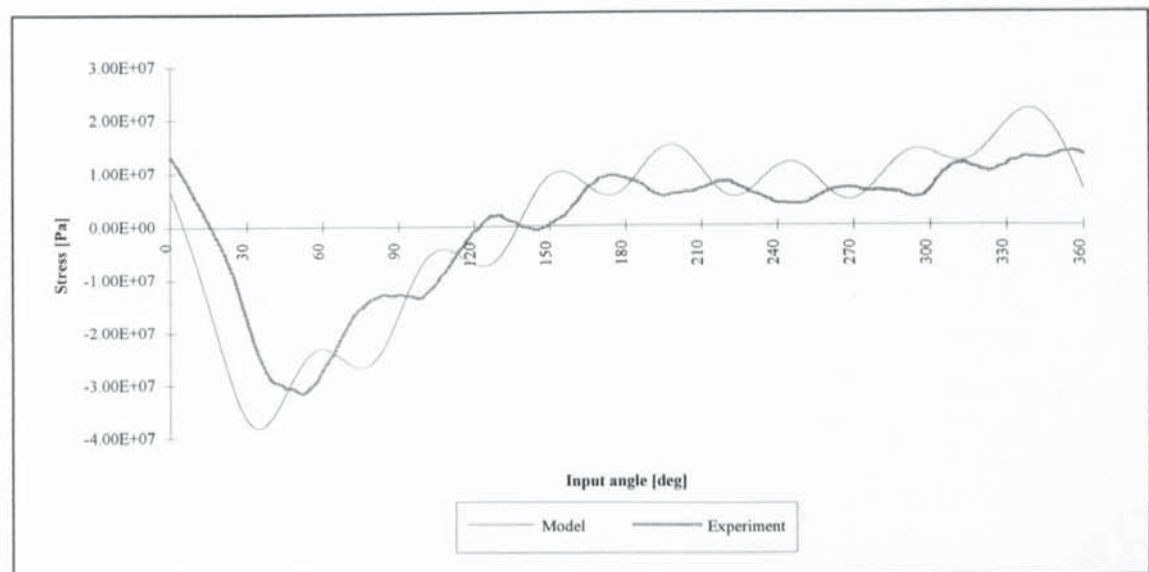


Fig. C.14.c: Stress at the follower midpoint for $\omega = 21.89$ rad/s

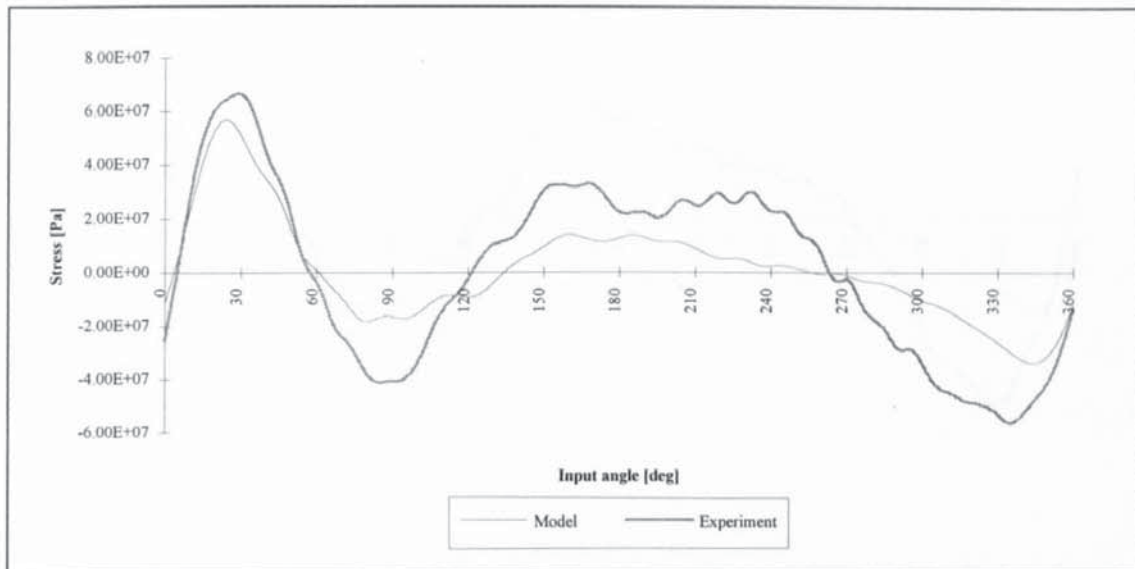


Fig. C.15.a: Stress at the input link midpoint for $\omega = 22.52$ rad/s

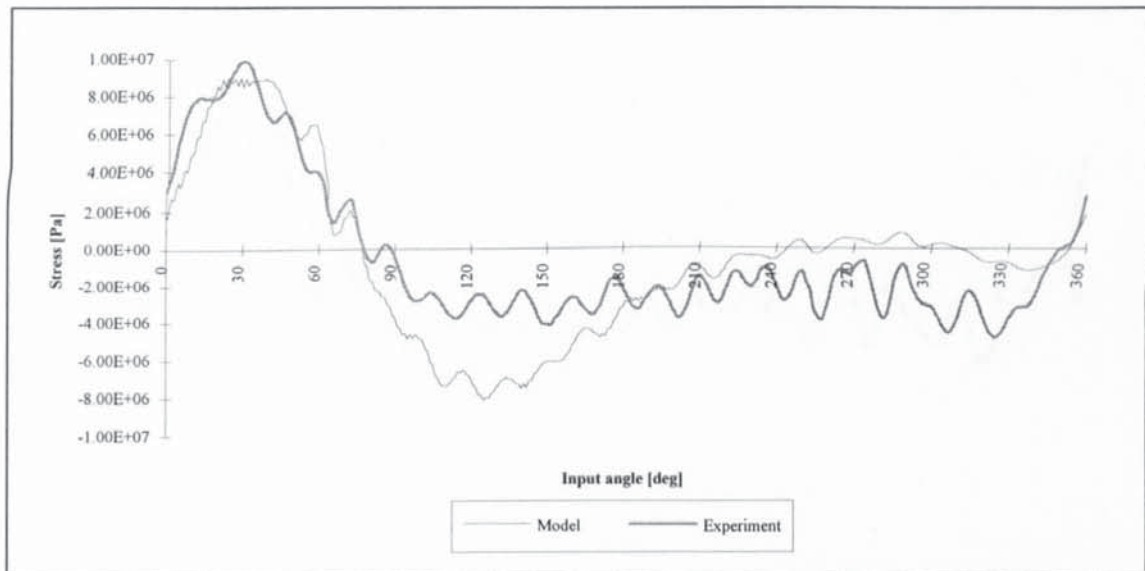


Fig. C.15.b: Stress at the coupler midpoint for $\omega = 22.52$ rad/s

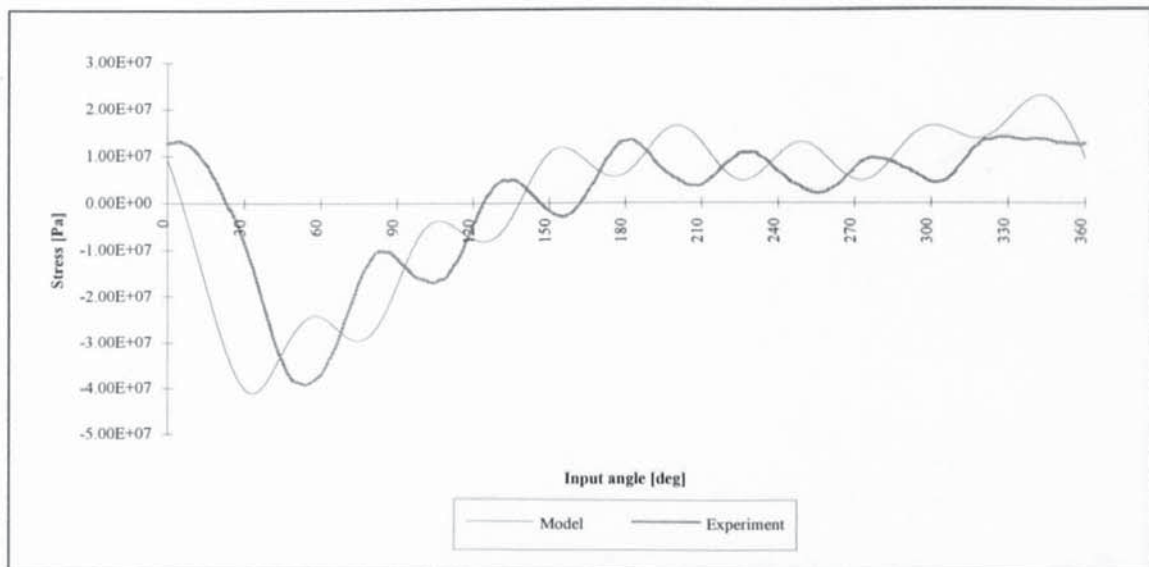


Fig. C.15.c: Stress at the follower midpoint for $\omega = 22.52$ rad/s

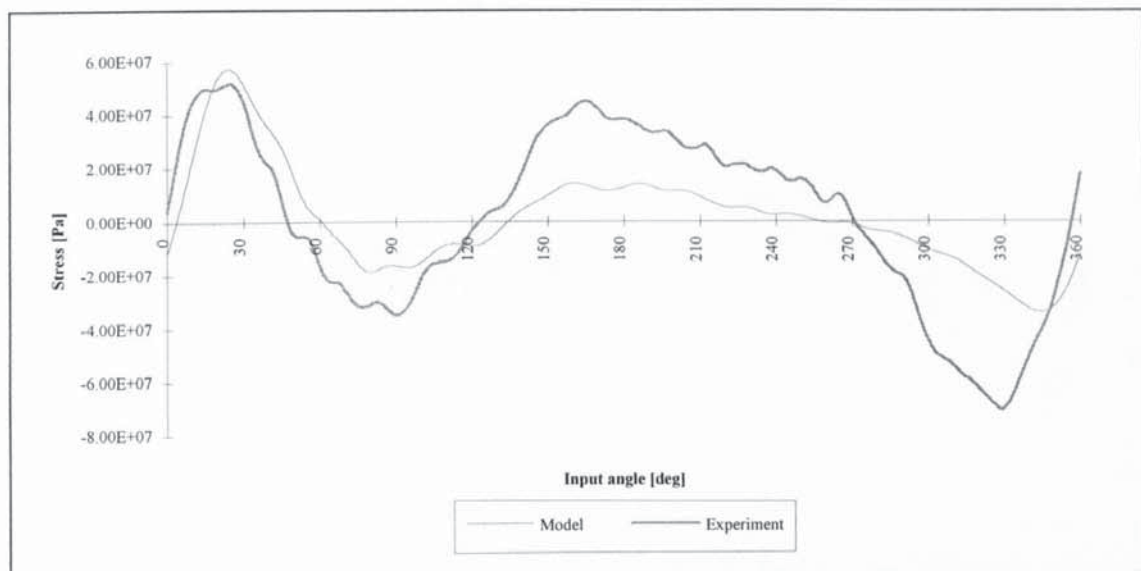


Fig. C.16.a: Stress at the input link midpoint for $\omega = 22.60$ rad/s

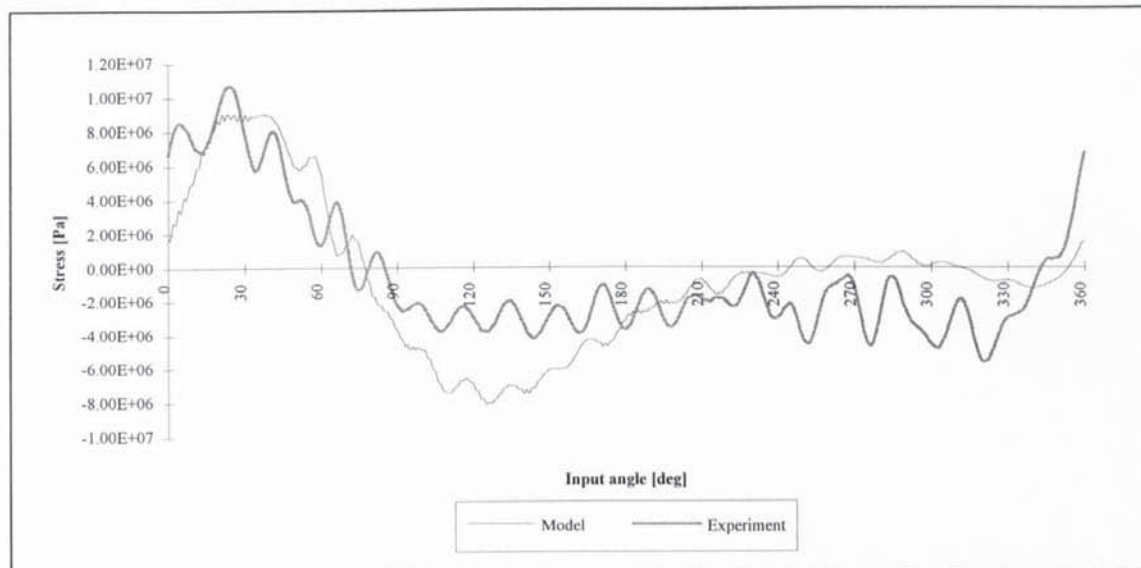


Fig. C.16.b: Stress at the coupler midpoint for $\omega = 22.60$ rad/s

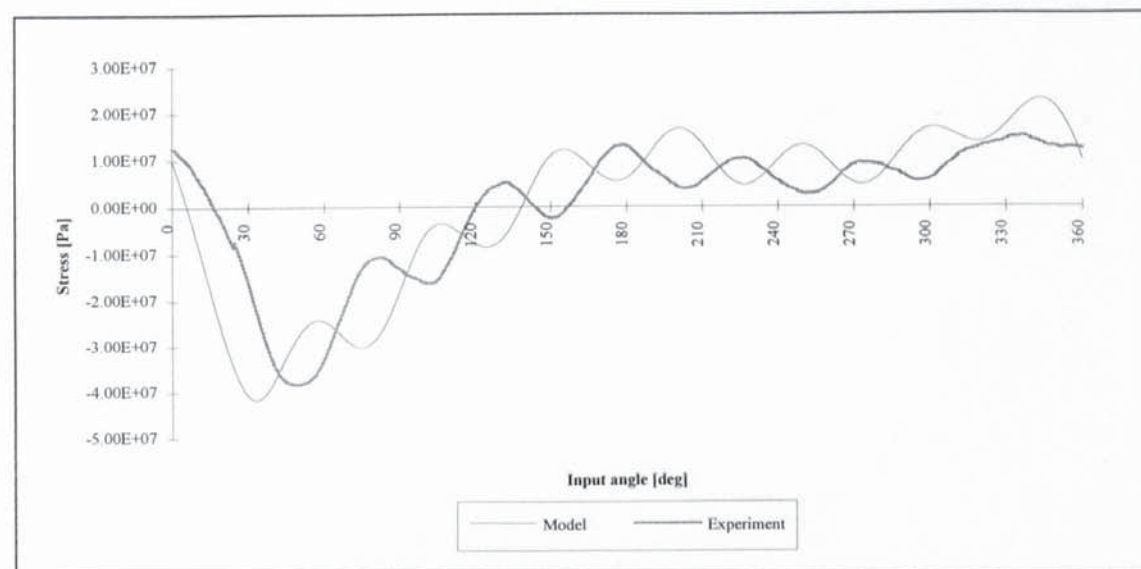


Fig. C.16.c: Stress at the follower midpoint for $\omega = 22.60$ rad/s

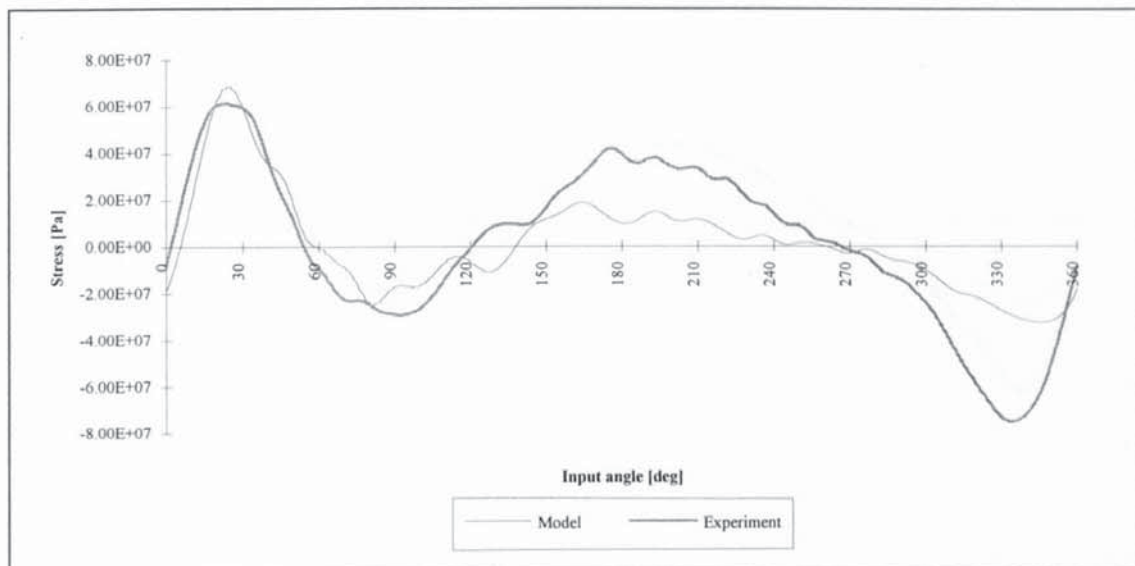


Fig. C.17.a: Stress at the input link midpoint for $\omega = 23.44$ rad/s

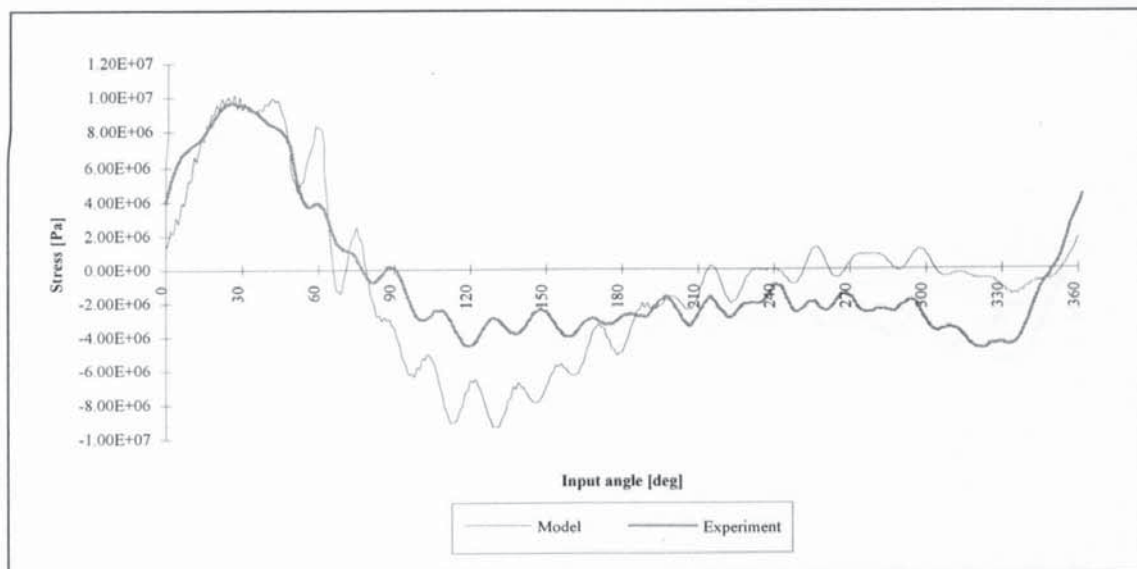


Fig. C.17.b: Stress at the coupler midpoint for $\omega = 23.44$ rad/s

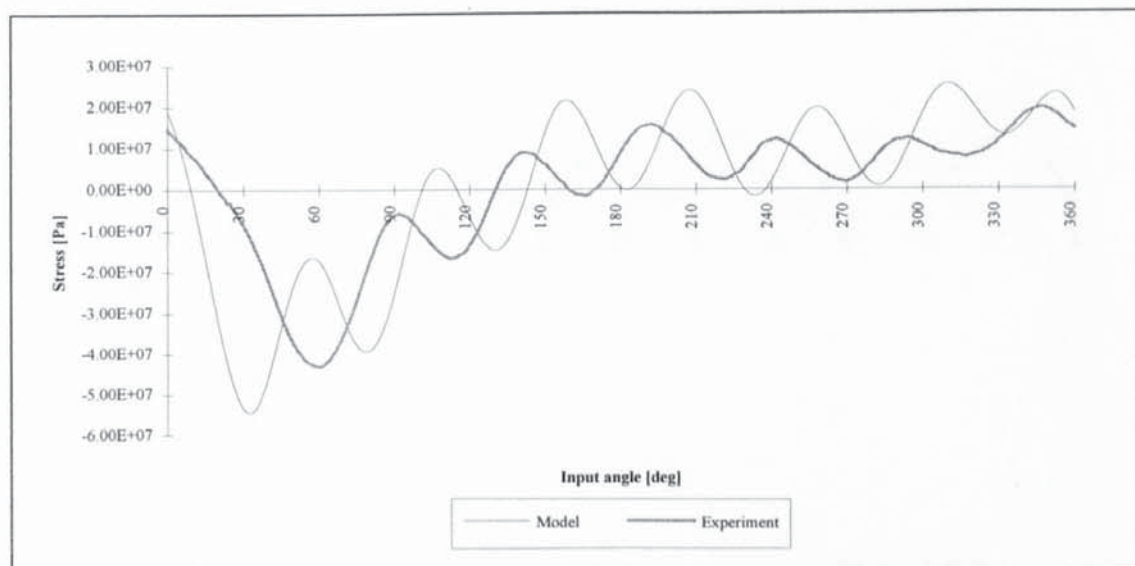


Fig. C.17.c: Stress at the follower midpoint for $\omega = 23.44$ rad/s

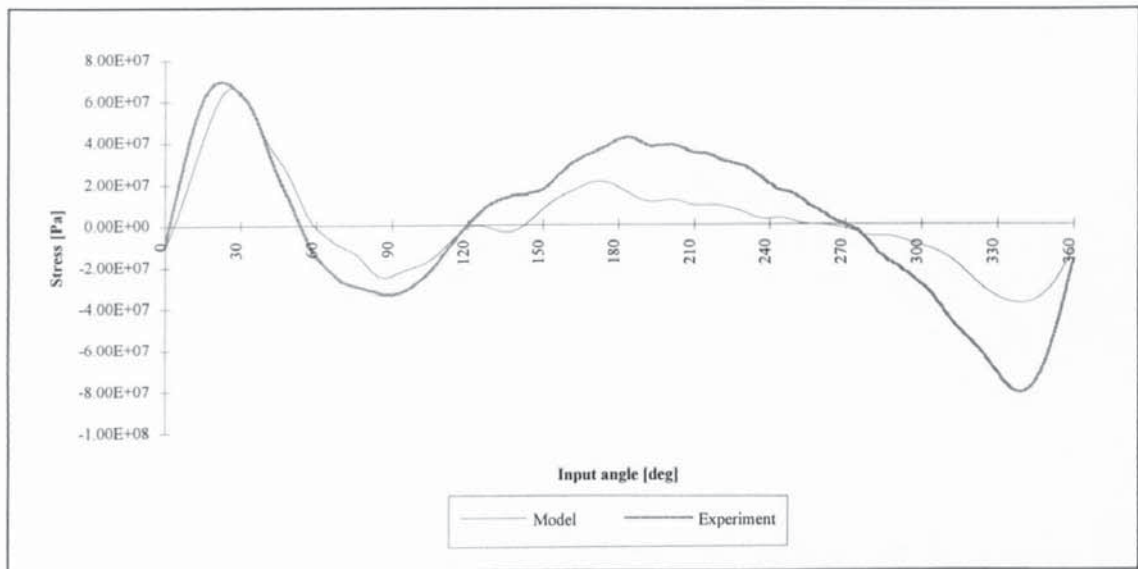


Fig. C.18.a: Stress at the input link midpoint for $\omega = 24.35$ rad/s

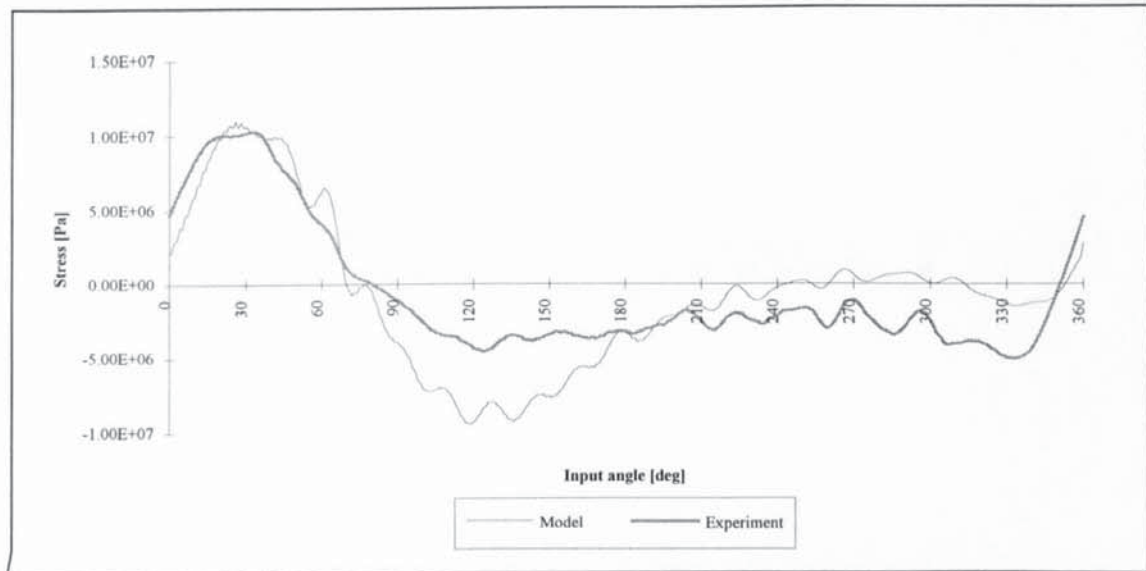


Fig. C.18.b: Stress at the coupler midpoint for $\omega = 24.35$ rad/s

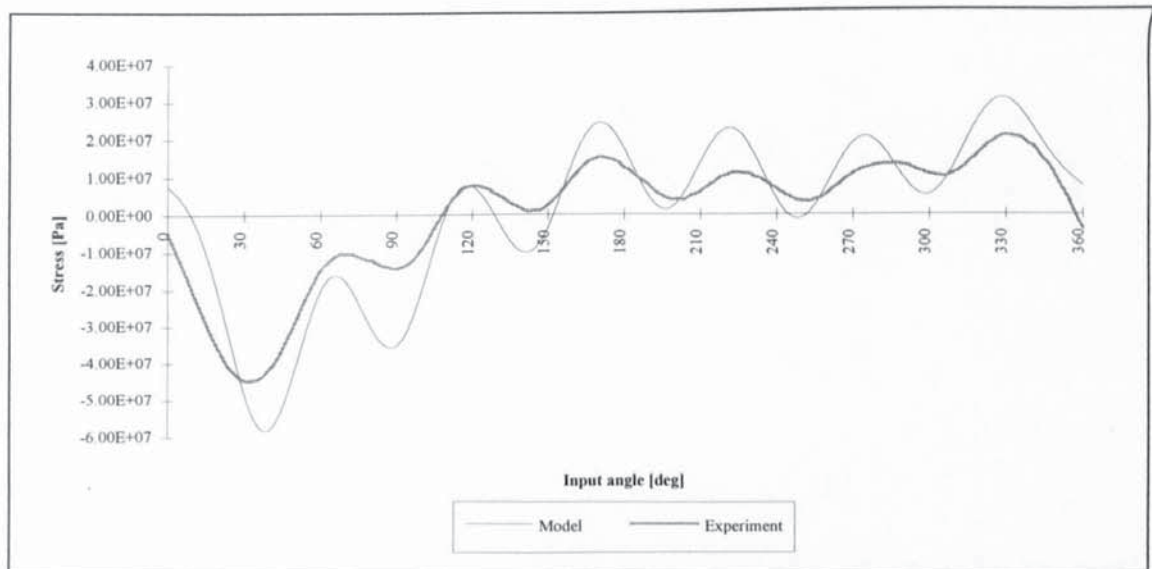


Fig. C.18.c: Stress at the follower midpoint for $\omega = 24.35$ rad/s

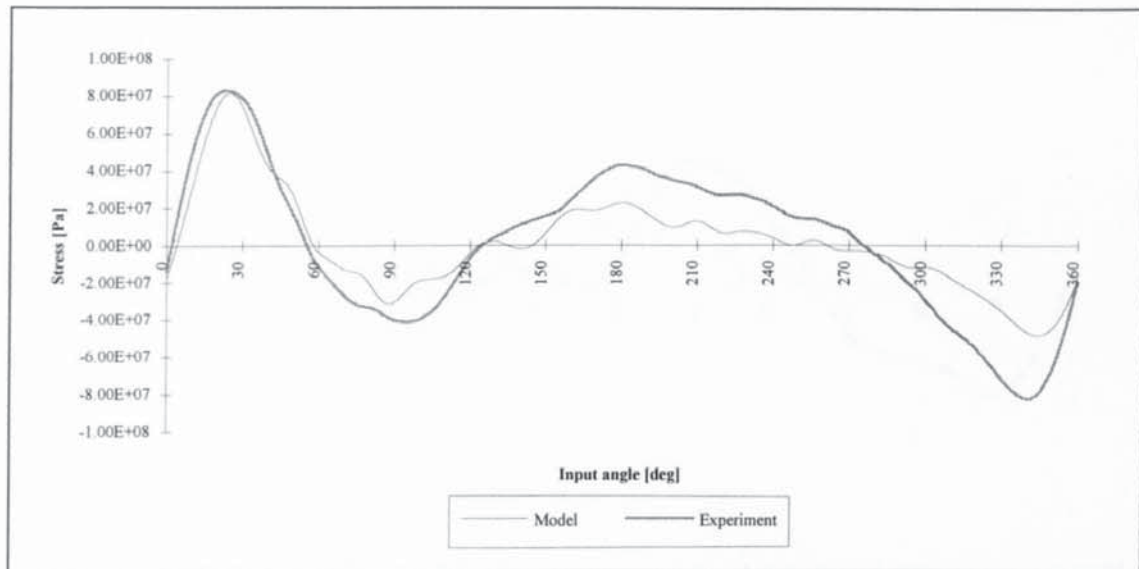


Fig. C.19.a: Stress at the input link midpoint for $\omega = 25.96$ rad/s

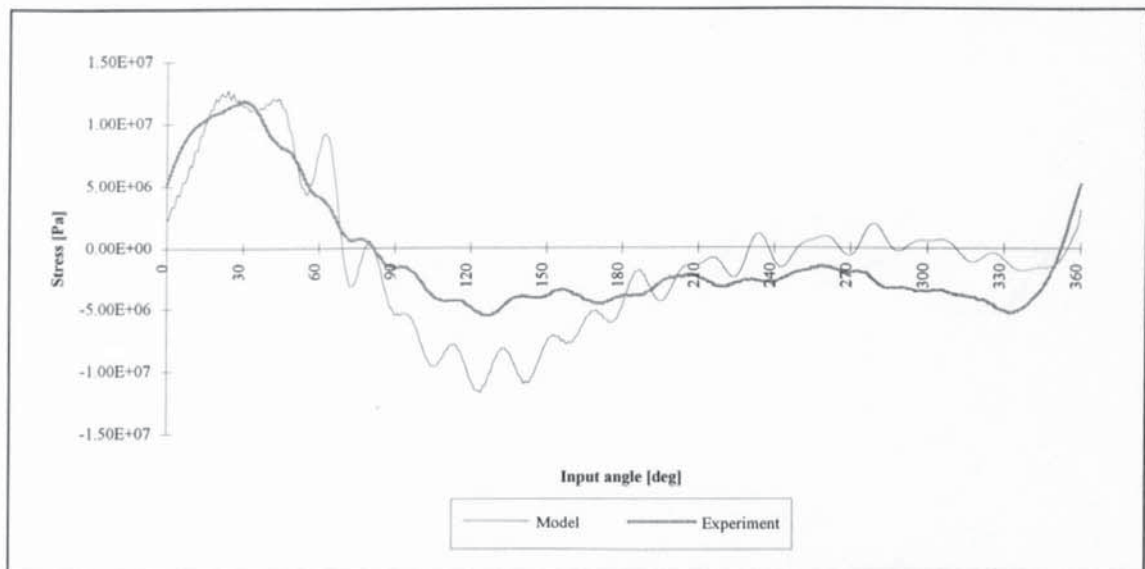


Fig. C.19.b: Stress at the coupler midpoint for $\omega = 25.96$ rad/s

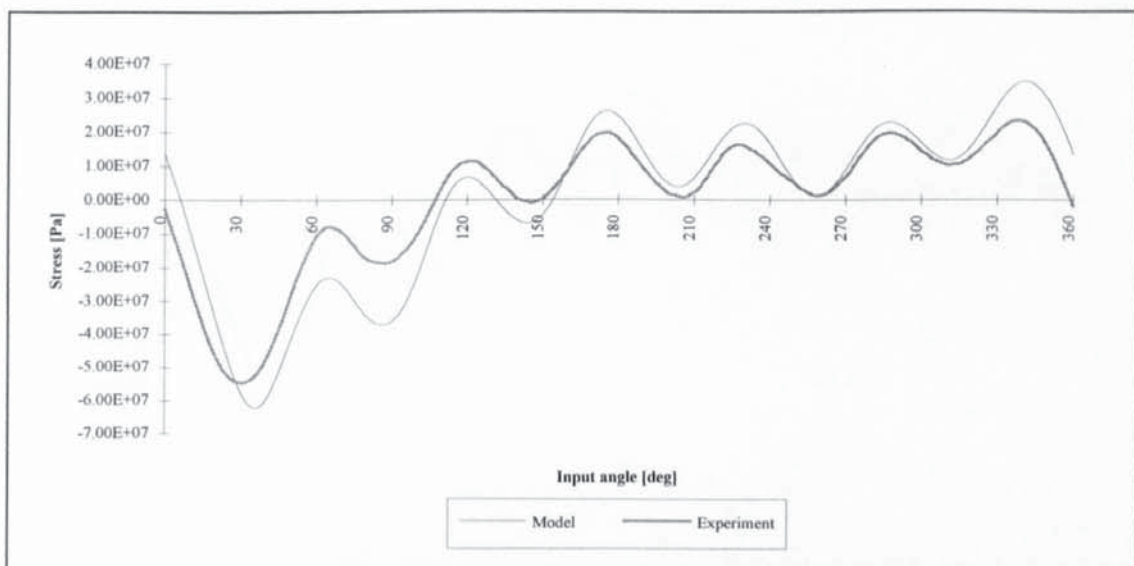


Fig. C.19.c: Stress at the follower midpoint for $\omega = 25.96$ rad/s

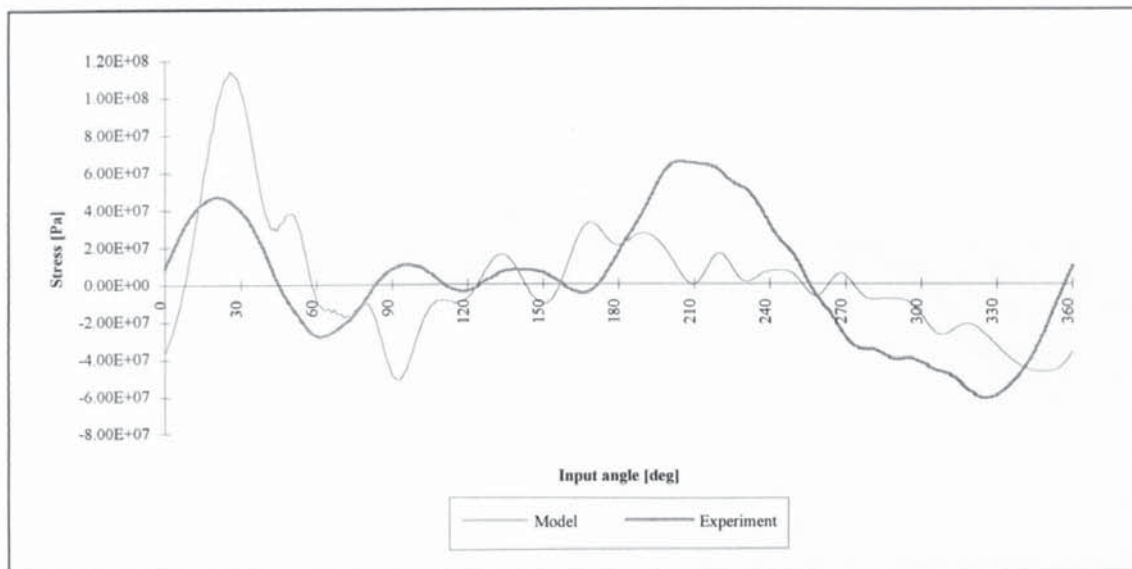


Fig. C.20.a: Stress at the input link midpoint for $\omega = 27.32$ rad/s

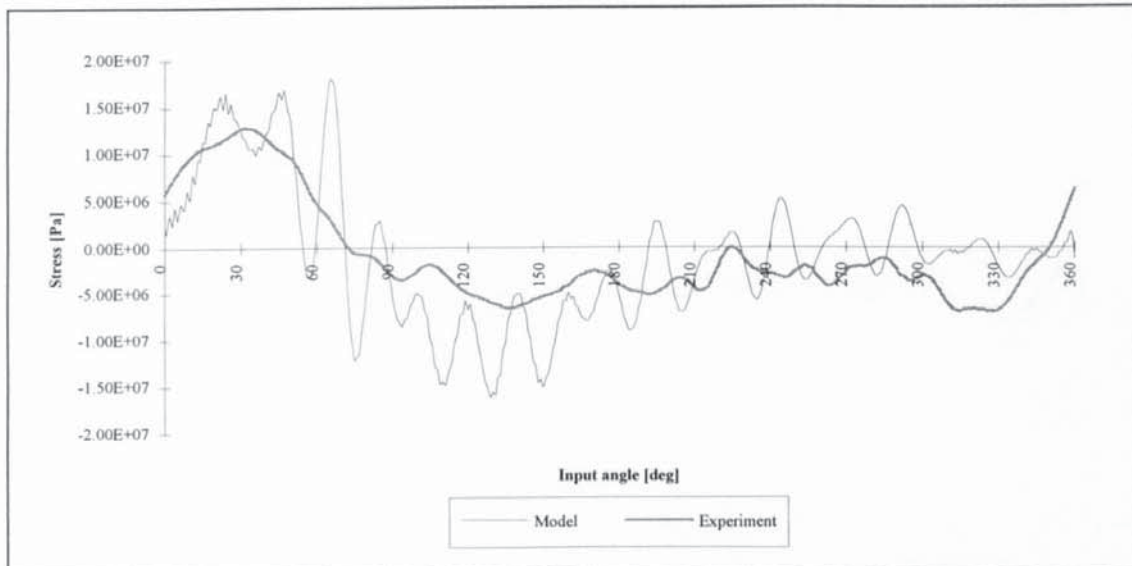


Fig. C.20.b: Stress at the coupler midpoint for $\omega = 27.32$ rad/s

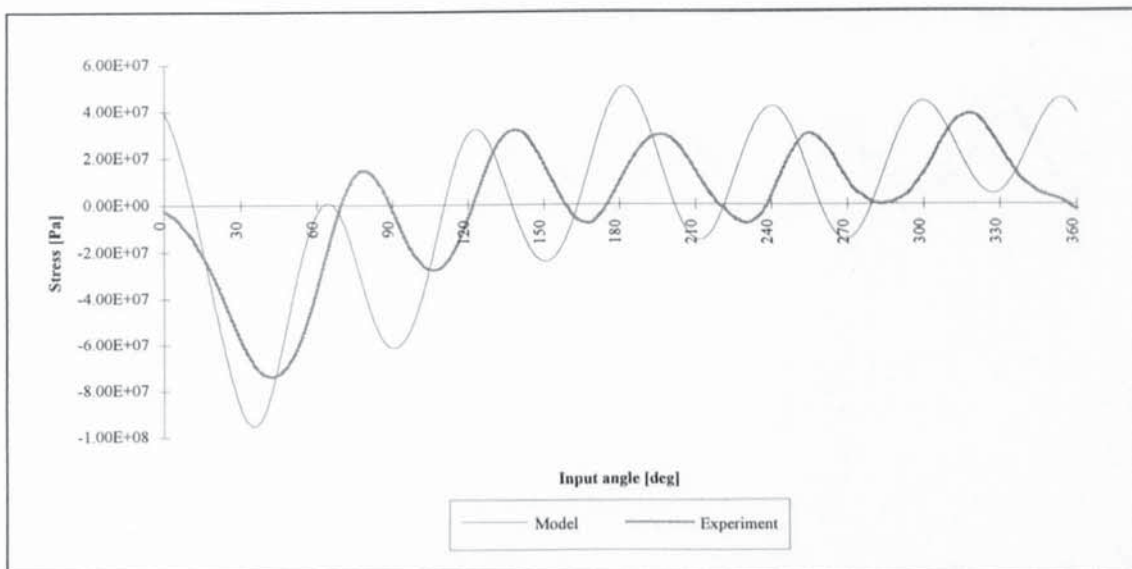


Fig. C.20.c: Stress at the follower midpoint for $\omega = 27.32$ rad/s

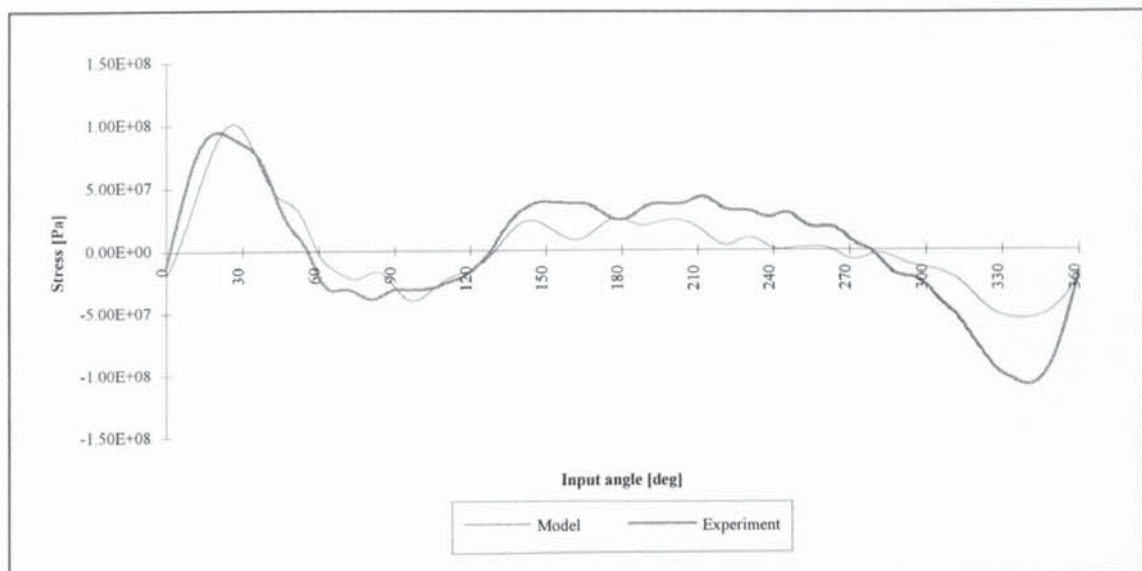


Fig. C.21.a: Stress at the input link midpoint for $\omega = 29.09$ rad/s

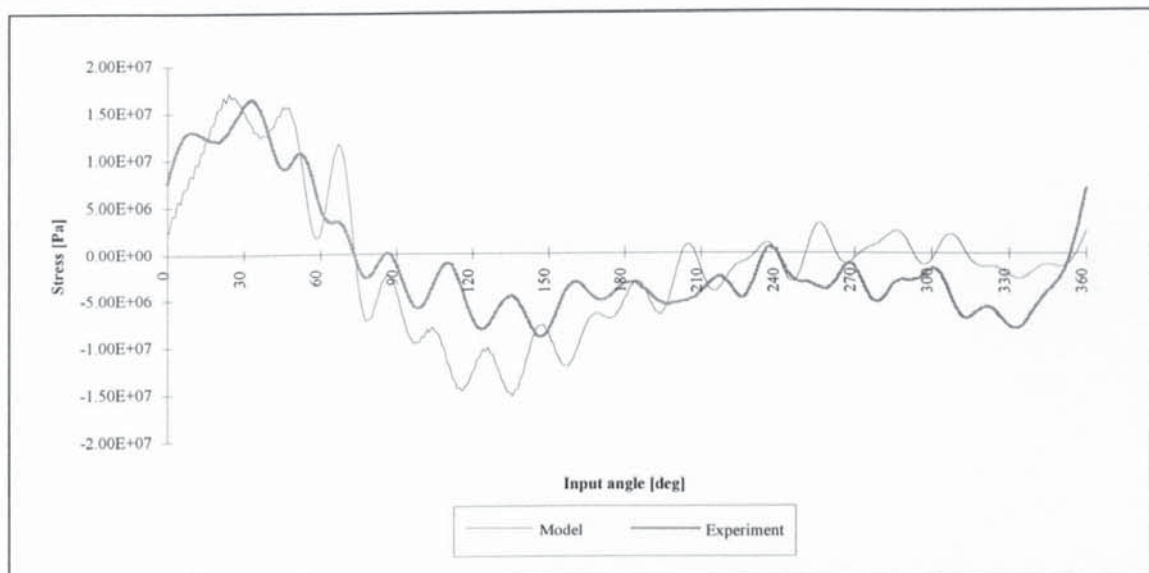


Fig. C.21.b: Stress at the coupler midpoint for $\omega = 29.09$ rad/s

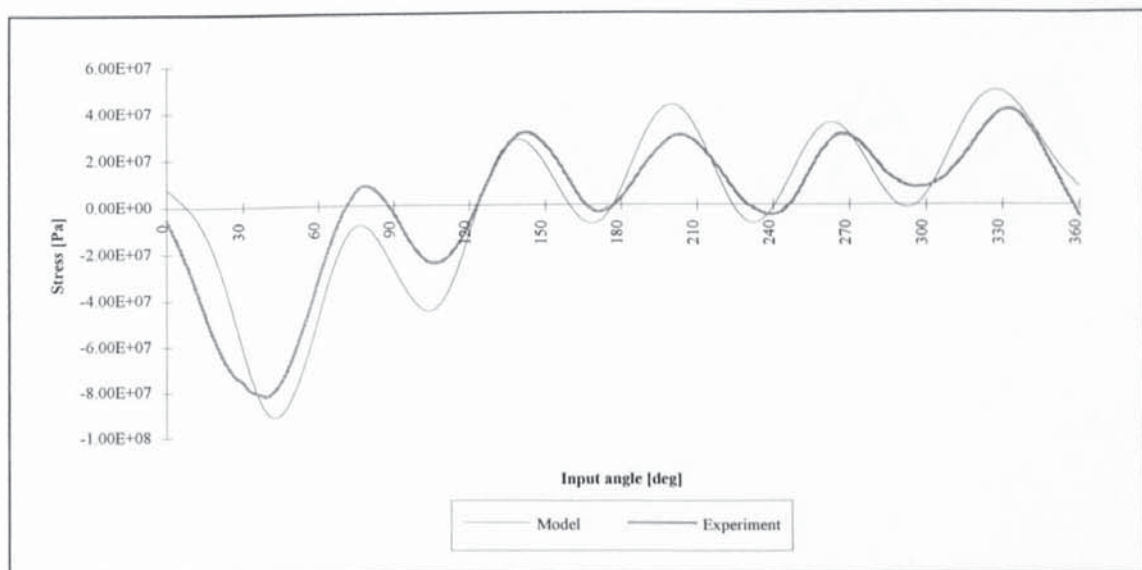


Fig. C.21.c: Stress at the follower midpoint for $\omega = 29.09$ rad/s

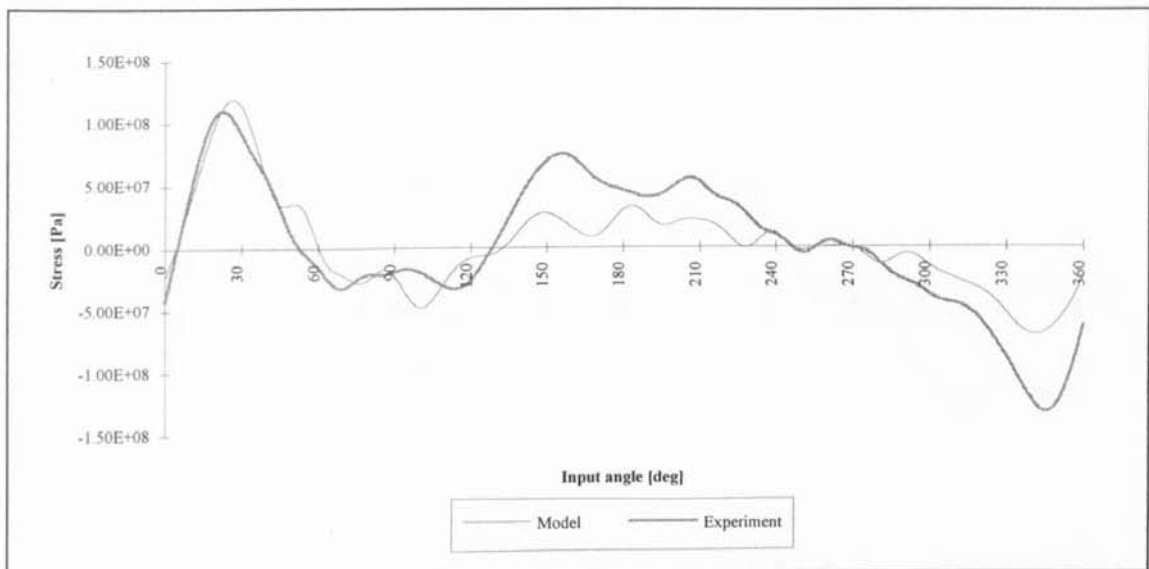


Fig. C.22.a: Stress at the input link midpoint for $\omega = 30.21$ rad/s

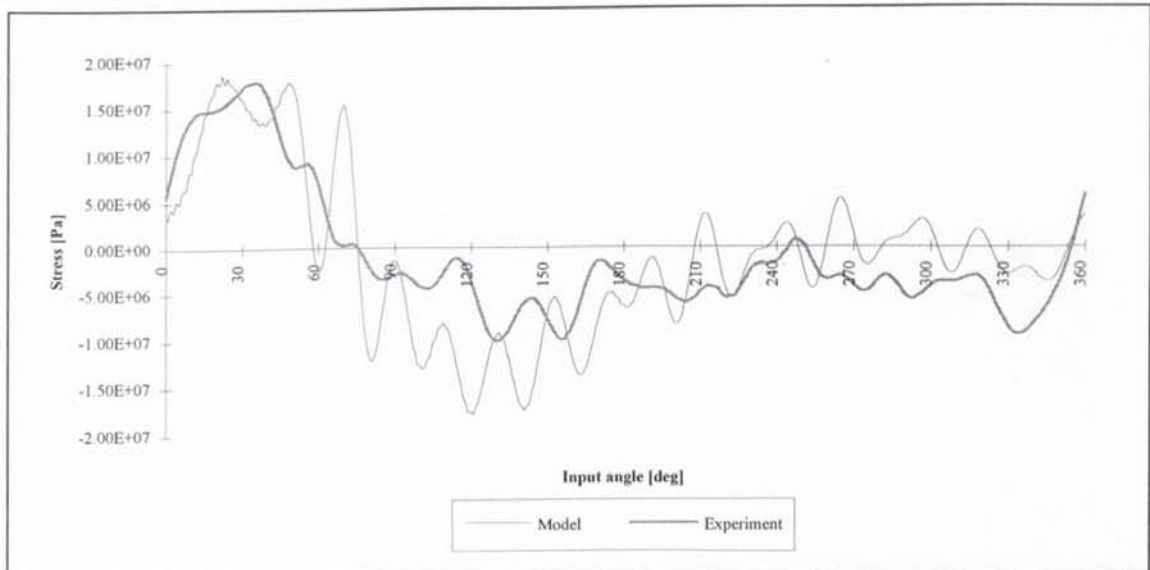


Fig. C.22.b: Stress at the coupler midpoint for $\omega = 30.21$ rad/s

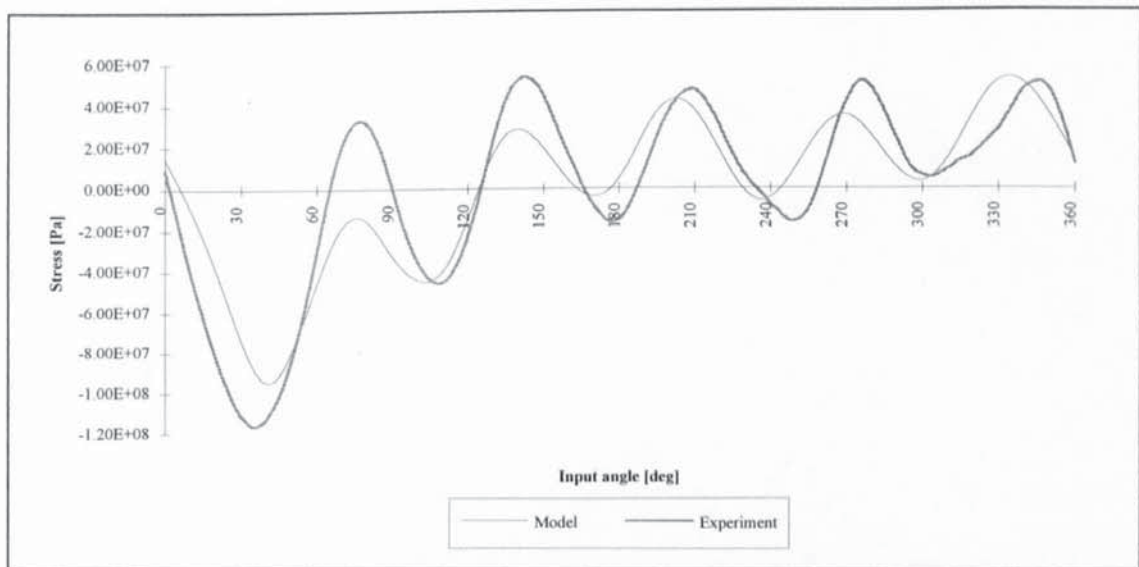


Fig. C.22.c: Stress at the follower midpoint for $\omega = 30.21$ rad/s

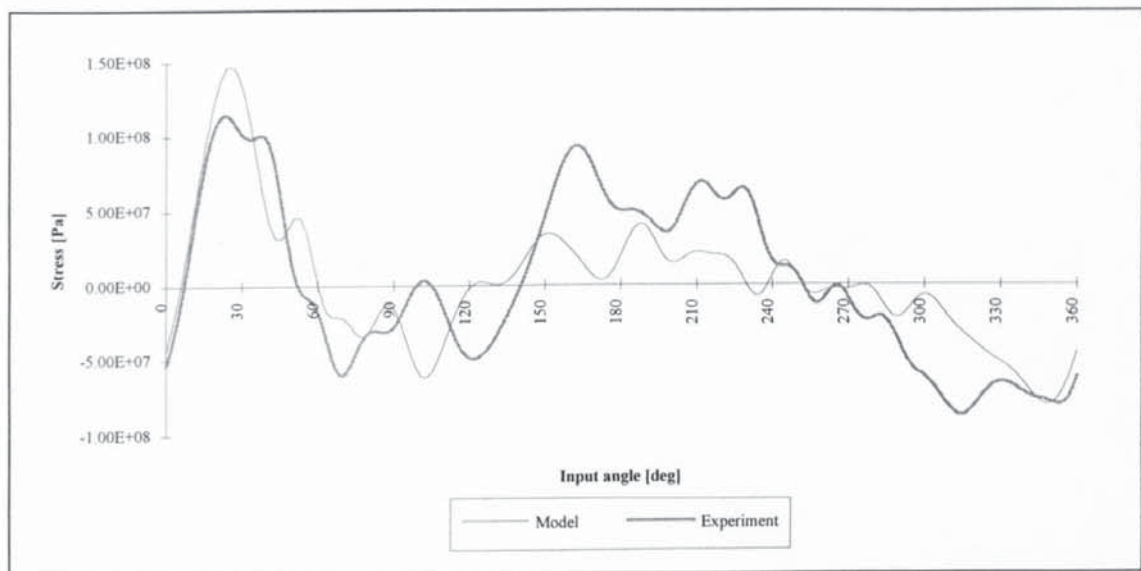


Fig. C.23.a: Stress at the input link midpoint for $\omega = 31.42$ rad/s

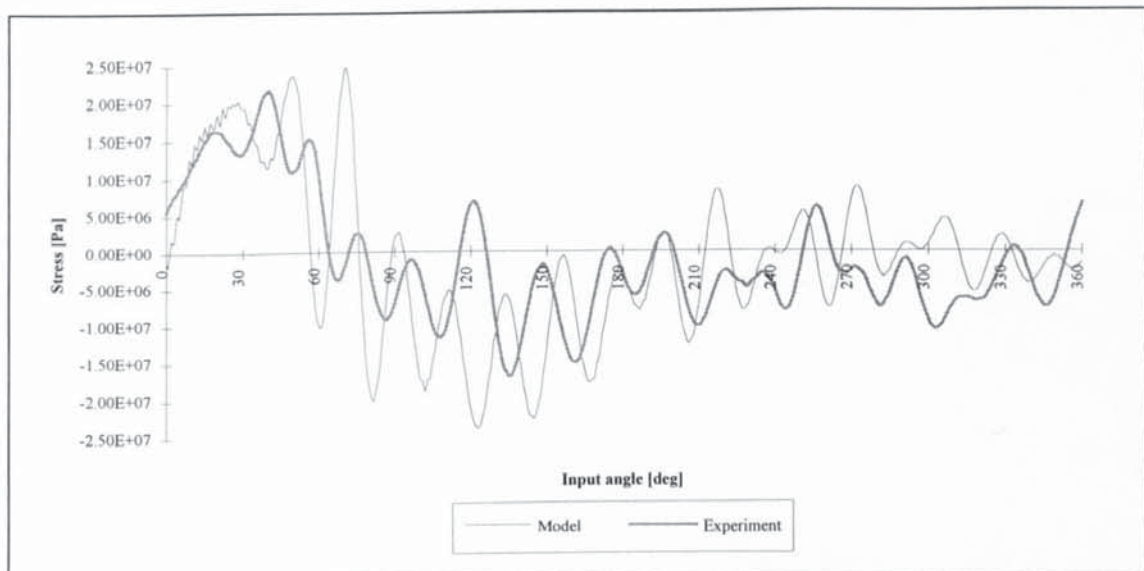


Fig. C.23.b: Stress at the coupler midpoint for $\omega = 31.42$ rad/s

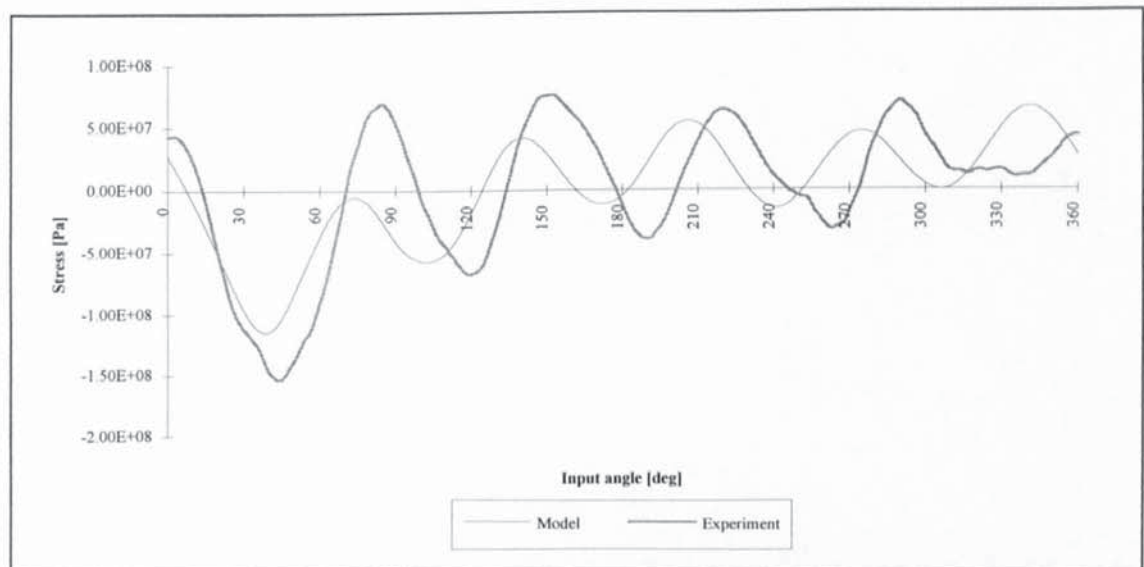


Fig. C.23.c: Stress at the follower midpoint for $\omega = 31.42$ rad/s

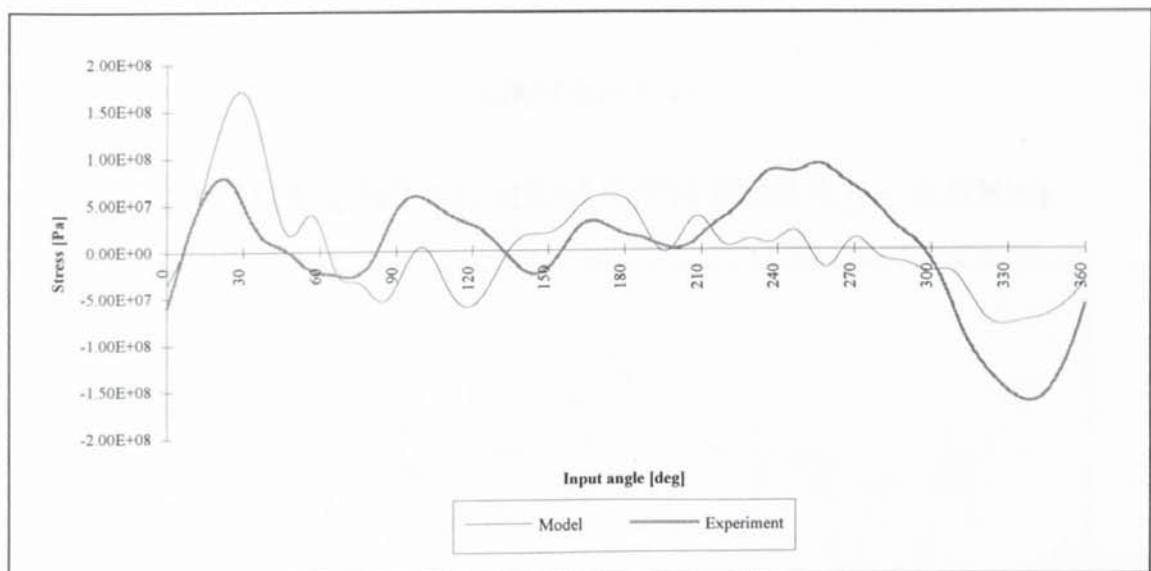


Fig. C.24.a: Stress at the input link midpoint for $\omega = 35.30$ rad/s

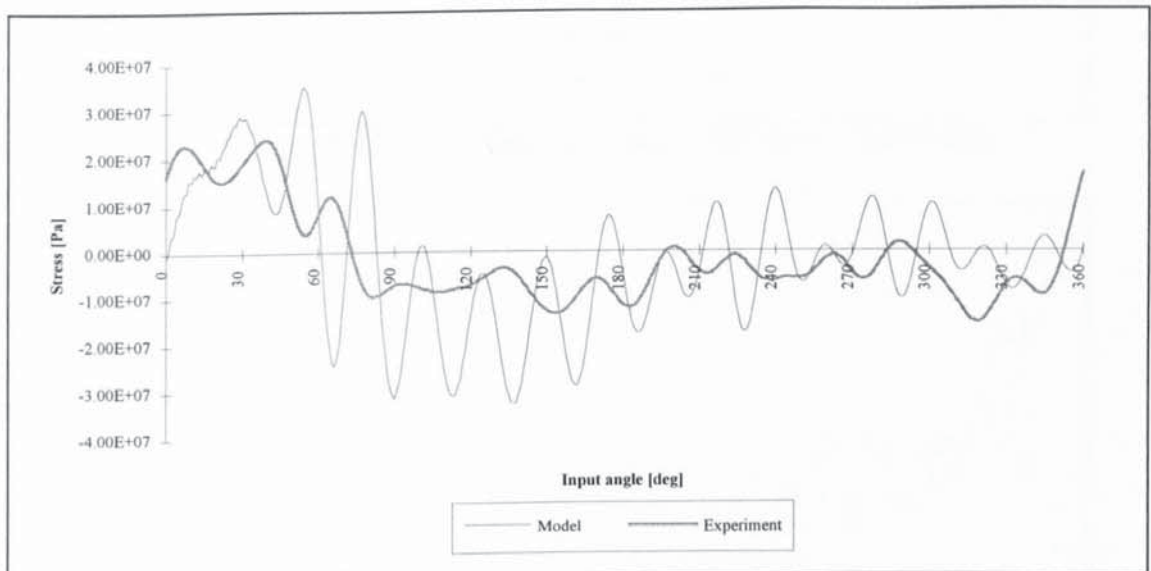


Fig. C.24.b: Stress at the coupler midpoint for $\omega = 35.30$ rad/s

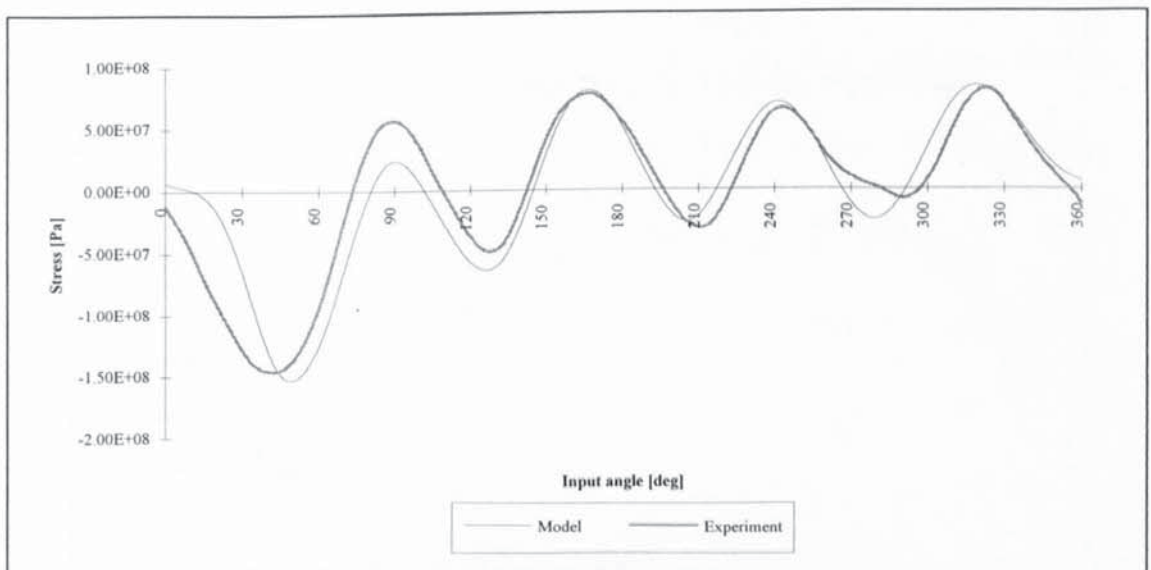


Fig. C.24.c: Stress at the follower midpoint for $\omega = 35.30$ rad/s

Appendix D

EXPERIMENTAL RESULTS FOR $L_2 = 0.636\text{m}$

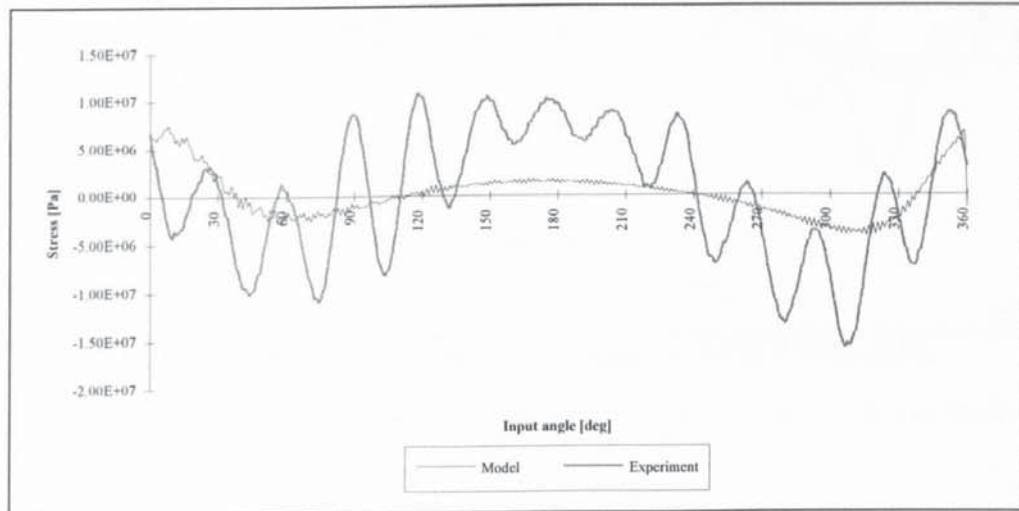


Fig. D.1.a: Stress at the input link midpoint for $\omega = 6.84\text{ rad/s}$.

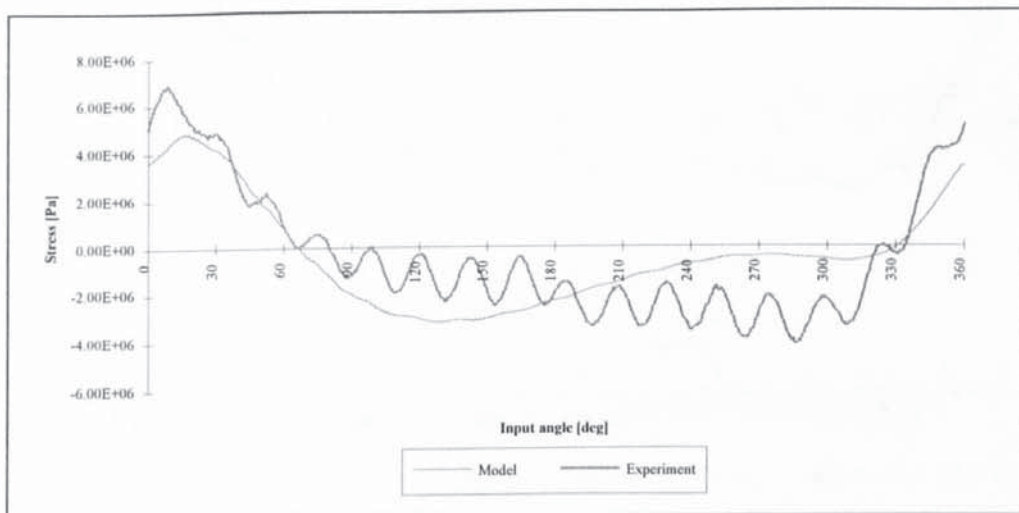


Fig. D.1.b: Stress at the coupler midpoint for $\omega = 6.84\text{ rad/s}$.

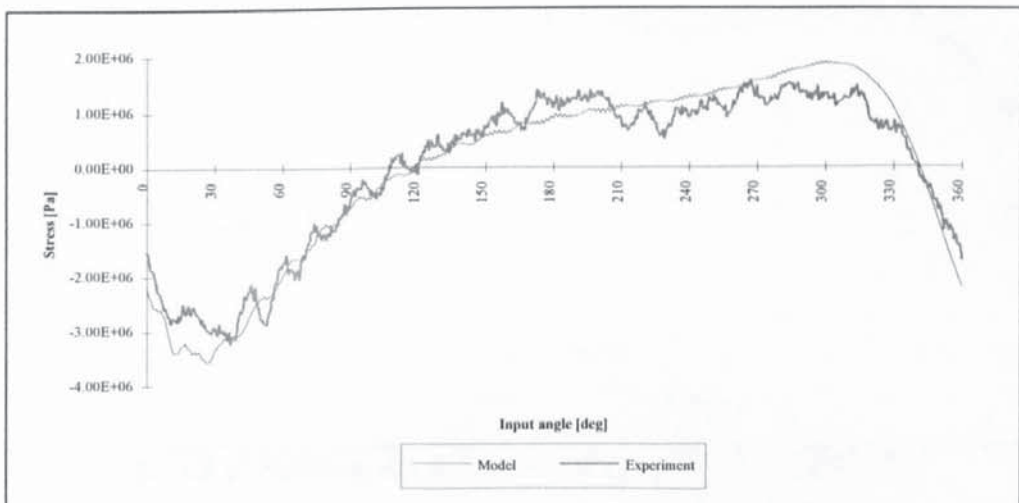


Fig. D.1.c: Stress at the follower midpoint for $\omega = 6.84\text{ rad/s}$.

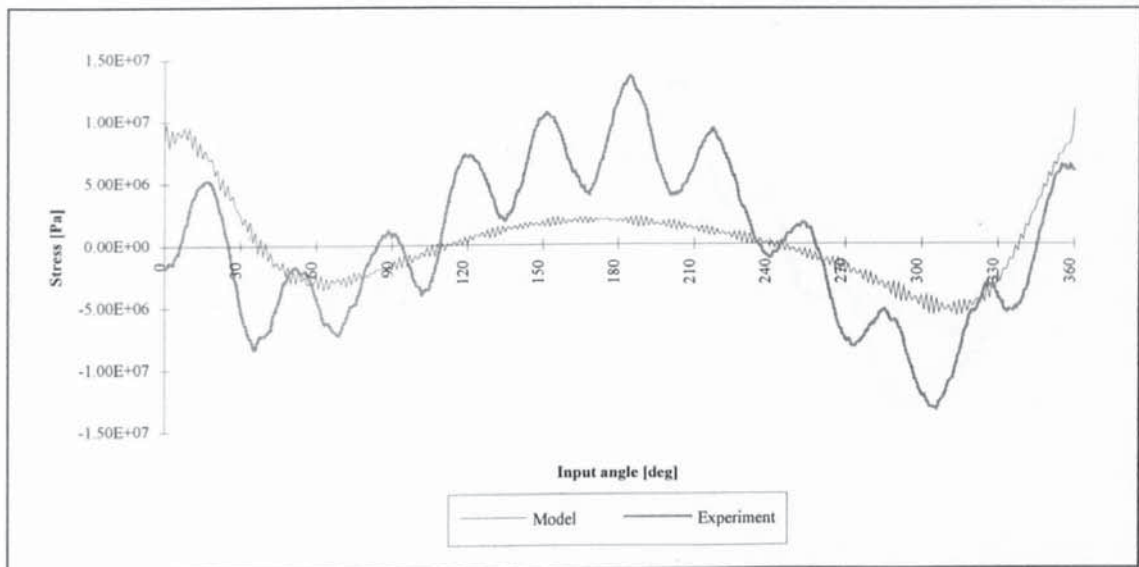


Fig. D.2.a: Stress at the input link midpoint for $\omega = 7.86$ rad/s.

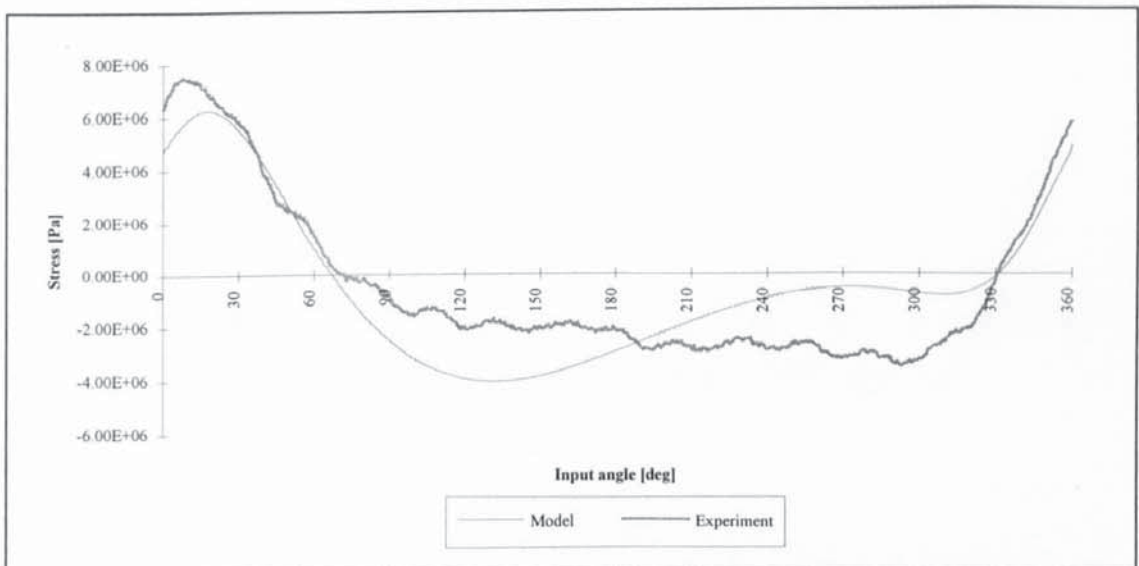


Fig. D.2.b: Stress at the coupler midpoint for $\omega = 7.86$ rad/s.

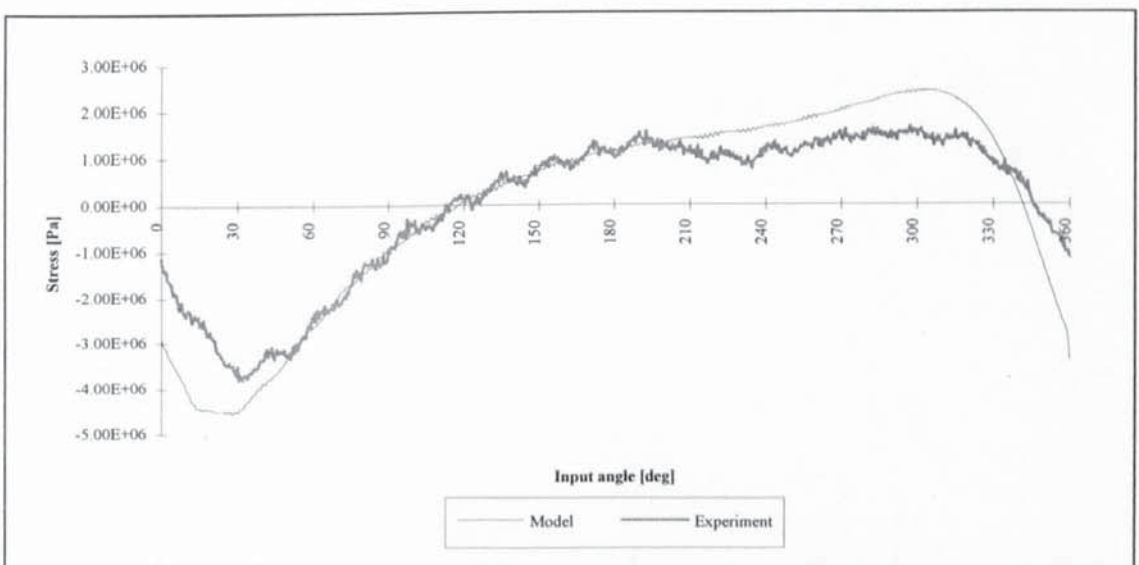


Fig. D.2.c: Stress at the follower midpoint for $\omega = 7.86$ rad/s.

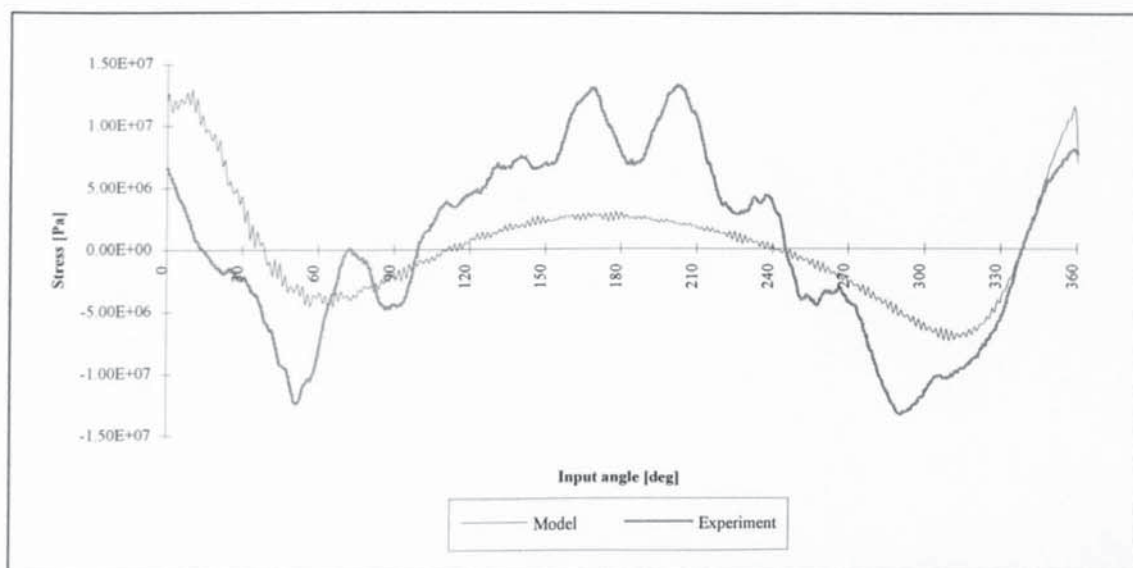


Fig. D.3.a: Stress at the input link midpoint for $\omega = 9.11$ rad/s.

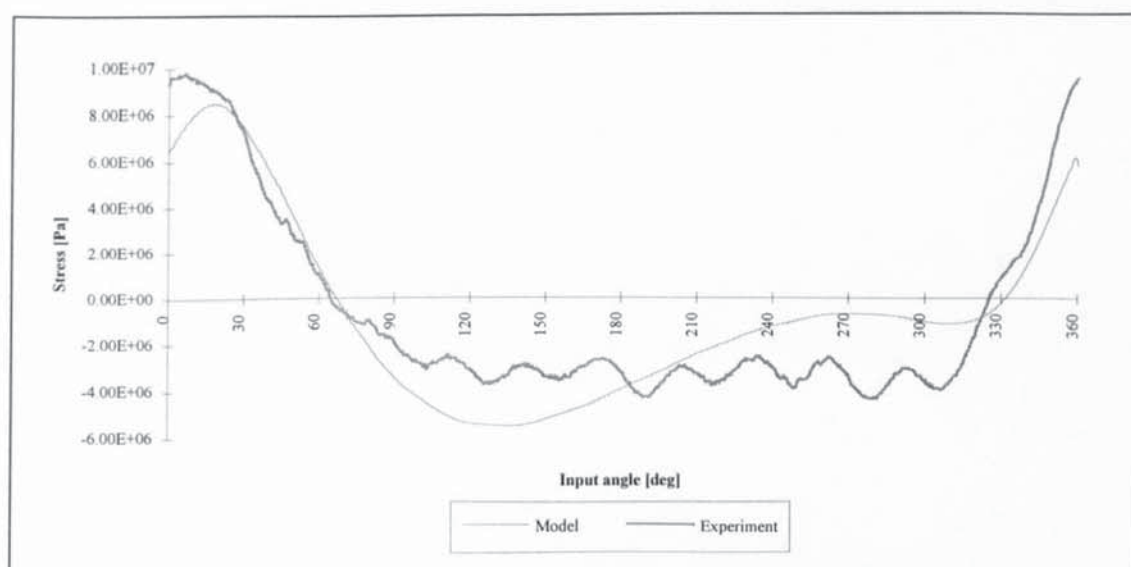


Fig. D.3.b: Stress at the coupler midpoint for $\omega = 9.11$ rad/s.

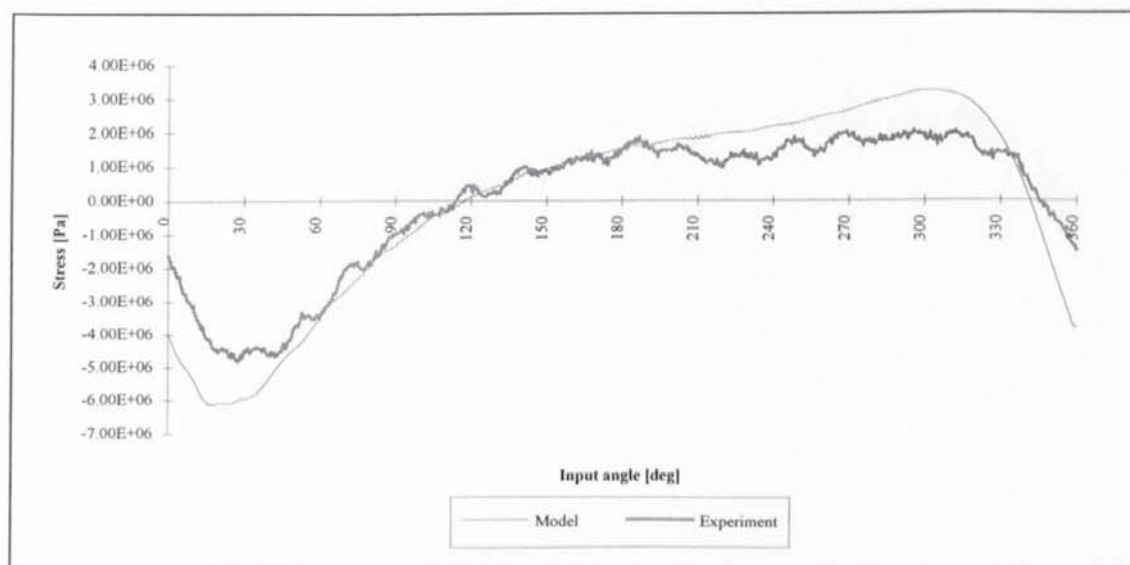


Fig. D.3.c: Stress at the follower midpoint for $\omega = 9.11$ rad/s.

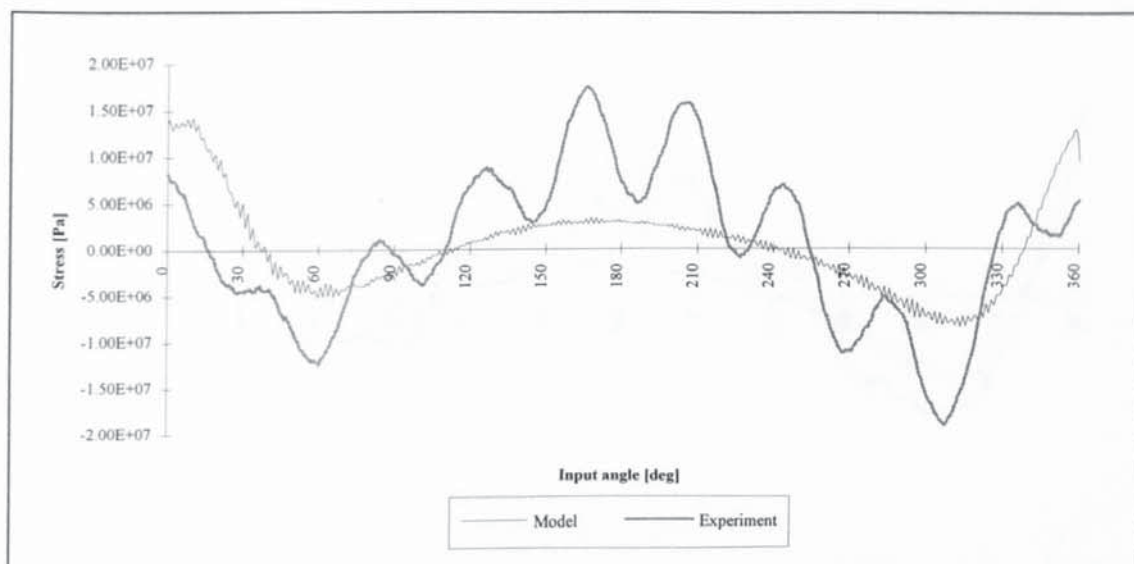


Fig. D.4.a: Stress at the input link midpoint for $\omega = 9.68$ rad/s.

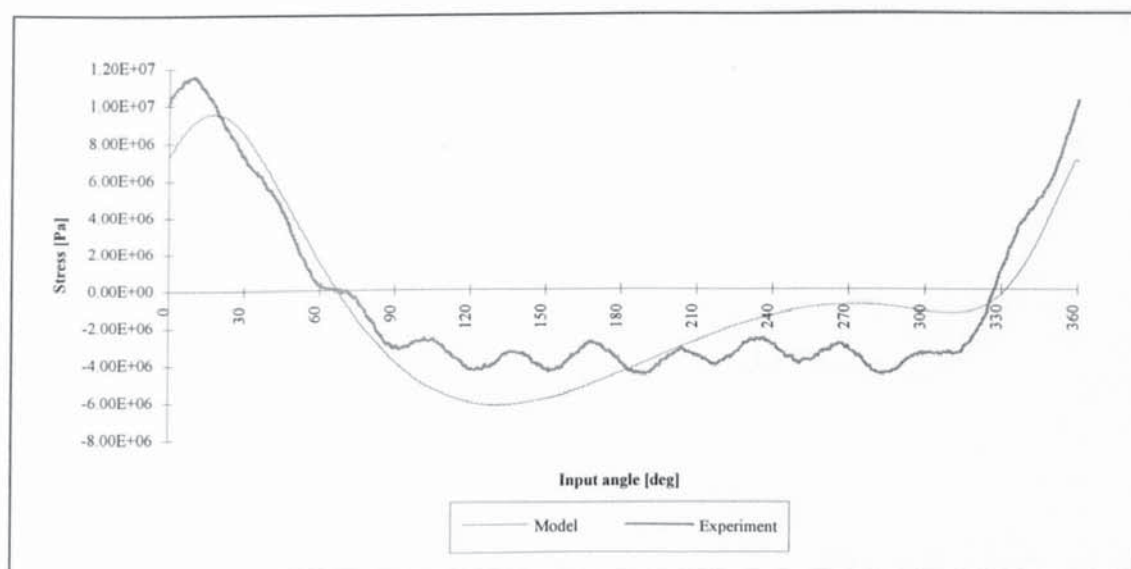


Fig. D.4.b: Stress at the coupler midpoint for $\omega = 9.68$ rad/s.

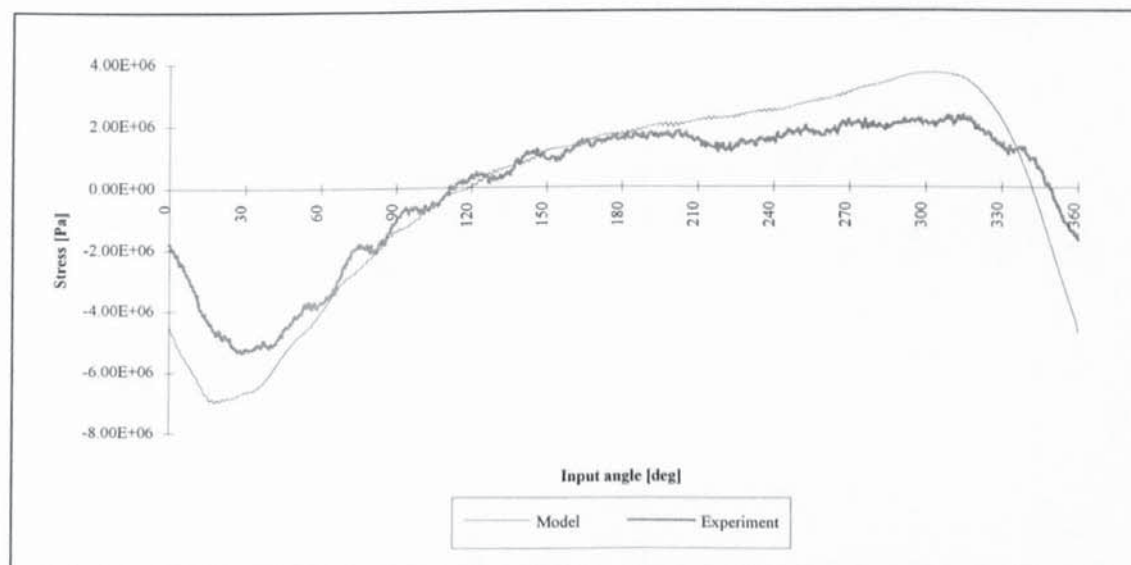


Fig. D.4.c: Stress at the follower midpoint for $\omega = 9.68$ rad/s.

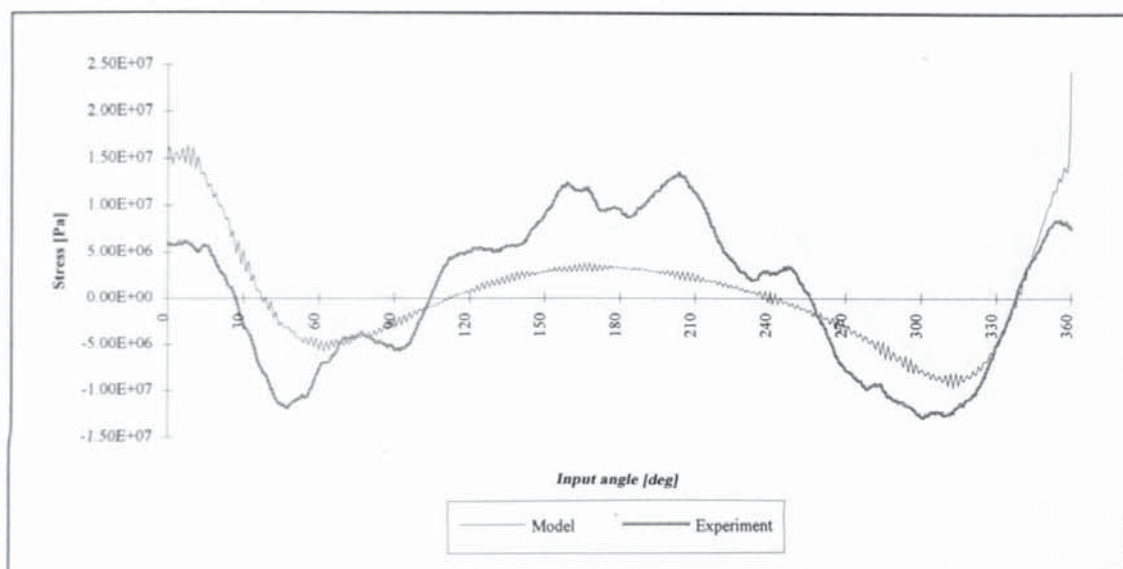


Fig. D.5.a: Stress at the input link midpoint for $\omega = 10.23$ rad/s.

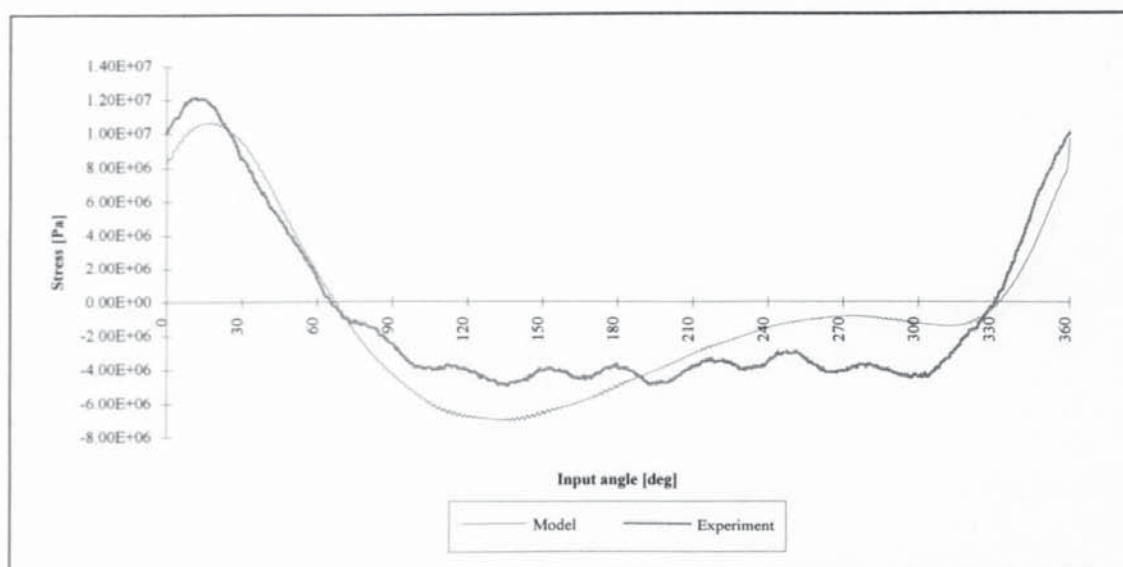


Fig. D.5.b: Stress at the coupler midpoint for $\omega = 10.23$ rad/s.

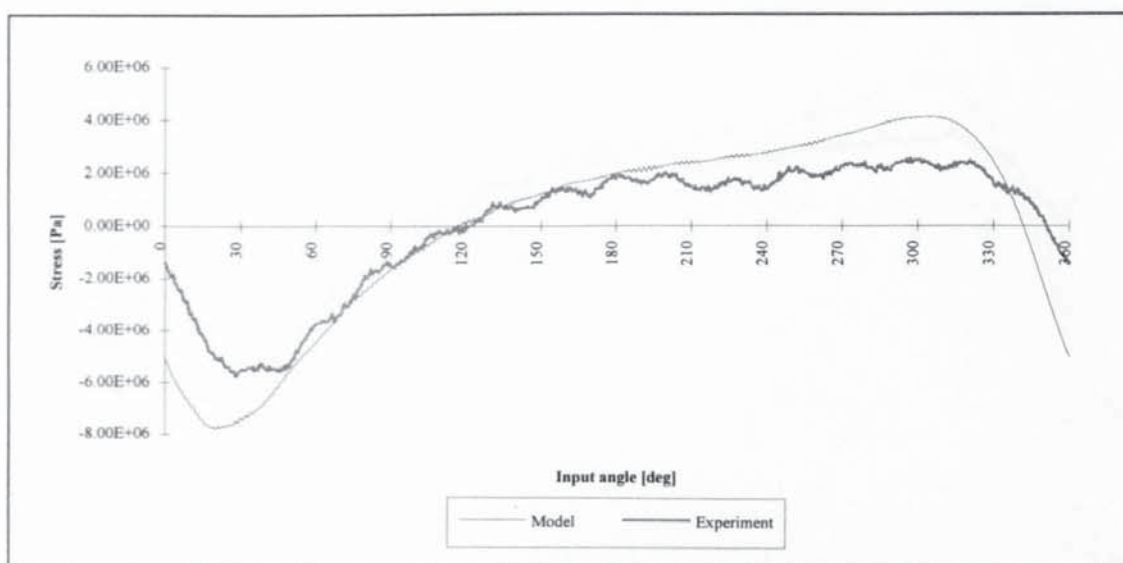


Fig. D.5.c: Stress at the follower midpoint for $\omega = 10.23$ rad/s.

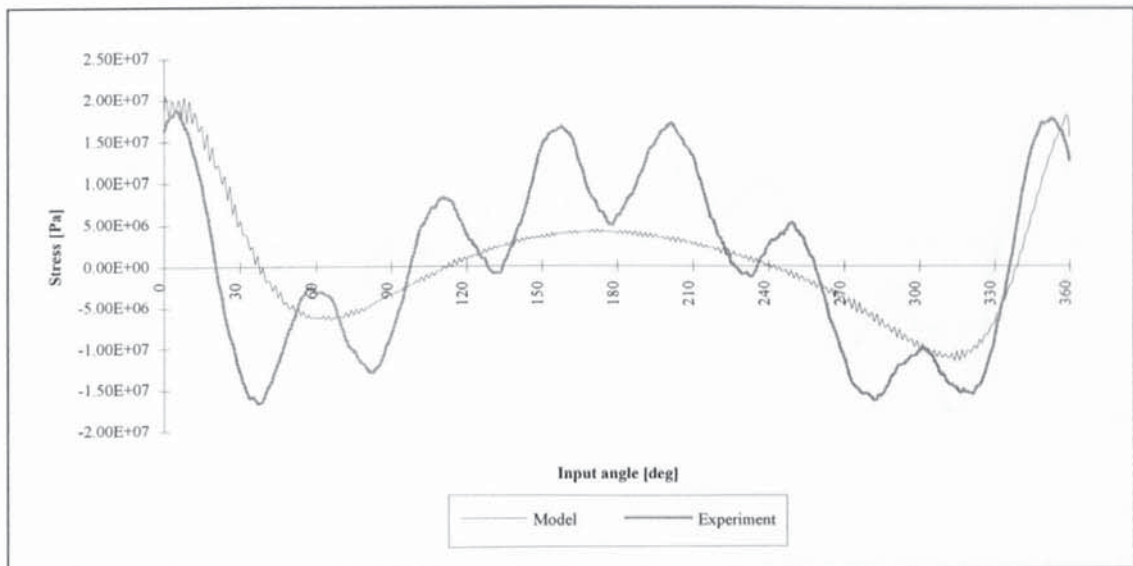


Fig. D.6.a: Stress at the input link midpoint for $\omega = 11.38$ rad/s.

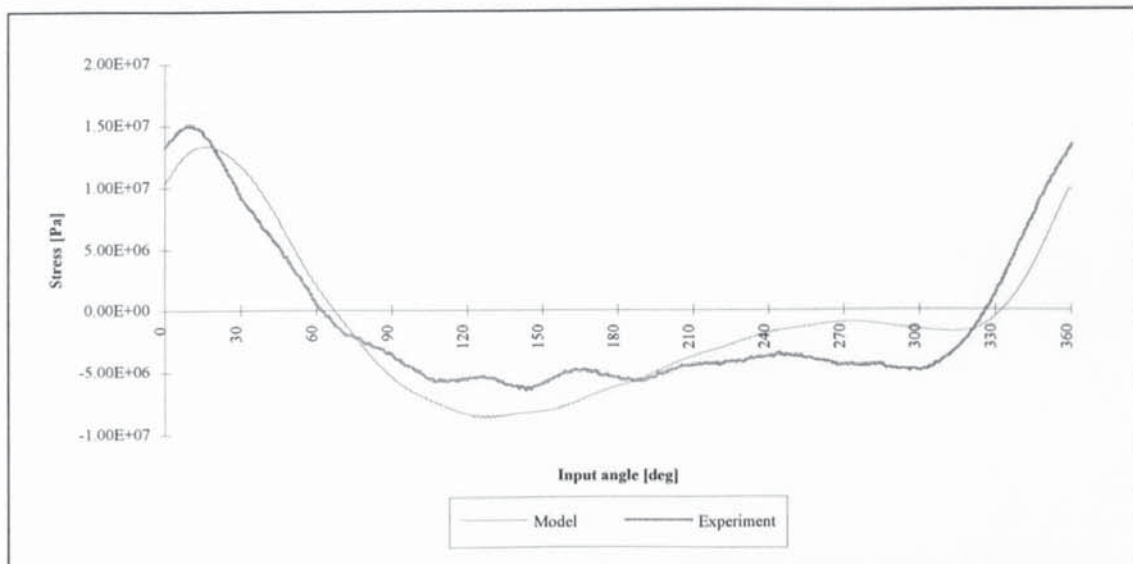


Fig. D.6.b: Stress at the coupler midpoint for $\omega = 11.38$ rad/s.

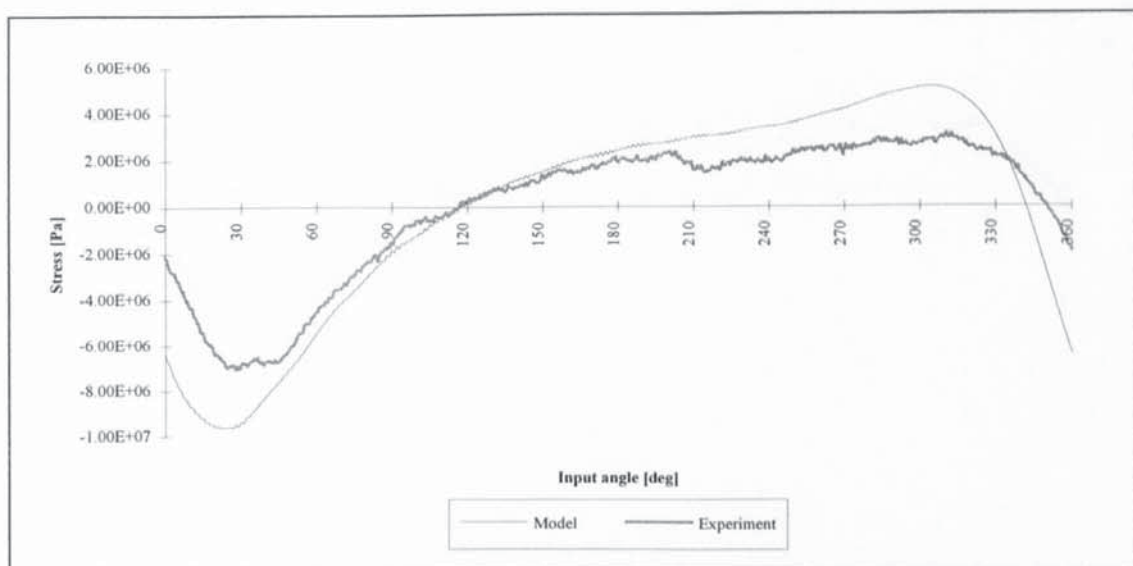


Fig. D.6.c: Stress at the follower midpoint for $\omega = 11.38$ rad/s.

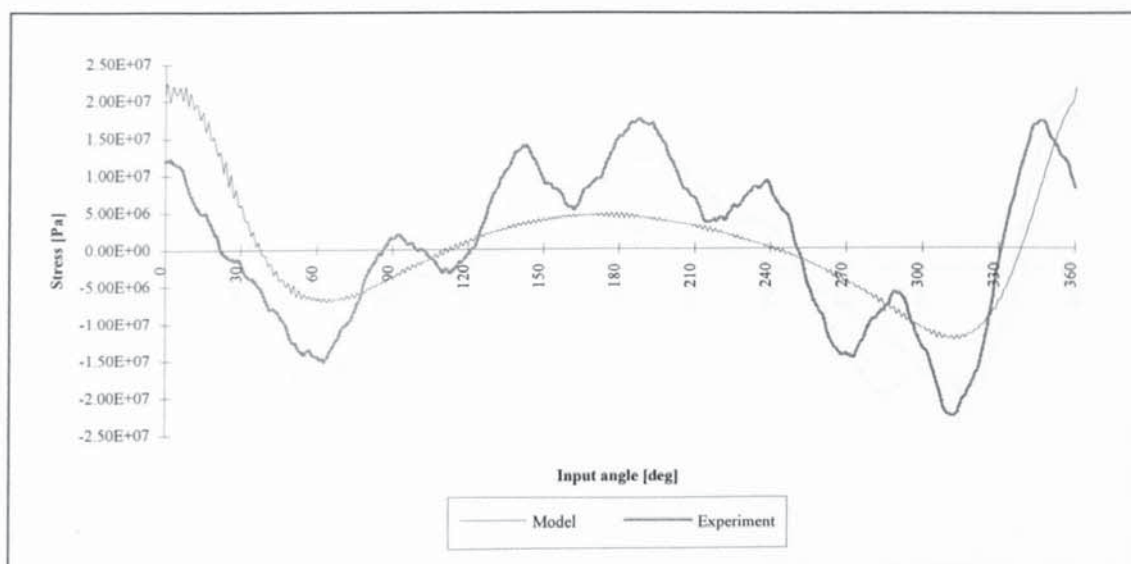


Fig. D.7.a: Stress at the input link midpoint for $\omega = 11.9$ rad/s.

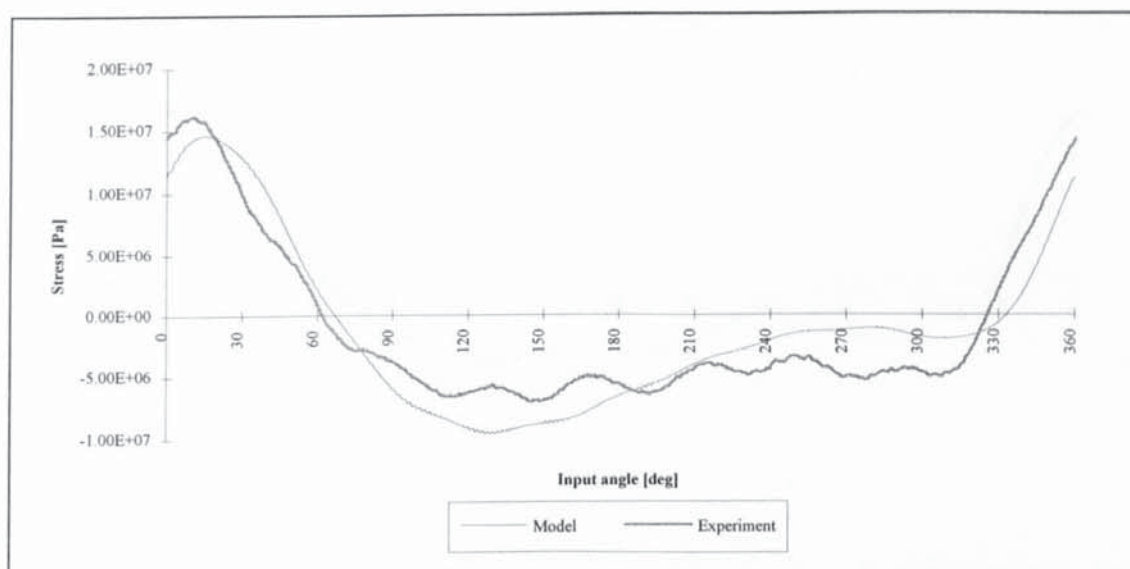


Fig. D.7.b: Stress at the coupler midpoint for $\omega = 11.9$ rad/s.

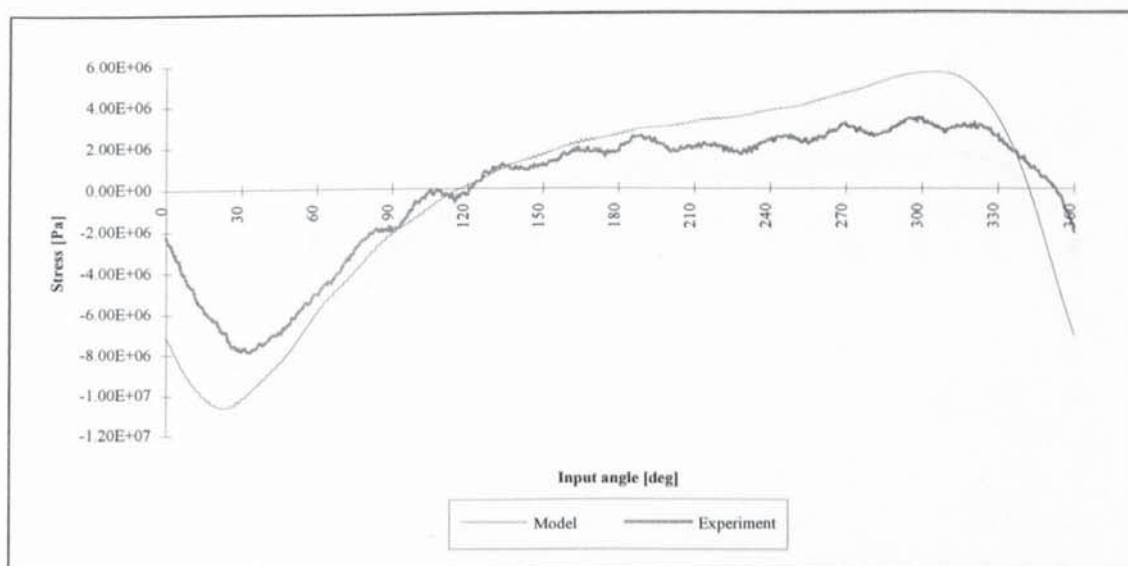


Fig. D.7.c: Stress at the follower midpoint for $\omega = 11.9$ rad/s.

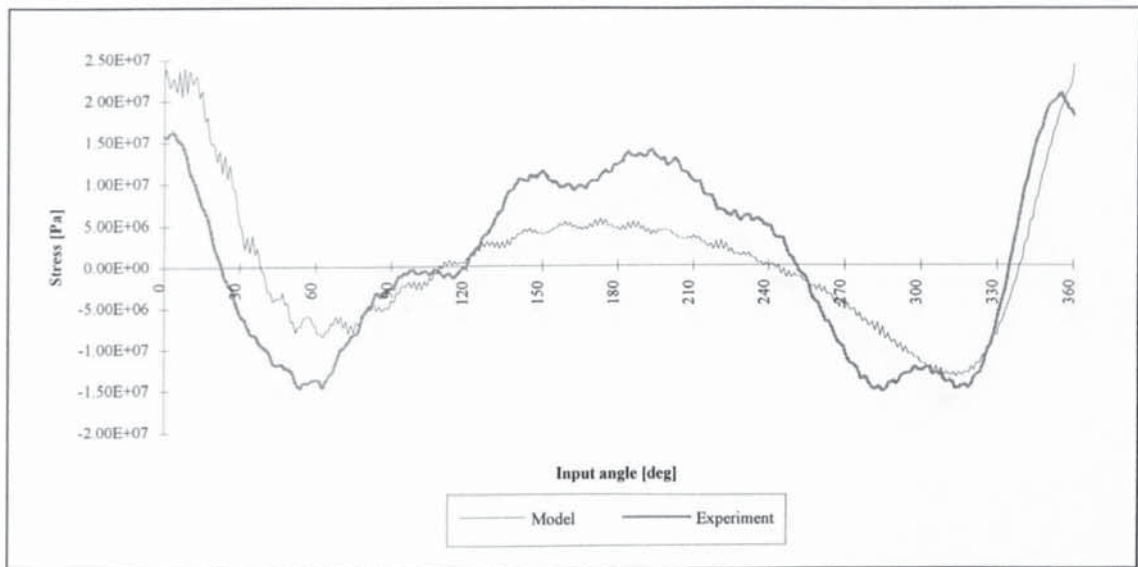


Fig. D.8.a: Stress at the input link midpoint for $\omega = 12.44$ rad/s.

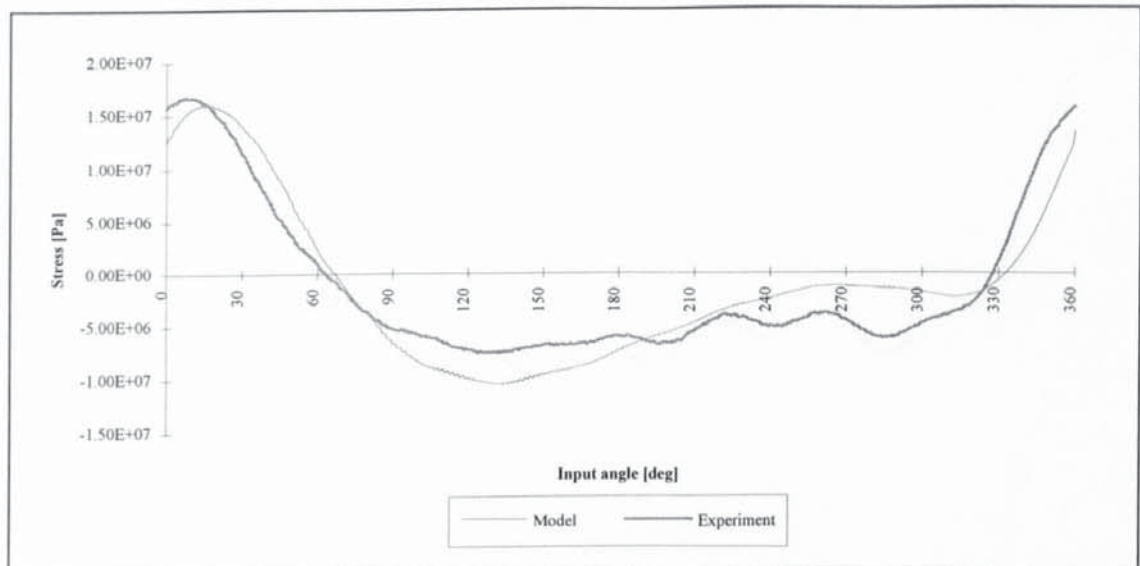


Fig. D.8.b: Stress at the coupler midpoint for $\omega = 12.44$ rad/s.

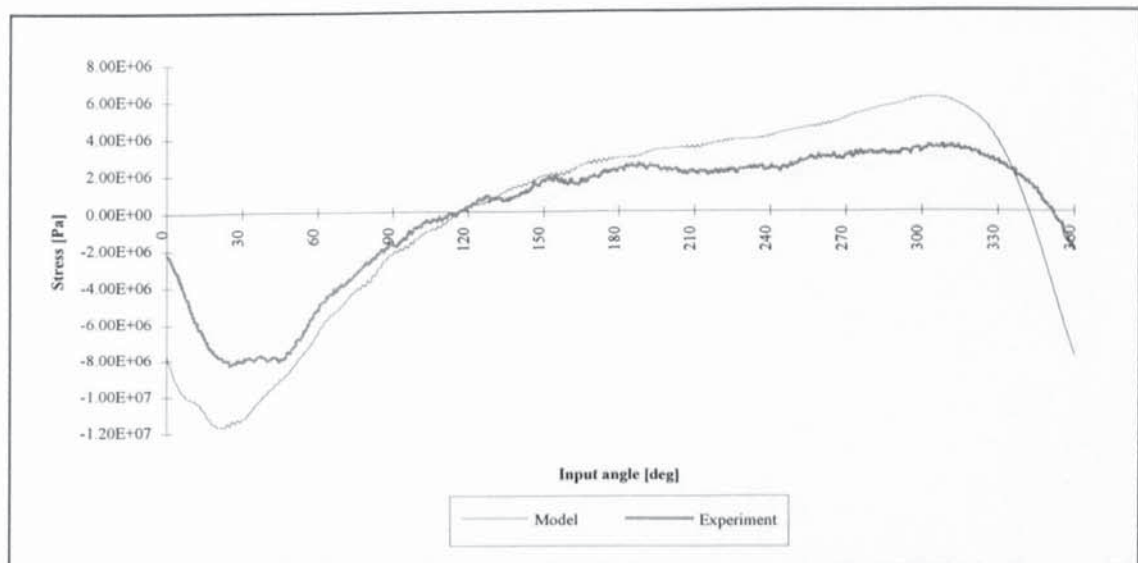


Fig. D.8.c: Stress at the follower midpoint for $\omega = 12.44$ rad/s.

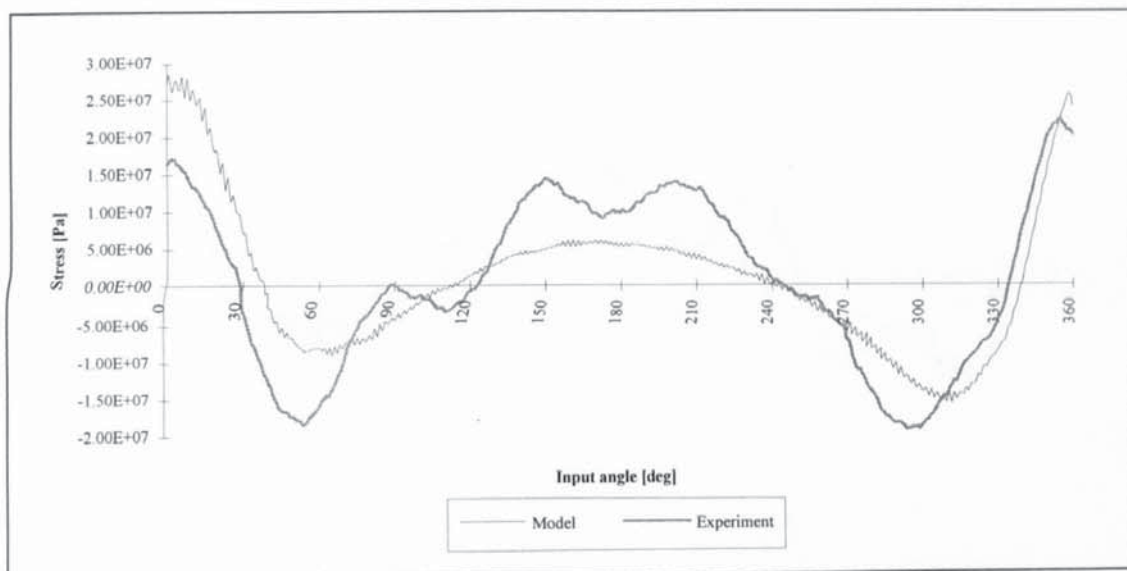


Fig. D.9.a: Stress at the input link midpoint for $\omega = 13.4$ rad/s.

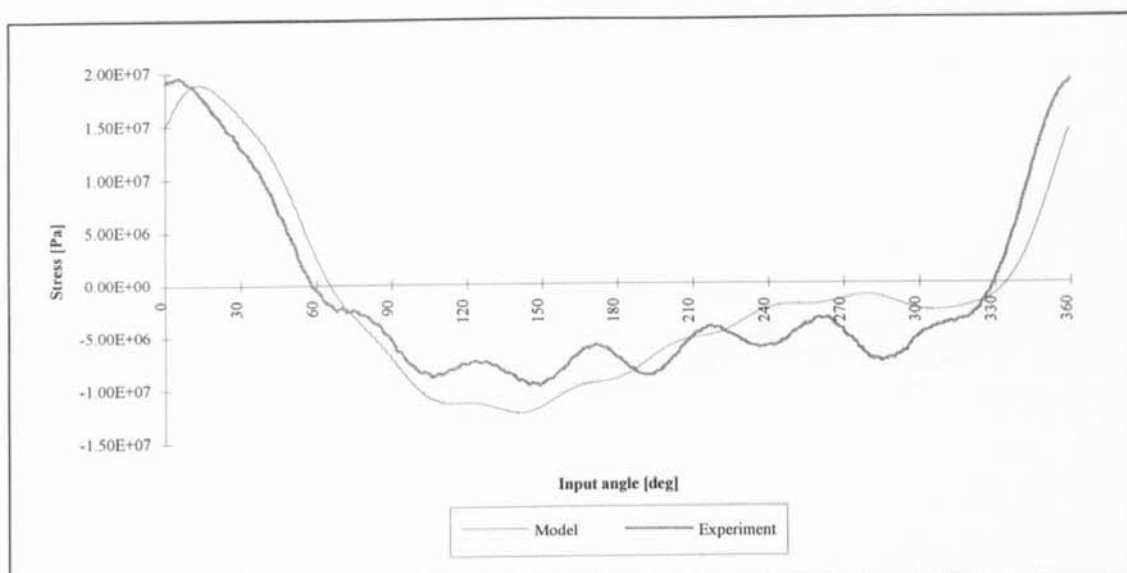


Fig. D.9.b: Stress at the coupler midpoint for $\omega = 13.4$ rad/s.

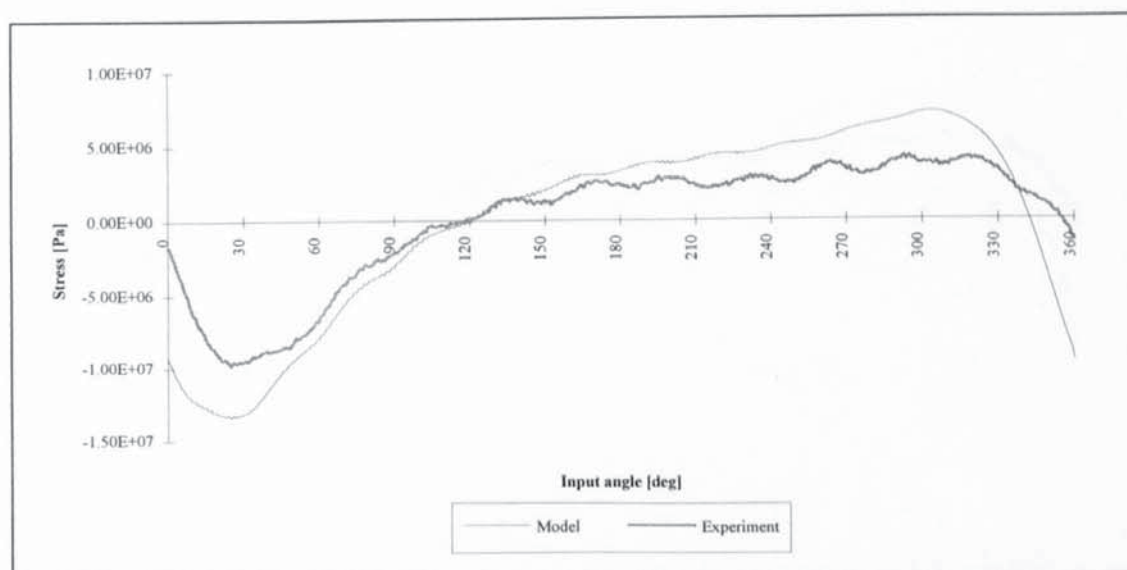


Fig. D.9.c: Stress at the follower midpoint for $\omega = 13.4$ rad/s.

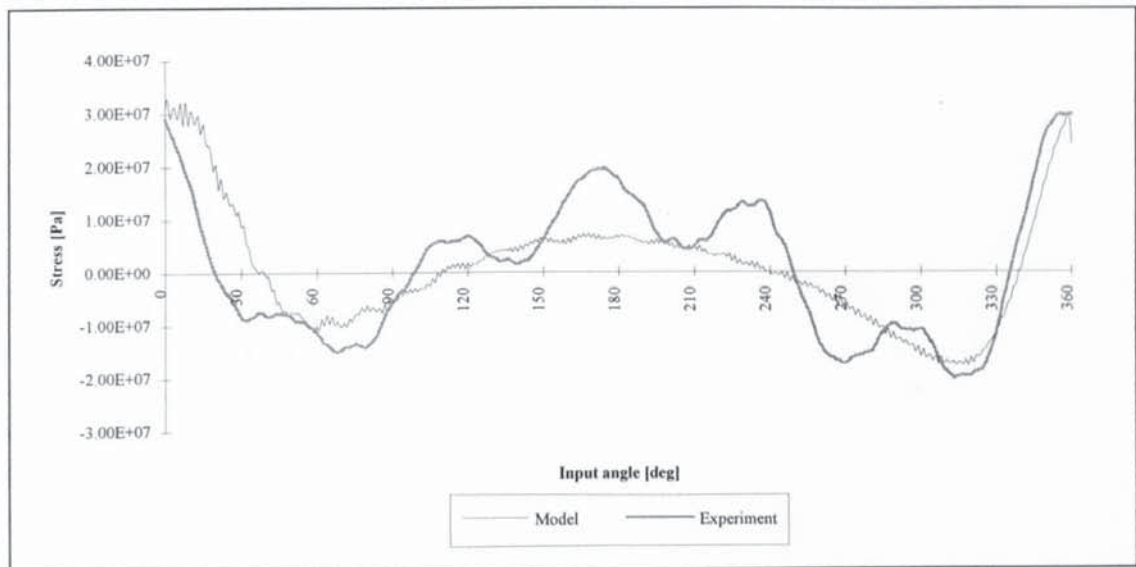


Fig. D.10.a: Stress at the input link midpoint for $\omega = 14.28$ rad/s.

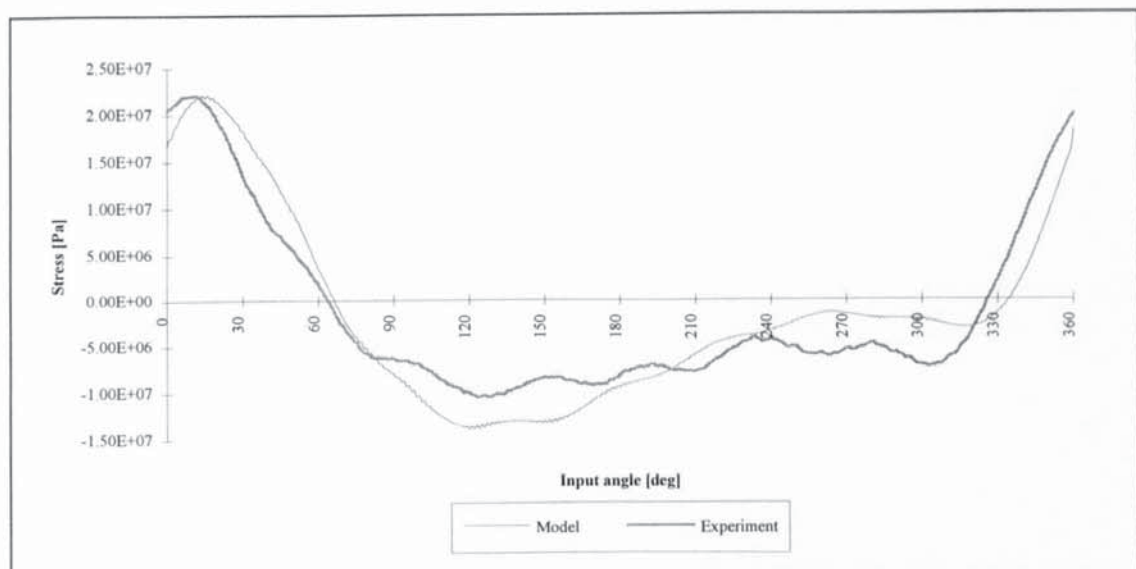


Fig. D.10.b: Stress at the coupler midpoint for $\omega = 14.28$ rad/s.

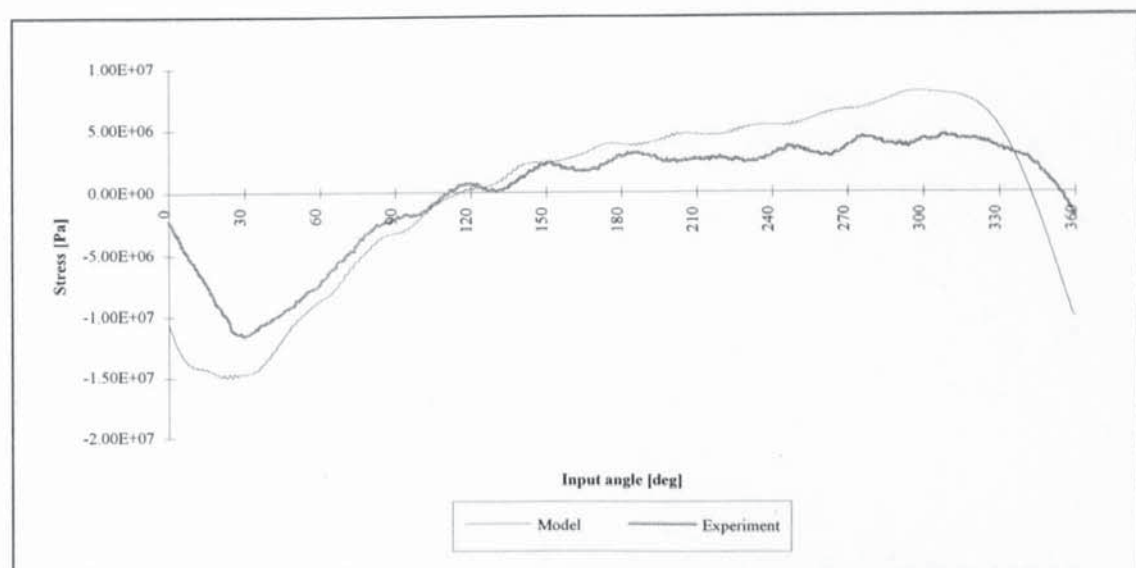


Fig. D.10.c: Stress at the follower midpoint for $\omega = 14.28$ rad/s.

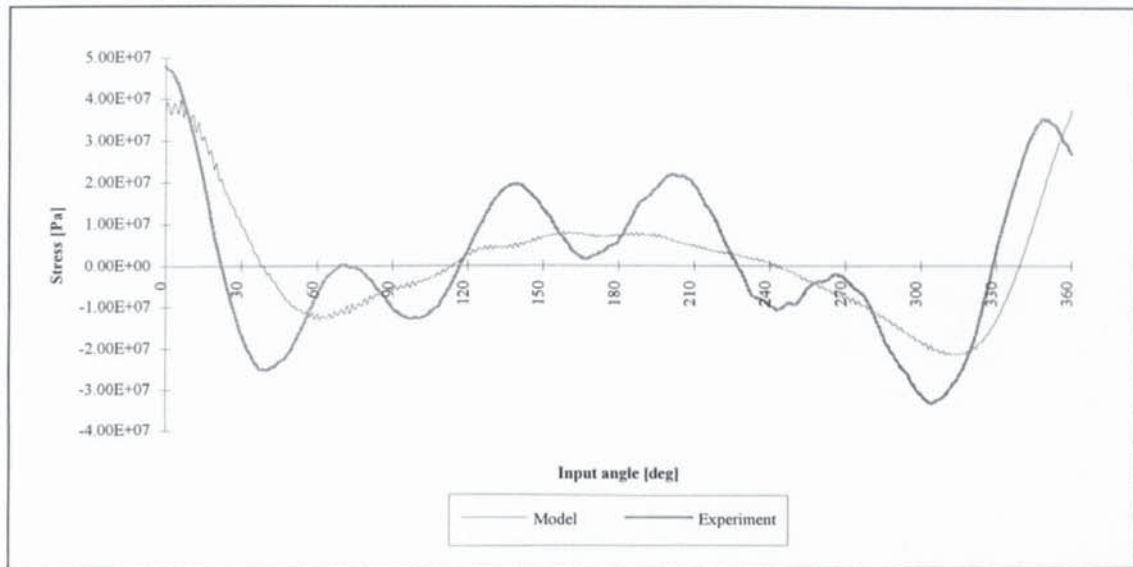


Fig. D.11.a: Stress at the input link midpoint for $\omega = 15.51$ rad/s.

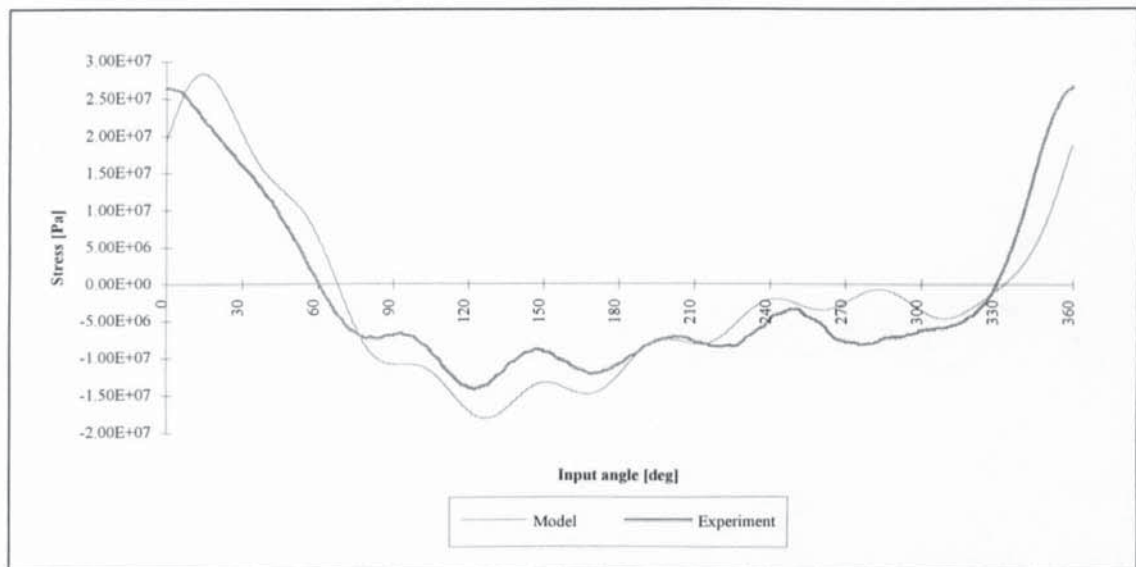


Fig. D.11.b: Stress at the coupler midpoint for $\omega = 15.51$ rad/s.

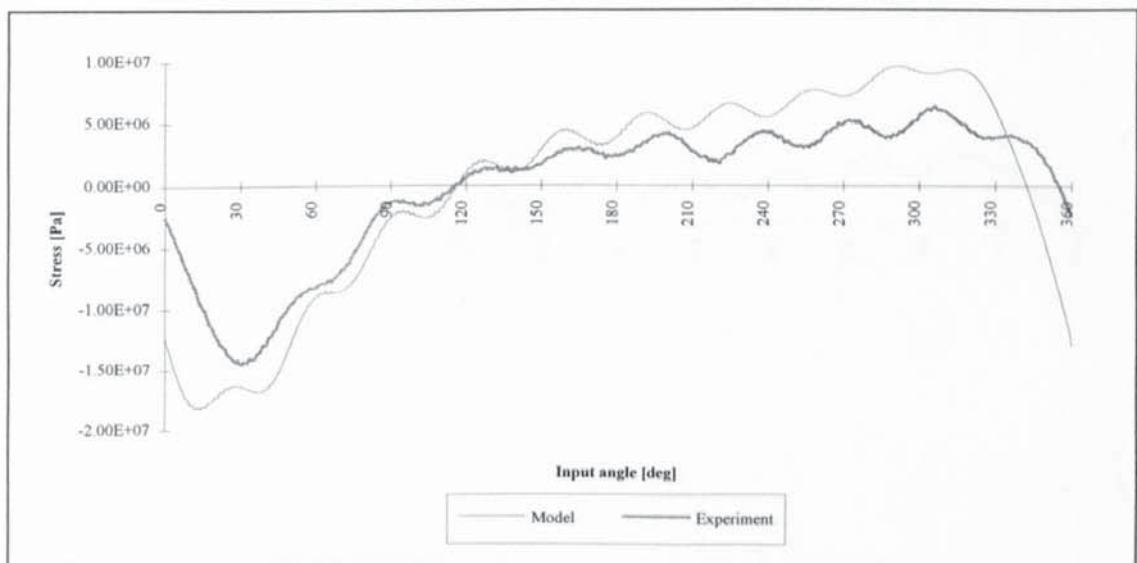


Fig. D.11.c: Stress at the follower midpoint for $\omega = 15.51$ rad/s.

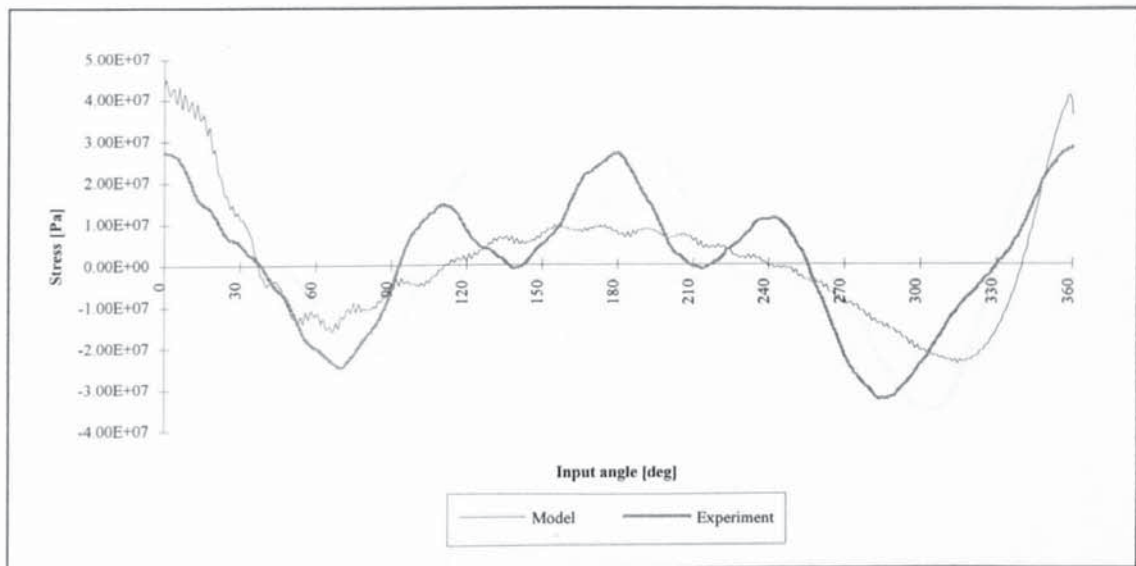


Fig. D.12.a: Stress at the input link midpoint for $\omega = 16.45$ rad/s.

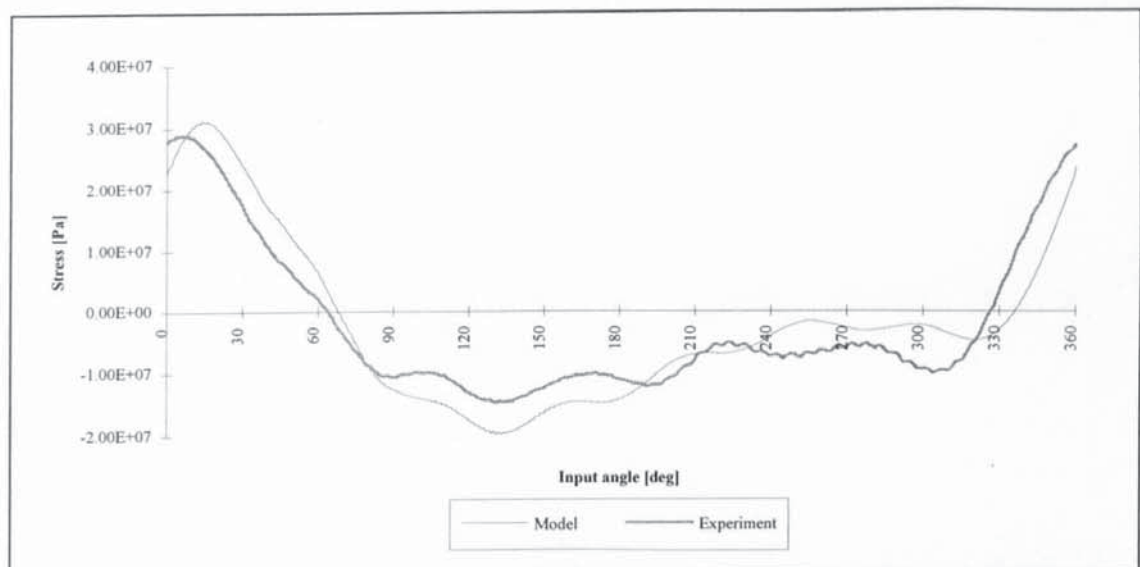


Fig. D.12.b: Stress at the coupler midpoint for $\omega = 16.45$ rad/s.

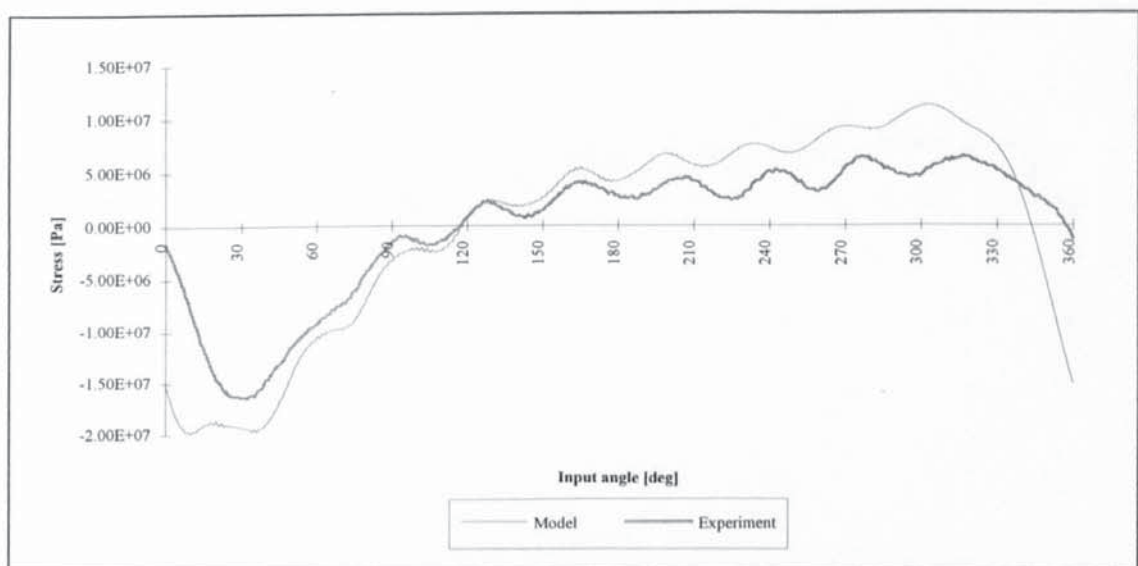


Fig. D.12.c: Stress at the follower midpoint for $\omega = 16.45$ rad/s.

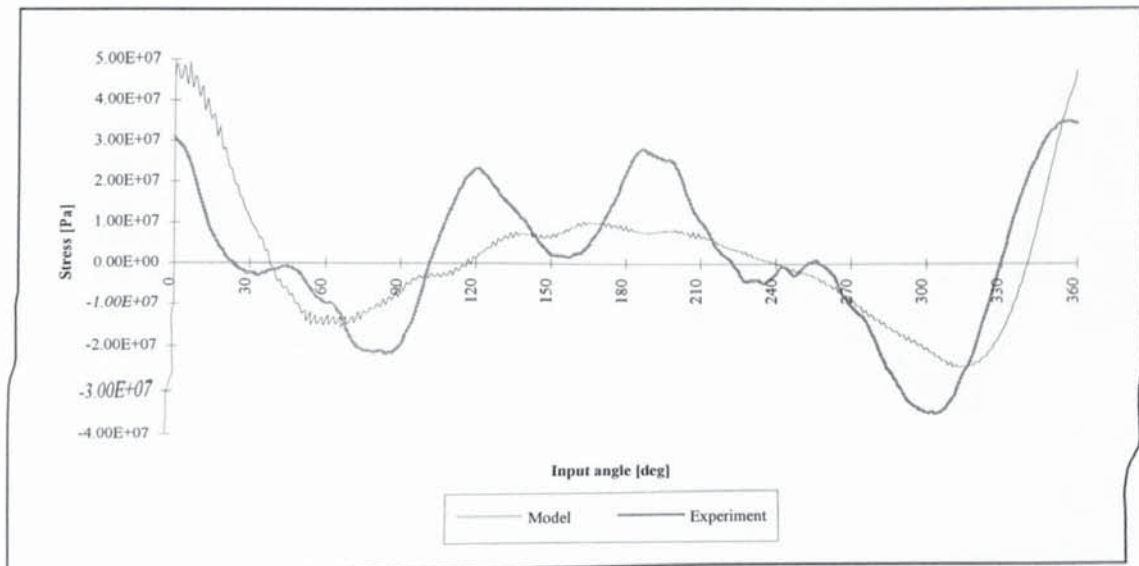


Fig. D.13.a: Stress at the input link midpoint for $\omega = 16.89$ rad/s.

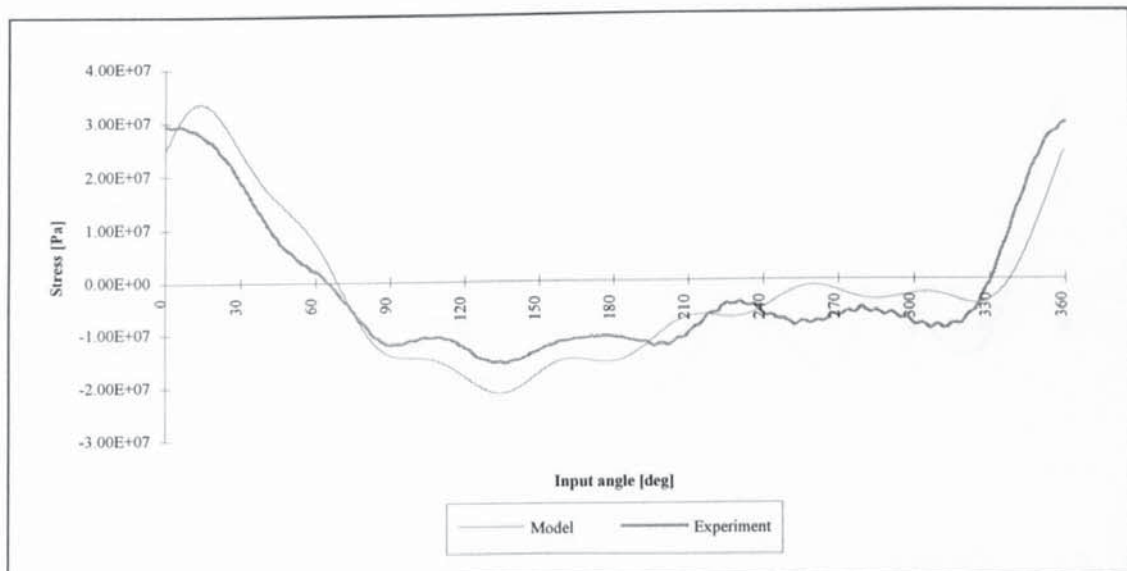


Fig. D.13.b: Stress at the coupler midpoint for $\omega = 16.89$ rad/s.

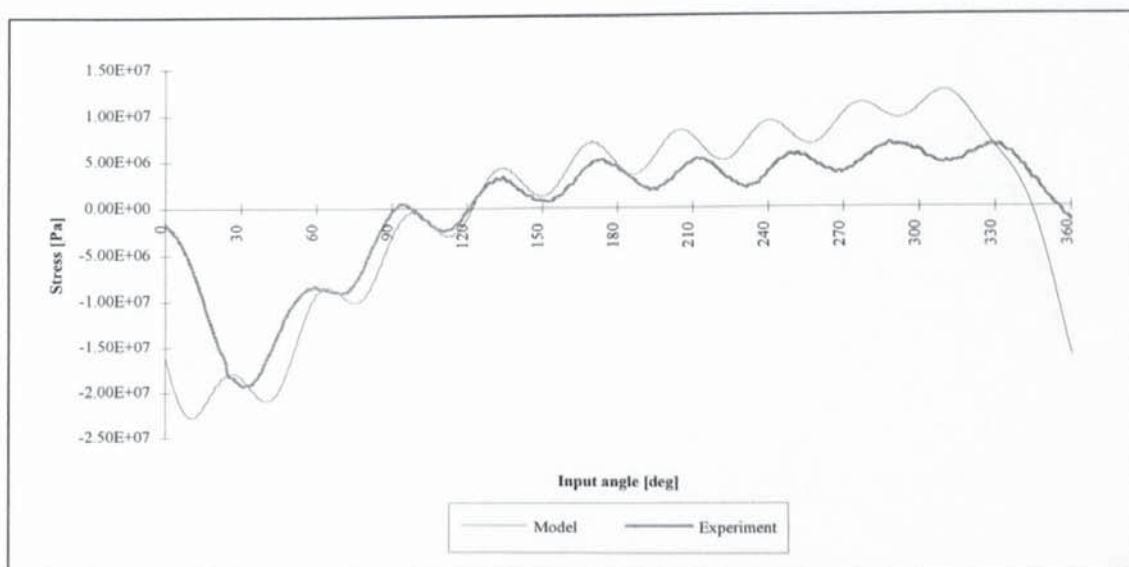


Fig. D.13.c: Stress at the follower midpoint for $\omega = 16.89$ rad/s.

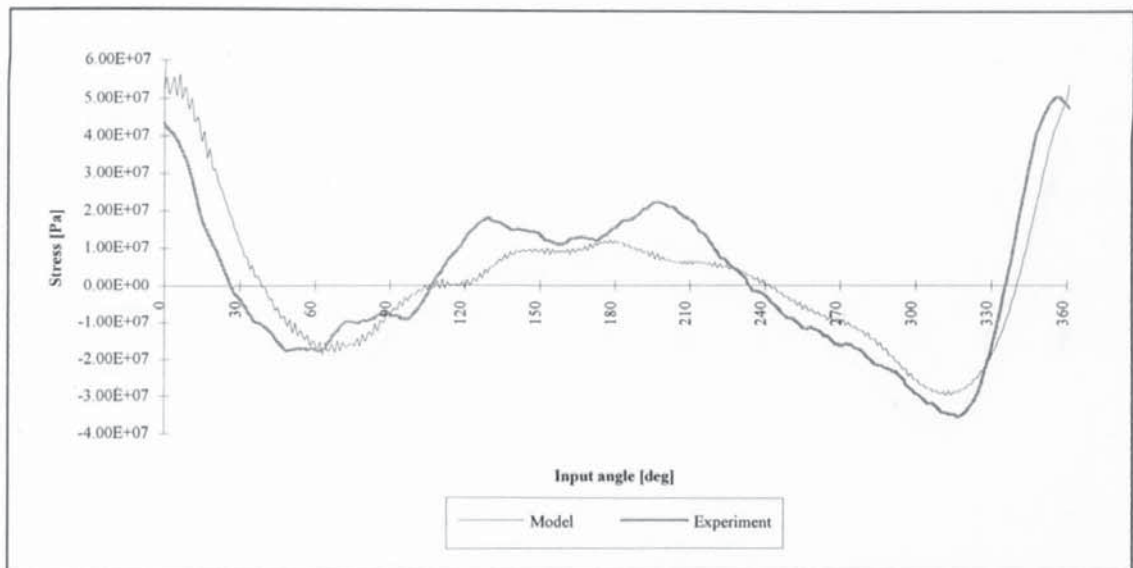


Fig. D.14.a: Stress at the input link midpoint for $\omega = 18$ rad/s.

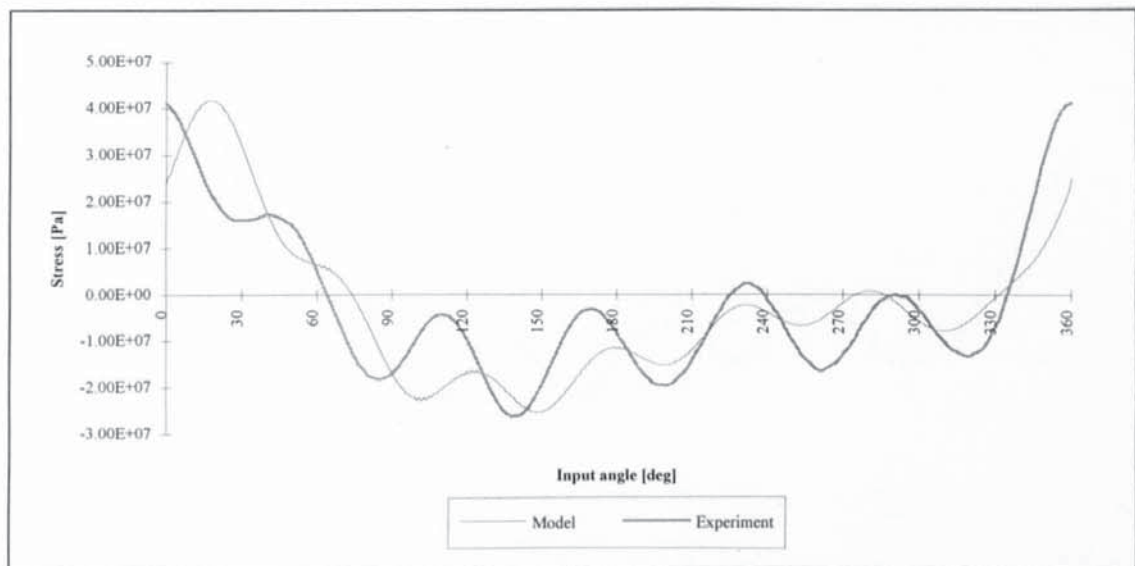


Fig. D.14.b: Stress at the coupler midpoint for $\omega = 18$ rad/s.

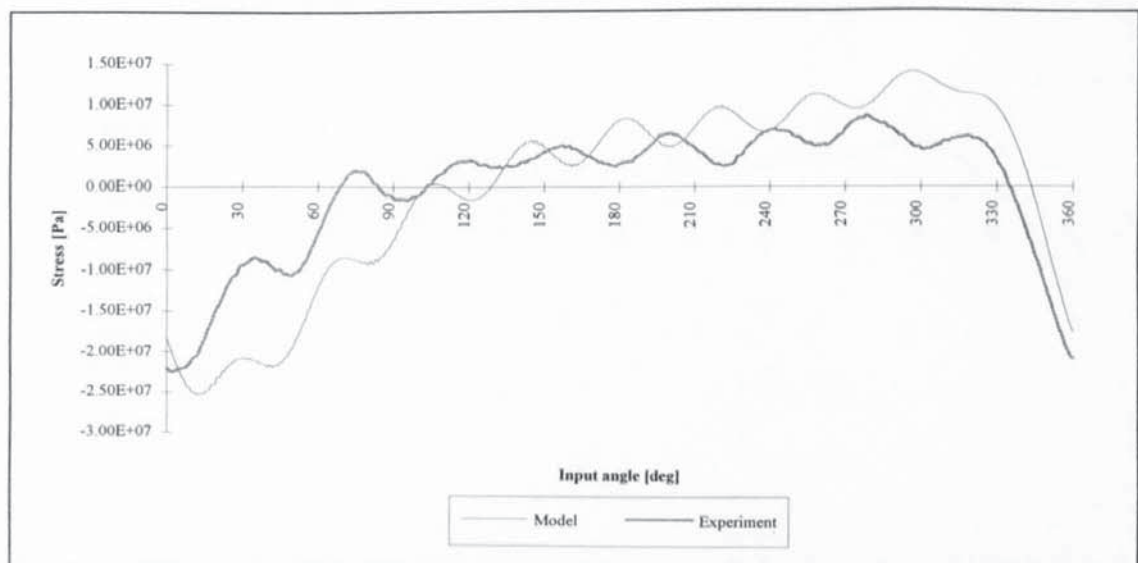


Fig. D.14.c: Stress at the follower midpoint for $\omega = 18$ rad/s.

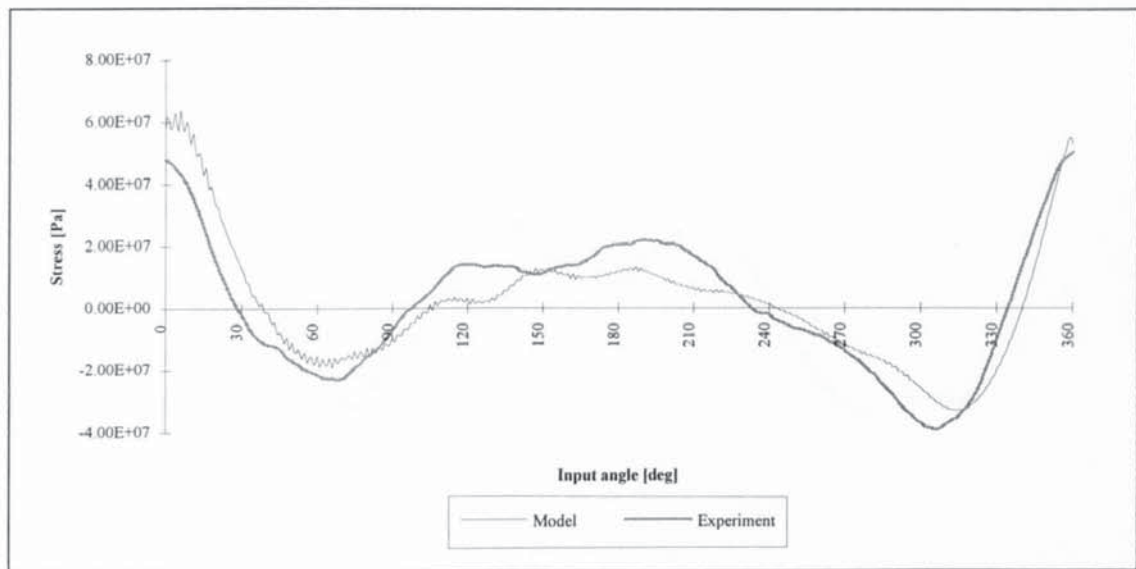


Fig. D.15.a: Stress at the input link midpoint for $\omega = 18.81$ rad/s.

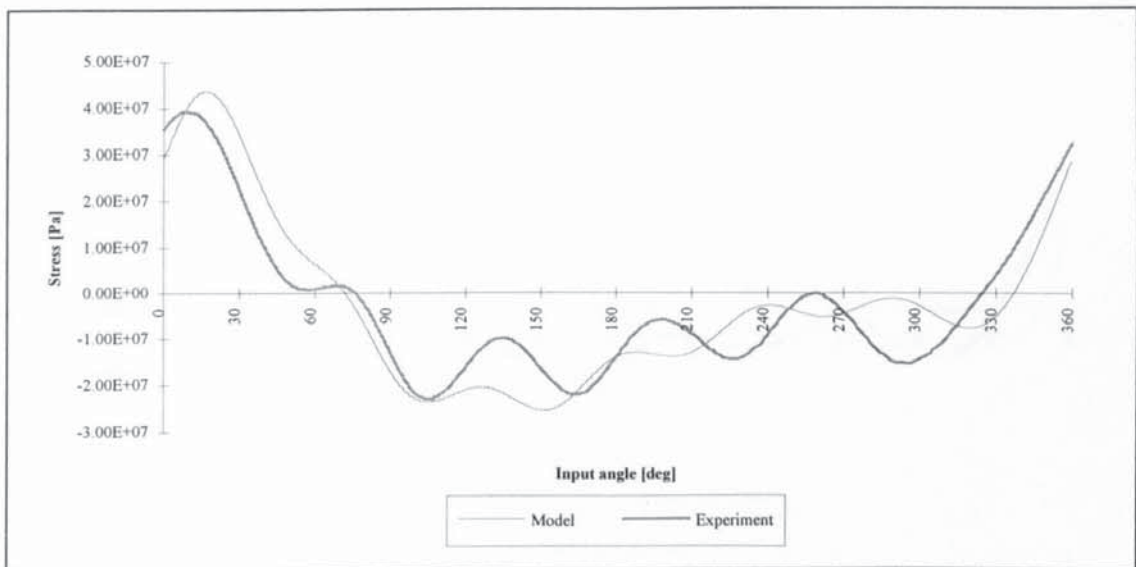


Fig. D.15.b: Stress at the coupler midpoint for $\omega = 18.81$ rad/s.

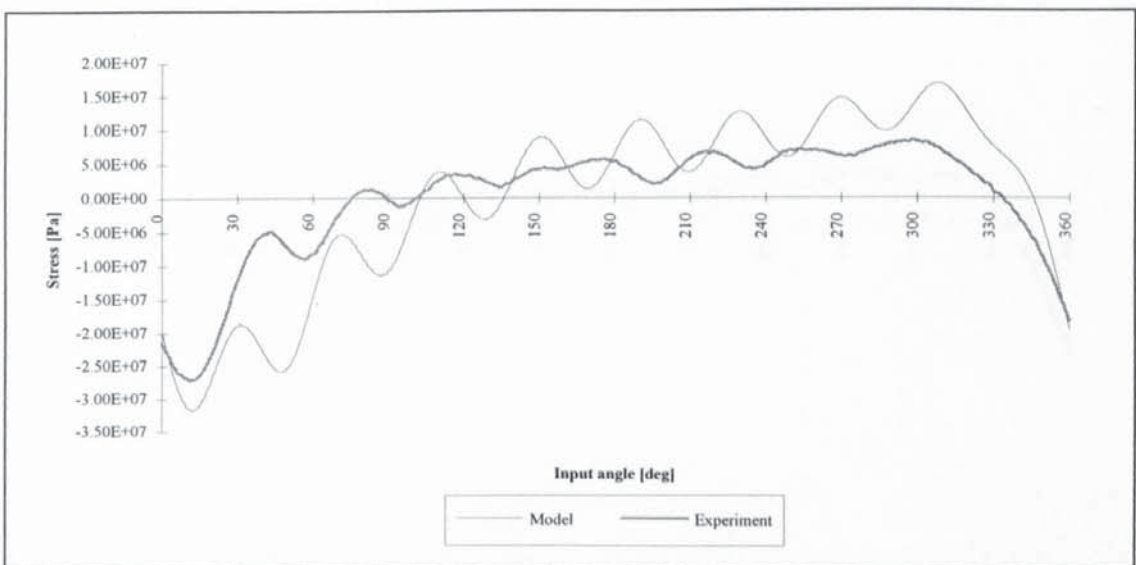


Fig. D.15.c: Stress at the follower midpoint for $\omega = 18.81$ rad/s.

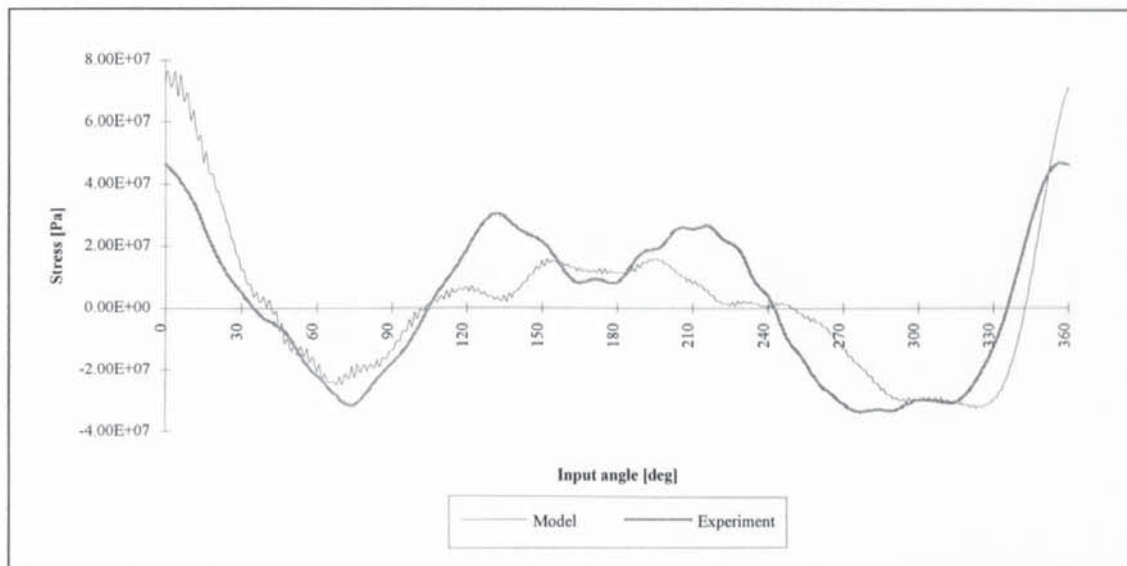


Fig. D.16.a: Stress at the input link midpoint for $\omega = 20.27$ rad/s.

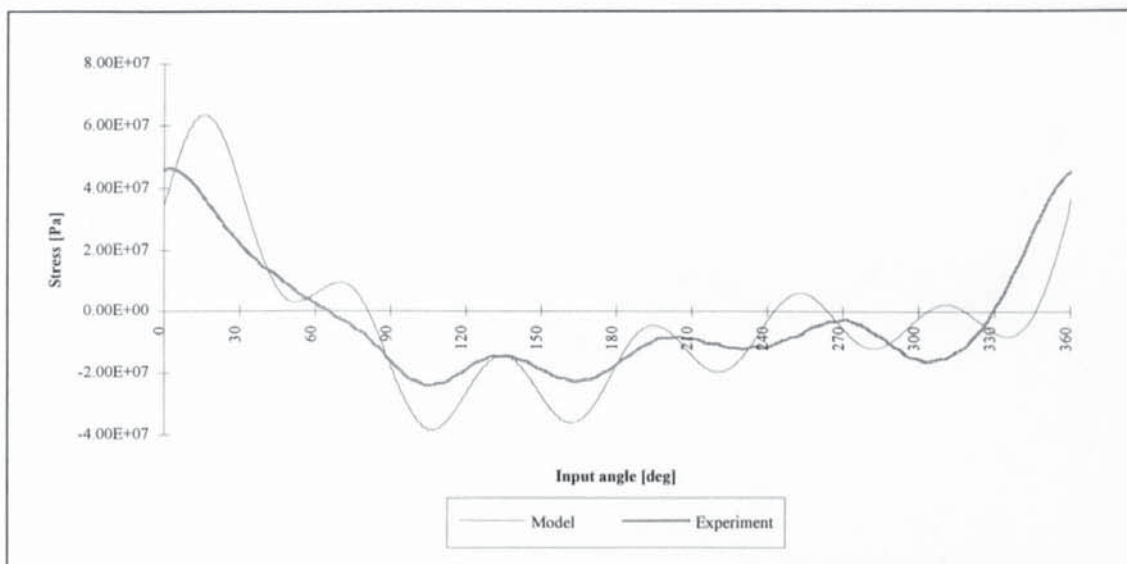


Fig. D.16.b: Stress at the coupler midpoint for $\omega = 20.27$ rad/s.

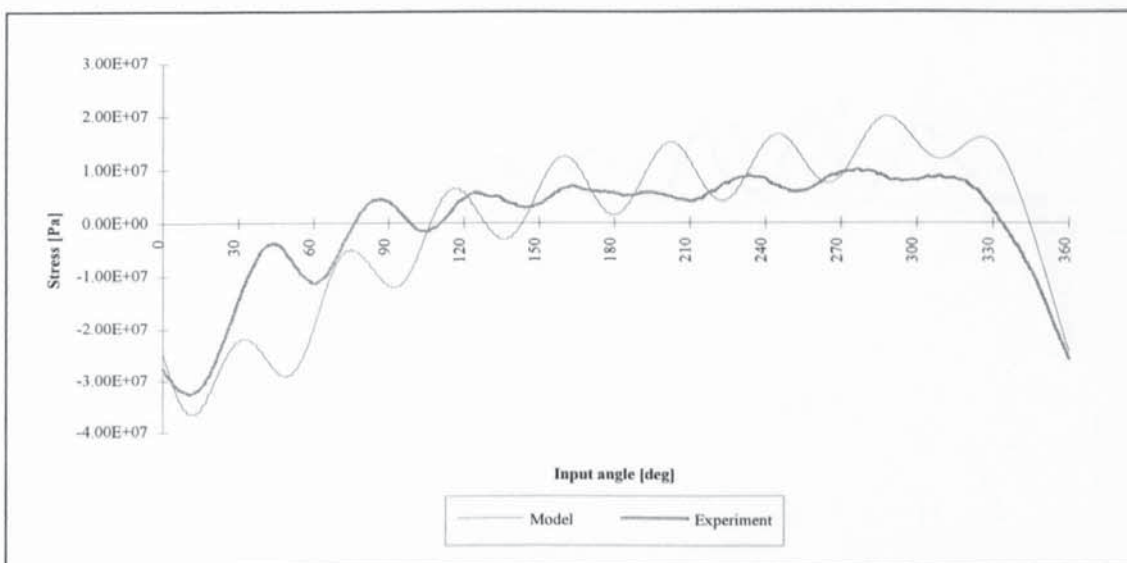


Fig. D.16.c: Stress at the follower midpoint for $\omega = 20.27$ rad/s.

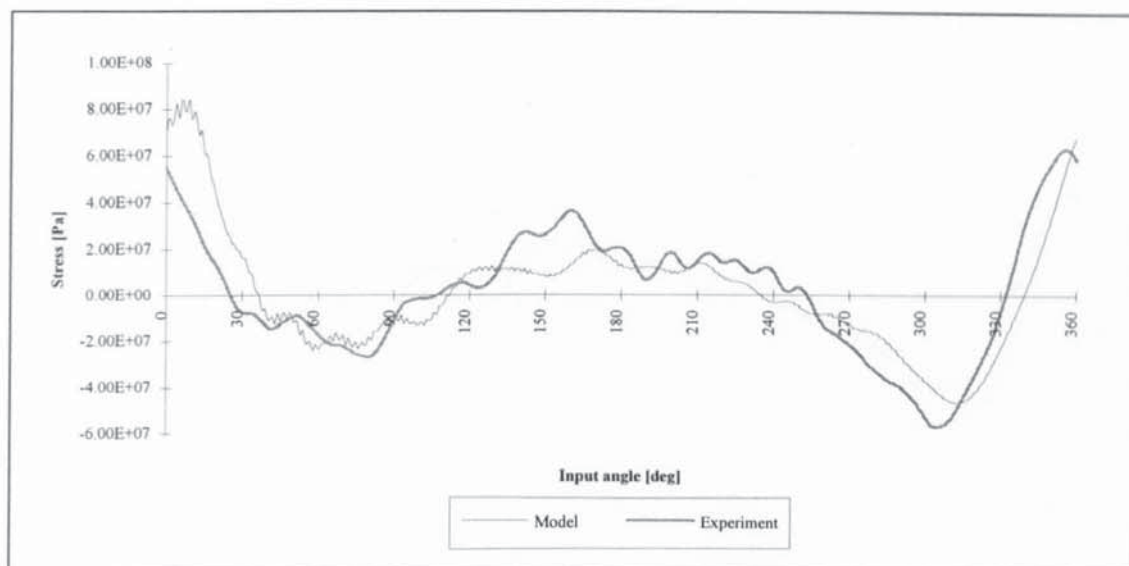


Fig. D.17.a: Stress at the input link midpoint for $\omega = 21.37$ rad/s.

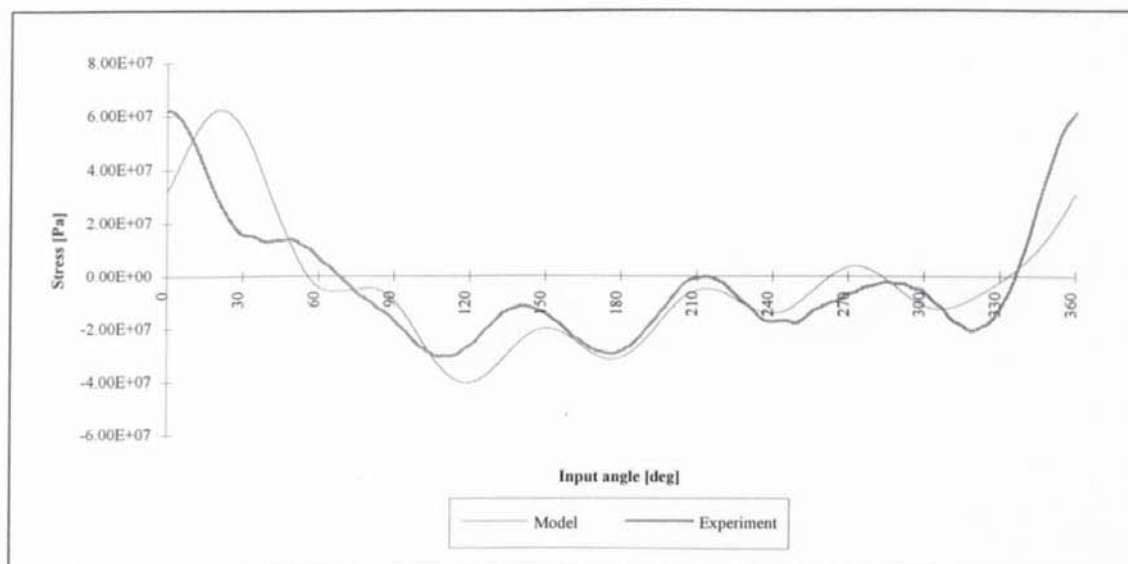


Fig. D.17.b: Stress at the coupler midpoint for $\omega = 21.37$ rad/s.

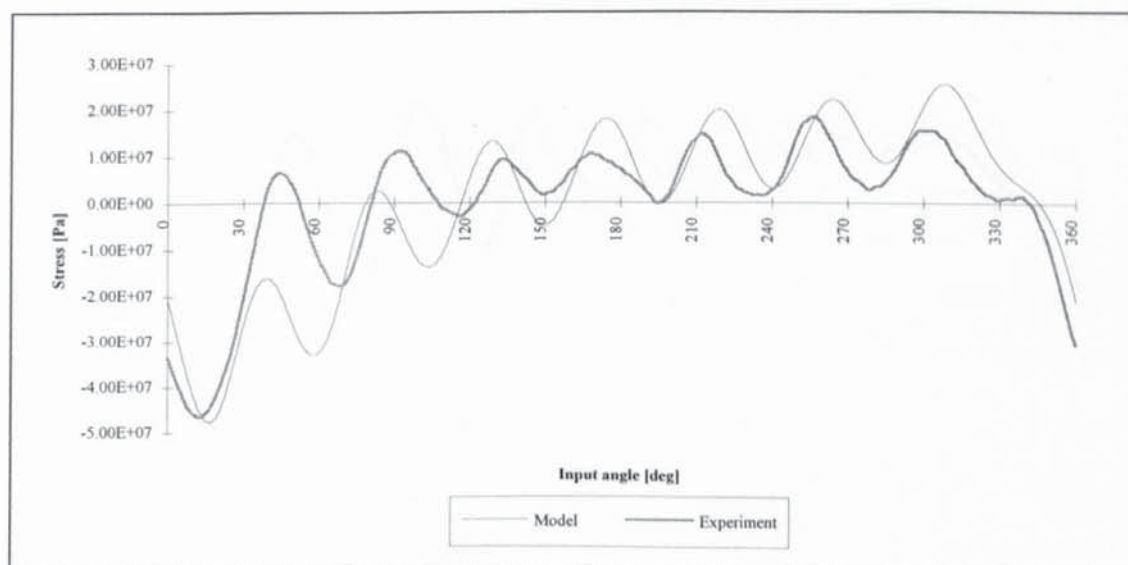


Fig. D.17.c: Stress at the follower midpoint for $\omega = 21.37$ rad/s.

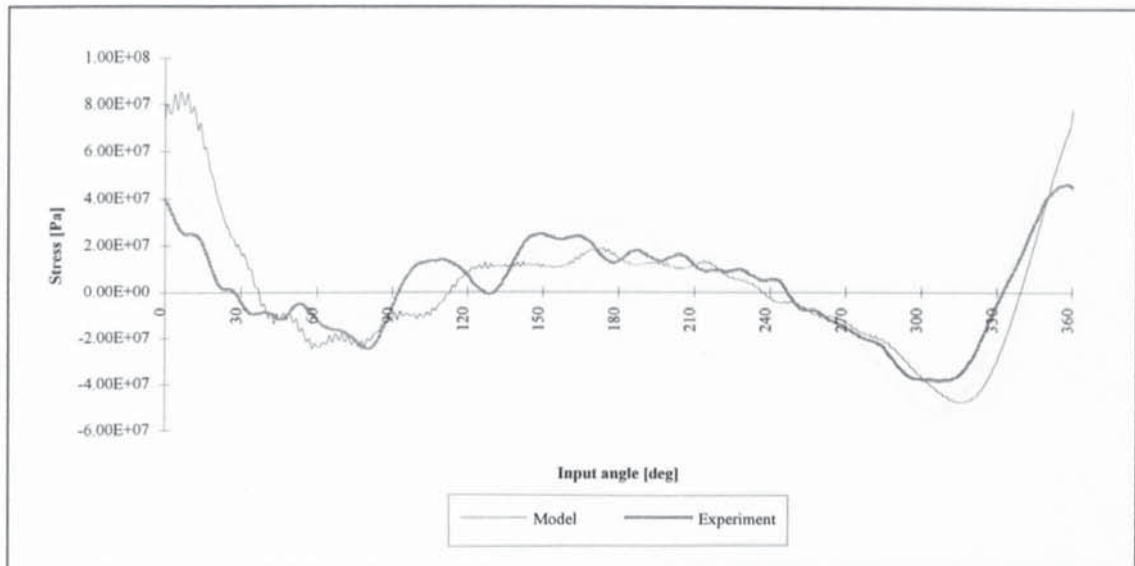


Fig. D.18.a: Stress at the input link midpoint for $\omega = 21.74$ rad/s.

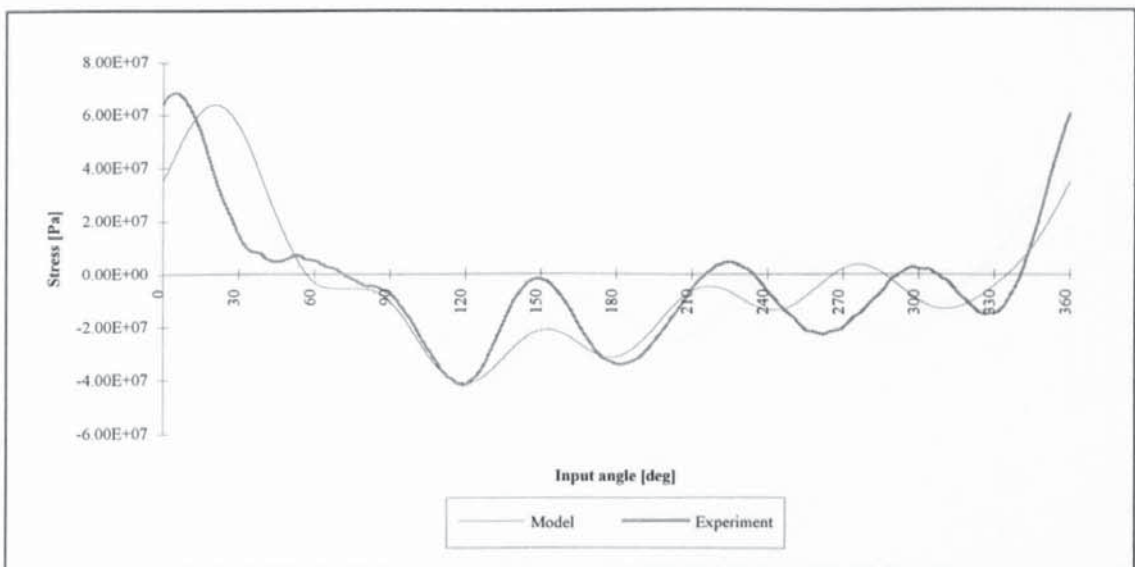


Fig. D.18.b: Stress at the coupler midpoint for $\omega = 21.74$ rad/s.

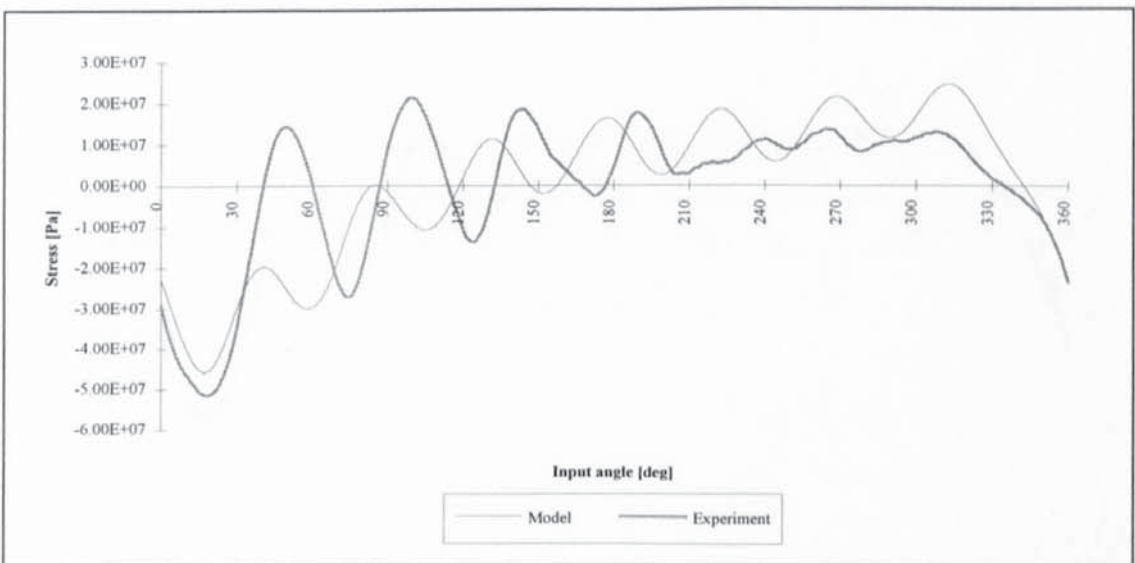


Fig. D.18.c: Stress at the follower midpoint for $\omega = 21.74$ rad/s.

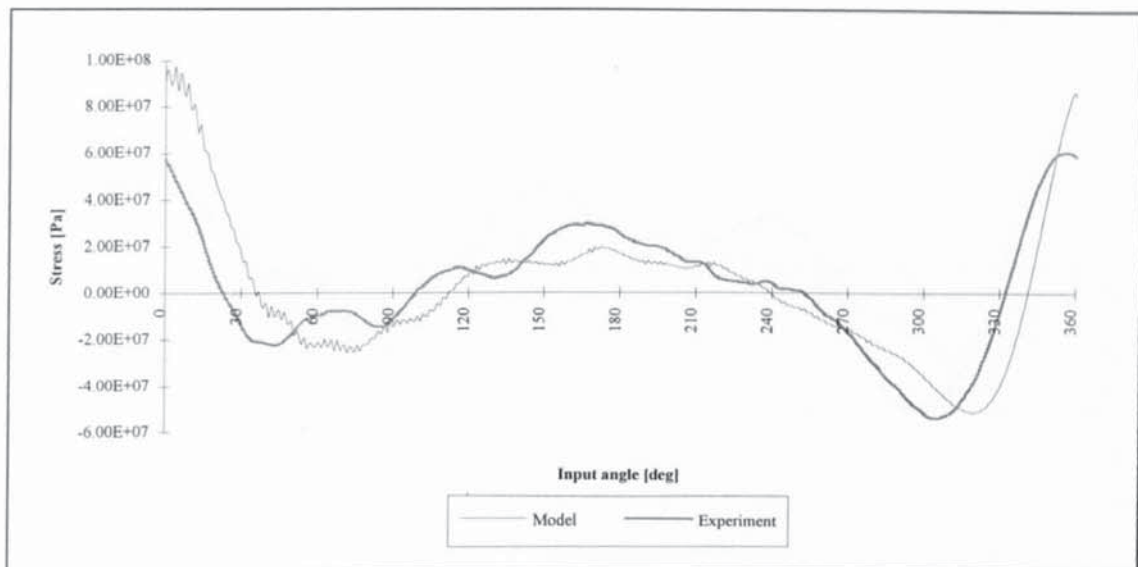


Fig. D.19.a: Stress at the input link midpoint for $\omega = 22.68$ rad/s.

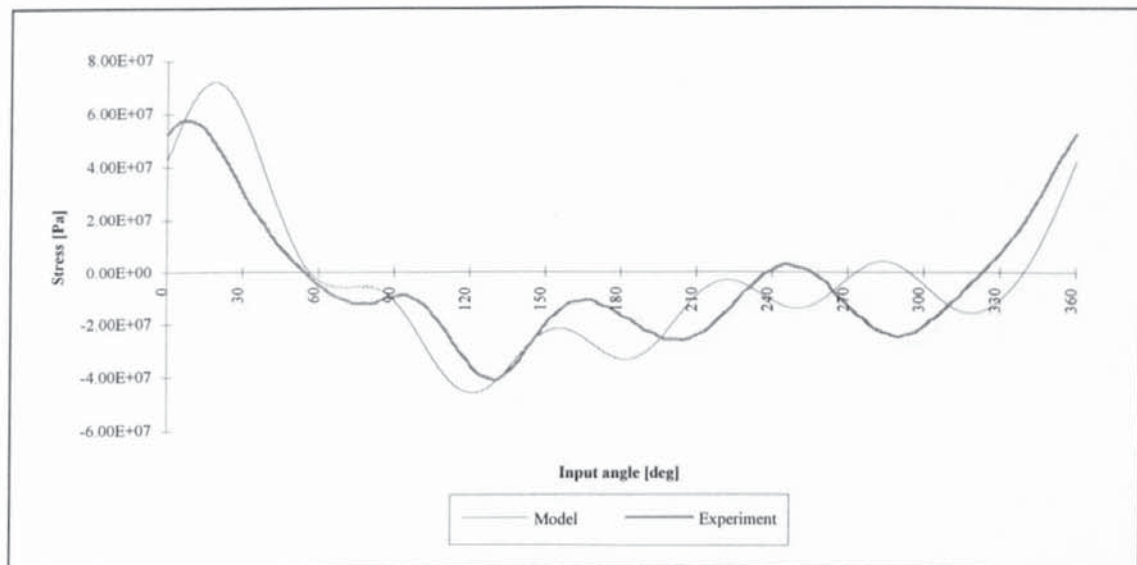


Fig. D.19.b: Stress at the coupler midpoint for $\omega = 22.68$ rad/s.

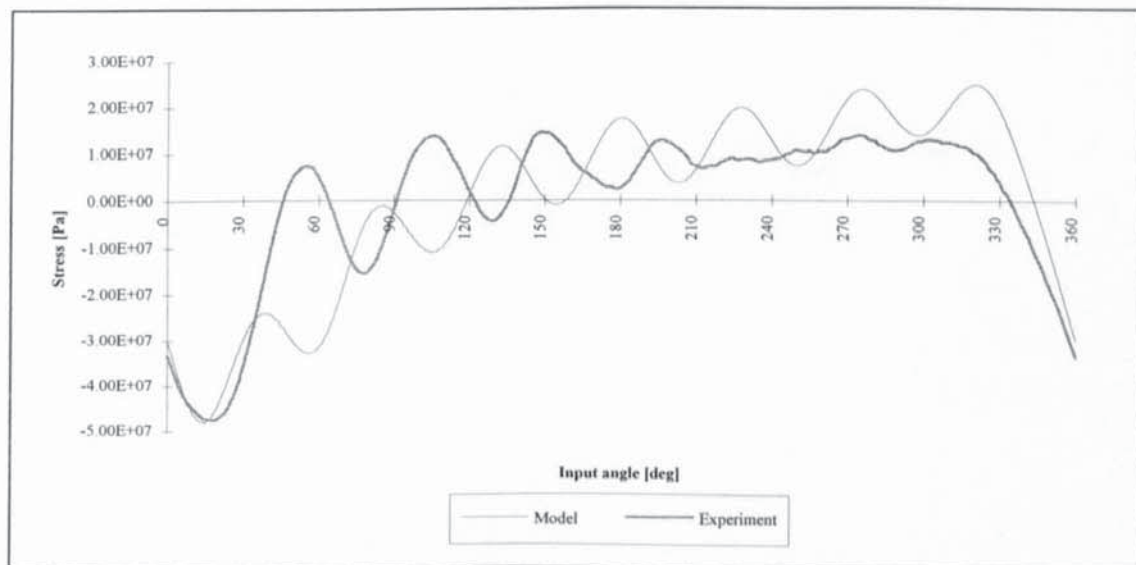


Fig. D.19.c: Stress at the follower midpoint for $\omega = 22.68$ rad/s.

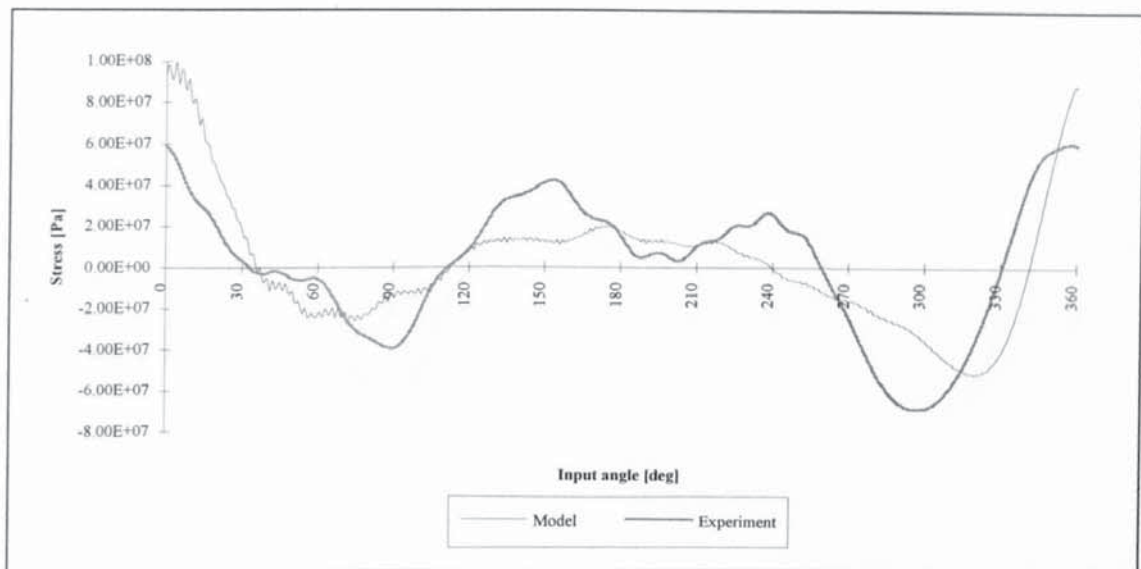


Fig. D.20.a: Stress at the input link midpoint for $\omega = 22.77$ rad/s.

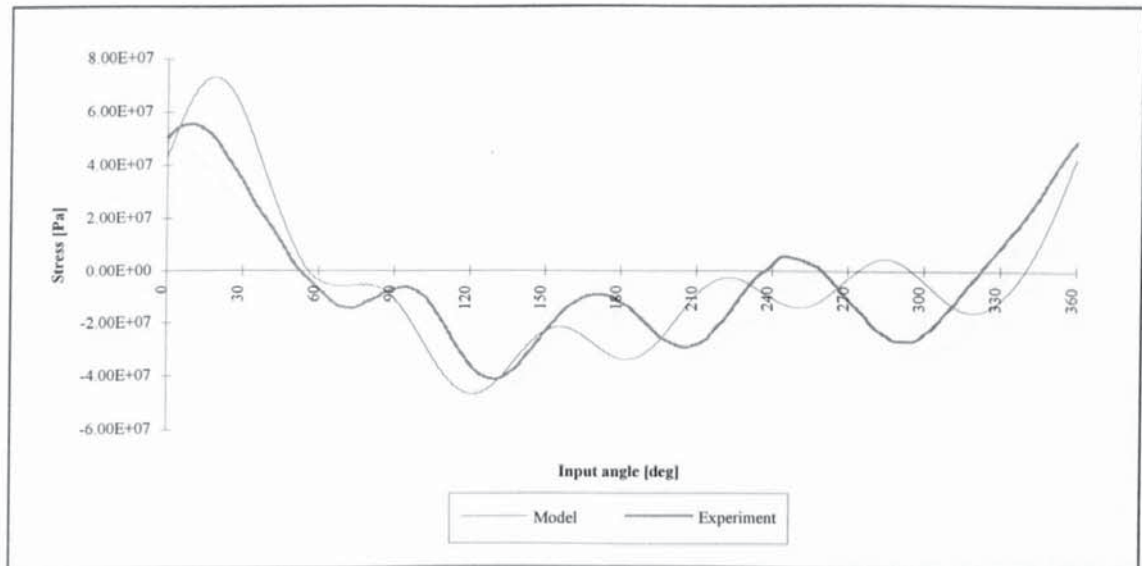


Fig. D.20.b: Stress at the coupler midpoint for $\omega = 22.77$ rad/s.

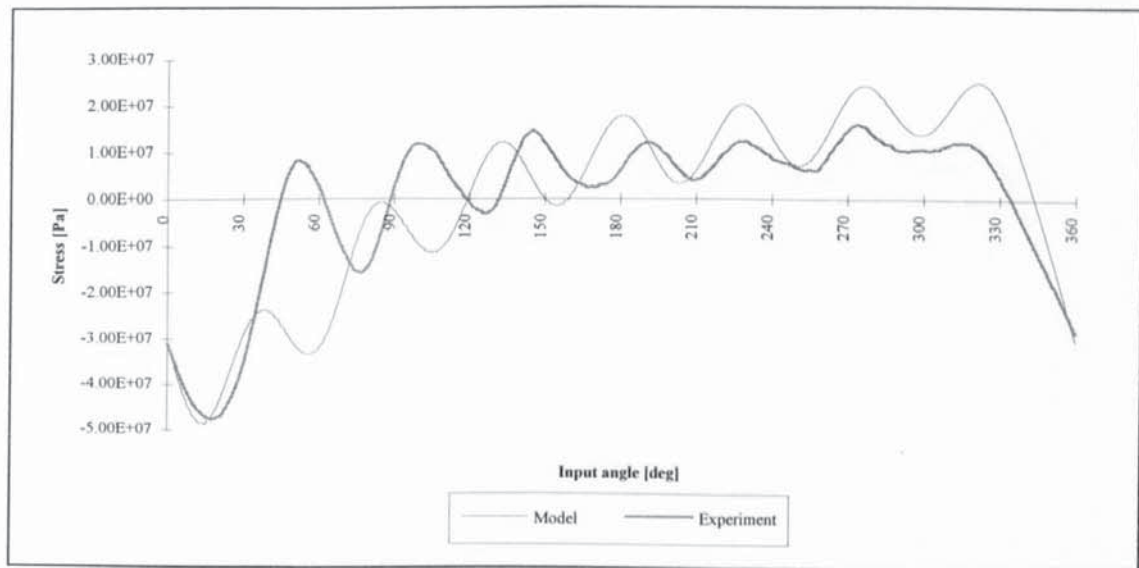


Fig. D.20.c: Stress at the follower midpoint for $\omega = 22.77$ rad/s.

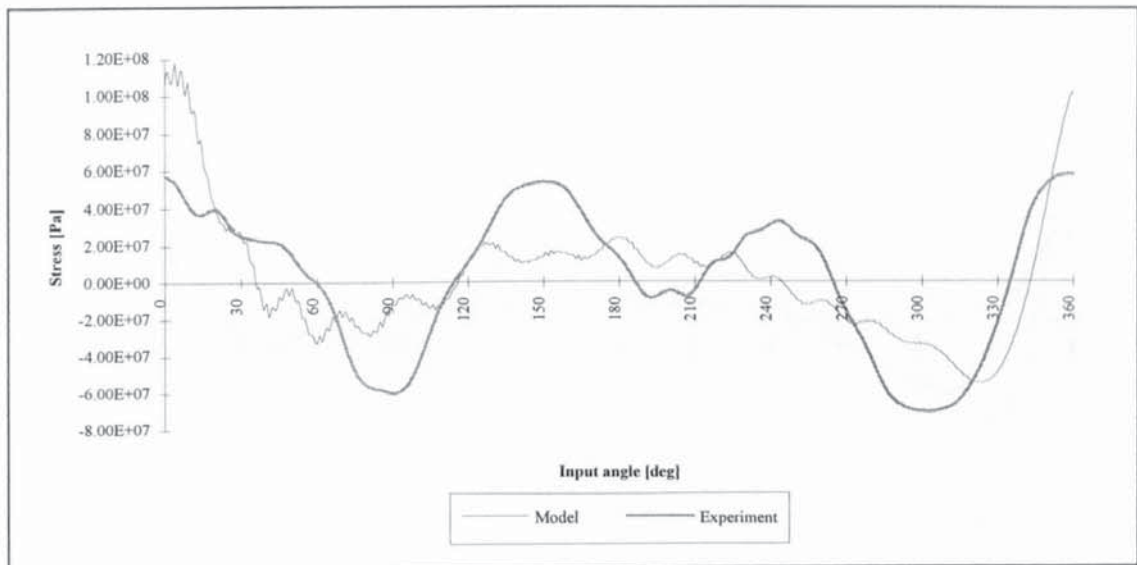


Fig. D.21.a: Stress at the input link midpoint for $\omega = 23.36$ rad/s.

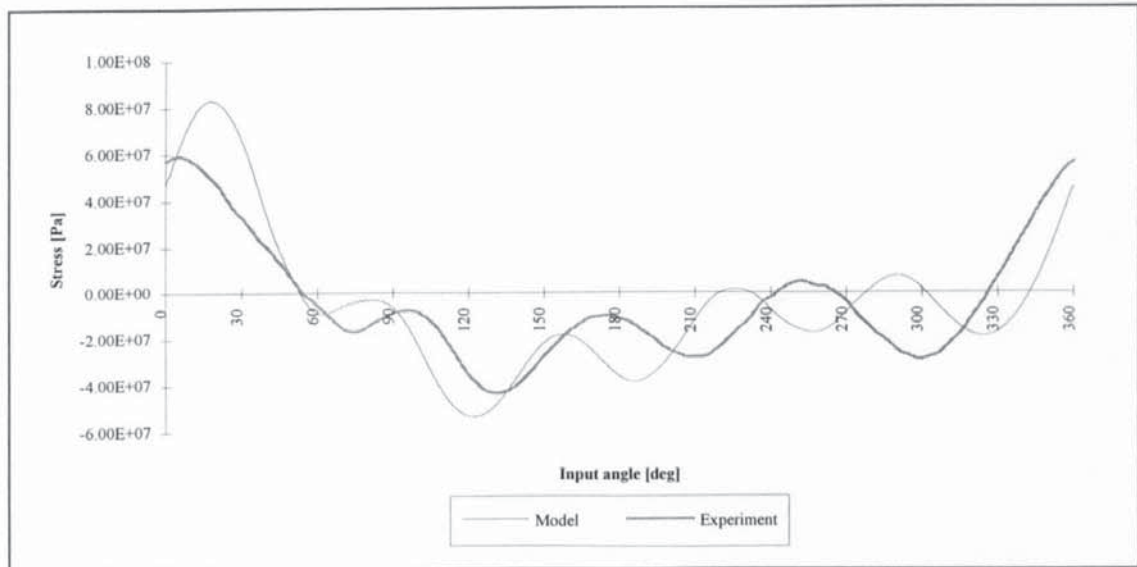


Fig. D.21.b: Stress at the coupler midpoint for $\omega = 23.36$ rad/s.

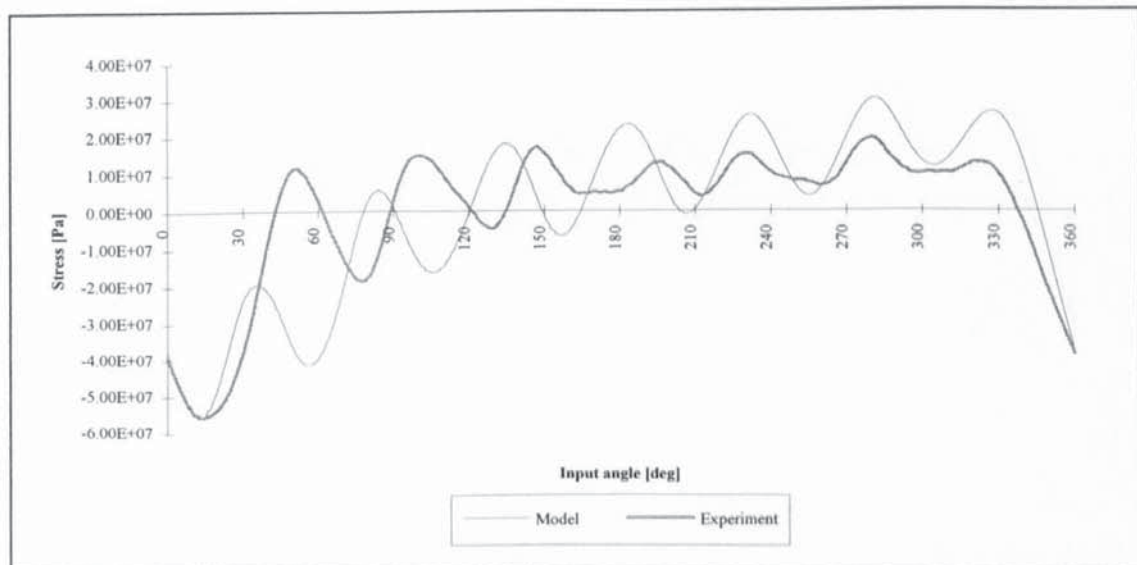


Fig. D.21.c: Stress at the follower midpoint for $\omega = 23.36$ rad/s.

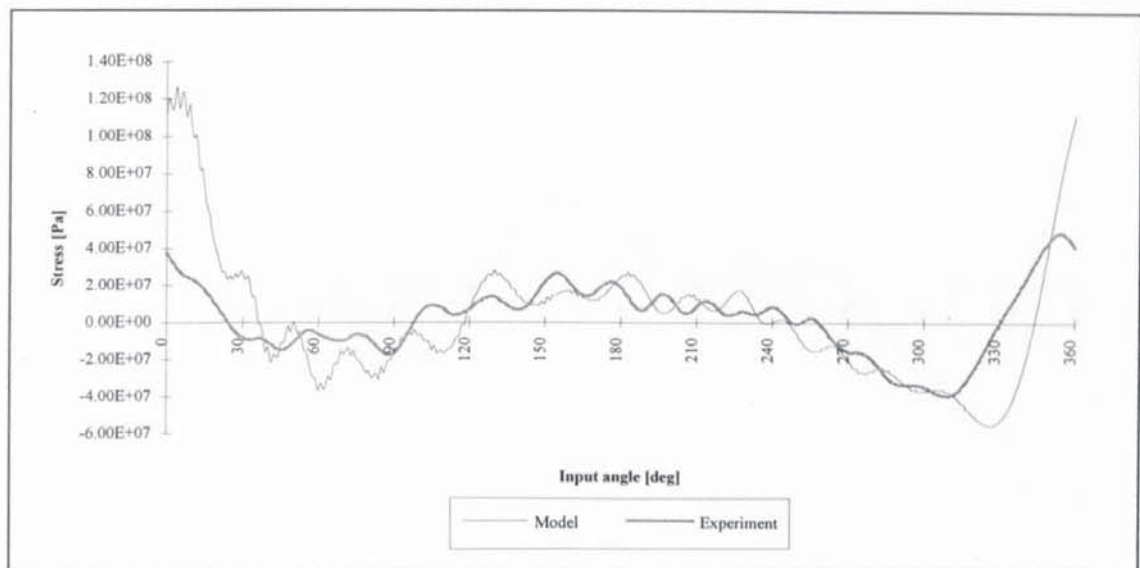


Fig. D.22.a: Stress at the input link midpoint for $\omega = 23.62$ rad/s.

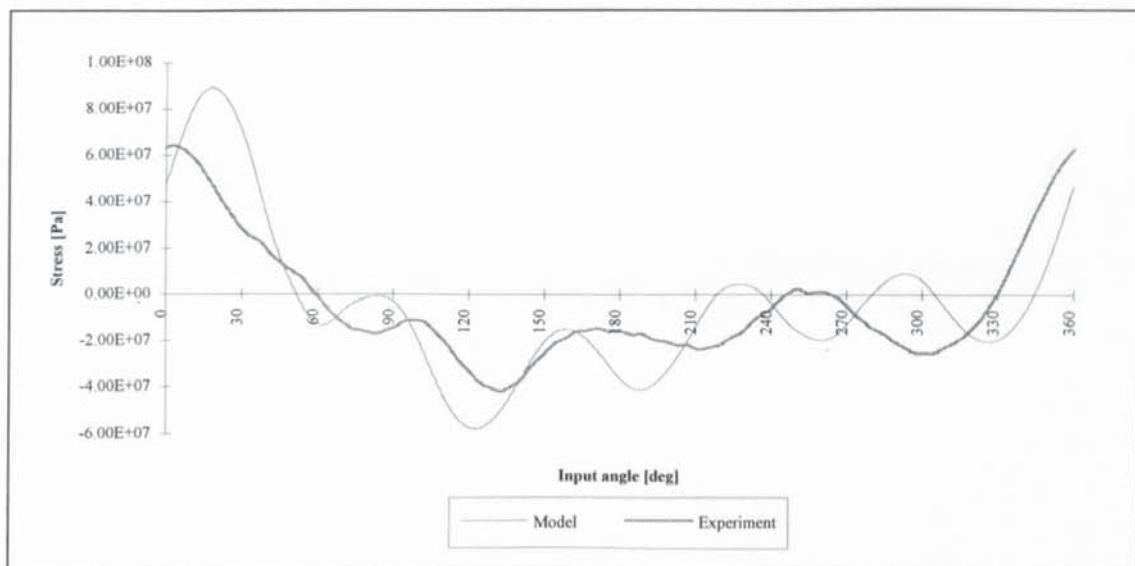


Fig. D.22.b: Stress at the coupler midpoint for $\omega = 23.62$ rad/s.

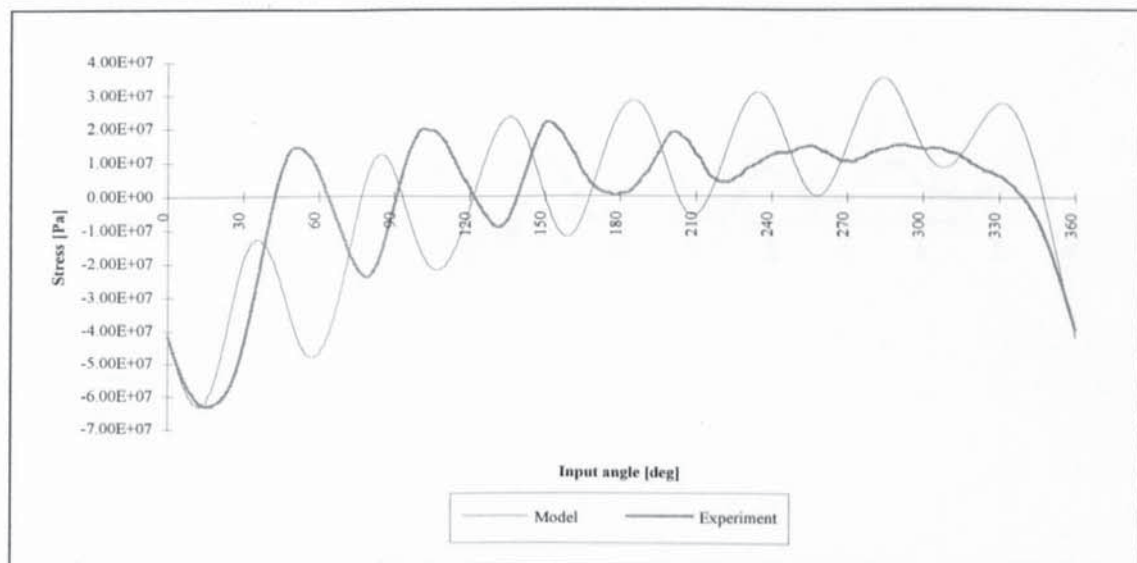


Fig. D.22.c: Stress at the follower midpoint for $\omega = 23.62$ rad/s.

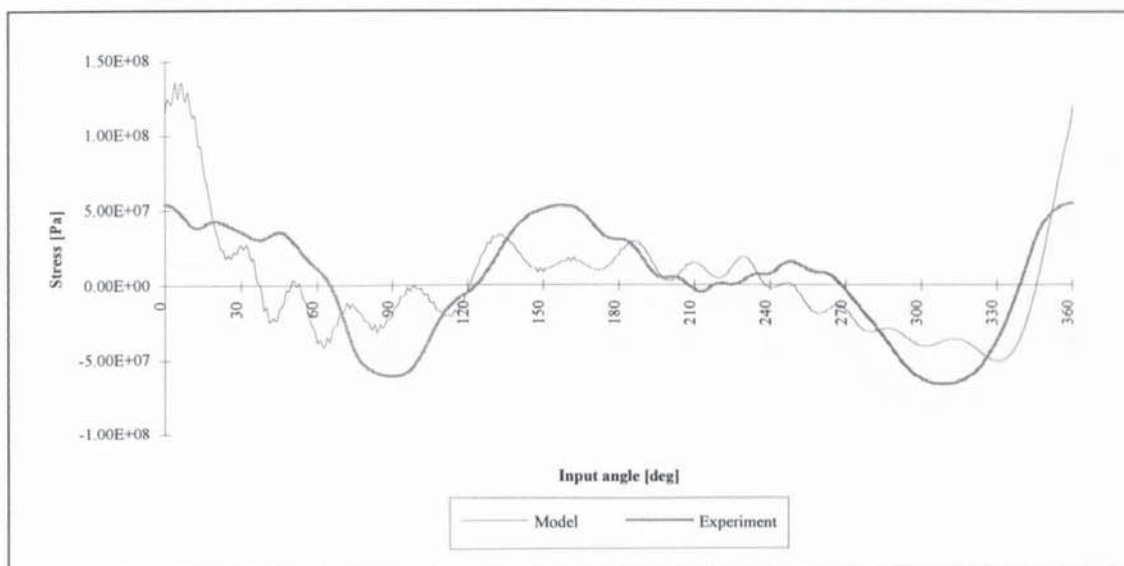


Fig. D.23.a: Stress at the input link midpoint for $\omega = 23.89$ rad/s.

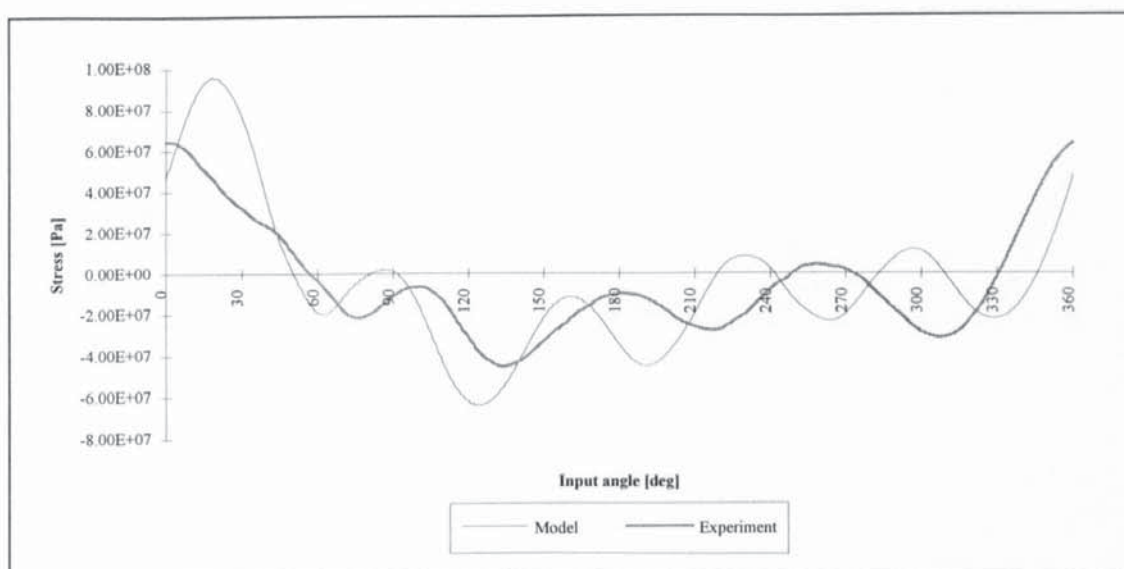


Fig. D.23.b: Stress at the coupler midpoint for $\omega = 23.89$ rad/s.

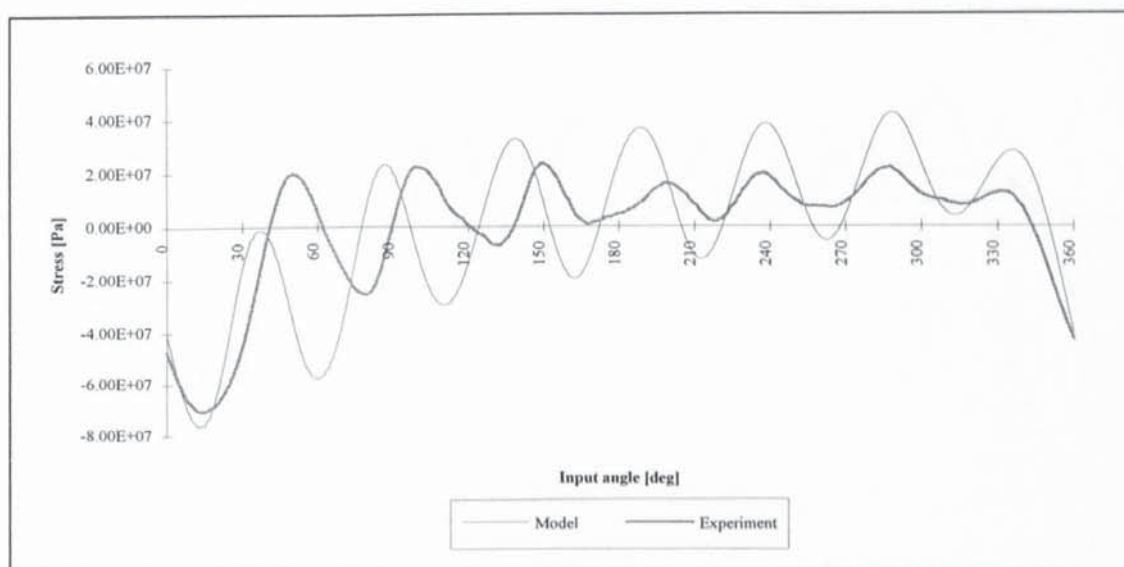


Fig. D.23.c: Stress at the follower midpoint for $\omega = 23.89$ rad/s.

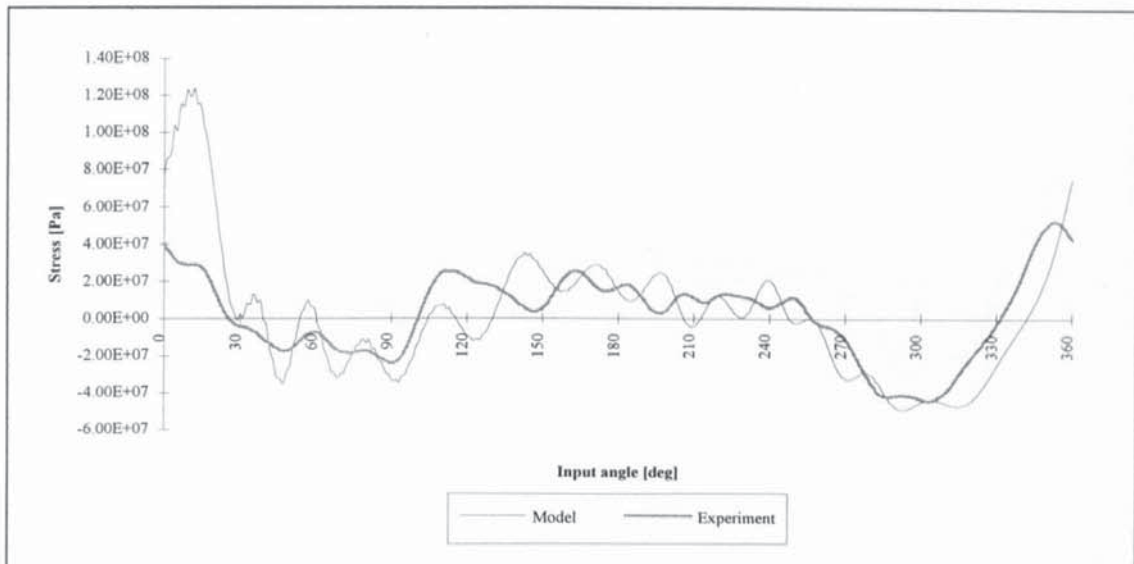


Fig. D.24.a: Stress at the input link midpoint for $\omega = 24.74$ rad/s.

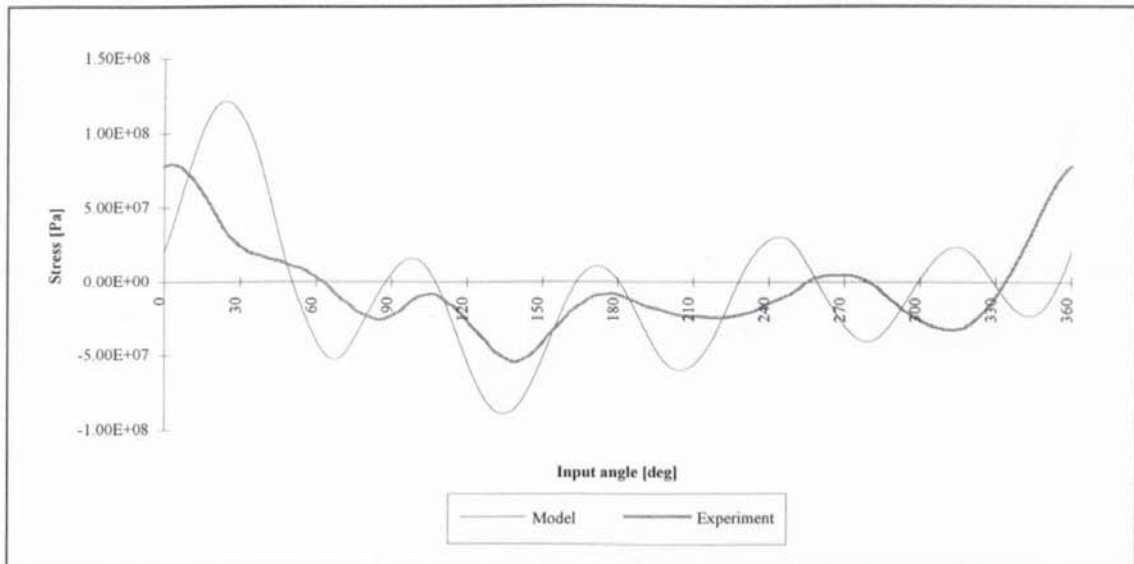


Fig. D.24.b: Stress at the coupler midpoint for $\omega = 24.74$ rad/s.

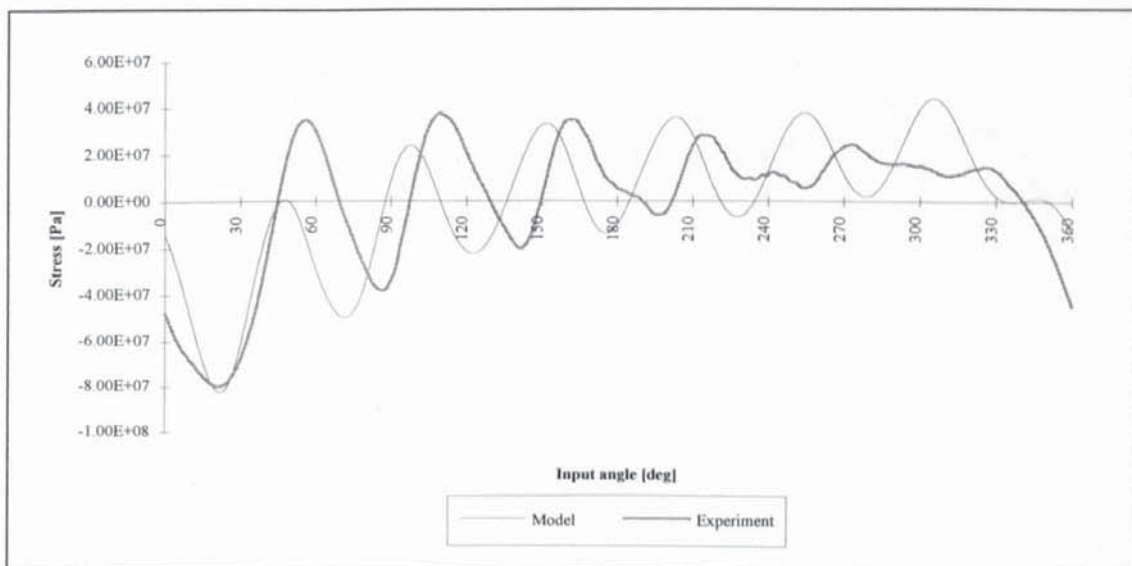


Fig. D.24.c: Stress at the follower midpoint for $\omega = 24.74$ rad/s.

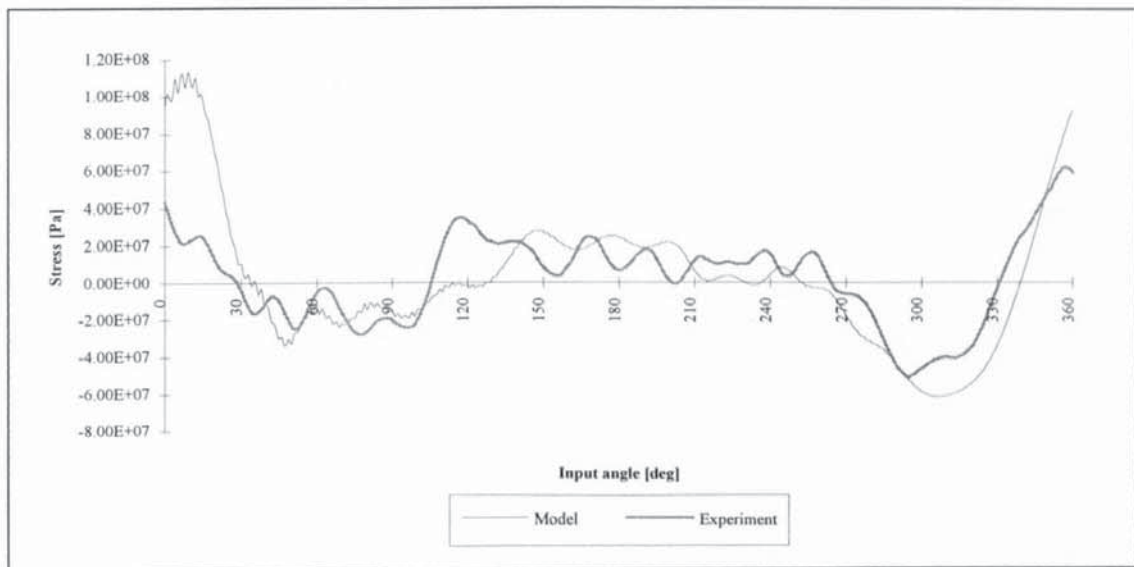


Fig. D.25.a: Stress at the input link midpoint for $\omega = 25.34$ rad/s.

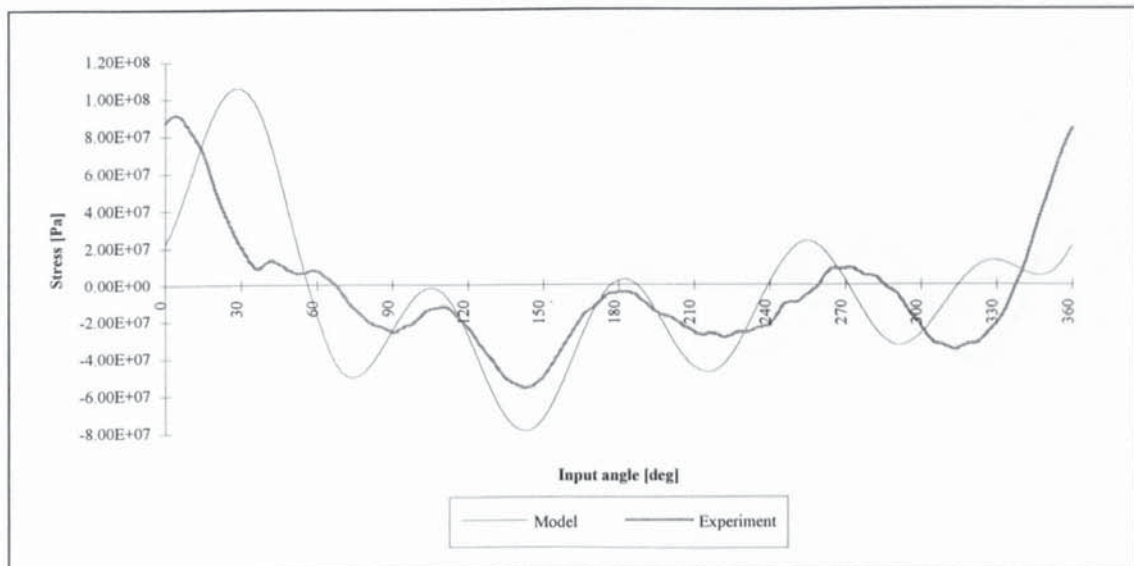


Fig. D.25.b: Stress at the coupler midpoint for $\omega = 25.34$ rad/s.

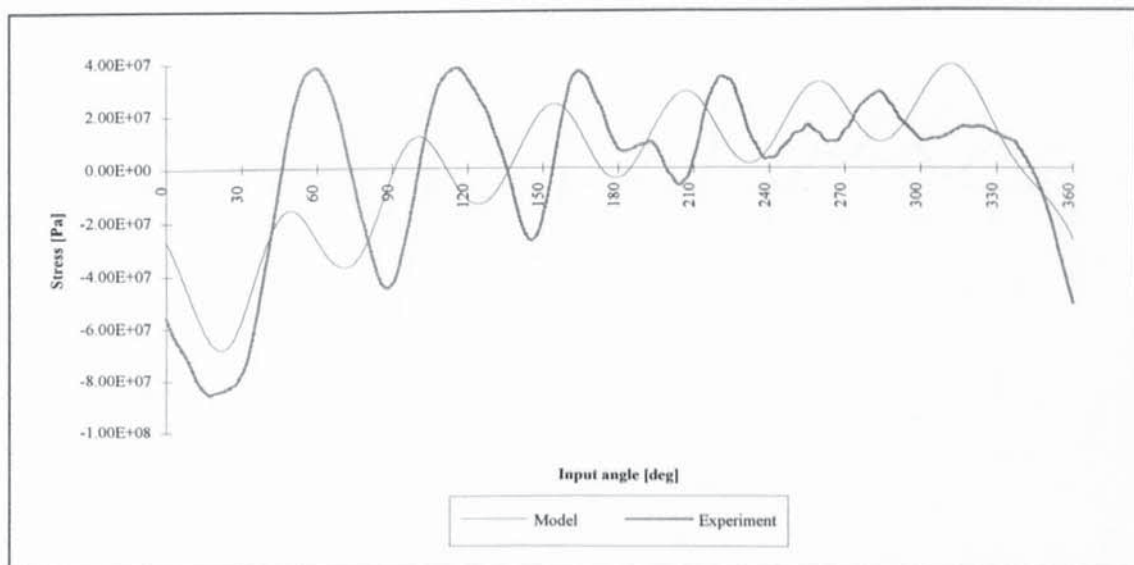


Fig. D.25.c: Stress at the follower midpoint for $\omega = 25.34$ rad/s.

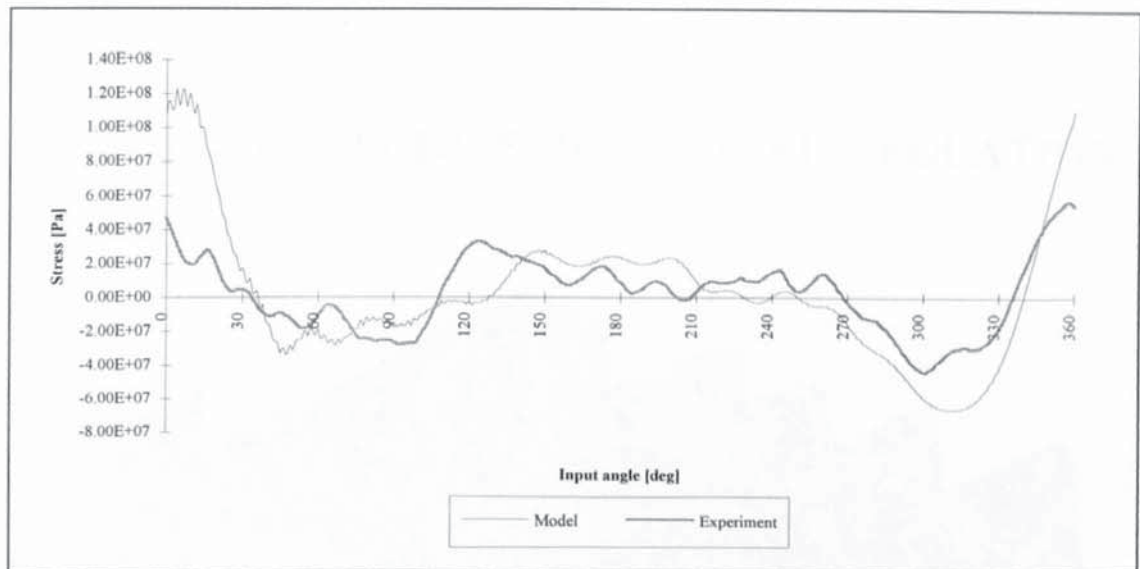


Fig. D.26.a: Stress at the input link midpoint for $\omega = 25.75$ rad/s.

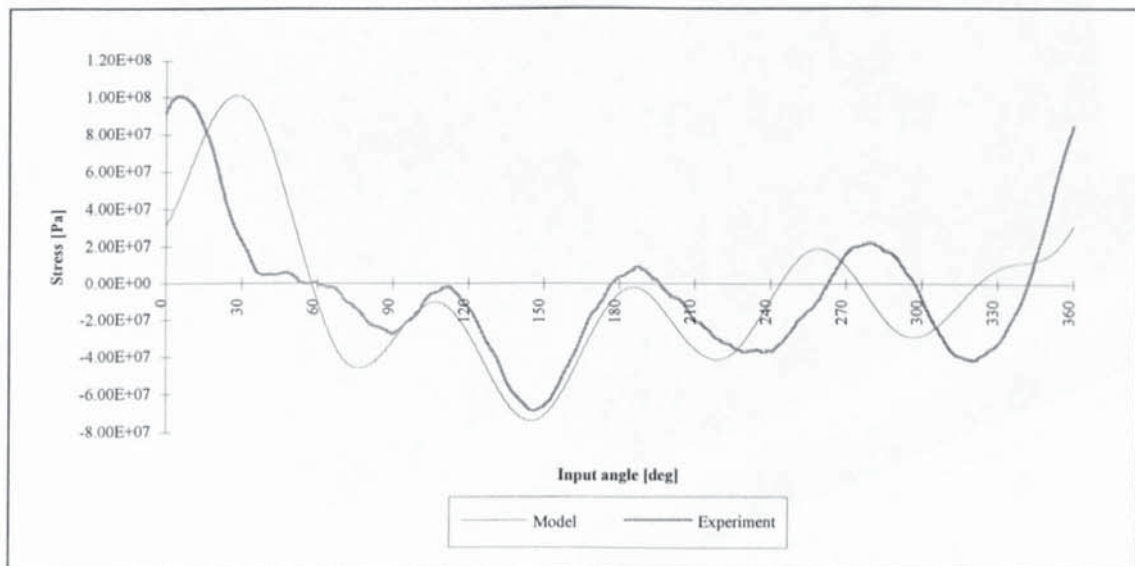


Fig. D.26.b: Stress at the coupler midpoint for $\omega = 25.75$ rad/s.

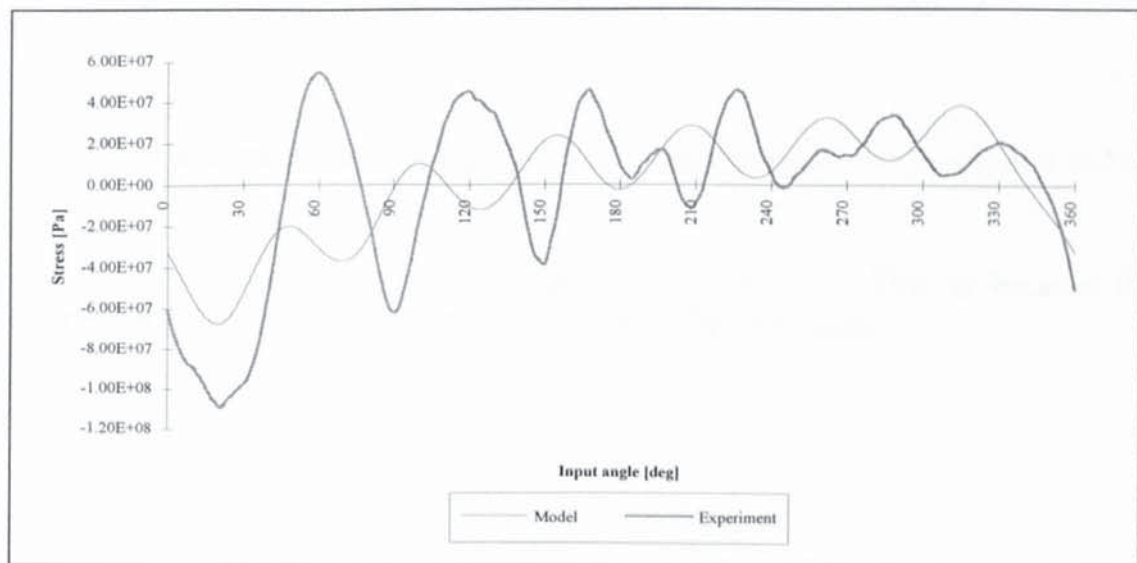


Fig. D.26.c: Stress at the follower midpoint for $\omega = 25.75$ rad/s.

Appendix E

STABILITY REGIONS OF MATHIEU'S EQUATION

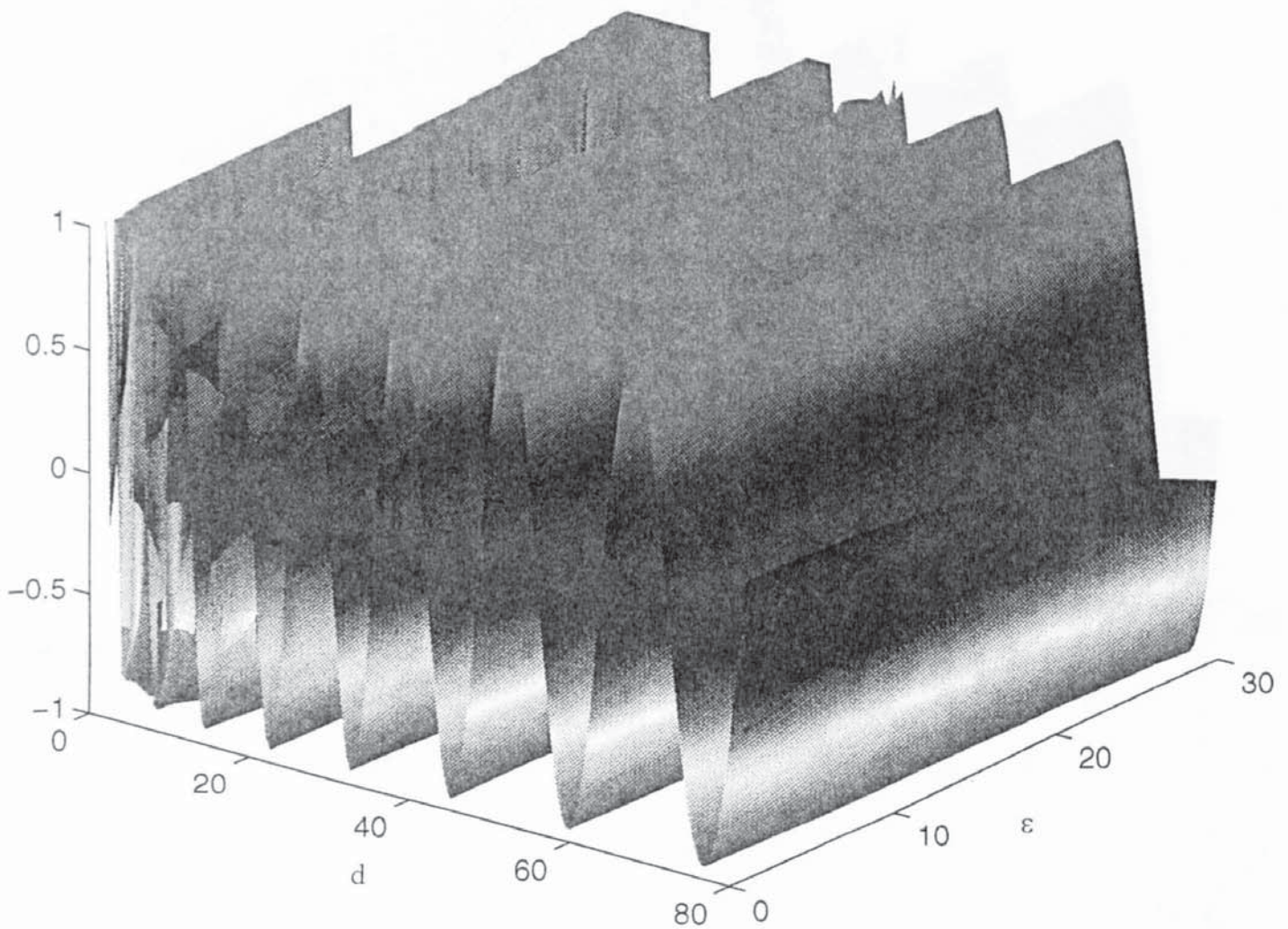


Fig. E.1: Variation of the first eigenvalue of the monodromy matrix versus d and ϵ .

The limits of z axis have been deliberately set to $[-1,1]$. This is because the eigenvalues of the monodromy matrix are larger when d is small.

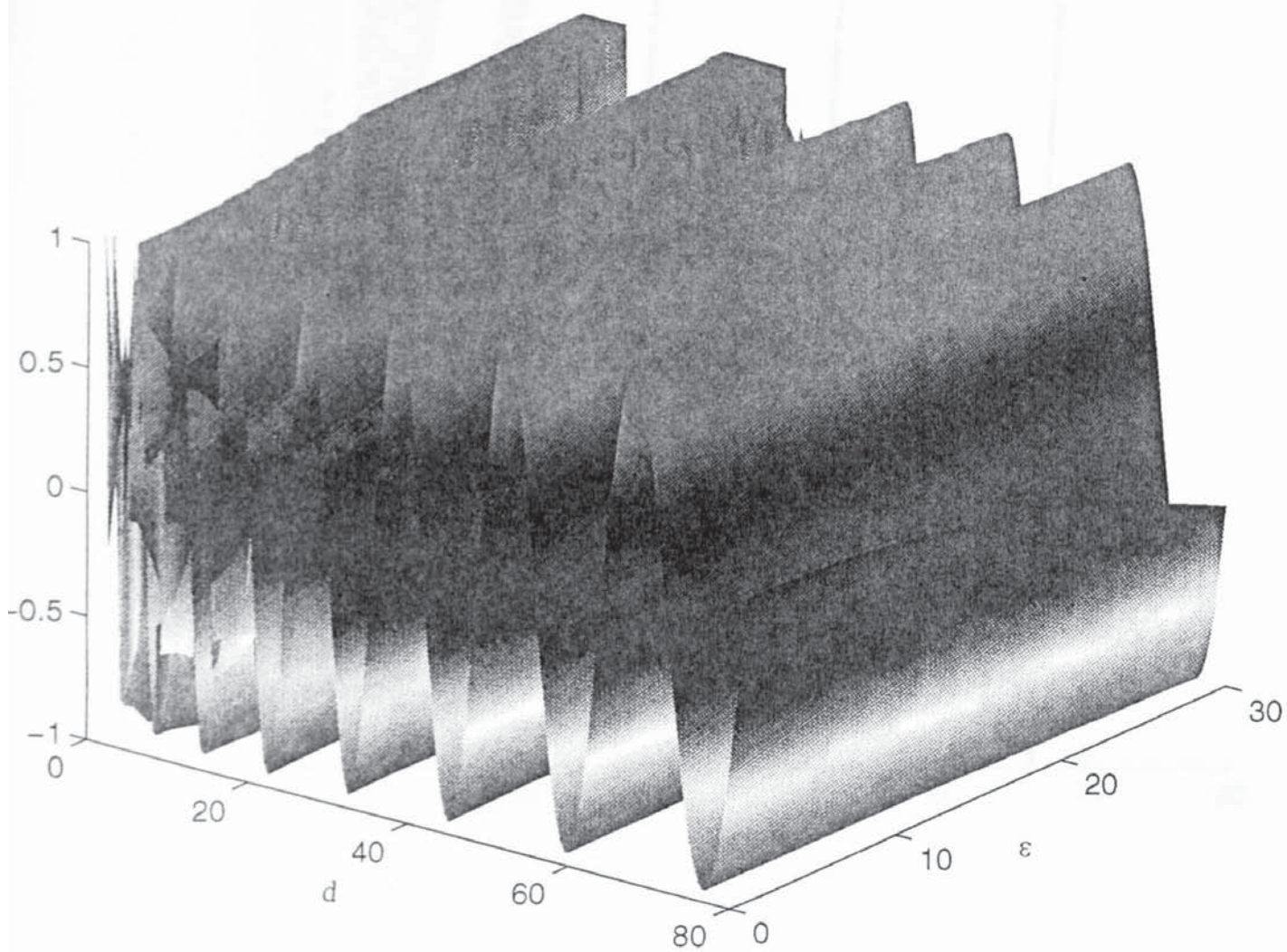


Fig. E.2: Variation of the second eigenvalue of the monodromy matrix versus d and ϵ .

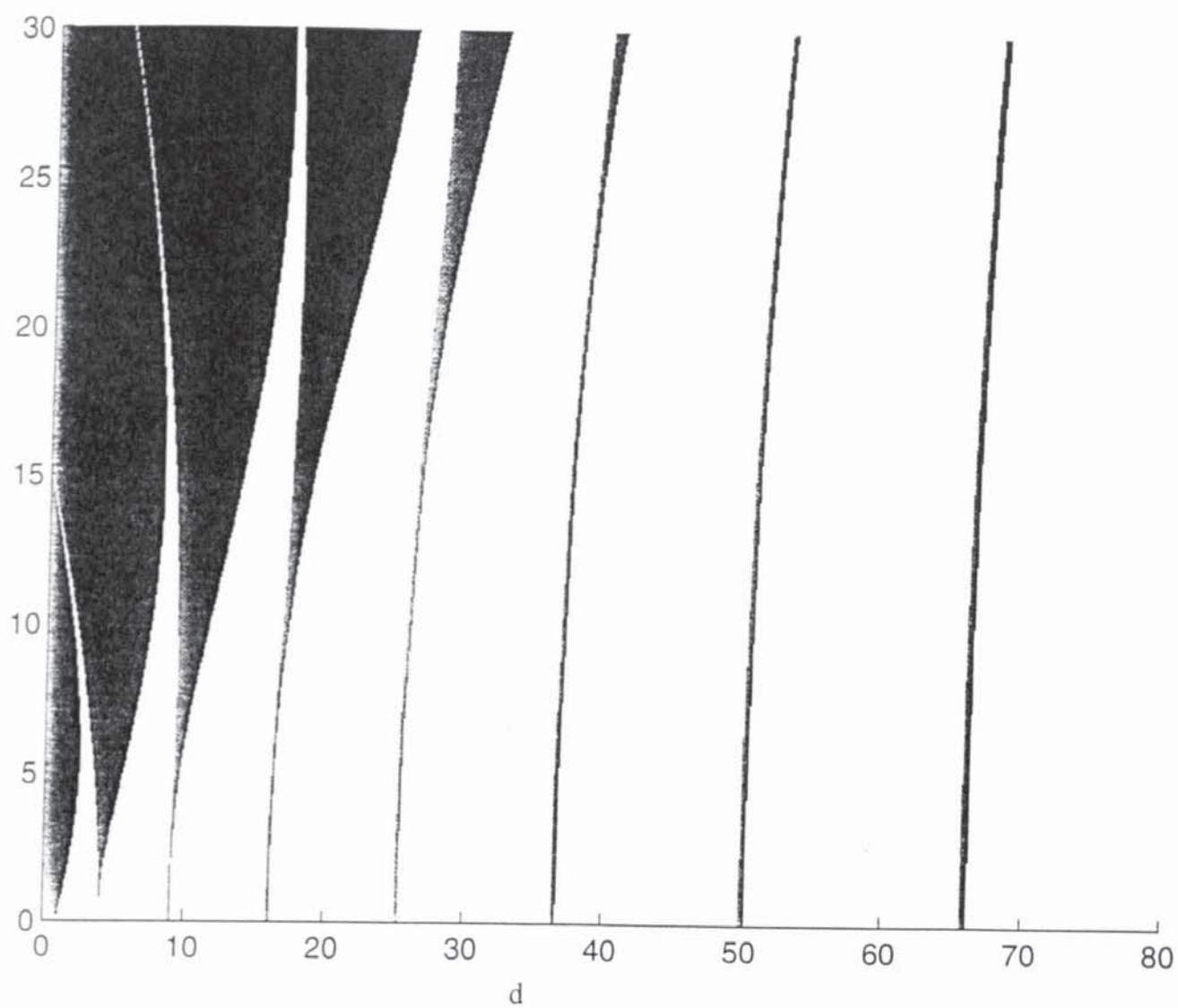


Fig. E.3: Stability chart in (d, ϵ) space.